
Habitat loss and species interactions

An in silico investigation of the structure and dynamics of ecological communities

By

CHRIS MCWILLIAMS



Department of Engineering Mathematics
UNIVERSITY OF BRISTOL

A dissertation submitted to the University of Bristol in accordance with the requirements of the degree of DOCTOR OF PHILOSOPHY in the Faculty of Engineering.

JUNE 2016

Word count: about sixty six thousand

It is interesting to contemplate a tangled bank, clothed with many plants of many kinds, with birds singing on the bushes, with various insects flitting about, and with worms crawling through the damp earth, and to reflect that these elaborately constructed forms, so different from each other, and dependent upon each other in so complex a manner, have all been produced by laws acting around us.

- Charles Darwin, 1859 [1]

ABSTRACT

This thesis represents a computational investigation of ecological community dynamics and structure. The communities are simulated using an individual-based model, and their properties are studied using a range of ecological metrics relating to diversity, network structure, and stability. A significant portion of the thesis focuses on community responses to two different types of habitat loss: random and contiguous. Particular attention is paid to the strength of species interactions, which are found to drive variability in population dynamics and also to mediate the effects of habitat loss. The modelling framework involves several features that make this a novel treatment of the subject. Specifically, the model is spatially explicit, multi-trophic, and the behaviour of individuals is constrained by bioenergetic parameters. Furthermore, the communities consist of two types of interaction: mutualism and antagonism.

Random habitat loss is found to reduce the temporal variability of population dynamics by reducing species interaction strengths. At the same time, communities are observed to become more *even*, in terms of species abundance and spatial distributions. Under contiguous habitat loss communities become more variable, which is associated with an increase in interaction strengths. However, when subject to a high rate of immigration, communities under contiguous habitat loss do not display significant changes in diversity properties, or network structure. Community responses to habitat loss are seen to depend on the spatial structure of the landscape, with random habitat loss providing barriers to the motion of individuals. Immigration also emerges as a key mechanism in driving community structure and dynamics. At high immigration rates species do not go extinct.

Community *dynamics* under variable immigration rates are studied in detail. Closed communities (without immigration) display poor persistence, with most non-basal species going extinct. High immigration rates are seen to promote community stability in several others ways. Specifically, high immigration reduces temporal variability in species dynamics; increases the stationarity of species long-term abundance distributions; and reduces the signature of determinism associated with oscillatory trophic dynamics. Differences also emerge within single communities, with high abundance species displaying less stationary but more deterministic dynamics, while low abundance species display the converse.

Under variable immigration rates many community responses to habitat loss are unchanged. However, the removal of the *rescue effect* provided by immigration means that species do go extinct. Also certain differences are found between mutualistic and antagonistic communities, as well as further unexpected differences between random and contiguous habitat loss. Mutualistic communities are seen to be insensitive to immigration rates in terms of total biomass, but display more extinctions than antagonistic communities. Contrary to previous findings, contiguous habitat loss produces more extinctions, while random habitat loss is found to result in trophic collapse of communities.

Finally, a novel method for the inference of species interactions from population dynamics is

presented. Interactions are inferred by fitting a generalised Lotka-Volterra model to discretely sampled time series data. The method is tested against data generated using both ordinary differential equation models, and using the individual based model. In the case of two species dynamics the method is shown to accurately recover interaction strengths, and in the case of three and five species the method shows promise for prediction the demographic rates (including biomass flows between species). However the reliable identification of interaction network topologies from systems of more than two interacting species remains unsolved. An application of the method to 60 species systems is presented, reducing the size of the system by aggregating the dynamics according to functional groups.

DEDICATION AND ACKNOWLEDGEMENTS

A Ph.D. thesis does not happen without external influence. I was incredibly lucky to be given the funding to pursue a project of my own choice. For this I thank the University of Bristol, and the invisible hands of the BCCS academic board and EPSRC. I sincerely hope that the future will bring with it an enhanced appreciation of the value of public investment in research and education. Not only in the sciences, but in all spheres of knowledge.

This thesis would not have been possible without the support of collaborators, advisers, friends and family. I would like to thank them all, but to name a few explicitly. Michael Gastner and Lars Rudolph helped me in many ways in the early stages on the project. Daniel Montoya has been an inspiration throughout, and has taught me all that I know about the field of Ecology. Alan Champneys took me on as a student when times were rough, and from him I have learned a lot. I also thank my collaborators in the realm of public engagement. Specifically, Espen Knoop and Lewis Roberts and all the others involved in the Tangible Networks project. My heartfelt thanks extend to my friends, in particular Patrick McGovern who has helped me throughout this process, and to my parents whose boundless support I value beyond measure. The ultimate thanks goes to Tam. She has experienced the turbulence of this process first hand, and without her I may never have completed this body of work.

AUTHOR'S DECLARATION

I declare that the work in this dissertation was carried out in accordance with the requirements of the University's Regulations and Code of Practice for Research Degree Programmes and that it has not been submitted for any other academic award. Except where indicated by specific reference in the text, the work is the candidate's own work. Work done in collaboration with, or with the assistance of, others, is indicated as such. Any views expressed in the dissertation are those of the author.

SIGNED: DATE:

LIST OF TABLES

| TABLE | Page |
|---|------|
| 2.1 Default parameter values. | 34 |
| 4.1 Testing stationarity metrics. | 100 |
| 6.1 Parameter ranges for <i>type I</i> and <i>type II</i> models. | 169 |
| 6.2 Demographic rate predictions. | 194 |

LIST OF FIGURES

| FIGURE | Page |
|--|------|
| 1.1 A trophic cascade | 5 |
| 1.2 Illustration of nestedness | 9 |
| 2.1 Niche space | 26 |
| 2.2 A sixty species food web | 27 |
| 2.3 Schematic of interaction network, with mutualism | 29 |
| 2.4 Motion of individuals | 30 |
| 2.5 Community dynamics by trophic level | 37 |
| 2.6 Community dynamics by trophic level, with mutualism and habitat loss | 38 |
| 2.7 Spatial depiction of IBM community | 39 |
| 3.1 Number of individuals versus HL | 53 |
| 3.2 Diversity versus HL | 54 |
| 3.3 Diversity by trophic level | 55 |
| 3.4 Rank abundance distributions for mutualistic communities under random HL | 56 |
| 3.5 Rank abundance distributions for mutualistic communities under contiguous HL | 56 |
| 3.6 Evenness according to rank abundance model fits | 57 |
| 3.7 Relative abundance by functional group, under random HL | 59 |
| 3.8 Relative abundance by functional group, under contiguous HL | 60 |
| 3.9 Number of links versus HL | 61 |
| 3.10 Total interaction frequency versus HL | 62 |
| 3.11 Generality versus HL | 63 |
| 3.12 Vulnerability versus HL | 64 |
| 3.13 Interaction diversity versus HL | 65 |
| 3.14 Specialisation versus HL | 65 |
| 3.15 Species area variability versus HL | 66 |
| 3.16 Interaction strength and variability versus HL | 67 |
| 3.17 Moran's I versus HL | 69 |
| 3.18 Geary's C versus HL | 69 |
| 3.19 Minimum invariability versus HL | 71 |

LIST OF FIGURES

| | |
|--|-----|
| 3.20 Ecosystem synchrony versus HL | 72 |
| 3.21 Interaction strength distributions under random HL | 75 |
| 3.22 Interaction strength distributions under contiguous HL | 75 |
| 3.23 Species mobility in under random and contiguous HL | 77 |
| 3.24 Dependence on immigration. | 78 |
| | |
| 4.1 Fractional persistence at zero IR. | 84 |
| 4.2 Dynamics at zero IR for different MAI ratios. | 86 |
| 4.3 Number of persistent species versus MAI ratio. | 87 |
| 4.4 Fractional persistence by trophic level, for different reproduction rates. | 87 |
| 4.5 Dynamics at zero IR for different reproduction rates. | 88 |
| 4.6 Dynamics at zero IR for different reproduction rates, MAI=0.5. | 89 |
| 4.7 Landscape size versus persistence. | 90 |
| 4.8 Number of initial species versus persistence. | 92 |
| 4.9 Number of initial species versus persistence, MAI=0.5. | 92 |
| 4.10 Network structure with high persistence. | 94 |
| 4.11 Network structure with low persistence. | 94 |
| 4.12 Temporal variability versus immigration rate. | 96 |
| 4.13 Control dynamics for testing stationarity metrics. | 99 |
| 4.14 Testing stationarity metrics: sample length. | 101 |
| 4.15 IBM dynamics at IR=0.001. | 102 |
| 4.16 Stationarity by trophic level at high immigration. | 103 |
| 4.17 Species dynamics at high IR, by trophic level. | 104 |
| 4.18 Stationarity of high and low abundance species. | 105 |
| 4.19 Average number of stationary species for a single network. | 107 |
| 4.20 Average number of stationary species over a region of parameter space. | 108 |
| 4.21 Average number of stationary species versus HL, and IR. | 109 |
| 4.22 Recurrence quantification plots for various time series. | 113 |
| 4.23 Percentage determinism calculated from the IBM. | 114 |
| 4.24 Linear regression to evaluate estimator performance. | 116 |
| 4.25 Accuracy of estimators versus sample length. | 117 |
| 4.26 Rank abundance spectra to test repeatability. | 119 |
| | |
| 5.1 Comparison of sampling methods for calculation of diversity. | 125 |
| 5.2 Diversity metrics for random HL. | 127 |
| 5.3 Diversity metrics for contiguous HL. | 128 |
| 5.4 Interactions and variability for random HL. | 130 |
| 5.5 Interactions and variability for contiguous HL. | 131 |
| 5.6 Ecosystem synchrony. | 133 |

| | | |
|------|---|-----|
| 5.7 | Shannon equitability versus HL, fixed IR. | 135 |
| 5.8 | Shannon equitability by trophic level versus HL, fixed IR. | 137 |
| 5.9 | Rank abundance distributions under random HL, MAI=0.0. | 138 |
| 5.10 | Rank abundance distributions under random HL, MAI=1.0. | 139 |
| 5.11 | Rank abundance distributions under contiguous HL, MAI=0.0. | 140 |
| 5.12 | Rank abundance distributions under contiguous HL, MAI=1.0. | 140 |
| 5.13 | Relative abundance by functional group, under random HL. | 142 |
| 5.14 | Relative abundance by functional group, under contiguous HL. | 143 |
| 5.15 | Generality versus habitat loss. | 144 |
| 5.16 | Vulnerability versus habitat loss. | 145 |
| 5.17 | Rank abundance distributions under fixed random HL, MAI=0.0. | 146 |
| 5.18 | Rank abundance distributions under fixed contiguous HL, MAI=0.0. | 146 |
| 5.19 | Rank abundance distributions under fixed random HL, MAI=1.0. | 147 |
| 5.20 | Rank abundance distributions under fixed contiguous HL, MAI=1.0. | 147 |
| 6.1 | Schematic of inference methodology. | 155 |
| 6.2 | Functional response for <i>type I</i> and <i>type II</i> models. | 165 |
| 6.3 | Dynamics of the <i>type I</i> model. | 170 |
| 6.4 | Dynamics of the <i>type II</i> model. | 171 |
| 6.5 | Effect of noise on parameter estimates for <i>type I</i> model. | 172 |
| 6.6 | Effect of the number of samples on parameter estimates for <i>type I</i> model. | 173 |
| 6.7 | Effect of the number of samples on parameter estimates for <i>type I</i> model, with high noise. | 174 |
| 6.8 | Effect of noise on parameter estimates, ensemble of 100 simulations of <i>type I</i> model. | 175 |
| 6.9 | Effect of number of samples on parameter estimates, ensemble of 100 simulations of <i>type I</i> model. | 175 |
| 6.10 | Effect of noise on parameter estimates, <i>type II</i> model. | 176 |
| 6.11 | Effect of noise on parameter estimates for both <i>type I</i> and <i>type II</i> models. | 177 |
| 6.12 | Effect of number of samples on parameter estimates for both <i>type I</i> and <i>type II</i> models. | 178 |
| 6.13 | Non-linear functional response in <i>type II</i> model. | 179 |
| 6.14 | Linearity of functional response as a predictor for estimate quality. | 180 |
| 6.15 | Demonstration of range sampling procedure. | 180 |
| 6.16 | Range sampling results. | 181 |
| 6.17 | Example dynamics of the IBM for two species. | 185 |
| 6.18 | Functional response (FR) of the herbivore. | 187 |
| 6.19 | Numerical response (FR) of the herbivore. | 188 |
| 6.20 | Intrinsic growth and mortality functions. | 189 |
| 6.21 | Convergence of parameter estimates for low immigration rate, 2 species. | 191 |
| 6.22 | Convergence of parameter estimates for high immigration rate. | 192 |

LIST OF FIGURES

| | |
|--|-----|
| 6.23 Comparison between true and fitted dynamics | 193 |
| 6.24 Two species demographic rate predictions, low IR. | 195 |
| 6.25 Two species demographic rate predictions, high IR. | 196 |
| 6.26 Relative error in rate predictions, low IR. | 197 |
| 6.27 Relative error in rate predictions, high IR. | 197 |
| 6.28 Potential topologies for three species. | 199 |
| 6.29 Convergence of parameter estimates, three species. | 200 |
| 6.30 Three species IBM dynamics. | 201 |
| 6.31 Demographic rate predictions, three species, low IR. | 202 |
| 6.32 Demographic rate predictions, three species, high IR. | 203 |
| 6.33 Relative error in three species predictions, low IR. | 204 |
| 6.34 Relative error in three species predictions, high IR. | 205 |
| 6.35 Model selection, three species, low IR. | 206 |
| 6.36 Model selection, three species, high IR. | 207 |
| 6.37 Competing topologies, five species. | 208 |
| 6.38 Five species IBM dynamics. | 208 |
| 6.39 Number of stable five species topologies. | 209 |
| 6.40 Frequency of stability for competing five species topologies. | 210 |
| 6.41 Five species demographic rate predictions. | 211 |
| 6.42 Inferred topology, five species. | 213 |
| 6.43 Inferred topology, sixty species without mutualism (1). | 214 |
| 6.44 Inferred topology, sixty species without mutualism (2). | 214 |
| 6.45 Inferred topology, sixty species with mutualism (1). | 215 |
| 6.46 Inferred topology, sixty species with mutualism (2). | 216 |
| 6.47 Phase plane analysis, three species. | 217 |

INTRODUCTION

1.1 Motivation

An ecosystem is a subset of the *biosphere* - the entirety of the living systems on this planet. Ecosystems are of fundamental importance to humanity because the multitude of services they provide support human civilisation [2]. Additionally living systems are closely coupled, in a two way relationship, to the abiotic systems of the planet. Lovelock, and other proponents of the *Gaia theory* [3], suggest that these biotic and abiotic components together form a single homoeostatic system which maintains conditions that are harmonious to life. Regardless of the validity of this theory, it has become increasingly clear that human activity is currently changing these global (biotic and abiotic) systems. It is well established that the recent increase in global temperatures is anthropogenic [4, 5]. Furthermore it has been conservatively estimated that the rate of species extinctions during the last century was between 8 and 100 times the background extinction rate [6]. This elevated extinction rate is undeniably related to human activities, with land-use-change and loss of habitat cited as the primary causes [7, 8]. Therefore studies into the detailed effects of habitat loss, and into the development of ecological theory in general, are urgently required in order to mitigate the effects of this *biodiversity crisis*. Together such studies represent a body of knowledge with important implications for conservation, restoration and ecological stewardship.

The breadth and scale of human impact on ecological systems is in itself sufficient motivation for this thesis. Much work has been done already in this area but, as we shall see, many questions remain open. In particular the dynamics and structure of *hybrid-ecological communities* - collections of species that interact in diverse ways - are relatively unstudied [9, 10]. Furthermore, the response of such communities to habitat loss has not yet been considered. In general, several recent studies have highlighted the importance of subtle and underlying changes to the structure of ecosystems that result from habitat loss, and which precede species extinctions [11–17]. As

we shall see the field is moving beyond a focus on species extinctions only, towards a more detailed understanding of these underlying structural changes. In this thesis we conduct a number of experiments, using computer simulations, that aim to contribute to this understanding. Particular attention is paid to the role of species interactions in generating observable patterns, and in mediating the effects of habitat loss. *In silico* investigations such as this are a useful tool in the development of ecological theory. However, their scope and interpretation must not be misunderstood (see section 1.4). In the current chapter we present an overview of the literature that is relevant to the investigation, but before departing on that journey it is necessary to explain the context of the project as a whole.

This work is funded by the Bristol Centre for Complexity Sciences (BCCS). Therefore the content of the thesis falls under that generously sized umbrella term - *complexity science* - which may leave some readers perplexed. They would not be to blame, especially given that the project motivation just provided rests on real-world *ecological* concerns. Complexity science may be understood as the study of *complex systems*. Ladyman, Lambert and Weisner review the various definitions of a complex system [18]. They attempt to synthesise a concrete definition of this concept, which they argue has previously been rather loosely and carelessly applied. The authors arrive at the following tentative definition of physical complexity:

"A complex system is an ensemble of many elements which are interacting in a disordered way, resulting in robust organisation and memory."

They assert that this definition contains conditions necessary, but perhaps not sufficient for complexity, and propose an alternative *data driven* definition under which a complex system is one that generates data with a high measure of statistical complexity [19]. Indeed to define a complex system is no easy task. Depending on who you ask there may be further necessary conditions such as *emergence*, *hierarchical organisation*, *de-centralised control* and even anti-reductionist properties such as *top-down causation*.

Given the lack of a concrete definition of complex systems, many of my contemporaries prefer a more *pragmatic approach* to the question - what is complexity science? A fair summary of the consensus view is that complexity science represents a broad set of mathematical and computational tools which find application in increasingly diverse areas of the natural and social sciences. This expansion is driven by the ever increasing availability of data; advances in high performance computing; and the development of the tools themselves. For some the tools used, and the fields of study in which they find use, are too disjoint to call complexity science a unified field. This pragmatic approach is not dissimilar to the *instrumentalist*, or "shut-up-and-calculate", interpretation of quantum mechanics [20], which finds popular support in the face of the difficult and unresolved philosophical questions posed by that theory. Further discussion on the nature of complexity is not relevant to this thesis, other than to say that if a general definition of a complex system were arrived at, then its criteria may be met by the concept of the *ecological community*.

1.2 Community ecology

An ecological community may be broadly defined as a collection of species that coexist in time and space. The study of these collections, *community ecology*, attempts to understand their structure, dynamics and function. A fundamental tenet in the field is that coexisting species interact with one another. This multitude of interactions gives rise to a *tangled web* of inter-dependence between species, that ecologists have been aware of at least since the time of Charles Darwin [1] (see quote in front matter), and probably long before. The interactions occur locally between individual members of species (e.g. two rabbits mate, one rabbit is eaten by a fox) in a manner that is arguably *disordered*. On a larger scale robust patterns of organisation exist, in particular the biodiversity patterns of species richness and abundances [21, 22]. Therefore it is tempting to conclude that the ecological community fits the definition of physical complexity quoted in the previous section.

Perhaps the key question is whether large scale community patterns do in fact result from low level mechanics, such as the interactions between individuals. This question has been an ongoing source of debate. Numerous studies have suggested that empirically observed biodiversity patterns may be consistent with *random* models of community assembly. In particular *neutral theories of biodiversity* [23, 24] assert that the species in a community are functionally identical, or at least that any difference between species is *neutral* with regards to their fitness. The fact that such neutral models are able to predict aggregate community patterns appears to reduce the complexity of the system. As stated by Purves et al. [22], in a truly neutral community all species may be replaced by a single species without loss of community function. In such a case all biodiversity patterns are meaningless artefacts of randomness. However, empirical observations tell us that species are not functionally identical, instead they display differential traits. Purves et al. give the example of carbon uptake and storage in a forest. Trees have different life cycles (growth and decay rates especially), and therefore they display functionally different temporal profiles of carbon sequestration. As such, altering the species composition of the tree community, will alter the *function* of the community (at least in terms of carbon storage, but most likely in other ways too). Therefore even proponents of *neutral* theories cannot claim that they explain it all. RatherIn general neutrality may provides useful *null models* against which to test the relative importance of other factors ,such as species interactions, in shaping communities. It seems that community assembly in nature is driven by a combination neutral and non-neutral processes [22, 25]. Therefore departures from neutrality are likely (although not necessarily [22, 26]) indicative of non-random and therefore ecologically meaningful mechanisms.

In general, the consensus view is that species interactions, and the non-random patterns that they form, do play a role in community assembly. Strong support for the influence of species interactions on community structure comes in the form of empirically observed *trophic cascades* [27, 28]. A trophic interaction is one in which energy is transferred between the interacting partners. Food webs and food chains represent collections of species interacting in such a way.

The connectivity in these systems means that an action which influences one species may have knock-on effects on the other species. Consider a simple three species food chain, in which grass is eaten by rabbits, which in turn are eaten by foxes. Grass represents the *basal trophic level* and is the sole source of all energy in this system, being the only *auto-trophic* species. If all grass is removed from the system the species in higher trophic levels go extinct: both the rabbits, and indirectly the foxes, will starve. This is a *bottom up* trophic cascade. Alternatively an action may be taken which benefits the fox population. An increased numbers of foxes is likely to have *top-down* cascading effects. For example, more foxes means fewer rabbits, which in turn means more grass. Clearly there is a dynamic element to any such changes, as we shall see throughout this thesis.

The reintroduction of wolves into Yellowstone National Park is perhaps the most famous example of a real-world trophic cascade. The grey wolf (*Canis lupus*) was reintroduced to Yellowstone in 1995. Analysis by Ripple and Beschta [28] suggests that the abundance of mature aspen and cottonwood trees increased during the following 15 years, and attributed this increase to a reduction in elk numbers due to predation by wolves. They also noted an increase in beaver and bison numbers, which they speculate resulted from reduced competition for resources with the elk. However, the observed changes displayed a spatial pattern. Specifically they recorded differences in the response to wolf reintroduction between the southern and northern regions of the park, and between highland and riparian (riverside) areas. Subsequent research [29] supports the existence of a trophic cascade in Yellowstone, but highlights the importance of other factors, such as landscape heterogeneity and environmental conditions, in determining its effect. From this we conclude that species interactions can indeed play an important role in ecology, but that their effects cannot be fully understood in isolation.

Another informative example of a trophic cascade was published by Knight et al. [27]. In their study it was shown that the presence of fish in pond communities can indirectly facilitate plant reproduction in neighbouring terrestrial communities. The pathway of influence is depicted in figure 1.1. Fish feed on dragonfly larvae in ponds, reducing the number of adult dragonflies which predate on pollinators. The presence of fish was shown to measurably benefit nearby plants by increasing pollination rates. This example again highlights the importance of species interactions, but carries with it a warning to the community ecologist. The definition of a community as an object of study (given at the beginning of this section) requires a delineation according to spatial scale or habitat type. From [27] it is clear that such a delineation can prove problematic because communities may influence one another. The pathways of influence are not confined to species with complex life histories, such as the dragonfly. More simply communities may influence one another via dispersal and immigration: the movement of individuals throughout space.

It is necessary to be aware of the limitations faced when focusing on a *local* community. Ricklefs argues [30] that the ecological community is an *epiphenomenon*, and that the strong focus of ecologists on local collections of species has hindered progress in our understanding of

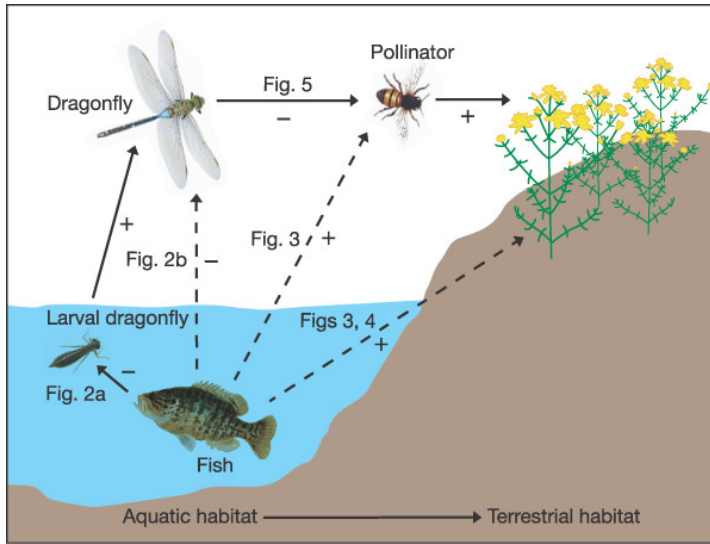


Figure 1.1: An example of a trophic cascade that crosses community boundaries. The presence of fish in ponds was empirically determined to indirectly benefit plant reproduction in neighbouring communities. Figure reproduced from Knight et al. [27].

biodiversity at regional scales. Certainly spatial considerations are fundamental to our understanding of ecology. Whittaker showed that the concept of *biodiversity* must be considered on different spatial scales [31], and it is well known that *species richness* (simply the number of species present) scales with spatial area [32]. More recently it has been shown that the choice of spatial scale also affects calculations of stability. Wang and Loreau [33] demonstrated empirically that temporal variability in biomass can decrease with spatial scale, possibly due to averaging over asynchronous fluctuations at the landscape level.

In general we see that the ecological community is an abstraction of nature, that is sensitive to spatial scale. Geographic boundaries may exist which validate this abstraction. For example islands present useful study systems of relatively isolated natural communities. However, in most cases the consideration of multiple spatial scales leads naturally to the concept of the meta-community [34]. At the landscape level one may think of a number of interacting communities, where local assemblages of species are connected via the dispersal of individuals. Meta-community modelling has increased in popularity [34, 35], and provides an important link between the local and the regional scales. However, such models tend to use a simplistic representation of the local community (e.g. [36]). Generally each locality is represented as a patch, containing information on species abundances but no spatial structure. Therefore meta-community modelling represents a trade-off in resolution at different spatial scales. For this reason *community modelling* remains useful for understanding the details of local dynamics and structure, but we must be aware of the wider context in which the local community exists.

1.2.1 Species interactions

In a local community, interactions occur between individual organisms. However, it is common to use a condensed representation by defining which *species* interact. If the interacting individuals belong to the same species the interaction is referred to as *intra-specific*; if they belong to different species it is referred to as *inter-specific*. Inter-specific interactions broadly fall into three groups: *antagonism*, *mutualism* and *competition*, based on the effect that each species has on the other. An antagonism is an interaction where there is benefit to one species and harm to the other. A mutualism benefits both parties, whereas a competition harms both parties. Whatever the type of interaction being studied, it is possible to represent the pattern of interactions between the species in the community as a network. Such a network may be referred to as a *species interaction network*, or simply an interaction network, and they have proven a useful tool for community ecologists [37]. There is a widely held view that the *structure* of these networks provides insight into the function and dynamics of ecological communities (see section 1.2.1). Correspondingly an arsenal of network metrics have been developed, drawing on the mathematics of *network theory*, with which ecologists attempt to characterise meaningful aspects of network structure. Several of these metrics are introduced in section 2.8.4, and used in the analysis throughout the thesis.

It has been, and largely remains, common practice to define a community by the way in which its constituent species interact. So in addition to the spatial delineation already discussed, a delineation exists according to interaction type, such that studies may refer to *antagonistic communities* [14], *mutualistic communities* [38] or *competitive communities* [36]. Antagonistic communities in the form of food webs are perhaps the most general since all non-basal species must feed in some manner, although studies of host-parasitoid communities are also common [13]. Mutualistic communities have received much attention in the form of plant-pollinator communities, given the key role of pollination as an ecosystem function that helps maintain plant biodiversity [39]. However, in nature there exists no clear delineation based on interaction type. It is possible for all types of interaction to occur between species that co-exist in time and space. Therefore there has been a recent move towards studies of communities that contain multiple types of interaction, or *hybrid communities* [9, 10, 40–43]. Some of these studies have brought into question previous results derived from communities with single interaction types (see section 1.2.1), and so represent an important development in the field.

Another recent development is the quantification of *interaction strengths* in ecological network studies. Early network metrics used by ecologists were based on binary networks [44], i.e. networks without weights associated with the links. This is in part because it is easier to empirically identify the presence of an interaction (to define the existence of a link in the network), than it is to quantify the strength of the interaction (to define the weight of that link). However, metrics have since been developed that incorporate interaction strength [26, 44, 45] and several studies have highlighted the improved descriptive power of such *quantitative network metrics* over their *qualitative* counterparts (see sections 1.2.1 and 1.3.2). A key feature of ecological

networks is their propensity to contain a few strong interactions and many weak interactions. Qualitative descriptors do not capture this structural feature [44]. It is common in empirical studies to use the *observed frequency* of an interaction as a proxy for its strength [26, 46]. In many cases this interaction frequency is a good approximation of the biomass flow or energy transfer along a trophic link, and therefore serves as a useful measure for how important that link is in the network. However, other metrics may be used to quantify link weight. For example plant-pollinator studies may measure pollen transport in order to quantify the amount of pollen that ‘flows’ along each interaction pathway [47].

There are many reasons to *quantify interaction strengths*, aside from the assignment of link weights to interaction networks. Strong interactions between species are thought to be destabilising for a community. A seminal theoretical study on this topic is May’s 1973 paper [48]. Using *random matrix theory* he derived results on the dynamic stability of interaction networks with random link weights. Specifically the weights were assigned randomly from a distribution with mean zero and variance σ^2 . May concluded that the probability for such a system to be dynamically stable (in terms of the linear stability of the equilibrium) decreased with σ^2 , and also with the *connectance* C (the fraction of non-zero link weights in the full coupling matrix). Subsequently a number of theoretical studies confirmed that strong interactions are destabilising in food webs [49, 50], and the effect has been empirically observed by O’Gorman [51]. From a dynamical systems perspective this result is intuitive. Strong coupling increases the dependence between variables. From a practical perspective the result is significant because by quantifying interaction strengths we may understand aspects of community stability.

Returning to the example of trophic cascades, we see further motivation for quantifying interaction strengths. In the case of the *Yellowstone cascade*, we may want to quantify the effect that a change in one population (wolves) has on the populations of other species (elk, aspen, bison, beavers). This is one definition of interaction strength, and we have seen that in Yellowstone it was spatially dependent. Similarly one may want to determine the effect that the removal of one species would have on a community. Extinction of one species may result in cascading extinctions [41], which are likely determined by interaction strengths [52, 53]. Extensive reviews on the subject of interaction strengths are provided in [46, 54]. A general theme emerging from the two papers is that methods (both empirical and theoretical) for quantifying interaction strength are dependent on the question being asked. Various methods capture different aspects of the effect of one species on another, and any two metrics are not necessarily comparable. Wootton and Emmerson [54] in particular call for more clarity from researchers on the metrics being used, and for an improved dialogue between theorists and empiricists regarding the issue of interaction strengths. In this thesis interaction strengths play a central role. The way in which they are defined is discussed in section 2.8.4, and revisited in chapter 6.

Much work in community ecology has focused on the question: how does the structure of an interaction network relate to properties of the community. This is what we refer to as *the*

role of network structure. Community properties that may be related to network structure include stability, diversity (species richness and abundances), and ecosystem functions such as pollination and nutrient cycling. We focus here on work that relates structure to *stability* because it is of particular relevance to the current project. In later chapters we will be interested in how community stability is affected by habitat loss. In depth treatments of the role of network structure on community properties in general are provided in [55] and [56]. As discussed in section 1.2.1, the metrics used to capture aspects of network structure are either qualitative or quantitative. Given that links weights represent a structural feature of weighted networks that provide more information about the system being studied, it seems natural to include link weights when that information is available. Banašek-Richter et al. [57] have shown that quantitative network metrics generally provide more accurate representations of network structure when link weights are included. Correspondingly most ecological network studies now quantify link weights (interaction strengths) in some form.

Community stability is a multifaceted and evolving concept [58–61], that includes aspects such as *robustness*, *persistence*, *variability* and *resilience*. These are discussed further in section 2.8.2, where definitions of associated metrics are provided. A general observation is that large and complex ecological communities can be remarkably stable given the extent of the external perturbations they face. There is an apparent contradiction between this empirical observation and some theoretical results regarding stability. May’s work [48] showed that large and highly connected communities are unlikely to be stable. Subsequent work by Gross [50] has shown that indeed the probability of obtaining a stable network *at random* is vanishingly low for networks of many species ($P(\text{stable}) < 10^{-4}$ for networks of 50 species). Despite these theoretical results large and stable communities are observed in nature. Either there is something wrong with the way these studies compute stability, or there are some non-random properties of real-world network structures that confer stability on communities. (A third possibility, discussed in section 2.8.2, is that the focus of theorists on stability is mistaken because communities in nature are in fact unstable.)

As we saw in section 1.2.1 community ecology has historically focused on communities with single interaction types. This focus has produced results that connect structural properties with stability in such systems. For example it is well documented that *compartmentalisation* promotes stability in antagonistic communities [62, 63]. Conceptually compartmentalisation is the tendency for groups of species to interact strongly within the group, while interacting weakly with species outside the group. This property has been observed in empirical food webs [62], suggesting that it may indeed play an important role in stabilising natural communities. Weak connectance [48, 63] and high variability in interaction strengths [64, 65] have also been suggested to play a role. The structural properties of mutualistic communities appear to differ from those of antagonistic communities. Empirically it has been observed that mutualistic communities have a *nested* structure [38]. Nestedness can be thought of as the tendency for specialist species to interact with

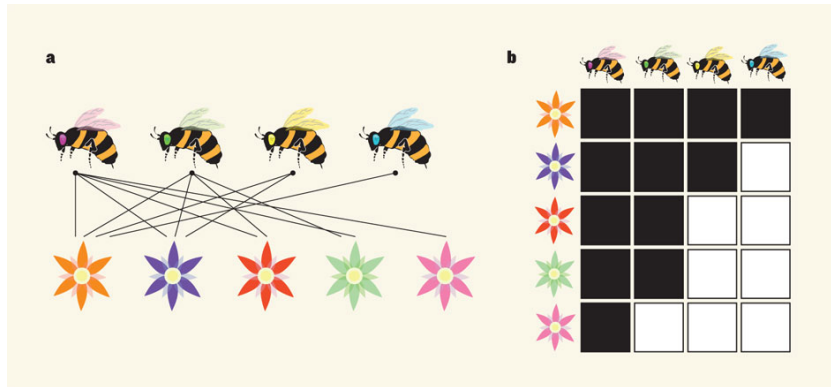


Figure 1.2: **Nestedness** is the property that the diets of specialist species are subsets of the diets of generalist species. It is common in mutualistic communities. Figure reproduced from [66]: **a**, In the mutualistic interactions that occur between plants and their pollinators, some species (generalists, such as the pink-eyed bee) interact with many partners, whereas other species (specialists, such as the blue-eyed bee) have few partners. **b**, Such networks have been described as ‘nested’, as they produce a triangular pattern when the interactions (depicted by black squares) are arranged in a matrix.’

subsets of the interaction partners of more generalist species. This concept is illustrated in figure 1.2. The property of nestedness has been shown to promote stability in mutualistic communities, as has high connectance [63].

However, more recent work on *hybrid communities* by Sauve et al [40] has brought into question some of the structural properties commonly associated with stability. They modelled communities comprising mutualistic and antagonistic interactions, and demonstrated that the effects of modularity and nestedness on stability were strongly reduced. This controversial finding indicates the importance of the recent push to study hybrid communities (previously discussed in section 1.2.1). It has also been shown, by Mougi et al. [43], that the introduction of mutualism can stabilise antagonistic communities. The novelty of these results highlights how far there is to go in order to understand the role of different interaction types as they occur in nature: simultaneously. This thesis represents one step on that journey.

1.3 Habitat loss

A significant portion of this thesis (chapters 3 and 5) is devoted to the study of community responses to habitat loss. As we saw in section 1.1, habitat loss is one of the leading causes of the extensive damage to ecosystems that we are witnessing globally. Therefore understanding the effects of habitat loss, and how to mitigate them, is more important now than ever. In this section we introduce the current state of knowledge regarding this issue, from a community ecology perspective. We cite certain key papers, however the field is too vast to provide a comprehensive overview. The reader is referred to reviews in [16] and [17] for such information. In section

[1.3.1](#) we outline how habitat loss has been modelled previously, and discuss the results of this modelling. In section [1.3.2](#) we then compare the modelling results to certain key empirical studies. In the literature a range of related concepts are studied, including *habitat alteration*, *degradation* and *fragmentation*. In what follows we use *habitat loss* to refer to all these concepts, except where a specific distinction is warranted.

In nature habitat may be destroyed in a number of ways. In general there is some spatial structure to the human activity that causes loss of habitat. Development often follows lines of infrastructure such as roads, which themselves represent linear loss of habitat. On a local scale, human activity is usually aggregated. Urban development is approximately contiguous, and agricultural land use is usually concentrated in certain areas. However, there is also a random element to the loss of habitat, particularly on a larger spatial scale. For example, the spatial distribution of exploitable resources (fertile land, mineral deposits etc.) is approximately random. Therefore we may consider there to be two extremes to the spatial pattern in which habitat is lost. At one end of the spectrum contiguous regions of habitat may be lost, leaving the rest of the landscape untouched. At the other extreme is habitat loss which is totally random, i.e. without spatial structure. In this thesis we consider [these two extreme cases](#). [Throughout we shall refer to either random or contiguous habitat loss \(see section 2.5\)](#). However, in section ?? we consider [some of the subtle interplay between these two cases. both extremes \(see section 2.5\)](#).

1.3.1 Modelling studies

Historically studies of habitat loss have focused on species extinctions, since the loss of species is arguably the most visible consequence of any perturbation. Numerous theoretical studies have investigated how the species extinctions resulting from habitat loss depend on the spatial pattern of the perturbation [67–73]. The studies cited employ spatially explicit (either lattice-type or meta-community type) modelling, such that habitat can be destroyed according to different spatial patterns. In general these studies agree that species extinctions occur at a higher level of habitat loss when the destruction occurs in some spatially-correlated way, rather than at random.

Other modelling has indicated that the loss of species is mediated by properties of the interaction network structure. Fortuna and Bascompte [74] modelled the dynamics of mutualistic communities under habitat loss. They demonstrated that random network structures produced species extinctions at lower levels of habitat loss, compared to network structures empirically derived from real-world communities. Similarly Melian and Bascompte [75] used a meta-community model to demonstrate that certain network properties can help to prevent extinctions in simulated antagonistic communities. Both increasing levels of omnivory, and reducing top-down control by predators were shown to increase extinction thresholds. However, both studies cited pertain to small model networks, and the results remain to be demonstrated empirically.

Understanding the full effects of habitat loss on a community necessarily requires the consideration of multiple trophic levels [12, 76]. We saw in section [1.2.1](#) that changes to a single

species in a community can have effects that cascade across trophic levels. Modelling by both Dobson et al. [76], and by Sole and Montoya [12], suggests that species in higher trophic levels are most vulnerable to habitat loss. Dobson et al. describe how diversity, and associated ecosystem functions, are lost first from higher trophic levels. They refer to this effect as *trophic collapse* of the community.

We have previously noted a move towards the study of hybrid communities with multiple types of interaction (section 1.2). Since this is a recent trend, such communities have yet to be studied extensively in the context of habitat loss. The only relevant study we are aware of at the time of writing is by Evans et al. [41]. They empirically constructed a network of networks, spanning several habitats on a farm ecosystem and comprising multiple interaction types. A robustness algorithm was then used to determine how vulnerable the hybrid network was to the loss of different habitats from the farm. Interestingly they reported that two of the most important habitats, relative to their sizes, were hedgerow and wasteland. However, their approach was spatially implicit and did not consider the *dynamics* of the farm community. As we shall see, such an approach is insufficient for understanding the spatio-temporal effects of habitat loss (sections ??). Therefore a more detailed modelling treatment of hybrid-communities under habitat loss is required.

Species extinctions are not the only effect of habitat loss on communities. Other effects may include changes in stability, in the distribution of species abundances and in network properties. These more subtle changes may be thought of, in some sense, as representing a decline in ecosystem ‘health’, and a loss of ecosystem function, which may occur prior to the loss of any species. Of particular concern are changes in *species interactions* resulting from habitat loss. We saw in section 1.2 that species interactions play a key role in generating community patterns and maintaining ecosystem function. This led Janzen to comment in 1974 that, when considering the effects of deforestation

“what escapes the eye, however, is a much more insidious kind of extinction: the extinction of ecological interactions” [77].

Modelling studies have investigated the loss of interactions due to habitat loss. For example Fortuna et al. [78] used a meta-community model to show that mutualistic interactions may be lost rapidly beyond a critical threshold of habitat loss. As we shall see in the following section, empirical studies have revealed that interaction networks may display structural changes in response to habitat loss. Such changes clearly result from the non-random loss of interactions between species. However, despite extensive empirical evidence for how interaction networks respond to habitat loss, theoretical models have yet to reproduce these effects. Therefore, by simulating multi-trophic community dynamics under habitat loss, we intend to reveal some of the low level mechanisms responsible for known structural changes (see section 1.6). However, we are not aware of any modelling that has attempted to reveal changes in network structure at

the community level. Our knowledge of such changes under habitat loss comes from empirical studies.

1.3.2 Empirical studies

There are certain empirically observed responses to habitat loss that appear to be general. Namely habitat loss affects species in higher trophic levels more strongly than those in lower trophic levels [79, 80], it is generally de-stabilising, and beyond a certain level of destruction it results in the loss of species [17]. These effects are consistent with the theoretical studies cited in the previous section (1.3.1). Another key theoretical result - that communities respond differently to random and correlated habitat loss - also has empirical support, although the situation is more complex in nature than in the simple models cited. Empirically studying the effect of the spatial pattern of habitat loss is a challenge because this requires controlled destruction. In empirical studies a distinction is often made between *habitat fragmentation* and *area loss* [81]. In the context of this thesis we may broadly think of fragmentation as resulting from random destruction at some spatial scale, whereas highly correlated destruction results in contiguous area loss. However, there are certain issues with these analogies, which will become clear in the discussion below. Habitat fragmentation is of particular concern. One such project, the *Stability of altered forest ecosystems* (SAFE) project [82], aims to do just that by agreeing a fixed spatial pattern for the logging of an area of rainforest in Borneo. This project is beginning to produce output on the effects of fragmentation and the resulting edge effects, which are particularly concerning given that globally '70% of the remaining forest is within 1km of the forest's edge' [83]. Most important, from a conservation perspective, is understanding the relative contributions of fragmentation, area loss, and other spatial factors such as fragment distribution [81, 84] and landscape connectivity [85], in determining biodiversity patterns.

Perhaps the most general feature of habitat loss, in any form, is a reduction in area. When land use changes, some area of the original habitat is lost. We can think of this in the context of a single forest fragment. The fragment represents a certain area of forest habitat, embedded in a wider *landscape matrix*. In general, the smaller the area of the fragment, the fewer species it can support. This result is known as the species-area-relationship (SAR), and there appears to exist a power-law scaling between the number of species present and the area of the habitat [32]. To first-order, a smaller forest fragment has less productive ability in terms of plant biomass, and therefore less ability to support species in higher trophic levels [12]. The aforementioned effect may be compound by increased competition between species in the reduced area [86], and other second-order mechanisms such as *Allee effects* [87]. However, the scaling exponent of the SAR has been shown to be context dependent [84]. It is clear that there are mechanisms beyond area loss that drive changes in biodiversity under habitat alteration. One consequence of fragmentation results from the species-area-relationship (SAR). It appears that the number of species found within a given area, in a certain habitat, scales as a power law with the area of the habitat [32].

Therefore smaller fragments have lower species richness.

Several of the mechanisms associated with habitat fragmentation are distinct from, or supplemental to, those of area loss alone [88]. Of particular importance are *edge effects* [86, 89]. The boundary length of a fragment scales linearly with its size, whereas the internal area scales quadratically. Therefore, as habitat loss proceeds, edge effects become more significant. There are numerous abiotic mechanisms responsible for edge effects. For example, exposure to greater wind speeds and solar radiation intensity have been demonstrated to alter diversity patterns at fragment edges [86]. Biotic mechanisms may also contribute to edge effects. It has been shown that rates of parasitism and herbivory vary with distance from a fragment edge [90]. Additionally, some species may be more robust than others to the presence of edge effects, resulting in differential responses at the species level. Pioneer tree species are better adapted to deal with exposure and poor soil conditions [], and generalist consumers are better able to exploit alternative resources from the landscape matrix (beyond the fragment boundary []). The latter point highlights the importance of *landscape context* in determining the effects of habitat loss.

Landscape context refers to the properties of the wider landscape in which the local community is embedded (see section 1.2). It has been shown that close proximity of habitat fragments improves species richness at both the community [] and meta-community level []. Such a situation disproportionately benefits those species with general diets and higher dispersal abilities []. Other landscape features such as matrix type (edge effects are reduced by a gradual transition to a similar habitat type rather than sharp transition to a contrasting habitat []), and landscape connectivity (reduced connectivity limits dispersal making each fragment more isolated []) contribute to diversity patterns. In general, we see the importance of explicitly considering space. The response of communities to habitat loss cannot be explained only in terms of local processes, but must be understood in terms of the wider landscape context (see section 1.6.).)

THIS TO GO (BUT PRESERVE REFS): Additionally it has been shown that smaller fragments may increase variability in species abundances [33, 88], and result in increased predation pressure due to spatial compression of the community [17]. (The latter effect is only likely when the predator is mobile and can therefore exploit numerous fragments.) On a regional scale fragmentation has been shown to dramatically reduce the biomass of terrestrial communities [83], due to a reduction in landscape connectivity.

Discuss here stability, spatial compression, area relationship. Refers frowards to stability section in chapter 2.

In addition to altering species richness and abundance patterns, habitat can change the structure of species interaction networks. This topic has received much attention in recent years []. Several recent studies have empirically detected changes in the structure of interaction networks due to habitat loss [16]. Tylianakis et al. [11] showed that empirical antagonistic communities (host-parasitoid) responded to habitat degradation with reduced evenness in interaction frequencies. This means that certain interactions became relatively more frequent, so that energy

flow through the community became concentrated along certain pathways. The quantitative changes in network structure that they observed were not detectable by equivalent qualitative metrics. Neither were conventional diversity metrics, based on species abundance or richness, able to distinguish between habitats at different levels of degradation. The changes detected represent subtle and ‘hard to measure’ impacts of habitat degradation, that may well be missed if only certain metrics are used. In particular this study highlights the importance of using quantitative network metrics. Similarly, Albrecht et al. [14] detected a decline in antagonistic interaction diversity as a result of habitat alteration. They showed that insect food webs in a grassland system lost interaction diversity faster than species diversity. Therefore, although species were lost, the extent of the community response would be underestimated if only metrics based on species abundance or richness were used. Both of these examples ([11] and [14]) highlight the sensitivity of results to the metrics used, when studying community responses to habitat loss. This sensitivity motivates the large variety of metrics used in our analysis (see section 2.8), and in particular our use of quantitative network descriptors.

Further changes in network structure have been empirically detected. Habitat destruction has been observed to push mutualistic networks towards higher modularity, higher connectivity, and lower nestedness [15]. Such structural changes have traditionally been associated with reduced stability (see section 1.2.1). Similarly habitat loss has been shown to destabilise antagonistic communities by lowering modularity and increasing interaction strengths [16]. However, Kaartinen and RoslinTomas [91] observed that, although species composition of host-parasitoid communities varied between habitat fragments, quantitative network properties did not. This result suggests a possible generality of structural changes under habitat fragmentation. In general the literature suggests, as expected, that habitat loss reduces community stability, irrespective of the interaction type. However, it is suggested that the underlying changes driving this loss in stability differs between mutualistic and antagonistic communities. It is not clear how these results generalise to the stability response of hybrid-communities (see section 1.6).

It is clear that species interactions can be lost due to habitat alteration. However, which mechanisms are driving these changes is a subject of ongoing research. Osorio et al. [92] revealed host-parasitoid networks that displayed structural changes under a gradient of land use change (agricultural intensity). They demonstrated that local processes and community competition were driving these changes, with landscape context playing no significant role. Similarly, Aizen et al [] demonstrated that a reduction in habitat area resulted in a non-random loss of mutualistic interactions which was largely determined by local properties. Interactions that were less frequent and more specialised were found to be most vulnerable. Taken together these two studies suggest that local community processes play an important role in driving structural changes under habitat loss. However, this is not to discount the role of landscape context. for example, Rossetti et al. [93] suggest that insect herbivory responses to fragmentation bay be largely determined by edge effects. Ultimately, we know that interaction networks change under habitat loss but a solid

theoretical understanding of which changes are important, and what processes drive them is still being developed.

In general, the observation of structural changes under habitat loss, sometimes without the loss of species, supports the conclusion that we must move beyond a focus on species richness. From a conservation perspective this highlights the importance of targeting inter-specific interactions, and the maintenance of network structure and function, rather than focusing on species level effects [94]. The position is summarised by Valiente et al. [95], who stress “*the importance of focusing on species interactions as the major biodiversity component on which the ‘health’ of ecosystems depends.*”

1.4 Ecology *in silico*

Computational modelling has proven a useful tool in the mathematical sciences, and has grown in popularity with the ever increasing power of modern computers. The field of ecology is no exception. In fact, given the difficulty and expense of ecological field work, computational modelling has provided a valuable complement to empirical studies. However, it is important to note that *in silico* ecology is no substitute for ecology in the field. The review papers on species interaction strengths [46, 54], discussed in section 1.2.1, have already hinted at certain problems arising from a gulf between theory and experiment. Especially in the field of theoretical population dynamics there is a sense that some mathematical models are studied as objects in their own right, rather than with a purpose of rigorous application to empirical data. In such cases the term *ecological modelling* is incorrect. Barraquand is especially critical of this issue [96], and calls for better communication between theorists and empiricists. With this in mind it is appropriate to define the scope and purpose of the investigation presented in this thesis.

The work undertaken for this thesis is purely theoretical. We do not fit our models directly to empirical data. However, the modelling framework, which is fully specified in chapter 2.4, is grounded in ecological realism. We attempt to model *realistic* demographic processes and species interactions for multi-trophic communities. This is achieved by the use of bio-energetic constraints and, where possible, parameter values derived from the literature. However, the simplifying assumptions required of any model inevitably mean that the simulated communities represent a departure from the communities of the natural world. As such the modelling serves as a tool for *hypothesis generation*. Results are analysed in detail, and presented in such a way that they may be subsequently tested against empirical observations derived from natural communities. Differences, if found, between simulated and natural communities would be suggestive of mechanisms that are either wrong or missing from the model. This is informative in itself. Equally, an apparent agreement between the model and reality does not necessarily indicate that the model accurately describes the true mechanisms of the natural world. We have already seen an example of such a case in the neutral models of biodiversity (section 1.2). Neutral models are

able to produce realistic patterns, despite evidence that mechanisms in nature are not neutral [22]. Therefore the interpretation of our modelling results, as always, must be treated with caution.

The modelling framework employed in this thesis is *individual-based*. The model, which was developed by Lurgi et al. [58], involves a two dimensional landscape on which individuals move around and interact according to certain rules. Such models have widely used in ecology [97]. In this context they are known as individual-based models (IBMs), while in other fields they are often called *agent-based models* (ABMs). These two modelling concepts are equivalent, and represent a reductionist approach to the complex systems paradigm (introduced in section 1.1). The idea is that by explicitly modelling the behaviour of individual agents at a low level, one is able to study the aggregate patterns that emerge on a higher level as a result of the interplay between these agents. If the high level properties are realistic, this is evidence that the low level mechanisms in the model may be meaningful. Such modelling allows us to conduct experiments to determine how simulated communities respond to different perturbations. A challenge posed by the IBM approach is that the large number of parameters, and the complexity of the models, are such that simulations are capable of producing an overwhelming variety of output. The IBM model used in this thesis was previously parametrised in [58], using some parameter values taken from the literature and other values tuned in order to generate realistic and stable community level patterns (see section 2.4.2). Our applications of the model are novel, and so a significant amount of the work in this thesis represents *stress testing* of the model under new parameter conditions (especially the work in chapter 4).

IBM models have been used previously in the study of habitat loss (see section 1.3.1). However, our model combines certain features that, taken together, represent a novel modelling framework. The model is spatially explicit, ~~rather than implicit which is realistic since communities are naturally embedded in space~~. This spatially explicit treatment also allows us to study the effect of the spatial pattern of habitat loss, which as we have seen can determine the impact on a community. Previously models have typically focused on a small number of interacting species [36, 68, 75], whereas our model simulates a multi-trophic community of many species. Such models are less common [58, 98], and partly facilitated by increased computational power. The multi-trophic aspect is key. We have seen that different trophic levels often respond differently to habitat loss [12, 79, 80], and in fact the interplay between species in different trophic levels can mediate the response of the community as a whole [12]. As discussed in [58], our *bioenergetic* model is more realistic than previous models of multi-trophic food web dynamics [99–101] in the following ways: 1) There is no need to define extinction probabilities (e.g. [12, 78]) since survival of individuals depends on available energy (non-basal species starve without food). 2) Complex demographic processes such as reproductive ability, are defined by energy availability. 3) Differential traits such as energy gathering efficiency model heterogeneity between trophic levels (but not within levels). Furthermore our model incorporates two types of direct interaction

between species (antagonism and mutualism). The simulation of such *hybrid communities*, as we have seen, situates this work at the forefront of community ecology, especially in regards to theoretical treatments of habitat loss.

1.4.1 The role of immigration

A key feature of our modelling framework is *immigration*. The IBM is a model of *local community dynamics*, and as we saw in section 1.2 communities are embedded in a larger spatial context. Therefore we model an inflow of individuals from outside the local landscape. The mechanism for modelling this immigration is defined in section 2.4, and without it the simulations represent *closed communities* that are isolated from the wider landscape. In meta-community modelling the immigration (or dispersal/colonisation) mechanism is fundamental, and generally has positive effects on biodiversity [36, 102, 103]. Experimentally immigration also been observed to increase the diversity of plant communities [104], and to buffer the risk of plant extinctions in tropical forest fragments [105]. In such studies the source of immigration is referred to as the *regional species pool*. Increased species diversity in the regional pool has been shown to increase diversity in local communities [106], and to reduce variability between different communities [36, 107]. In highly productive sites immigration has been experimentally shown to contribute less to community diversity than local ecological processes [106]. Whereas in sites of low productivity immigration is the more important factor, an observation referred to as *shifting limitations* on plant diversity along a gradient of habitat quality.

1.5 Inferring species interactions

Most of the work presented in this thesis consists of studying communities simulated using the IBM model. The full model specification is given in chapter 2, but the basic idea is that we define which species are able to interact and the rules by which they interact, move around and reproduce. We then investigate the community level properties and dynamics that emerge from the local interactions of individuals belonging the constituent species. However, in the final chapter, we explore what might be considered the *inverse problem*. That is, given the observed community dynamics, is it possible to infer which species are interacting and how strongly. This problem finds parallels in other areas of science where high level aggregate properties of a system are relatively easy to observe, compared to the low level structural properties. For example the biochemical networks responsible for gene regulation in cells are highly complex and adaptive, and as such determining their topological structure presents an experimental challenge. Gene expression profiles (the high level result of the regulatory networks) are comparatively easier to measure via microarray experiments [61]. Therefore numerous methods have been developed to infer the structure of regulatory networks from gene expression profiles [108, 109].

In the field of ecology several attempts have been made to infer the network of species interactions from measurements of high level properties. Previous approaches may be thought of as falling into two categories: methods based on spatial data [110, 111], and those based on population dynamics [112–116]. Spatial approaches have looked at correlations in species spatial distributions. In the simplest approximation, if species affect each other negatively (for example via competition) then we may expect a negative correlation between species distributions in space. The converse would be expected for positive interactions (such as mutualism). However, such an approach is hampered by *indirect effects* mediated by interactions with other species. More advanced statistical methods have attempted to overcome such problems (see [111]), with promising results. However, in this thesis the focus is on the population dynamics approach. Although the empirical measurement of population dynamics requires a more sustained effort in the field, it does provide more information from which interactions may be inferred.

Some authors have attempted to detect signatures of species interactions via geometric analysis of observed population dynamics [112–114]. For example it may be possible, in certain contexts, to detect predation or competition interactions from the phase relationships between species dynamics [113] (see section 6.4.7). However, as with the simplistic spatial correlation approach described above, phase-plane analysis neglects the dynamic complexities arising from indirect effects due to the presence of many interacting species. To give an example, consider the case of *apparent competition*. In this scenario two prey species are fed upon by a single predator. Therefore there are two direct antagonistic interactions. However, an *indirect competition* may emerge between the two prey species. If one prey species performs well this confers benefit to the predator. The resulting increase in predator numbers may be detrimental to the second prey species, because of increased predation pressure. In a large and complex community the potential for such indirect effects increases dramatically. This problem may be overcome by the fitting of *population dynamics models* to empirical time series. Such models explicitly characterise the interactions between species, and their effects on dynamics. Therefore fitting population models, if successful, may account for all direct and indirect effects present.

Both Ives et al. [115], and Mutshinda et al. [116], have published similar methods that statistically fit variations of a *stochastic Gompertz model* [117] to time series data. The fitted models provide estimates of interaction strengths and other parameters. Ives et al. focus on the stability of the fitted models, while Mutshinda et al. attempt to quantify the relative importance of species interactions compared to environmental forcing. However, neither study stresses the importance of correct identification of interaction network topologies. The methodology we develop in chapter 6 is inspired by the paper of Shandilya and Timme: ‘*Inferring network topology from complex dynamics*’ [118]. They present a method which is used to fit a system of differential equations to the dynamics of up to 32 coupled chaotic oscillators. The results demonstrate that, in the presence of substantial noise, the method can successfully recover the structure of the network of coupling between the oscillators. Therefore the method appears well suited to the

problem of inferring species interactions from population dynamics, which may be modelled by a system of differential equations and which are generally subject to noise. Our work represents a novel application of their method to this problem.

A requirement of the method from [118] is that the form of the equations governing the dynamics is known, and particularly the coupling function between the oscillators is known and parametrised. Regarding our application of the method, this assumption raises a fundamental issue that has been the focus of much debate in the ecological modelling literature: what mathematical functions should be used to describe the interactions between species. When modelling the antagonistic interaction between a prey and a predator the function in question is known as the *functional response* (FR). The FR defines the rate of consumption of prey pre-capita of predator (see section 6.2.1). Over the years theorists have proposed numerous forms for this feeding function [119–122], and empiricists have endeavoured to determine its form experimentally [123, 124]. Empirically the efforts to obtain a general form for the FR have been hampered by context dependence in feeding relationships (for example [125, 126]). While theoretical investigations on the subject abound they suffer, in many cases, from a lack of experimental validation and weak dialogue with empiricists [46, 96]. Therefore no general consensus has been reached on the appropriate functional form for the FR in natural systems. The position was summarised by Wootton in 2005 [54], and has not changed greatly since:

“We still have a rudimentary understanding of which of the infinite possible forms of nonlinear interaction-strength functions we should attempt to apply a priori, particularly for interaction modifications. Identification of the most appropriate functional forms requires more extensive empirical exploration.”

Jost and Ardit have contributed to the debate [122] by fitting models with different forms of FR to population dynamics, and using model selection criteria to determine the ‘best’ form. Their results suggest that such an approach may be promising, although sufficient noise can easily lead to incorrect model identification. Another problem with their approach is highlighted by the quote from Wootton, since an *a priori* form of the FR must be defined before model fitting. In the context of inferring species interactions, it is likely that the use of an incorrect form for the FR will lead to errors in the estimated network topology. Therefore the choice of FR with which to fit to dynamics is a fundamental and non-trivial concern. However, our choice is somewhat constrained by the model fitting method used.

As stated, the model fitting method of Shandylia and Timme [118] requires an interaction function that is known and parametrised. The simplest modelling assumption is therefore to use an FR that is *linear and parameter-free*. The famous Lotka-Volterra equations [127, 128] contain such an FR (see section 6.2 for more details). Therefore the model that we fit to population dynamics is the generalisation of these equations to systems of N interacting species. The additional benefit of this choice is that it makes no assumptions about species roles, or about the

types of interactions between them. Therefore the fitting of this model enables the detection of antagonisms, competitions and mutualisms alike. A limitation of this modelling choice is that species interactions in nature are unlikely to take such a simple form (again see the quote from Wootton above). In chapter 6, the extent of this limitation is investigated (section 6.3.6). Also a novel method for the characterisation of the non-linearity in the interaction strength function between two species is proposed (section 6.3.7).

1.6 Scope of the present research

It would seem then, in reviewing this literature, that there is a pressing need to understand how natural communities respond to habitat loss. Furthermore, it is clear that this understanding can only be advanced by a dialogue between theorists and empiricists. The individual based modelling framework, employed in this thesis, contributes to the theoretical side of this dialogue. We will study how simulated communities respond to habitat loss, determine the low level mechanisms that drive the observed responses, and relate our findings to the body of empirical knowledge introduced in the previous sections. We aim to establish how simulated communities respond to habitat loss, and what we can learn about the low level mechanisms that mediate these responses. Additionally we look to further the general understanding of how local interactions between individuals contribute to community dynamics and structure. By also considering the inverse problem of inferring interactions from high level properties (section 1.5) we look towards a future ecology, in which there exist stronger links between modelling and empirical data. All theoretical results presented in this thesis must be understood in the context of the literature discussed in the previous sections. As we have seen, our treatment of multi-trophic hybrid-communities, and explicit consideration of spatial structure (in the way that habitat is destroyed, but also in the way the communities are modelled), makes this work well poised to answer new and relevant ecological questions.

We have seen that the spatial pattern of habitat loss is a key determinant of community response. Theoretical studies suggest that random loss is more detrimental to species richness than contiguous loss (section 1.3.1). This is broadly in agreement with empirical results, which suggest that fragmentation compounds the effects of area loss alone (section 1.3.2). The spatially explicit nature of our modelling allows us to investigate further the role of spatial pattern, at the local scale, in determining the effects of habitat loss. We have seen repeatedly in the previous sections that the local community cannot be understood in isolation from the wider landscape context. In our modelling the landscape context is defined by the immigration mechanism (section 1.4.1), whereby the local community is coupled to an external species pool. The simplicity of this mechanism in our model (section ??) represents basic assumptions about a stable landscape context (discussed further in sections ?? and ??). This simplicity allows us to study community responses to habitat loss that are driven by local processes alone. Related to landscape context,

it is necessary to state here that our modelling does not explicitly include edge effects (section 1.3.2). This simplification allows us to focus on spatial structure at the local scale. At this scale the difference between random and contiguous habitat loss relates to connectivity. Both types of habitat loss reduce the productivity (or carrying capacity) of the local landscape, by reducing the number of available sites that can support plants (or animals). However, contiguous loss results in a connected area of sites, while random loss results in a fragmented area with reduced connectivity. We predict that random loss will hinder the ability of individuals to interact, and therefore produce greater changes in network structure and diversity properties.

It is clear from empirical work (section ??) that interaction networks change in response to habitat loss, and it is believed that these changes are related to community dynamics and function. What is less clear is the mechanisms that drive these changes. Furthermore, most empirical studies in this area have focused on bipartite networks of single interaction types. Although such systems are naturally embedded in a larger multi-trophic community, little is known about how the observed changes in bipartite networks correspond to responses at the whole community level. Our modelling allows us to investigate these relationships. In particular, we look for changes in the mutualistic sub-network (see section ??) that are concurrent with community level responses. We know that habitat loss can push mutualistic network towards high modularity and lower nestedness [], and conversely push antagonistic networks towards lower modularity and higher interaction strengths []. Traditionally both of these changes are associated with a loss of stability. Therefore, we are interested in whether such structural changes are observed when modelling hybrid- rather than single-interaction communities, and if they are associated with changes in stability. Based on the work of Sauve et al. [], we predict that the role of such structural properties (nestedness and modularity) may be reduced in the context of hybrid-communities (see section ??).

In section ?? we saw empirical evidence that habitat loss destabilises population dynamics []. Therefore, we may expect to see a decrease in the stability of simulated communities (see section ??). In nature such destabilisation has been observed to result from loss of area [], and possibly due to increased interaction strengths in habitat fragments []. We will investigate these as possible mechanisms behind any loss of stability detected. Additionally we will investigate the role of mutualism, both in driving stability and determining responses to habitat loss. We have seen evidence that the introduction of mutualism can stabilise antagonistic communities [], and can promote spatial aggregation thus conferring reproductive stability []. Based on these two findings, and the fact that the benefits of mutualism can increase the availability of biomass at the base of food chains [], we predict that mutualistic communities may be more robust to habitat loss. If such an effect were detected it would constitute a novel result that warrant empirical investigation. Indeed, any differential response to habitat loss between communities with and without mutualism, will shed new light on the potential for mutualistic interactions to shape multi-trophic hybrid communities.

1.7 Outline of the thesis

The thesis is structured as follows. In chapter 2 the individual based model (IBM) of community dynamics is defined. This model was previously used by Lurgi et al. [58] to study the stability of hybrid mutualistic-antagonistic communities in space (see section 2.2). The IBM is central to this thesis, and is used for the majority of simulations conducted. In this chapter we also define, and provide interpretations for, a range of ecological metrics that are used throughout the thesis for analysis of community structure and dynamical properties. Further methods and metrics are introduced throughout the subsequent chapters as they become relevant. Chapter 3 presents a detailed analysis of community responses to habitat loss, under the *default parameter values* of the IBM. In chapter 4 the properties of community dynamics under changing *immigration rates* are explored. The analysis in this chapter considers species persistence, and ways to quantify stationarity and determinism in the simulation output. We then return, in chapter 5 to a study of habitat loss, extending the scope of the analysis in chapter 3 by considering community responses under different immigration rates. At the end of this chapter we provide a summary of the findings regarding community responses to habitat loss, and discuss their ecological relevance. Finally, in chapter 6, we move on to address the problem, introduced in section 1.5, of inferring species interactions from simulated population dynamics. The conclusion in chapter 7 provides a general summary of key results from all chapters, and suggests potential directions for further research.



CHAPTER

2

METHODOLOGY

2.1 Introduction

The research presented in this thesis represents an *in silico* investigation of ecological community dynamics; how they respond to habitat loss and the role of species interactions. All of the experimental results, except for those at the beginning of chapter 6, are generated using the same modelling framework. This modelling framework was previously developed by Lurgi, Montoya and Montoya [58]. In this chapter we provide the details of that framework; including how the model was previously used (section 2.2); the procedure for generation of interaction network topologies (section 2.3); the specification of the individual-based model (IBM) used for simulations (section 2.4); and the two algorithms used to model habitat loss (section 2.5). We also outline the implementation of this framework in code (section 2.6) and give examples of the dynamics generated by the IBM model (section 2.7). At the end of the chapter (section 2.8) we define the suite of ecological metrics and analysis methods that are used to characterise simulated communities throughout the thesis. This suite is not exhaustive. In particular additional analytic techniques are introduced in chapters 4 and 6. However the methods defined in this chapter have all been used previously in empirical or theoretical ecology studies - together they represent a *community ecology* toolbox.

2.2 Previous use of the model

The modelling framework outlined in this chapter is largely the same as that presented in [58]. The model specification provided here is more detailed than in that paper, and is mostly in original wording. Where material is reproduced from [58], it is cited explicitly. The fundamentals of the model remain unchanged, and the implemented code is largely reused with minor

amendments (see section 2.6). The novel elements of the modelling presented in this thesis are: 1) the implementation of habitat loss algorithms (section 2.5); and 2) the exploration of new model parameter values.

In [58] the authors use the model to study the effects of increasing levels of mutualism on the stability of simulated communities. The communities are multi-trophic food webs, in which some fraction of the antagonistic links between the bottom two trophic levels are replaced by mutualistic links (section 2.3.3). This link replacement alters the behaviour of the corresponding species by making them mutualistic (either plant or animal mutualists). The authors consider multiple aspects of community stability. Namely, temporal variability, spatial variability, spatial aggregation and interaction strengths (section 2.8.2). The study found that increasing levels of mutualism increased stability in some respects, but had no significant effect in other respects. Specifically, higher mutualism was associated with greater spatial aggregation and weaker interactions, but did not change either temporal or spatial variability. Furthermore, mutualism was seen to increase the total number of individuals in a community, while reducing diversity and producing few changes in structural network properties. The reduction in diversity was attributed to the dominance of mutualistic species, which accounted for the increased overall abundance. The only network properties that significantly changed were *generality* and *specialisation* (section 2.8.4), which both decreased. In the case of generality this was attributed to changes in the relative abundances of prey, while the change in specialisation was argued to result from the overall reduction in interaction strengths. We do not provide a detailed discussion of these results here, since it can be found in [58]. However these previous findings provide some context for the current investigation.

2.3 The interaction network

Before we can simulate community dynamics we need to define the network of interactions between the species. We refer to this as the *underlying interaction network* because it defines the potential for interactions in the IBM. If two individuals meet, and they belong to species that share a link in the underlying network, they may interact. This is in contrast to the *realised interaction network*, which is simply the network of all interactions that actually occur between members of species during a given period of time. As motivated in section 1.2.1, the inclusion of multiple interaction types in the model is a key feature of this research. Therefore we require underlying interaction networks that contain both *antagonistic* (predator-prey) and *mutualistic* (plant-pollinator) links. This allows individuals to interact either via predation or mutualism depending on the type of link that they share. Additionally the networks must be multi-trophic since we wish to study whole community patterns and responses. It would be possible to use empirically derived topologies for the underlying network. Indeed there is some precedent for this in simulation studies [78]. However we use a method, pioneered by Lurgi et al. [58], to generate

artificial network topologies with desired properties. The method first creates an artificial food web (section 2.3.1), and then replaces some of the links to introduce mutualism between some species in the first two trophic levels (section 2.3.3). The strength of this approach is that it allows us to specify the ratio of mutualistic to antagonistic interactions between species in the first two trophic levels, whilst controlling the total number of species (S) and the connectance (C) of the network. Therefore we are able to vary the level of mutualism and determine the effect that this has on community responses to habitat loss.

2.3.1 The niche model

The niche model (NM) of Williams & Martinez [129] is used in the first stage of network generation to create artificial food webs. The model was first published in 2000 and it was shown to produce networks with statistical properties similar to empirical food webs. Since that date numerous competing models have been proposed [130] to explain the structure of complex food webs. However the NM has been shown to outperform the other methods in the generation of *realistic* food web topologies [131], and has proven a useful tool for the creation of artificial networks in theoretical studies such as our own [58, 132–134]. Part of the attraction of the model is its simplicity - species are randomly distributed along a one-dimensional trophic niche, and are then assigned to consume all other species that fall within a certain region of the niche space. The details of the procedure are as follows.

The model has two parameters: the number of species S , and the desired connectance C . The model output is a binary adjacency matrix \mathbf{a} that defines the presence/absence of links between species. The element $a_{ij} = 1$ implies that species i consumes species j , and $a_{ij} = 0$ implies the absence of an interaction. Connectance is defined as the proportion of the maximum possible number of links that are realised i.e. $C = L/S^2$, where L is the number of links in the network.

Figure 2.1 illustrates the concept of niche space, and shows the niche value n_i and feeding range r_i for a particular species i . Niche space is the 1-dimensional range of real numbers $[0, 1]$. Each of the S species is assigned a niche value n_i , drawn uniformly at random from the niche space. The species is then assigned a feeding range with a central value c_i and a width r_i . Species i consumes all species, including itself, whose niche values fall within its feeding range. To determine the width of the feeding range, a beta function with expectation $2C$ is used to draw a number x_i from the range $[0, 1]$. This number is then multiplied by the species niche value n_i to give the feeding range width: $r_i = x_i \times n_i$. Since $n_i \sim U(0, 1)$, we know that the expectation value $E(n_i) = 0.5$, and so $E(r_i) = C$. Therefore on average each species consumes a fraction C of the total number of species, resulting in a network with close to the desired connectance (an approximation that improves for larger number of species). The only departure from the above is for the species with the smallest niche value n_i , which is assigned a zero-width feeding range $r_i = 0$. Therefore this species consumes no others, and there is guaranteed to be at least one basal

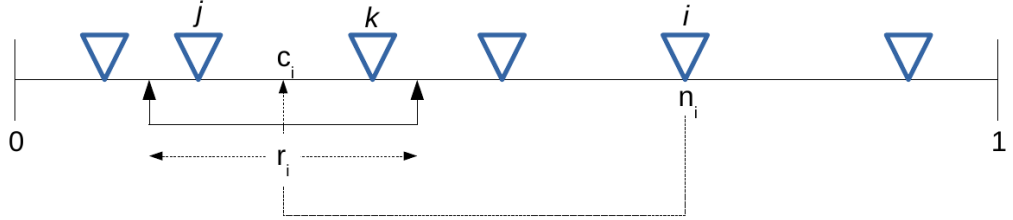


Figure 2.1: A representation of 1-dimensional *niche space* as visualised in the original publication [129], for number of species $S = 6$. The blue triangles represent the placement of species in niche space. The *niche value* of species i is given by n_i . The width and centre of the *feeding range* for species i are denoted by r_i and c_i respectively. Species i consumes all species whose niche values fall within its feeding range, here j and k .

species in the web.

A beta function has two parameters: $\alpha, \beta \in \mathbb{R}^+$. The choice of $\alpha = 1$ simplifies the probability density function to:

$$f(x; 1, \beta) = \begin{cases} \beta(1-x)^{\beta-1} & \text{if } 0 < x < 1, \\ 0 & \text{otherwise.} \end{cases}$$

The cumulative distribution function is derived by:

$$\begin{aligned} P(x) &= \int_0^x \beta(1-x')^{\beta-1} dx' \\ &= 1 - (1-x)^\beta. \end{aligned}$$

Therefore, by choosing a probability value y uniformly at random from the interval $[0, 1]$, we can draw an x value from our beta distribution:

$$\begin{aligned} y &= 1 - (1-x)^\beta, \quad \text{such that} \\ x &= 1 - (1-y)^{1/\beta}. \end{aligned}$$

The expectation value of this beta distribution is given by $E(x) = \frac{1}{1+\beta}$, therefore we choose

$$\beta = \frac{1}{2C} - 1$$

to give the desired expectation of $E(x) = 2C$.

Once the width r_i has been chosen, the feeding range is placed in niche space by drawing the range centre c_i uniformly at random from the interval $[r_i/2, n_i]$. Therefore cannibalism and

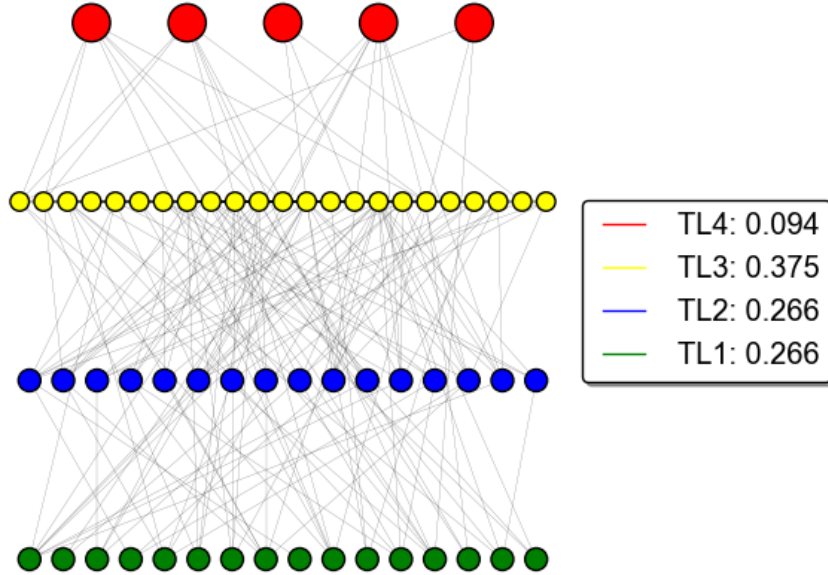


Figure 2.2: An example food web of 60 species, generated using the niche model with trophic constraints (described in the text). Numbers given in the legend are the fraction of species belonging to each trophic level.

looping are possible because up to half of the feeding range may contain niche values $\geq n_i$. In some cases the generated network may not be connected (i.e. contains one or more disconnected components), or two species may be trophically identical (i.e. have the exact same links as another species). In these cases the guilty species are deleted and reassigned new niche values (n_i, r_i, c_i) until the resulting network is connected and without identical species.

2.3.2 Trophic constraints

As alluded to previously the niche model produces multi-trophic food webs. Specifically the resulting networks have four trophic levels (see figures 2.2,2.3). The first trophic level consists of basal species, which have no prey and therefore represent plants. The second trophic level comprises species which feed only on plants. Therefore these species represent animals which are either strictly herbivorous, or may in fact be mutualists (see section 2.3.3). The third trophic level contains species which feed on other animal species, but which are also predated upon

by other animals. These species may also feed on basal species, in which case they represent omnivores. The fourth trophic level contains species which feed on animal species, but which have no predators of their own. Therefore these species represent top-predators. It is worth noting here that the niche model does not require top-predators to be strictly carnivorous. Therefore top-predators may happen to be omnivorous, feeding both on basal and non-basal species. We address this artefact of the niche model later in chapter 4.

The niche model gives us control over the number of species and the connectance. However the proportion of species belonging to each trophic level cannot be specified. Williams and Martinez [129] showed that on average the proportion of species belonging to basal, intermediate (levels two and three) and top trophic levels closely match those proportions found in empirical webs. However this is an ensemble statistic and so does not guarantee proportions for an individual web. Furthermore it is known that the niche model, and other food web assembly models, significantly underestimate the number of herbivore species[131]. That is, although the number of intermediate species may be ‘correct’, there are often too many species in the third trophic level and not enough in the second. To ensure that all the networks we generate contain a reasonable distribution of species across trophic levels we impose *trophic constraints*. We stipulate that at least 25%, 25% and 5% of species must belong to the first, second and fourth trophic levels respectively. If the niche model output does not meet these constraints the network is rejected and we generate another. The percentages used were determined heuristically in the development of the model by Lurgi et al. [58]. They ensure that there is always sufficient species richness at each level, especially at the base of the web, and that the community is not dominated by the third trophic level. An example of a niche model network which meets the trophic constraints is shown in figure 2.2.

2.3.3 Link replacement

The second stage in network creation, having obtained a food web from the niche model, is to introduce mutualistic interactions. This is done by replacing some of the links between species in the first two trophic levels i.e. between plants and herbivores. This changes the way that some species interact from antagonism to mutualism (see section 2.4.1). The fraction of these links switched is defined as the *mutualistic vs. antagonistic interaction ratio* (hereafter MAI ratio). Figure 2.3 is a schematic of a possible interaction network generated by this procedure, for a nineteen species community. In this case there are twelve links between the first two trophic levels, and six of these have been replaced by mutualistic links. The other six links remain antagonistic. Since half of the basal links have been replaced, the MAI ratio for this community is 0.5.

The result of link replacement is a hybrid network that defines two types of interaction between species (although only one between any given pair). We can identify two functional groups in each of the first two trophic levels, based on the way species interact. In the first trophic

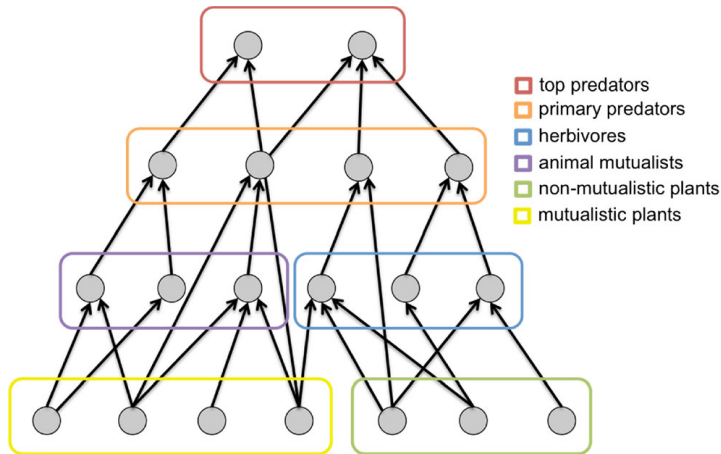


Figure 2.3: Schematic of an underlying interaction network (reproduced from [58]). Nodes correspond to species, and arrows to trophic links (antagonistic or mutualistic) from resource to consumer. The six *functional groups* of species are colour coded, and named in the legend. In this case there are twelve links between the first two trophic levels, six of these have been replaced by mutualistic links giving a MAI ratio of 0.5. Mutualistic plants and animal mutualists are defined by any species that has *at least* one mutualistic link. However species in both these groups may also have antagonistic links.

level *non-mutualistic plants* are basal species which do not have any mutualistic links. This group represents wind-dispersed plants which only have antagonistic interactions with the trophic level above. *Mutualistic plants* are any basal species with at least one mutualistic link. This group are dispersed by species from the second trophic level via their mutualistic interactions and can no longer be wind dispersed. They may also be predated upon by herbivores, if they have such links. Similarly *herbivores* are members of the second trophic level which only predate on basal species, whereas *animal mutualists* are any species in the second trophic level with at least one mutualistic link. The top two trophic levels represent distinct functional groups, which we refer to as *primary predators* and *top predators*. See figure 2.3 for a visualisation of these functional groups.

For most of the results presented networks were generated with eleven different MAI ratios in the range: $[0, 0.1, 0.2, \dots, 1.0]$. Communities with $\text{MAI} = 0.0$ contain no mutualism, whereas those with $\text{MAI} = 1.0$ contain only mutualistic interactions between the first two trophic levels. This is in accordance with the previous study [58], and allows us to look at how communities with different MAI ratios respond to habitat loss.

2.4 Individual-based model

Community dynamics is simulated using a spatially explicit, individual-based model (IBM) that was developed by Lurgi et al. [58]. The landscape consists of a homogeneous two-dimensional

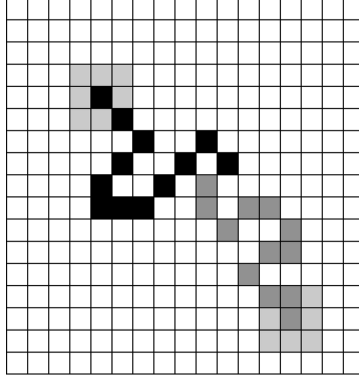


Figure 2.4: The trajectories of two individuals over 12 time steps are shown in *black* and *dark grey*. The distance-1 neighbourhoods of the two individuals on the first time step are shown in *light grey*. Figure reproduced from [58].

lattice (200×200 cells) on which individuals move around and interact subject to bio-energetic constraints. The lattice has periodic boundary conditions such that the topology of the landscape is toroidal. Each lattice cell has a space for an *inhabitant* and a *visitor*, such that a cell may contain at most two species. Basal species may only occupy the inhabitant space, whilst all other species may occupy either or both spaces. Distance on the lattice is defined as follows. The immediate neighbours of any given cell are the eight adjacent cells, including diagonals (i.e. a Moore neighbourhood). These eight neighbours are distance-1 from the central cell, whilst the sixteen cells surrounding them are distance-2, and so on (see figure 2.4). This distance metric is used in the rules for movement and reproduction (section 2.4.1), the habitat loss algorithms (section 2.5), and also in the calculation of the spatial metrics (section 2.8.3).

The model has a large parameter space - there are seventeen free parameters, which are defined in table 2.1. A discussion of the values chosen for these parameters can be found in section 2.4.2. Initial conditions are defined randomly by the following procedure. For each cell in the landscape an individual belonging to a randomly selected basal species is placed in the inhabitant space, so that all cells contain a plant individual. Then individuals from randomly selected non-basal species are placed in the visitor space of randomly selected cells, until the desired fraction of the landscape (given by parameter *OCCUPIED_CELLS*) is filled with animal individuals. The simulation is then run for a given number of time steps following the local rules described in section 2.4.1 below.

2.4.1 Local rules

The following local rules define the behaviour of individuals, which together generate the global dynamics of the IBM. In what follows capitalised-italicised words refer to model parameters, which are defined in table 2.1. Each individual stores energy (or resource), which it expends to perform actions. Initially all individuals are given a random amount of energy between *MIN_RESOURCE*

and $MAX_RESOURCE$. If the energy of an individual drops below $MIN_RESOURCE$ it dies and is removed from the landscape. On each time step an initial cell is randomly selected and all cells are updated sequentially, starting at the initial cell. Cell update consists of the following ordered processes which occur first for the visitor individual and then for the inhabitant:

1. Immigration
2. Death
3. Movement
4. Reproduction
5. Feeding
6. Metabolic loss

1) Immigration

An immigrant individual is created with probability given by $IMMIGRATION$. The species of the immigrant is selected uniformly at random from the original species pool. There must be space in the cell for the immigrant to be placed, or the immigrant must be able to feed upon the species present in the cell (in which case it does so and replaces it). Otherwise the immigrant is discarded. If placed, the immigrant is given a random starting energy.

2) Death

If the energy of an individual in the cell has fallen below $MIN_RESOURCE$, it is removed from the landscape.

3) Reproduction

An individual may only reproduce if its stored energy is greater than $MATING_RESOURCE$. This is true for all species. Animals reproduce sexually, plants reproduce asexually.

- **Sexual reproduction:** If an individual's energy exceeds $MATING_RESOURCE$ it searches its distance-3 neighbourhood. If it finds an individual of the same species, with sufficient energy to mate, and it finds a destination cell with space for an animal (inhabitant or visitor space), then mating occurs. Both parents give a fraction of their stored energy ($MATING_ENERGY$) to the offspring, which is placed in the destination cell. If an individual has reproduced it carries out no further actions on that time step.
- **Asexual reproduction:** This occurs for plants via two possible mechanisms.

1. If the individual is a non-mutualistic plant it reproduces with a probability equal to *REPRODUCTION_RATE*. If reproduction occurs the offspring is placed in a randomly selected available cell in the distance-3 neighbourhood. For plants, available means empty or only occupied by an animal individual. If no cells are available the plant cannot reproduce. Again a fraction of the parent plant's stored energy (*MATING_ENERGY*) is given to the offspring.
2. Mutualistic dispersal occurs for mutualistic plants. This action is carried out by the animal partner, and is done in the 'feeding' phase (see 5). The 'seed' of the parent plant is carried by the animal partner, so it may be placed beyond the distance-3 neighbourhood.

4) Movement

If the individual is a plant it does not move. Otherwise a neighbouring cell (distance-1) is selected uniformly at random. If the selected cell contains a prey species, feeding occurs (see 5). Otherwise, if there is an available space in the selected cell, the individual moves there. The motion is therefore a two-dimensional random walk, as represented in figure 2.4.

5) Feeding

Having selected (in 4) to move into a cell containing prey, there are three possible trophic interactions:

1. **Predation:** If neither individual belongs to a basal species a predation event occurs with probability *CAPTURE_PROB*. The prey species dies and a fraction of its energy *EFFICIENCY_TRANS* is given to the predator. The predator moves into the new cell.
2. **Herbivory:** If one individual is a non-mutualistic animal, the other is a plant, and there is space to move into the selected cell, they interact. A fraction of the plant's energy *HERB_FRACTION* is lost, and a fraction (*HERB_EFFICIENCY*) of this energy is given to the herbivore. Both individuals continue living and the herbivore moves into the new cell. If the animal is an omnivore an additional trade-off (*OMNI_TRADEOFF*) is applied to its energy gained, since omnivores are less efficient at digesting plant matter than straight herbivores.
3. **Mutualism:** If the individuals share a mutualistic link, and there is space for the animal to move, they interact. A fraction of the plant's energy (*MUT_FRACTION*) is transferred to the animal. The animal also keeps track of which plant it interacted with. If it later reaches an available cell in the landscape it creates a new individual belonging to this plant species, with probability *MUT_EFFICIENCY*. On each time step that an offspring is not produced, the mutualistic efficiency is reduced by a fraction *MUT_COOLING*.

6) Metabolic loss

If the individual is an animal it reduces its stored energy by a fraction *LIVING_EXPEND*, to account for metabolic losses. If the individual is a plant it auto-trophically increases its energy by a fraction *SYNTHESIS_ABILITY*. This, along with the randomly generated immigrants, are the only energy input to the system.

2.4.2 Model Parameters

A complex model such as this may display great variation in output depending on parameter values. During the model development by Lurgi et al. [58] a set of parameter values were selected that produced *realistic community patterns* and stable dynamics (see section 2.7). In particular the rank-abundance (see section 2.8.1.1) and degree-distributions were shown to be well fitted by log-normal and exponential functions, which is a pattern that has been observed in natural communities [135]. Where possible these parameters are based on *ecological realism*; the main example being trophic assimilation efficiency. It is well known that energy is lost when transferred between trophic levels, and that transfer rates are different depending on the type of resource consumed (plant vs. animal biomass) [136]. As such the assimilation rate is higher for plant biomass than animal biomass (*HERB_EFFICIENCY* > *EFFICIENCY_TRANS*). The extra reduction in transfer efficiency *OMNI_TRADEOFF* models the fact that omnivores are less well adapted to consume plant material because they also consume meat. Other than the omnivory trade-off all species within a functional group have identical parameters, and therefore differences between species are defined only by feeding relationships.

A key mechanism, and novel feature of the model, is mutualism. Mutualistic interactions are trophic, so energy is transferred from plant to consumer, but less than in a herbivorous interaction (*MUT_FRACTION* < *HERB_FRACTION* × *HERB_EFFICIENCY*). Therefore a mutualistic animal benefits energetically from the interaction, but less so than if it were herbivorous. A mutualistic plant benefits significantly by having less of its resource consumed, and receiving improved dispersal ability. There is a potential disadvantage to the plant that it must wait for a partner to reproduce. However the combined effect is that mutualism shifts some of the benefit of interaction in favour of the plant, whereas herbivory only benefits the consumer and harms the plant.

Lurgi et al. conducted a sensitivity analysis, which showed that their results were not significantly affected by a ±10% variation in the value of all parameters (see S.I. for [58]). Given the extensive effort that went into finding a stable and interesting region of parameter space, we choose to begin the investigation of habitat loss by using the same parameter values. These values, hereafter referred to as the *default values*, are given in table 2.1. In chapters 4 and 5 we explore the effect of varying certain parameters, with particular focus on the immigration rate.

CHAPTER 2. METHODOLOGY

| Parameter name | Value | Description |
|-------------------|-------|--|
| OCCUPIED_CELLS | 0.4 | Fraction of the grid initially occupied by individuals randomly placed on it. |
| MAX_RESOURCE | 20 | Maximum amount of resource an individual may possess at any given time. |
| MIN_RESOURCE | 3 | Death threshold: minimum amount of resource at individual may possess. Any individual possessing less than this amount at any given iteration will die (see text). |
| LIVING_EXPEND | 0.01 | Fraction of resource an individual spends in living every iteration of the model. Metabolic rate. |
| MATING_RESOURCE | 0.5 | Fraction of MAX_RESOURCE that is required for an individual to be able to reproduce. |
| MATING_ENERGY | 0.2 | Fraction of resource given to the offspring by the parent during reproduction. Each parent gives the same fraction. The total amount depends on how much resource the parent possesses at the time of reproduction. |
| IMMIGRATION | 0.005 | Probability that a new individual will appear in a cell of the grid each iteration. The species this individual belongs to is randomly chosen from the original species pool. |
| SYNTHESIS_ABILITY | 0.1 | Fraction of resource that is autotrophically created by each individual from the basal species every iteration. This is the only energy input to the system. |
| HERB_FRACTION | 0.7 | Fraction of resource lost to herbivores by individuals belonging to a basal species during a trophic event, i.e. a species in the first trophic level feeding on a species in the basal level. |
| OMNI_TRADEOFF | 0.4 | Fraction of resource that omnivores are effectively able to gather when feeding on a species from the basal level (a plant). |
| MUT_FRACTION | 0.25 | Fraction of resource of a primary producer (basal species individual) that a mutualistic partner obtains when an interaction of this type occurs. |
| CAPTURE_PROB | 0.4 | Probability that a predator individual embark upon a trophic relationship with one of its prey individuals when it encounters it. |
| EFFICIENCY_TRANS | 0.2 | Fraction of the resource the prey that is assimilated by the predator in a carnivorous interaction, i.e. trophic interaction not involving individuals from the basal species. |
| HERB EFFICIENCY | 0.8 | Fraction of the resource of the prey assimilated by the herbivore in an herbivorous interaction. |
| MUT_EFFICIENCY | 0.8 | Efficiency of an individual mutualist when dispersing a plant partner. In other words, the probability with which a mutualistic individual will facilitate the creation of a new individual of the last species of plant it visited when it is positioned on an empty cell immediately after it interacted with a mutualistic plant partner. |
| MUT_COOLING | 0.9 | Cooling factor for the mutualistic efficiency of plant dispersers (mutualists). This is the fraction of mutualistic efficiency that remains after each iteration. |
| REPROD_RATE | 0.01 | Reproduction rate of non-mutualistic plant species. Probability with which an individual belonging to a plant species that does not possess mutualistic partners for dispersal will create an offspring in any given iteration of the simulation run. |

Table 2.1: Definitions of model parameters, and *default values* used. Reproduced from [58].

2.5 Modelling habitat loss

In order to study the effect of habitat loss (HL) on simulated communities we extend the IBM of Lurgi et al. [58] by implementing two habitat loss algorithms. Simulations are set up and run as detailed in the previous sections but on the 1000th time step, after the initial transience (see section 2.7), a given fraction of the lattice cells are destroyed. The individuals inhabiting the destroyed cells are removed. Subsequently an individual may select a destroyed cell to move into (see section 2.4.1), in which case it is unable to move and remains in place. In the reproduction phase destroyed cells are counted as unavailable for the placement of offspring. Throughout the thesis results are presented for incrementally affected landscapes, representing a gradient of habitat loss. The levels of destruction are referred to by the percentage of destroyed cells: HL = [0, 10, 20, .., 90]%. The cells to destroy are chosen by two simple algorithms, giving two habitat loss scenarios: 1) Random and 2) Contiguous. These scenarios represent two extremes of the spatial pattern in which we may expect habitat to be destroyed in nature (see section 1.3).

1) Random habitat loss proceeds by selecting lattice cells uniformly at random from the set of non-destroyed cells. This is repeated until the desired percentage HL is achieved. The result is a patchy and fragmented landscape.

2) Contiguous habitat loss proceeds by selecting a ‘seed cell’ uniformly at random from the pristine landscape. Destruction then spreads radially outwards from the seed cell, according to the distance metric defined in section 2.4 and the toroidal boundary conditions of the lattice. This results in contiguous regions destroyed and pristine habitat.

2.6 Implementation in code

The code for the simulation model was originally written by Miguel Lurgi for research leading to the publication [58]. He and Daniel Montoya were responsible for the bulk of the model development, testing and parameter selection - a considerable task. My task was to take this ‘legacy code’ and apply it to a study of habitat loss. The model is implemented in *Python* [137], with several switches that ensure portability between different versions of the language. The programme makes extensive use of *numpy* and *networkx*, amongst other *Python* libraries. A change in the return value of some methods in *networkx* (specifically some methods from v1.9 return *generator* objects, whereas in v1.7 they return *lists*) forced me to make some amendments to the code. During this process I profiled the code using *cProfile* and *pstats*, because I noticed it was running very slowly. I determined that the cause was repeated calls to methods of the *networkx* library, which were made every time an interaction needed to be checked in the network (for example to see if two individuals are able to interact). By storing two representations of the network - one as a *networkx* object and one as a simple *numpy* array - I was able to speed up the

simulations by almost an order of magnitude. The *networkx* methods need only be called when some network metric needs to be calculated. Having made the above changes I ran an ensemble of test simulations. Cross-checking the results with those in [58] confirmed that the simulations were behaving as expected.

The original code was well written to be extendible, and there was a prototype algorithm for contiguous habitat loss. Therefore my job of implementing and testing the habitat loss algorithms (section 2.5) was made easy. I also added methods to save the spatial state of the system. This allows for *post-hoc* spatial analysis, and also facilitated the creation of spatial animations of the evolution of the system (see animations at [138], and figure 2.7). All results presented in this thesis are from simulation ensembles run on *Blue Crystal Phase 3* [139], the university's high performance computer cluster. Ensembles were run as parallel job arrays, and output saved in pre-constructed directory trees. I conducted post-simulation analyses in the statistical package *R* [140] and in *Python* making extensive use of the *open source* libraries available.

2.7 Dynamics of the model

In the absence of habitat loss the dynamics of the model is characterised by an initial period of transient dynamics, with high amplitude oscillations, after which the populations settle into a *relatively steady state*. A typical example of the population dynamics, aggregated by trophic level (TL), is shown in figure 2.5. The simulation that produced this figure used default parameters, and no habitat loss. In general we observe that the main transience, characterised by relaxation from the initial conditions, is contained within the first 1000 time steps. Therefore we use the *heuristic* that habitat loss is applied on the 1000th time step. Figure 2.6 shows the trophic dynamics of a mutualistic community ($MAI = 1.0$), with 40% HL applied. The drop in abundance on the 1000th time step is clearly visible. The figure also appears to show that the system has not reached steady state before HL is applied - the abundance of TL1 in particular is still increasing. However there is no requirement that the system should be at steady state before habitat is destroyed. More important is for the system to be a steady state when we sample from it to conduct analysis - we want to characterise the system reliably, and not unwittingly perform calculations on some section of transience. This issue turns out to be non-trivial, and we return to it in chapter 4. However, for the initial analysis in chapter 3, we make the same assumption as in [58]: that the system has reached steady state after 5000 time steps, even with the addition of HL.

Figure 2.7 shows the spatial state of the system on the 5000th time step, for a community with $MAI = 0.5$. There is no HL. Obviously we cannot generalise from a single image. However observing the communities in space does provide intuition about the dynamics and other properties of interest. *Animations* of the spatial dynamics under various conditions can be viewed online at [138]. Insights gained from *watching* the simulated communities feed implicitly into

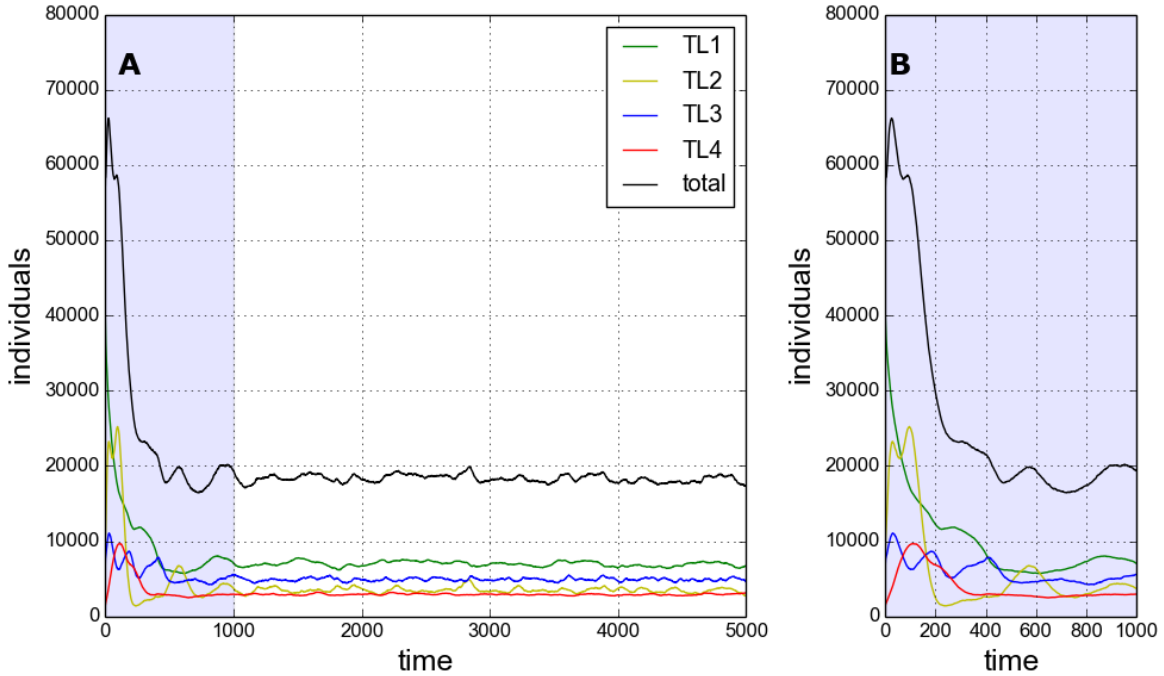


Figure 2.5: Example of community dynamics by trophic level, simulated using the IBM with *default parameters*. No habitat loss. Antagonistic community: $MAI = 0.0$. (A) The full dynamics for 5000 time steps. (B) Magnification of the first 1000 time steps, containing initial transience.

the analysis and discussion throughout the thesis.

2.8 Ecological metrics and analysis methods

In this section we introduce the metrics and methods used to analyse simulation output, which are standard tools of community ecology. These methods fall nicely into four categories. *Biodiversity* metrics (section 2.8.1) capture some aspect of the diversity of species. *Stability* metrics (section 2.8.2) try to quantify stability - a task that is fraught with confusion and therefore given some thought here. *Spatial metrics* characterise the properties of the distribution of species in space. *Network metrics* use properties of the *realised* interaction network to provide insight about community structure. The choice of metrics provides a balance across the aforementioned categories, and largely is determined by the analysis previously conducted by Lurgi et al. [58]. Additionally we present a way to use rank-abundance distributions to measure *evenness* in species abundances (section 2.8.1.1), and implement several new stability metrics based on *invariability* (section 2.8.2.1). In all that follows we use the number of individuals belonging to a species to measure *abundance*. An alternative would be to use *biomass*, which is potentially more informative due to allometric scaling [141]. However biomass information is not included in the model, and number of individuals is a commonly used alternative.

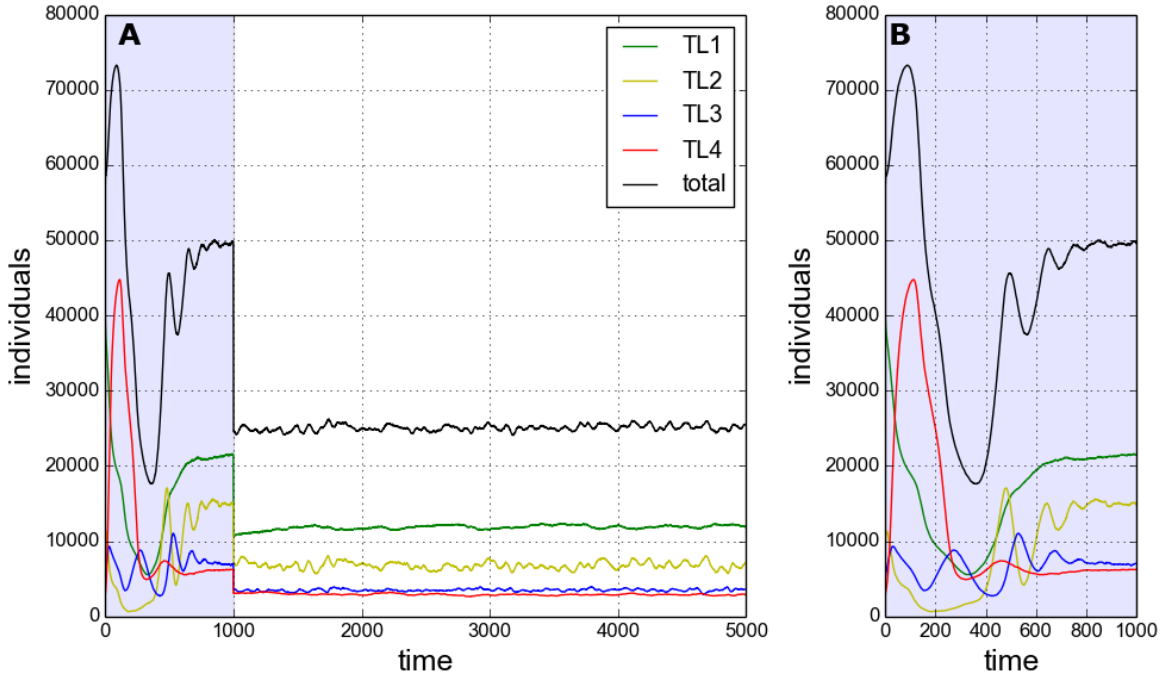


Figure 2.6: Similar to figure 2.5, but with $MAI = 1.0$, and with 40% contiguous habitat loss applied on the 1000th time step.

2.8.1 Biodiversity metrics

Species richness is very simply defined as the number of different species present (in a sample). As discussed in section 1.3, many HL studies have focused in species richness. However this metric only changes when species become locally extinct, or sufficiently rare that they are not present in samples. Therefore this metric is insensitive to many ways that a community may respond to perturbation. We define the **relative abundance** of a species i by:

$$(2.1) \quad r_i = \frac{N_i}{\sum_{j=1}^S N_j},$$

where N_i is the number of individuals belonging to species i , S is the number of species. Unless otherwise stated the sum in (2.1) is taken over all species, such that the relative abundance is the proportion of individuals in the whole community that belong to species i . The relative abundance of species within a subset of the whole community (such as a functional group) may also be calculated. In this case the sum is only over the subset of species, giving the abundance relative to the other species in the group. The relative abundance is used to calculate the **Shannon diversity index**:

$$D_{Sh} = -\sum_{i=1}^S r_i \log(r_i),$$

2.8. ECOLOGICAL METRICS AND ANALYSIS METHODS

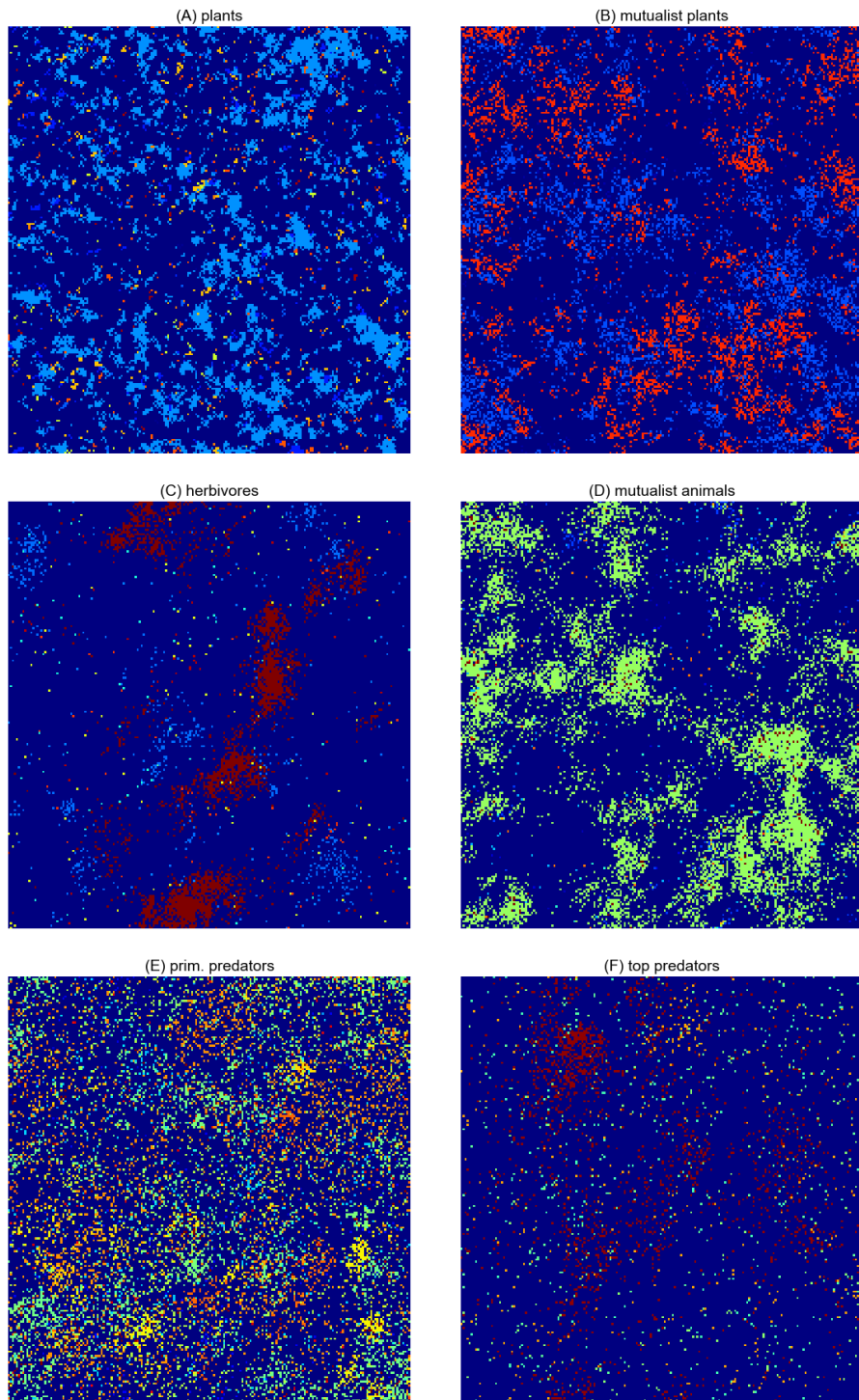


Figure 2.7: A spatial representation of each functional group. Each panel (A-F) shows the full landscape (200×200 cells). Dark blue represents empty cells. Other colours indicate presence of an individual, coloured by species. $MAI = 0.5$, $HL = 0\%$.

which is simply the Shannon entropy of species relative abundances. Therefore diversity, by this metric is maximal when all species have the same relative abundance, and approaches zero if one species out competes all others. There is no standard convention for base of the logarithm. Throughout this thesis we use the natural logarithm (base e) for all information theoretic measures. Normalising D_{Sh} by the maximum diversity gives us the **Shannon equitability index**:

$$(2.2) \quad E_{Sh} = \frac{D_{Sh}}{\log(S)},$$

since the maximum diversity is equal to the logarithm of the number of species S . The metric is constrained between 0 and 1, and is maximal when all species have the same relative abundance. Both the Shannon metrics can be computed for a subsets of the community (for example a functional group) by using the relative abundance within the subset (2.1), and reducing S accordingly. Throughout the thesis we use only the Shannon equitability index because it controls for the number of species present, and therefore changes in this metric are not driven by changes in species richness that may be induced by HL. Hereafter *we use the terms equitability and diversity interchangeably* to refer to the normalised metric given in (2.2).

2.8.1.1 Rank abundance distributions

Rank abundance distributions (RADs) provide another tool to study the patterns in species abundances. They are sometimes referred to as Whittaker plots, after his 1965 paper on species abundances in plant communities [142]. To construct the RAD, species are simply ranked from most to least abundant, such that the distribution is monotonically decreasing. It is conventional to use the logarithm of the abundance measure when plotting, because of the wide range of abundances often found in nature. We use RADS to *visually inspect* the distribution of species abundances, and to develop *alternative measures of evenness*. Example RADs for simulated communities can be seen in figure 3.4.

In natural communities it has been observed that RADs tend to be *long-tailed* - with relatively few species of high abundance, and relatively many species of low abundance. As such RADs have often been found to fit well to a *log-normal* distribution [58, 142], or modifications thereof [143]. However numerous alternative models have been proposed [144], and are implemented in the *vegan* package [145] of the programming language *R*. The power of RADs is that they condense a large amount of information about species abundances into a single plot. This information can be interpreted qualitatively via inspection, or quantitatively via the fitting of the aforementioned models. RADs may supplement other diversity metrics such as the Shannon metrics defined above, which being coarse-grained may miss subtle features of the abundance distribution (for example discontinuities or trophic sorting). Therefore we propose two measures of evenness to complement the use of the Shannon metrics. These measures are, calculated by fitting two alternative models to a RAD. We use two models from those available in *vegan*: the *Zipf* and the

preemption model, because both have a parameter which is easily interpreted as a measure of the evenness of the distribution. The **Zipf model** is given by the power law:

$$(2.3) \quad \hat{a}_r = N \hat{p}_1 r^\gamma$$

where \hat{a}_r is the predicted abundance of the species rank r ; N is the total number of individuals; \hat{p}_1 is the estimated proportion of the most abundant species (rank 1); and $\gamma \in \mathbb{R}^-$ is the estimated exponent of the power law. So γ gives the gradient of the line defined by (2.3) in log-log space. Therefore a smaller value of $|\gamma|$ indicates a shallower line and more even distribution of abundances (see for example figure 3.4). The **preemption model** is given by a geometric sequence:

$$(2.4) \quad \hat{a}_r = N\alpha(1 - \alpha)^{r-1}$$

where $\alpha \in [0, 1]$ is the single model parameter, and other symbols have the same meaning as in (2.3). Therefore the estimated abundance decreases by a fraction $(1 - \alpha)$ for each rank, and the choice of α is constrained such that the estimated abundances sum to N . In semi-log space, as is used to plot the RADs, the preemption model gives a straight line, since (2.4) implies:

$$\log(\hat{a}_r) = \log(1 - \alpha)r + C,$$

where C is constant. Therefore the smaller the value of α , the closer the gradient of the line is to zero, and the more even the distribution of abundances. In our case, as is common [145], we use relative abundances to allow comparison of the RADs between communities with a different total number of individuals. Therefore $N = 1$, and \hat{a}_r are fractions, in (2.3) and (2.4). The models are fitted using R , and the parameters γ and α used as complementary metrics for evenness - in both cases *the smaller the absolute value of the parameter, the more even the distribution of abundances in the community*. As with the Shannon metrics, RADs may be produced for subsets of the community.

2.8.2 Stability metrics

There are various different theoretical concepts relating to stability in ecosystems, which can lead to confusion [60, 146]. It is remarkable that complex ecosystems are able to function with relative consistency in the face of extrinsic variability and perturbations (e.g. due to environmental factors and human activity). Ecological theory does not yet fully explain this phenomenon. Donohue et al. [147] explain that stability is a multi-dimensional concept involving related but distinct components such as variability, resilience, robustness and persistence. Communities may appear stable in some respects, but unstable in others, especially under perturbations such as habitat loss. Our main approach to stability focuses on features of temporal population dynamics

and is outlined below. However we first introduce two key stability concepts for clarification. **Persistence** simply means lack of extinction i.e. a population of the species continues to exist through time [69]. In the current context persistence of a species is defined by the presence of individuals belonging to that species in the artificial landscape. This concept plays a key role in chapter 4. **Robustness** is a measure of how resistant a community is to perturbation. It is often used in the context of species extinctions, with robustness metrics measuring the expected extent of cascading extinctions after removal of some species [41]. **Dynamic stability**, in the current context, refers to properties of the dynamics of the system. Its definition requires further clarification.

As we saw in section 1.2.1, May demonstrated [48] that high connectance and strong interactions in random communities leads to instability. This led to the conclusion that ecosystem complexity reduces stability, which contradicts observations of nature and has been the subject of ongoing debate ever since (see discussion in section 1.2.1). The measure of stability used in this body of literature is derived from the mathematics of dynamical systems. The assumption is that the dynamics of an ecosystem can be modelled as a system of non-linear ordinary differential equations (ODEs). It is possible to calculate the local stability of the equilibrium state of this system - it is stable if all eigenvalues of the Jacobian have negative real parts. Therefore this commonly used theoretical concept of stability relates to the stability of ecosystem models. It is often referred to as *asymptotic resilience* [60] because the magnitude of the real parts of the eigenvalues determine the rate of return to equilibrium after perturbation.

Asymptotic resilience is used to measure stability in chapter 6. However, in practical applications, this measure cannot be used because of the difficulty in estimating the elements of the Jacobian from empirical data (see the aforementioned chapter). Therefore empiricists use an alternative measure that can be computed directly from population dynamic time-series [147, 148]. **Temporal variability** is measured as the coefficient of variation in the abundance time-series of a species. So for species i :

$$(2.5) \quad CV_i = \frac{\sigma_i}{\mu_i},$$

where σ_i and μ_i are the standard deviation and mean of the species abundance respectively, over the time period in question. To derive a community level measure we average CV_i over all species, and in all subsequent analysis refer to the resulting metric as **mean_CV**. The metric captures the variability of population dynamics, with the assumption that *higher variability implies lower stability*. However the relationship to asymptotic resilience (AR) is not clear. For example a system may exhibit a limit-cycle which is globally stable such that all trajectories approach it asymptotically (an attractor). Therefore AR classifies the system as stable. However the *mean_CV* may be high, depending on the amplitude of the limit cycle, suggesting instability. It appears that the two stability concepts are incompatible.

2.8.2.1 Invariability

A group of theoreticians at the *Station d'Ecologie Théorique et Expérimentale* in Moulis are currently attempting to clarify the issues surrounding stability, and characterise the relationship between AR and stability metrics based on variability [59, 60]. Their work is currently restricted to the case of systems with a stable equilibrium point, rather than an attractor. They introduce four new stability metrics based on *invariability*, which are named: ecosystem (I_{eco}), population (I_{pop}) and minimum invariability (I_{min}), and ecosystem synchrony ($Sync$). These are defined, respectively, as follows:

$$\begin{aligned} I_{eco} &= \frac{1}{CV(X_{tot})^2}, \\ I_{pop} &= \frac{(X_{tot}^*)^2}{(\sum_i \sqrt{Var(X_i)})^2}, \\ I_{min} &= \min_i \frac{(X_i^*)^2}{Var(X_i)}, \\ Sync &= \frac{Var(X_{tot})}{(\sum_i \sqrt{Var(X_i)})^2}, \end{aligned}$$

where X_i is the abundance time-series vector of species i ; X_{tot} is the total abundance time-series (i.e. $\sum_i X_i$); CV is the coefficient of variation (as defined in (2.5)); and X_i^* , X_{tot}^* are the species level and total abundance values of the stable equilibrium point respectively. Therefore I_{eco} is the squared inverse of the metric *mean_CV*, whilst I_{min} is the squared inverse of the coefficient of variation of the *most variable species*. I_{pop} is a weighted sum of the species level invariabilities, and $Sync$ is given by the ratio I_{pop}/I_{eco} . In [59] it is shown that AR is strongly dependent on species composition, and is closely related to I_{min} - it is often dominated by the least abundant and most variable species. Therefore they conclude that AR is not a reliable metric, and advocate some combination of invariability metrics to characterise stability. We implement and test these metrics in our analysis (chapter 3), and note here the following relevant properties:

- I_{eco} is a measure of system level stability, and should behave similarly to *mean_CV*.
- I_{min} is the stability of the most variable species, which is often the least abundant [59]
- I_{pop} is weighted in favour of the more abundant species, to reduce sensitivity to very rare species.
- $Sync$ is always less than or equal to one. If all species abundances vary in perfect synchrony $Sync = 1$. However any deviation from synchrony results in some cancellation in variability when abundance is aggregated over species, meaning that invariability is greater at the ecosystem level, than when summed over species i.e. $Sync < 1$.

2.8.3 Spatial metrics

As we saw in section 1.3, the spatial structure of the landscape at different scales has significant impacts on the community. Additionally we have seen that one main difference between mutualistic and antagonistic communities in the IBM relates to spatial aggregation (section 2.2). Therefore analysis of spatial patterns is pertinent to the current investigation. The spatially explicit nature of the IBM allows us to study the spatial structure of the communities. We use the spatial-autocorrelation metrics Moran's I and Geary's C to measure aggregation in species spatial distributions [58, 149]. **Moran's I** is a measure of global correlation, and for a single species s is given by:

$$(2.10) \quad MI_s = \frac{N}{\sum_{i=1}^N \sum_{j=1}^N w_{ij}} \frac{\sum_{i=1}^N \sum_{j=1}^N w_{ij}(X_i - \bar{X})(X_j - \bar{X})}{\sum_{i=1}^N (X_i - \bar{X})^2},$$

where N is the total number of cells; X_i is equal to 1 if the species is present in cells i and equal to 0 if not; \bar{X} is the mean of X_i over all cells; and w_{ij} is spatial weight between cells i and j . We take w_{ij} equal to 1 if the cells are neighbours (distance-1), and 0 otherwise. In the extreme of total aggregation, when every cell containing the species is surrounded by other cells containing the species, $MI_s = 1$. In the opposite extreme, when no cells containing the species are adjacent to each other, $MI_s = -1$. For a random distribution of individuals the expected value $E(MI_s) = -1/(N - 1)$, which is close to zero for large N . For a single species s , **Geary's C** is given by:

$$GC_s = \frac{(N - 1)\sum_{i=1}^N \sum_{j=1}^N w_{ij}(X_i - X_j)^2}{2W\sum_{i=1}^N (X_i - \bar{X})^2},$$

where W is the sum over all w_{ij} , and all other symbols have the same meaning as in (2.10). GC is a measure of local aggregation and is constrained between maximum aggregation at $GC_s = 0$, and minimum aggregation at $GC_s = 2$. The expected value for a random distribution is $E(GC_s) = 1$, indicating no local correlation structure. To obtain community level metrics, the species level aggregation values are averaged over all species. In [58] the aggregation metrics were associated with stability, since higher aggregation may confer species with greater reproductive stability and reduced vulnerability to predation. However this relationship is not concrete.

Three further spatial metrics are used to characterise species *spatial ranges*. The **species range centroid** is calculated as the two-dimensional centre of mass of all individuals on the lattice. The **species range area** is calculated as the area of the circle, centred on the centroid, that contains 97% of the individuals of that species. **Species density** is then defined as the number of individuals divided by the area of the range. These three metrics are used to calculate the temporal variability of species spatial ranges, by taking the coefficient of variation in each metric (as defined in (2.5)) over the time period of interest. The coefficients of variation are averaged over all species to obtain **community level metrics for spatial variability**: *mean_CV_centroid*,

mean_CV_area, and *mean_CV_density*. These metrics provide an interesting comparison with variability in species abundance, and represent another alternative component of system stability.

2.8.4 Network metrics

The importance of the structure of the interaction network in determining the high level patterns and functions of an ecological community was discussed in section 1.2.1. A wide range of *qualitative* and *quantitative* descriptors are available to characterise the structure of the interaction network [11, 26, 44, 58]. Qualitative metrics refer to those that depend only on the presence/absence of links i.e they are used on unweighted networks. Quantitative metrics refer to those that use some measure of interaction strength i.e. a weighted network. It has been shown that the quantitative metrics are less sensitive to sampling intensity and generally more reliable than their qualitative counterparts [45, 57]. Also Tylianakis and collaborators have shown [11] that quantitative metrics may be required in order to detect the effects of habitat degradation on ecological communities (host-parasitoid networks in their study). In our analysis we use the same metrics as in [58], which are defined below.

2.8.4.1 Qualitative network descriptors

The unweighted interaction network is defined by the asymmetric adjacency matrix **a**, where element a_{ij} is 1 if there exists a trophic link from prey i to predator j , and 0 otherwise. The **connectance** is defined as:

$$C = L/S^2,$$

where L is the number of links (non-zero elements in **a**), and S is the number of species. Qualitative **generality** (G) and **vulnerability** (V) are defined as the mean number of prey per predator, and the mean number of predator per prey respectively. These are given by

$$\begin{aligned} G &= \frac{L}{N_B + N_I}, \\ V &= \frac{L}{N_I + N_T}, \end{aligned}$$

where N_B , N_I and N_T are the number of species belonging to basal, intermediate and top trophic levels respectively. **Compartmentalisation** is a measure of how frequently species share common neighbours, and is given by:

$$P = \frac{1}{S(S-1)} \sum_{i=1}^S \sum_{j \neq i} c_{ij},$$

where c_{ij} is the number of species with which both i and j interact divided by the number of species with which either i or j interact [58]. Finally **nestedness** is a measure of the extent

to which the diets of specialist species are subsets of the diets of more generalist species [58] (see figure 1.2). As discussed in section 1.2.1 this is may be an important feature of mutualistic networks. Therefore nestedness is calculated for the mutualistic sub-network only, using the *NODF* algorithm of Almeida-Neto et al. [150].

2.8.4.2 Quantitative network descriptors

The quantitative network metrics used are based on the *Shannon entropy* of link weights - analogous to the way it is used to measure diversity of species abundances. It is common practice to use interaction frequency to define link weights [11, 45, 58], in part because this is easier to measure empirically than, for example, biomass flow. We present here the standard definitions of the Shannon network metrics using the notation of Bersier et al. [44]. As previously, the natural logarithm is used for all metrics. It is necessary in what follows to define $\log(0) = 0$, which is equivalent to excluding zero elements in the interaction matrix from the calculations. Also rows or columns with sum equal to zero are removed, to avoid division by zero.

The asymmetric weighted matrix of interaction frequencies is denoted by \mathbf{b} , where element b_{ij} is the number of individuals of species i consumed by species j during the sampling period. Therefore we can define interaction diversities for the links coming into a species k from its prey, and the links going from k to its predators:

$$\begin{aligned} H_{N,k} &= -\sum_{i=1}^s \left(\frac{b_{ik}}{b_{\bullet k}} \log \left(\frac{b_{ik}}{b_{\bullet k}} \right) \right) \\ H_{P,k} &= -\sum_{j=1}^s \left(\frac{b_{kj}}{b_{k\bullet}} \log \left(\frac{b_{kj}}{b_{k\bullet}} \right) \right) \end{aligned}$$

where $H_{N,k}$ is the diversity of inflows from prey; $H_{P,k}$ is the diversity of outflows to predators; s is the total number of species; and $b_{\bullet k}$, $b_{k\bullet}$ are column and row sums giving the total number of interactions that species k has with its prey and predators respectively. The interaction diversity metrics behave just as the Shannon entropy - the higher the number of interaction partners and the more even the interaction frequencies across these partners, the higher the interaction diversities. The exponents of (2.13) and (2.14) are used to calculate the *effective number* of prey and predators respectively:

$$\begin{aligned} n_{N,k} &= \begin{cases} e^{H_{N,k}} \\ 0 \text{ if } b_{\bullet k} = 0 \end{cases} \\ n_{P,k} &= \begin{cases} e^{H_{P,k}} \\ 0 \text{ if } b_{k\bullet} = 0 \end{cases} \end{aligned}$$

where the symbols have the same meaning previously. These metrics have the property that if the interaction frequencies of species k are distributed equally amongst its interaction partners,

then the effective number of prey/predators is equal to the actual number. However, if the interaction frequencies are not equal between partners, the effective number of prey/predators is reduced, since there is some preferential interaction. These effective number of species are used to calculate **weighted quantitative generality and vulnerability**, which are defined as:

$$G_q = \sum_{k=1}^s \left(\frac{b_{\bullet k}}{b_{\bullet\bullet}} n_{N,k} \right)$$

$$V_q = \sum_{k=1}^s \left(\frac{b_{k\bullet}}{b_{\bullet\bullet}} n_{P,k} \right)$$

where $b_{\bullet\bullet}$ is the total number of interactions. So the metrics in (2.17) and (2.18) give a weighted average of the effective numbers of prey and predators respectively. They are weighted by the fraction of the total interactions the species k is involved, such that species with more interactions contribute most to the average.

We also calculate metrics for **interaction diversity** ($H2$) and **specialisation** ($H2'$). These are applied to the mutualistic sub-network only because the specialisation metric $H2'$ is implemented in *R* in the *bipartite* package [151]. (It may be possible that a multi-trophic version of the specialisation metric can be derived.) We define:

$$p_{ij} = \frac{\sum_{j=1}^S b_{ij}}{\sum_{i=1}^S \sum_{j=1}^S b_{ij}},$$

as the proportion of the total number of interactions which occur between prey i and predator j . Then the interaction diversity is given by:

$$H2 = -\sum_{i=1}^S \sum_{j=1}^S p_{ij} \log(p_{ij}),$$

which is maximal when all interactions between prey and predator have the same frequency i.e. the distribution of interaction frequencies is most even. The specialisation metric ($H2'$) is obtained by standardising $H2$ with respect to the theoretical maximum and minimum diversity:

$$H2' = \frac{H2_{max} - H2}{H2_{max} - H2_{min}},$$

where $H2_{max}$ and $H2_{min}$ are the extremes of the diversity values that can be achieved if the total number of interactions of each species is held constant. As such $H2'$ is equal to 0 and 1 for maximum generalisation and specialisation respectively. We calculate $H2'$ using the *bipartite* package in *R*.

2.8.4.3 Interaction strength metrics

A key feature of ecological communities, and a central theme of this thesis, is the strength of interactions between species. As with stability (section 2.8.2), there are numerous ways to define the strength on an interaction [46]. We have already seen that interaction frequency (b_{ij})

serves as one proxy for interaction strength. In the IBM we may expect that the frequency of an interaction will be largely determined by the abundances of the interacting species. If two species are very abundant then the individuals of these two species are more likely to encounter each other in space. However other factors may contribute. The distribution of species in space may affect how often they interact. For example two species may be abundant but highly aggregated in different regions of the landscape, and so are unable to interact. Factors such as competition and stochasticity may also influence interaction frequencies.

In addition to frequency we define an interaction strength metric IS , which for the interaction between species i and j takes the value:

$$(2.19) \quad IS_{ij} = \frac{b_{ij}}{N_i N_j},$$

and as such represents the per-capita effect of a predator, per-capita of prey. In subsequent analysis IS refers to the mean value of (2.19) over all interactions in the network. This metric is useful because it is analogous to the Lotka-Volterra interaction coefficients and their generalisation to other ODE population dynamic models [46]. In the context of the IBM simulations, IS can also be interpreted as an estimate of the encounter probability between individuals of species i and j (see discussion in section 3.4). We return to look in more detail at the quantification of species interaction strengths in chapter 6.

CHAPTER



HABITAT LOSS WITH HIGH IMMIGRATION RATE

3.1 Introduction

In this chapter we conduct a preliminary investigation of how simulated communities respond to habitat loss. Using the individual based model (IBM) defined in section 2.4 we study the response of communities with *varying levels of mutualism* (MAI ratio) to the destruction of different percentages of the landscape. As discussed in section 1.2, a solid theoretical understanding of communities comprising multiple types of interaction is lacking. Studies in this area are relatively few and recent [9, 10, 40, 41, 43, 152], compared with studies of single interaction communities, ~~and have yet to address the response of hybrid-communities to habitat loss which have been ongoing for several decades~~. Therefore the inclusion of both mutualistic and antagonistic interactions in the model represents a key novel feature of this investigation.

To destroy habitat we use the two algorithms described in section 2.5. Therefore there are two habitat loss (HL) scenarios to study, which we refer to as the *random* and *contiguous* scenarios according the way in which habitat is destroyed. As we saw in section 1.3.1 numerous studies have found that the spatial pattern of habitat destruction plays an important role in determining the effect on the community or meta-community (for example [12, 68, 73]). The two HL scenarios represent two extremes of the way in which a natural habitat may be destroyed, ranging from almost complete spatial auto-correlation to complete randomness. Therefore we are able to study the differences between community responses at these two extremes, and ~~draw~~ comparisons with the results of previous studies.

To determine the effect of HL on the simulated communities we employ the suite of metrics defined in section 2.8, and study how they change along the gradient of increasing HL. These metrics capture aspects of diversity, stability, spatial organisation, and properties of the network

of interactions between species. We predict that both diversity and stability will be negatively impacted by HL, and that as the level of destruction increases beyond a threshold of destruction some species will become extinct from the landscape. Based on the findings of previous HL studies (discussed in section 1.3) we also expect that random HL will impact communities more than contiguous HL, at least in terms of the number of extinctions. However, following the work of Tylianakis et al. [11], we may also expect to see underlying changes in the community structure and network properties prior to the loss of any species from the landscape. This region of the HL gradient, prior to species extinctions, will be of particular interest since such underlying changes are not well understood, and may not be detected by conventional studies and metrics (see section 1.3 for more discussion on this). Therefore we expect changes in network properties, which will be detectable in particular by the quantitative metrics introduced in section 2.8.4.2. Based on the literature cited in section 1.3 we predict that the mutualistic sub-network will be pushed towards lower nestedness and higher modularity, and also expect a whole-network reduction in modularity and increase in interaction strengths. The literature also suggests that habitat loss should destabilise community dynamics, and we hope to explain changes in both stability and network properties in terms of low level mechanisms. The role of MAI ratio in mediating the effects of HL is also of interest. Based on the findings of Lurgi et al. [58], which used the same IBM, we may expect communities with high MAI ratio to be more robust to HL. In their paper it was shown that communities with higher MAI ratio tended have weaker stronger interactions and be more highly aggregated in space, and were also suggested to be more stable (see section 2.2). We hypothesise here that mutualism may confer stability in the face of habitat loss by improving the reproductive success of basal species, making more energy available to species in higher trophic levels. If this hypothesis holds we may also expect to see dominance of mutualistic plants and animals over their antagonistic counterparts.

3.2 Methods

Here we outline the experimental procedure used to generate the results presented in section 3.3 below. Full details of the methodology are given in chapter 2, including the analysis metrics which are defined in section 2.8.

3.2.1 Simulation procedure

For this chapter we ran two ensembles of simulations using the IBM model. One ensemble employed the random habitat loss algorithm, and the other employed the contiguous algorithm. In both ensembles the level of habitat loss (HL) is varied between 0% and 90% in steps of 10%. At each value of HL there are 25 repeat simulations at each of the 11 MAI ratios ($MAI = [0.0, 0.1, \dots, 0.9, 1.0]$). Therefore there are a total of 2750 ($= 25 \times 11 \times 10$) simulations in each ensemble. Each simulation uses a unique interaction network, generated using the method

described in section 2.3. Each ensemble contains the same simulations at $HL = 0\%$, since no habitat is destroyed and all else is held constant between HL scenarios. All model parameters take the *default values* as given in table 2.1 and published in [58]. The model, implemented in *Python* [137], was simulated on the Blue Crystal computer cluster [139] (details in section 2.6).

3.2.2 Sampling and analysis

To calculate the analysis metrics from the simulation output we follow the precedent set in [58]. Metrics based only on species abundances are calculated from a ‘snapshot’ of the simulation state on the final time step. Other metrics (for example temporal variability and network metrics) are calculated from samples aggregated over the final 200 time steps of the simulation. For such metrics we use the mean species abundance over the 200 time steps, where a measure of abundance is required. The *realised network* of interactions is constructed by counting the total number of interaction events between each pair of species during the 200 time steps. The use of snapshots and short time windows taken from the end of the simulations assumes that the system has reached steady state by then. For now we make this assumption, but return to assess its validity and consequences in chapter 4.

Throughout the analysis we look for robust changes of the metrics evaluated in response to HL. Therefore, as in [58], we fit linear models to identify *statistically significant* trends in the response variables, and where necessary we log-transform the data to attempt to linearise the response (see for example figure 3.16). The linear models are fitted using the *ordinary least squares* method of the *statsmodels* package in *Python*. The *p-value* of the *f-statistic* of the fits are given, which is a significance value for the test of the null hypothesis that the slope of the linear trend is equal to zero. Therefore a low *p-value* is evidence to reject the null hypothesis and conclude that the slope of the trend is non-zero. Different levels of significance are indicated in the plots throughout this chapter. However we always follow the convention that *p-values* < 0.05 are statistically significant, whilst $0.05 < p < 0.1$ indicates marginal significance. When fitting linear models the *p-value* of the *f-statistic* may be used to test for significance. In this case the null hypothesis is that the true slope of the linear trend is equal to zero. The *p-value* gives the probability of the observed trend arising by chance, from a random set of data. Therefore a low *p-value* indicates that the observed trend is unlikely to have arisen by chance, and therefore represents evidence to reject the null hypothesis. However, there are certain issues with this interpretation of *p-values* that mean they must be treated with caution, especially in computational studies such as this.

One issue is related to the *statistical power* of the test. Broadly, if a large sample size is used the test has high statistical power and can therefore detect small effects. However, it can be shown that, as sample size becomes large, *p-values* necessarily tend to zero regardless of the presence of an actual trend in the data [153, 154]. Computational studies are easily able to produce large numbers of replicates. Therefore there is a potential danger for such studies

to conclude that small or non-existent trends are statistically significant. Various authors have raised this spurious trend detection as a concern in computational experiments when sample sizes are on the order of 1000 and above [153–156]. For the linear regression modelling throughout this thesis we use sample sizes of 250 (25 replicates for each of the 10 levels of habitat loss). We argue that this number is sufficiently small that p-values are still meaningful. However, it is also sufficiently large that we should not be surprised to obtain low p-values even when the size of the trend appears small. In acknowledgement of this issue we use a high confidence threshold when interpreting results. Such an approach is advocated by Greene when using large samples [157], although he does not provide a scaling rule between confidence threshold and number of samples. We choose to use 99% confidence, such that a *p-value* must be less than 0.01 before we accept evidence for the existence of a robust trend.

A second issue with linear modelling in this context relates to the number of tests conducted. When testing trend significance at the 99% confidence threshold one expects a *type I error* rate of 1%. That is, on average one out of a hundred tests on data with no trend will give sufficient evidence to reject the null hypothesis. In the analysis presented in section 3.3 (and in subsequent chapters), a large number of response metrics are tested for trends. Therefore we must acknowledge the possibility of *type I error* in our results. The consequences of such errors are mitigated by three factors. Firstly, the high confidence threshold reduces the type I error rate. Secondly, the response metrics tested are all metrics which we have prior reason to believe will change under habitat loss (see sections ?? and ??). Thirdly, for all trends detected as significant, we do not blindly accept the result. All response trends are discussed in the context of the literature, and attempts are made to explain the observed trends in terms of the low level mechanics of the model (see for example section ??).

3.3 Results

We find that simulated communities respond differently under the two HL scenarios. Therefore throughout this section we draw comparisons between the results for *random* and *contiguous* HL, and seek to understand the differences. In general we find that there is little qualitative difference in the results for communities with different MAI ratios. Certain quantitative differences, reported in [58], hold true across the HL gradients. For example high MAI communities are more aggregated in space, have more biomass in the lower trophic levels, and support a greater total number of individuals. Despite these quantitative differences, we find that communities with different MAI ratios respond in qualitatively the same way to both types of HL. Therefore, to simplify matters, we present results for three MAI ratios only ($MAI = 0.0, 0.5, 1.0$). In general we refer only to qualitative trends in the response metrics which hold true across MAI ratios, but make it clear where this is not the case.

For clarity we separate the results into subsections according the type of metric analysed:

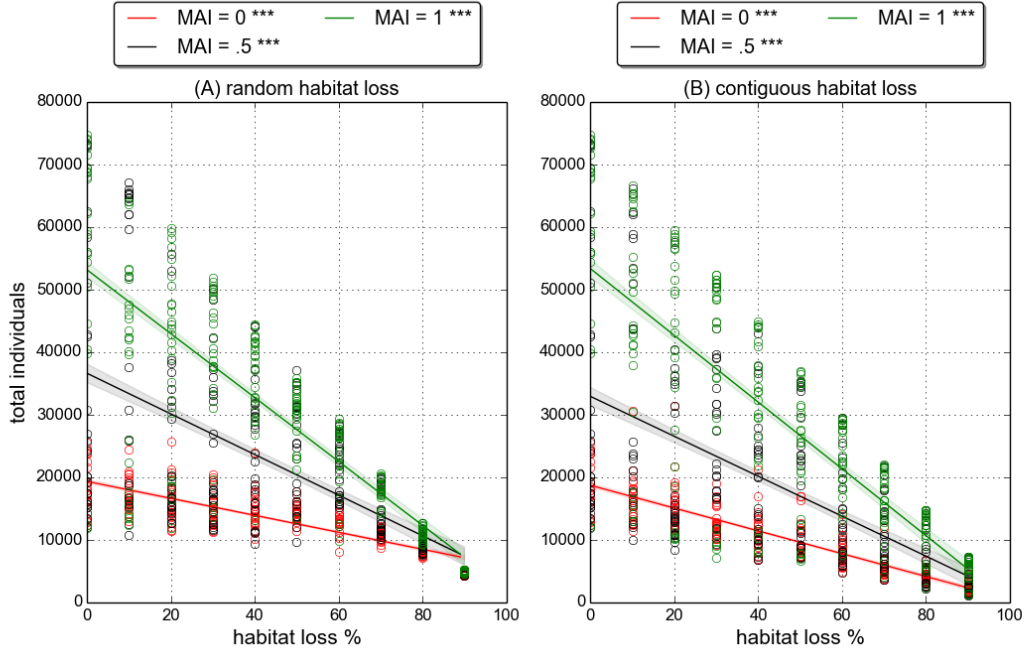


Figure 3.1: Total number of individuals against percentage habitat loss, for both scenarios: (A) Random HL, and (B) Contiguous HL. Circles represent the number of individuals for a single community; lines represent a linear fit to the data and the shaded regions indicate the standard error of the mean. p -value < 0.001 for all linear model fits (indicated by ***).

Diversity (section 3.3.1); *Network properties* (section 3.3.2); *Stability and space* (section 3.3.3); and *Invariability* (section 3.3.4). In general we find significant changes in the metrics associated with diversity, stability and space, whereas we find fewer significant changes in network properties.

3.3.1 Diversity

Figure 3.1 shows that the total number of individuals decreases in response to HL, in both the random and contiguous scenarios. This is expected because there are fewer available cells, so the landscape is able to support fewer individuals. The linear fits to the data suggest that the average number of individuals is similar at each point in the HL gradient in the two HL scenarios. Therefore there is little to distinguish between the two scenarios based on the number of individuals. The figure also shows that communities with higher MAI ratio support more individuals than those with lower MAI ratio, as was previously reported [58].

Despite the decrease in the total number of individuals, species do not go extinct (results not shown). At 90% HL, when averaged over all MAI ratios and replicates, we observed a mean of 0.0 and 0.23 species extinctions per community for random and contiguous HL respectively. Therefore we effectively see *no change in species richness* in response to habitat loss. The lack

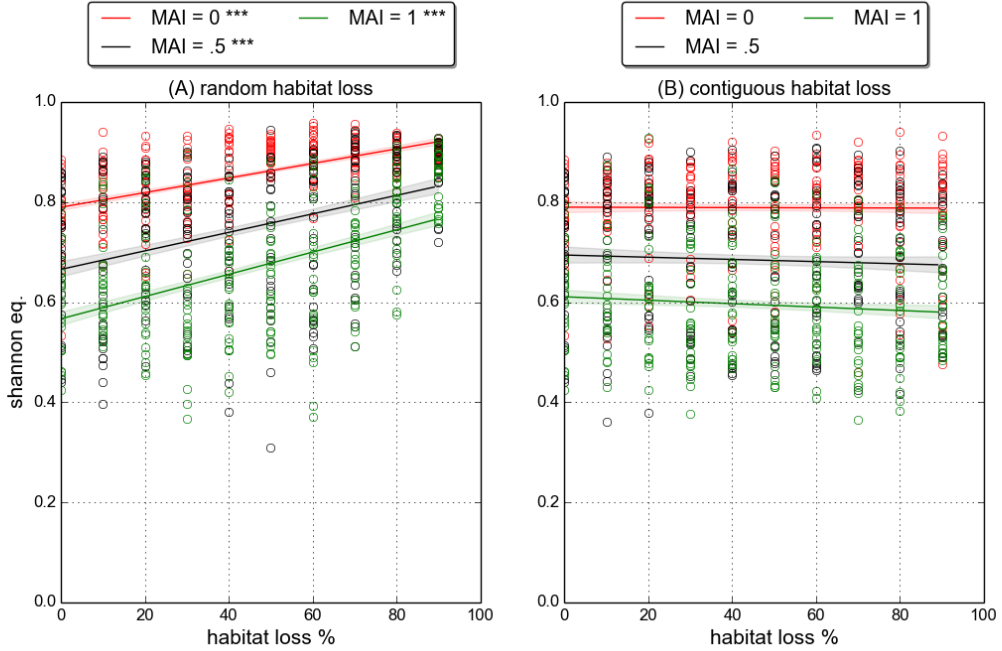


Figure 3.2: **Shannon equitability** against percentage habitat loss, for both scenarios: (A) Random HL, and (B) Contiguous HL. Circles represent the Shannon index value for a single community; lines represent a linear fit to the data and the shaded regions indicate the standard error of the mean. *** indicates p -value < 0.001 for linear model fit, whilst no marker indicates p -value > 0.1 .

of extinctions is due to a relatively high immigration rate (IR). The IR can be thought of as the probability per time step that an empty cell receives an immigrant (see section 2.4.1). Therefore at the default value ($IR = 0.005$), if the landscape were empty, we would expect on each time step an average of 200 ($= 0.005 \times 200 \times 200$) immigrant individuals drawn uniformly at random from the pool of 60 species. Therefore species can recover from extinction via a *rescue effect* that is common to all species. The immigration mechanism also allows for the maintenance of very low species abundances, which are sustained by immigration rather than feeding and reproduction. The absence of extinctions means that all changes observed across the HL gradient are not associated with changes in species richness. Therefore all of the results presented in this chapter represent the sort of underlying structural changes reported by Tylianakis et al. [11].

So, although there is no change in species richness under either HL scenario, there are changes in community structure. Figure 3.2 shows that the *Shannon equitability* (equation (2.2)) increases for random HL, but does not change significantly for contiguous HL. Figure 3.3 shows that the same trends hold when the Shannon equitability is calculated separately for each trophic level. Since there is no change in species richness we can interpret this metric in terms of both diversity and evenness. Therefore random HL seem to make communities more diverse by

3.3. RESULTS

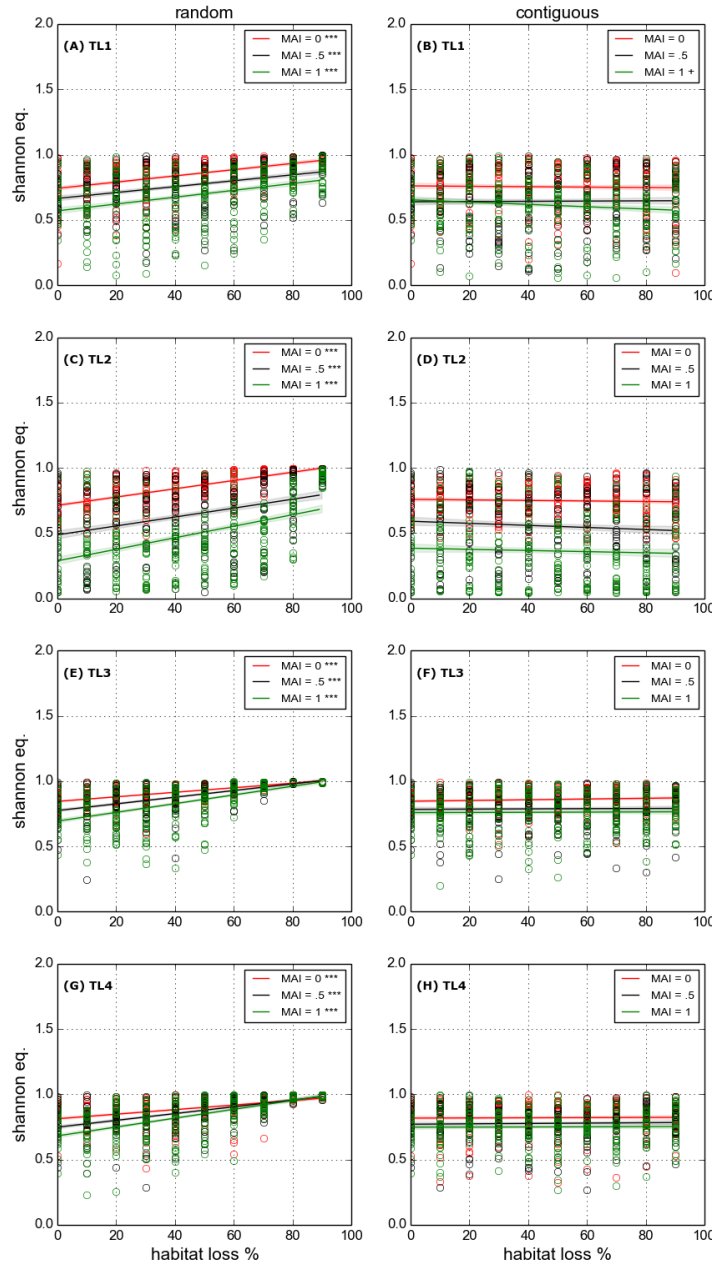


Figure 3.3: Shannon equitability against percentage habitat loss, for each trophic level. Left column: random HL. Right column: contiguous HL. Circles represent the Shannon index value for a single community; lines represent a linear fit to the data and the shaded regions indicate the standard error of the mean. *** indicates $p\text{-value} < 0.001$ for linear model fit, + indicates $p\text{-value} < 0.1$, and no marker indicates $p\text{-value} > 0.1$.

increasing the evenness in the distribution of species abundances. On the other hand, contiguous HL appears to have no significant affect on the diversity or evenness of species abundances.

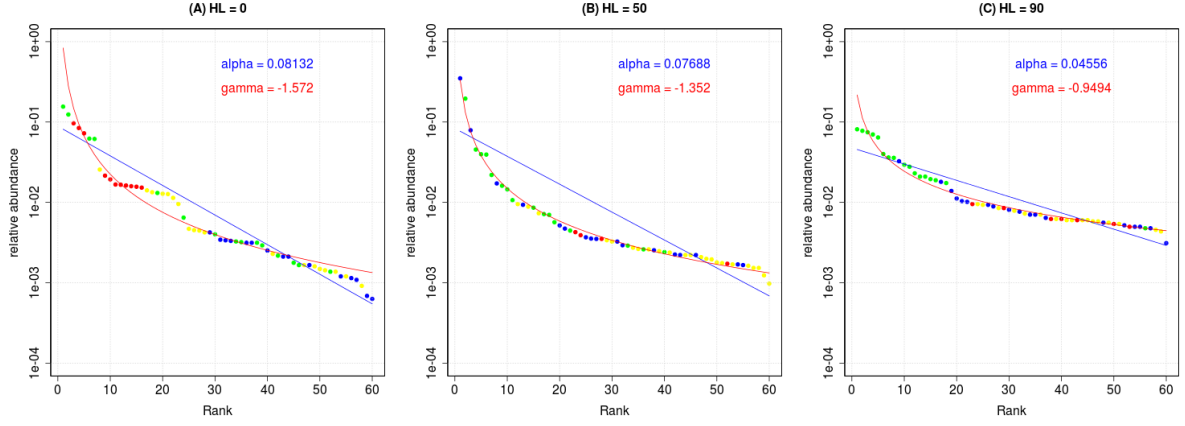


Figure 3.4: **Example rank abundance distributions (RADs)** for three communities with **MAI=0.5** at different levels of **random HL**: (A) HL= 0%; (B) HL= 50%; (C) 90%. Species abundances are relative to the total number of individuals in the community, and plotted on a logarithmic scale. Points represent species, coloured according to trophic level: green=basal; blue=herbivore/animal-mutualist; yellow=primary predator; red=top predator. Blue and red lines give the pre-emption and Zipf model fits respectively (see text in section 2.8.1.1 for definitions), best fit parameter value for each model given as annotations on plot.

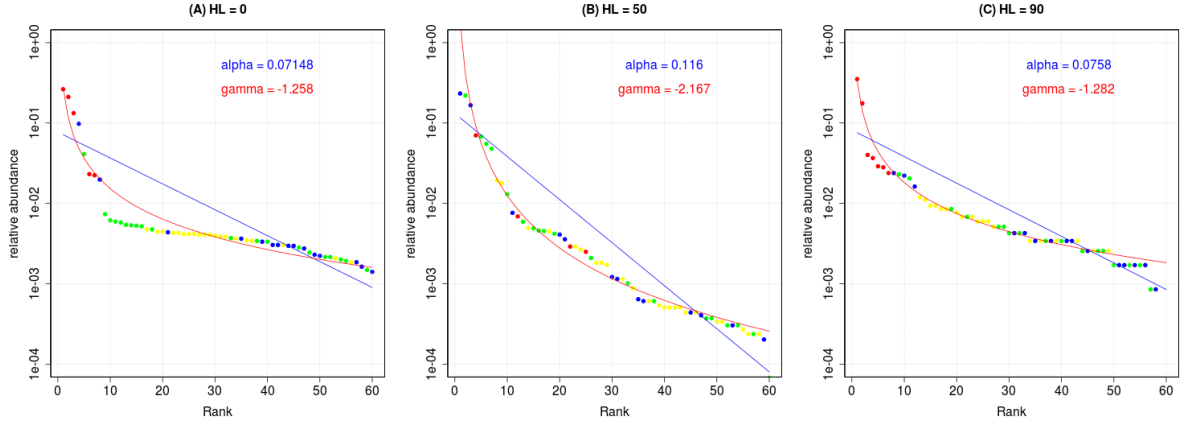


Figure 3.5: Similar to figure 3.4 but for **contiguous HL**.

To look explicitly at changes in evenness we construct *rank abundance distributions* (RADs) for each community, and fit standard models to these distributions (defined in section 2.8.1.1). Figures 3.4 and 3.5 show example RADs for three communities at different levels of HL, all with MAI= 0.5 (qualitatively the RADs and how they change under HL are similar across all MAI ratios). Since these plots are for single communities we cannot draw general conclusions from

3.3. RESULTS

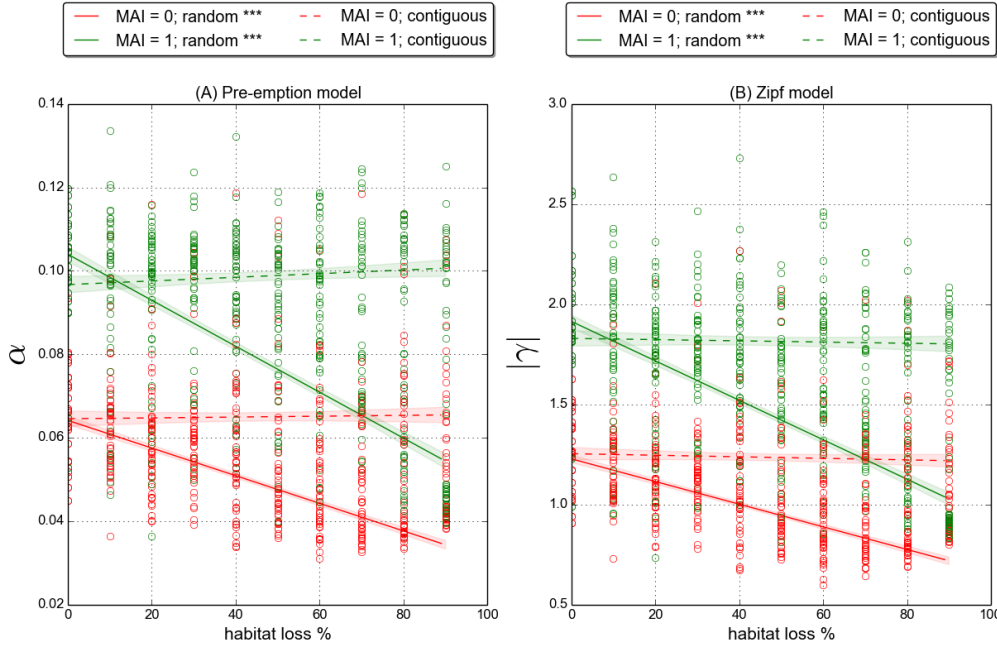


Figure 3.6: **Rank abundance model fit** parameters against HL. Panel A: Pre-emption model parameter α is smaller for more even distributions. Panel B: Absolute value of Zipf model parameter $|\gamma|$ is smaller for more even distributions. (See model definitions in section 2.8.1.1). Solid lines represent linear fits to the random HL data, dashed lines indicate linear fits to the contiguous HL data, and error bars give ± 1 standard-deviation. *** indicates p -value < 0.001 for linear model fit, whilst no marker indicates p -value > 0.1 .

them. However, they serve to visualise the model fits and their interpretation. The solid blue and red lines in these plots show the *preemption* and *Zipf* model fits, respectively. Each model has an evenness parameter and, as discussed in section 2.8.1.1, the lower the magnitude of the parameter the more even the distribution. From visual inspection panel C in figure 3.4 is the most even RAD of the six displayed. Correspondingly the model fits to this RADs have the lowest magnitude values for α and γ . Although the Zipf model appears to give a qualitatively better fits to the data, we use both models the test for evenness in our simulated communities. In this way we can check for consistency in the conclusions.

Figure 3.6 uses all replicates at a given MAI ratio to show how the evenness parameters, α and γ , change in response to HL. For clarity the results are shown for two MAI ratios only (0.0, 1.0), but are consistent across all MAI ratios. The modelling suggests that under contiguous HL the RADS show no significant change in evenness. However both the preemption and Zipf models indicate that communities under random HL show a significant increase in evenness. These findings are consistent with the changes in Shannon diversity discussed above.

The RADs in figure 3.4 suggest another trend in response to random HL - there appears to be

a systematic shift in the relative abundances according to trophic level. This is most visible for the basal and top trophic levels, shown in green and red respectively. For the example communities shown, the top predator species have high relative abundance in pristine landscape (panel A), but reduced abundances in damaged landscapes (panels B and C). At 90% HL all top predators in the depicted community have a relative abundance of less than 0.01. On the other hand basal species have a wide range of relative abundances in pristine landscape, but come to dominate the community at 90% HL with all but one basal species in the top 18 ranks. This is consistent with empirical observations, since species in higher trophic levels tend to be more sensitive to perturbations [76, 80]. To investigate this effect further we look at the relative abundances of all six functional groups in response to habitat loss. These are plotted in figures 3.7 and 3.8 for the random and contiguous scenarios respectively. For the contiguous scenario community structure is remarkably constant across the habitat loss gradient, according to the relative abundances of the functional groups. The only statistically significant changes are in the non-mutualistic plant and top predator species at MAI= 0, where there is a slight decrease in top predator abundance relative to plant abundance (figure 3.8, panels A and F). In the random scenario there are clear systematic shifts in the distribution of abundance across the functional groups (figure 3.7). In particular, and in agreement with the RADs in figure 3.4, there is a relative increase in plant abundance and decrease in top predator abundance, which is statistically significant across all MAI ratios. There is also a slight decrease in the relative abundance of species in the second trophic level (panels C and D). Overall there is a shift in relative abundance towards the basal level, but interestingly there is no significant change in the abundance of primary predator species (panel E). This suggests that there is some benefit to being a primary predator in this context (see discussion in 3.4).

3.3. RESULTS

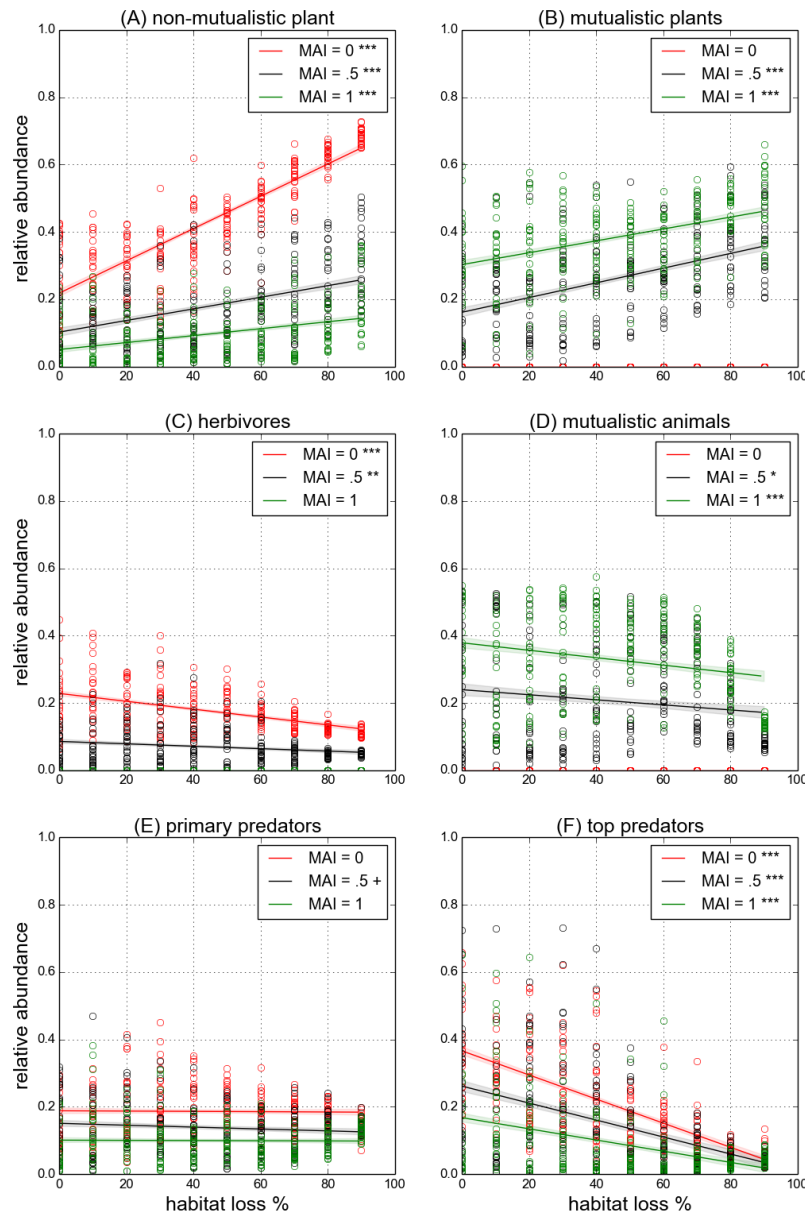


Figure 3.7: Relative abundance by functional group for random HL. Abundance relative to total number of individuals in the community. Circles represent the value for a single community; lines represent a linear fit to the data and the shaded regions indicate the standard error of the mean. The markers ***, **, *, + correspond to linear model fit p-values of < 0.001, < 0.01, < 0.05 and < 0.1 (marginal significance) respectively.

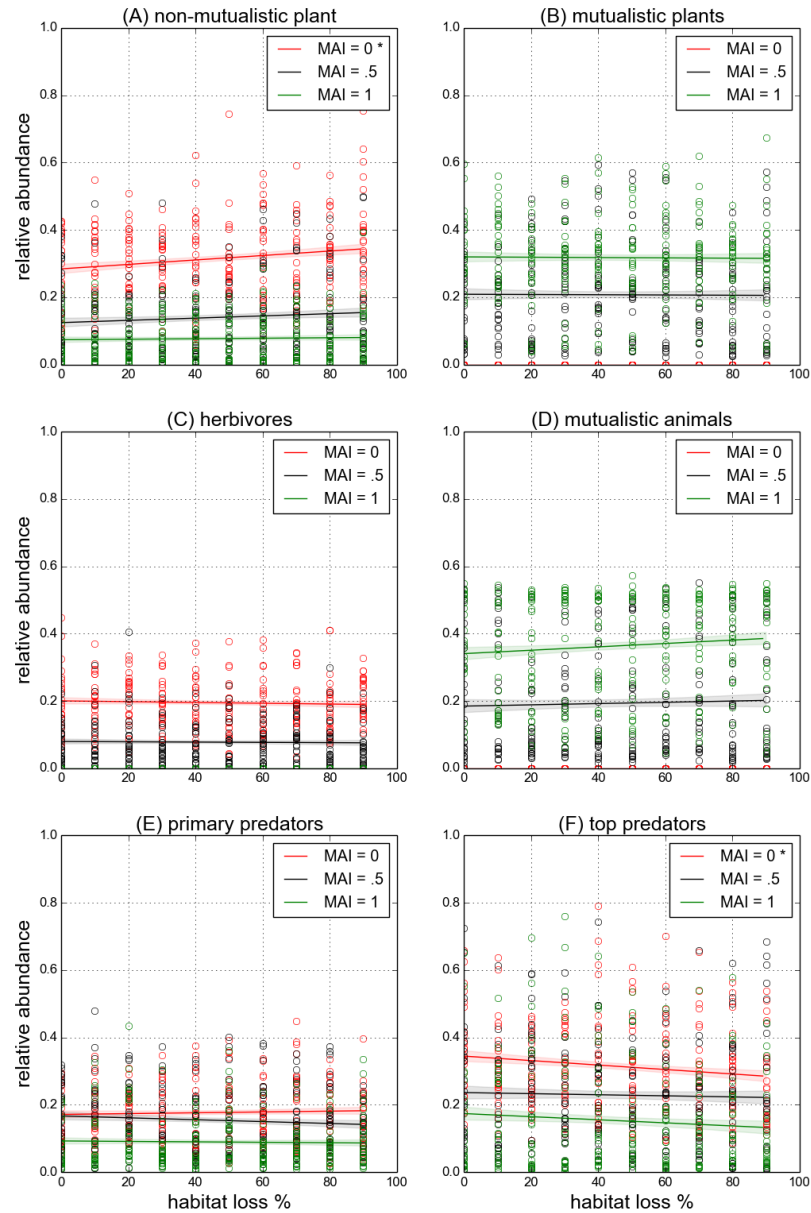


Figure 3.8: Similar to figure 3.7, but for **contiguous HL**.

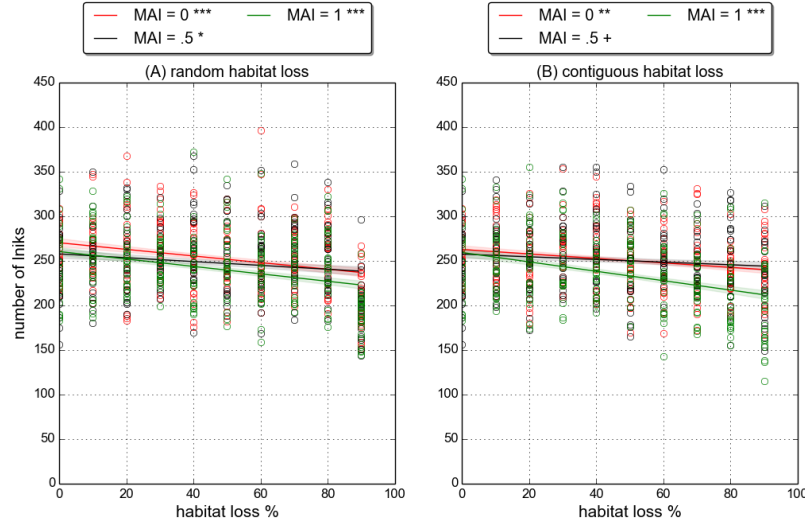


Figure 3.9: **Number of links** of links in the realised network (see text in section 3.2.2 for definition). Linear fits and p-value markers as in previous plots (see caption of figure 3.7).

3.3.2 Network properties

Figure 3.9 shows that, in both HL scenarios, there is a slight decrease in the number of links in the realised network. This result indicates that some species, which would be able to interact, do not encounter each other in space as a result of HL. The number of links lost, on average is few - the greatest loss according to the linear models is under contiguous HL for MAI= 1.0 where the number of links falls from ≈ 250 in pristine landscape to ≈ 200 at $HL = 90\%$. However loosing any number of links is enough to create changes in network topology that can be detected by the qualitative network metrics (section 2.8.4.1). In addition to the loss of links, figure 3.10 show that there is a decrease in the total number of interactions in both scenarios. This overall decrease in the frequency of interactions is not a surprising result of HL. As we argued in section 2.8.4.3, interaction frequencies are largely determined by the abundances of the interacting species. So when there are fewer individuals in the landscape (figure 3.1) we should expect fewer interactions. However it appears from figure 3.10 that more interactions are lost due to random HL than contiguous. For example at $HL = 70\%$ all communities in the random scenario have fewer than 50,000 interactions in total, whereas at the same level of contiguous destruction many communities have more than 50,000 interaction and several even exceed 100,000. Also the slopes of the linear fits in panel A are steeper than in panel B. These results suggest a mechanism that produces fewer interactions under random HL than under contiguous, despite similar numbers of individuals. We propose such a mechanism in section 3.4.

Together the loss of links, and the change in interaction frequencies indicate changes in realised network of interactions. Therefore we seek to characterise these changes, using the net-

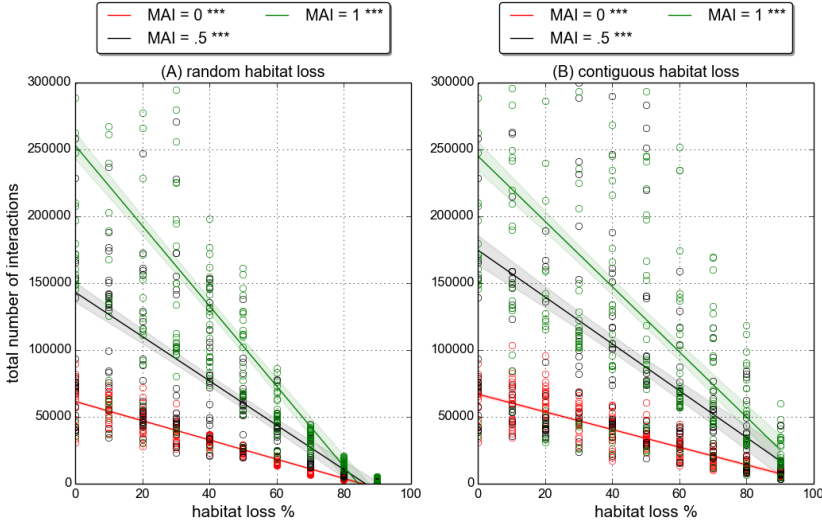


Figure 3.10: **Total number of interactions** between all species during final 200 time steps of a simulation. Linear fits and p-value markers as in previous plots (see caption of figure 3.7).

work metrics defined in section 2.8.4. The nestedness and compartmentalisation of communities showed no significant change under either HL scenario. Therefore these plots are not shown. The response of connectance, and qualitative generality and vulnerability, follows directly from the loss of links since there is no change in species richness. Therefore connectance, generality and vulnerability all decrease in both scenarios, as a direct result of the loss of links shown in figure 3.9 (results not shown). The response of the quantitative network metrics is more subtle because these metrics are based not only on the presence/absence of links, but on the frequency of each interaction.

The results for the weighted quantitative generality and vulnerability metrics (hereafter referred to as generality and vulnerability) are shown in figures 3.11 and 3.12. For contiguous HL neither metric shows significant change. This tells us that the loss of links and decrease in interaction frequencies occur in a such a way that the *average number of effective prey and predators* (equations (2.15) and (2.16)) per species is constant across the contiguous HL gradient. For this to occur the changes must be distributed homogeneously across the network such that there is no change, on average, in the number of interactions per species and the relative frequencies of those interactions. This finding relates to the previous observation that diversity and rank-abundance patterns do not change under contiguous HL (section 3.3.1). If the relative abundance of all species is constant across the HL gradient, and interaction frequencies are mainly driven by species absolute abundances, then the lack of change in quantitative network metrics follows directly. This appears to support the conclusion that interaction frequencies are driven by species abundance patterns.

In the random scenario generality and vulnerability decrease and increase respectively (fig-

3.3. RESULTS

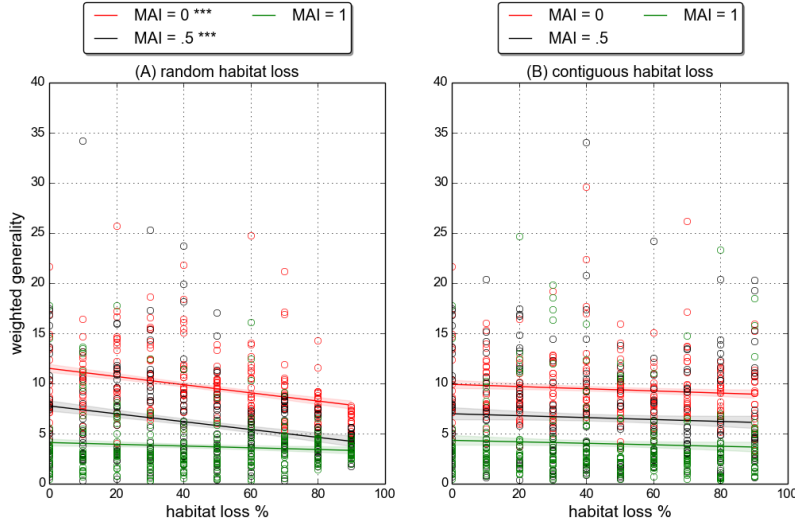


Figure 3.11: **Weighted quantitative generality**, of whole network (see section 2.8.4 for definition). Linear fits and p-value markers as in previous plots (see caption of figure 3.7).

ures 3.11 and 3.12). This represents an asymmetry between the responses of predator interactions compared to prey interactions. The increase in vulnerability means that the average *effective* number of predators per prey increases. It is unlikely that the *actual* number of predators per prey increases, since links are lost from the network. Therefore the only way that vulnerability could increase is if the interaction frequencies of prey with their predators became more even. We know from section 3.3.1 that species abundances become more even in response to random HL, and that diversity increases both at the community level and within functional groups. Therefore the change in vulnerability appears to be explained by the increased evenness of prey and predator species, leading to more even interaction frequencies between the two.

The decrease in generality, shown in figure 3.11(A), tells us that the average *effective* number of prey per predator decreases under random HL. Since we have just concluded that interaction frequencies must become more even, we must attribute this to a decrease in the *actual number of prey* per predator. Since we know that the relative abundance of top predators is greatly reduced (figure 3.7), it is reasonable to conclude that some struggle to find prey. Interestingly the change in generality at MAI = 1.0 is not significant (although it was significant at all ten other MAI ratios) suggesting that either prey are not lost, or more likely that the loss of prey to top predators is offset by the increased evenness of interactions. We know that high MAI communities have fewer individuals in the top trophic level (figures 3.7 and 3.8) and so the top predator contribution to generality is likely to be lower. Also high MAI communities contain more individuals than low MAI communities across the HL gradient, meaning a greater absolute number of prey. Together these two mechanisms explain why generality does not change significantly at MAI = 1.0.

The results for the bipartite network metrics, interaction diversity and H2', are shown in

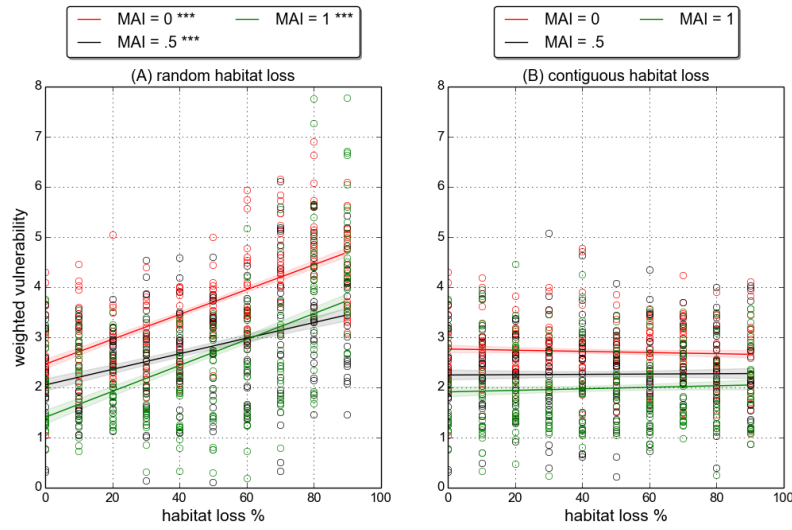


Figure 3.12: **Weighted quantitative vulnerability**, of the whole network (see section 2.8.4 for definition). Linear fits and p-value markers as in previous plots (see caption of figure 3.7).

figures 3.13 and 3.14. They support the conclusion that the changes in quantitative network metrics are driven by changes in species relative abundances. In the contiguous scenario neither metric shows significant change, in agreement with the generality and vulnerability results. In the random scenario interaction diversity increases, whereas the specialisation metric $H2'$ shows no significant change. The increase in interaction diversity means that the interactions frequencies between plant and animal mutualists become more even. Again we assert that this is due to the observed increase in evenness of species relative abundances in these two groups (figure 3.3).

The fact that $H2'$ does not change significantly means that interactions in the mutualistic sub-network become neither more even nor less diverse relative to the minimum and maximum interaction diversity, $H2_{min}$ and $H2_{max}$ (see definition in section 2.8.4). $H2_{min}$ and $H2_{max}$ are theoretical values calculated with the constraint that the total number of interactions of each species is fixed. If we assume, as we have argued, that the interaction frequencies are determined by species abundances, then the constraint is equivalent to holding all species abundances constant. The $H2'$ result then implies that interactions do not become more diverse than expected, given the abundance of each species. In other words, the change in the diversity of interactions is due to changes in species relative abundances.

3.3. RESULTS

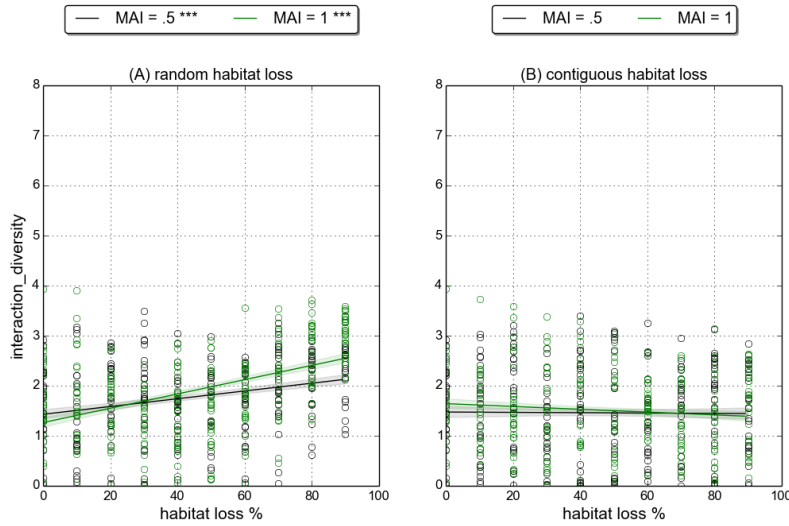


Figure 3.13: **Interaction diversity** in the mutualistic sub-network (see section 2.8.4 for definition). Linear fits and p-value markers as in previous plots (see caption of figure 3.7).

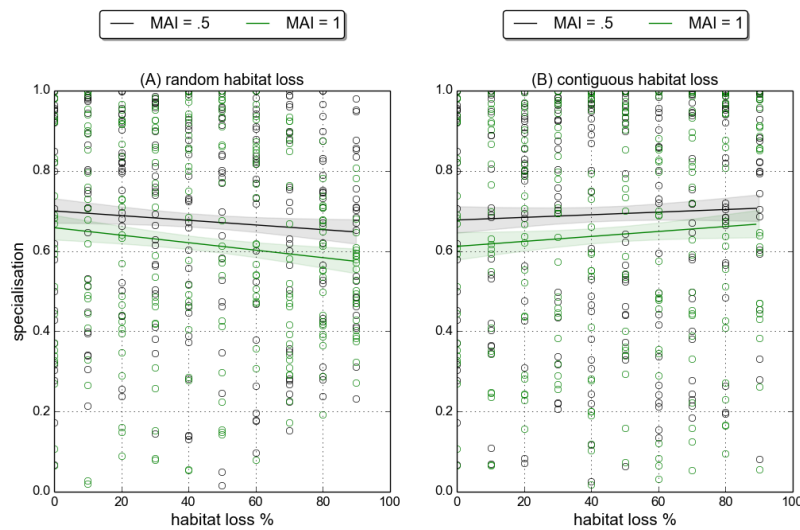


Figure 3.14: **Specialisation H2'** in the mutualistic sub-network (see section 2.8.4 for definition). Linear fits and p-value markers as in previous plots (see caption of figure 3.7).

3.3.3 Stability and spatial metrics

In this section we measure temporal stability using four metrics for temporal and spatial variability defined in sections 2.8.2 and 2.8.3: the temporal coefficients of variation (CV) in species abundances (*mean CV*), species range area (*mean CV area*), species range centroid (*mean CV centroid*), and species spatial density (*mean CV density*). At the end of the section we also look at the spatial aggregation metrics, as defined in section 2.8.3. All metrics are calculated at the species level, and then averaged over all species in the community. In the following section (3.3.4) we show that the stability results are consistent with the alternative *invariability* metrics, which are defined in section 2.8.2.1.

The stability results are consistent across the four variability metrics - *communities become more variable under random HL, and less variable under contiguous HL*. The raw data for these metrics show trends that are clearly non-linear, and appear approximately exponential (responses change at an increasing rate). Therefore we log-transform the data prior to fitting linear models. The log-linear trends are illustrated for species area variability in figure 3.15, and for species abundance variability in the middle row of figure 3.16. The same trends are observed for the other two variability metrics (results not shown), and they are statistically significant across all MAI ratios. Therefore we conclude that the aforementioned variability responses are robust. The variability response also represents a striking difference between the two HL scenarios. In all other metrics presented communities either respond in the same way (e.g. number of

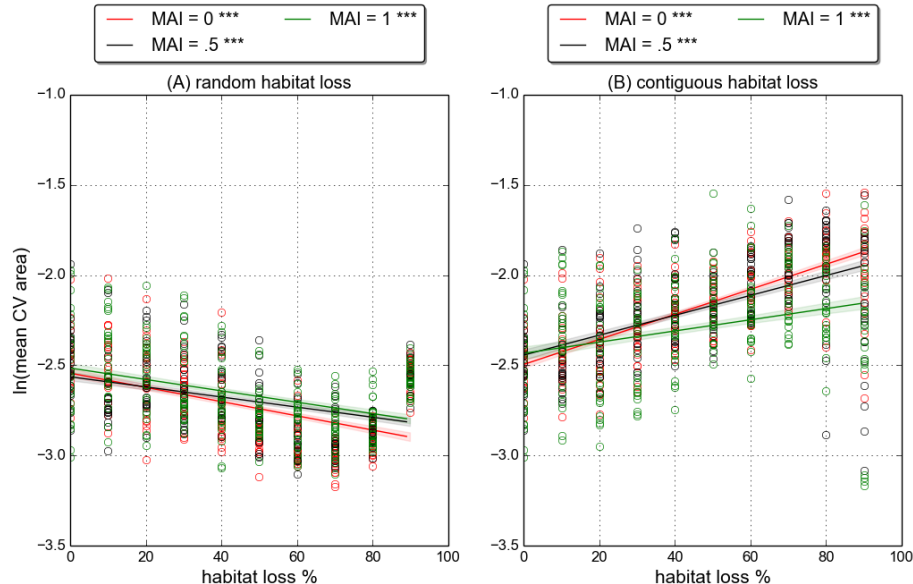


Figure 3.15: Species area variability: coefficient of variation in area of species range, averaged over all species (definition in section 2.8.2). Linear fits and p-value markers as in previous plots (see caption of figure 3.7).

3.3. RESULTS

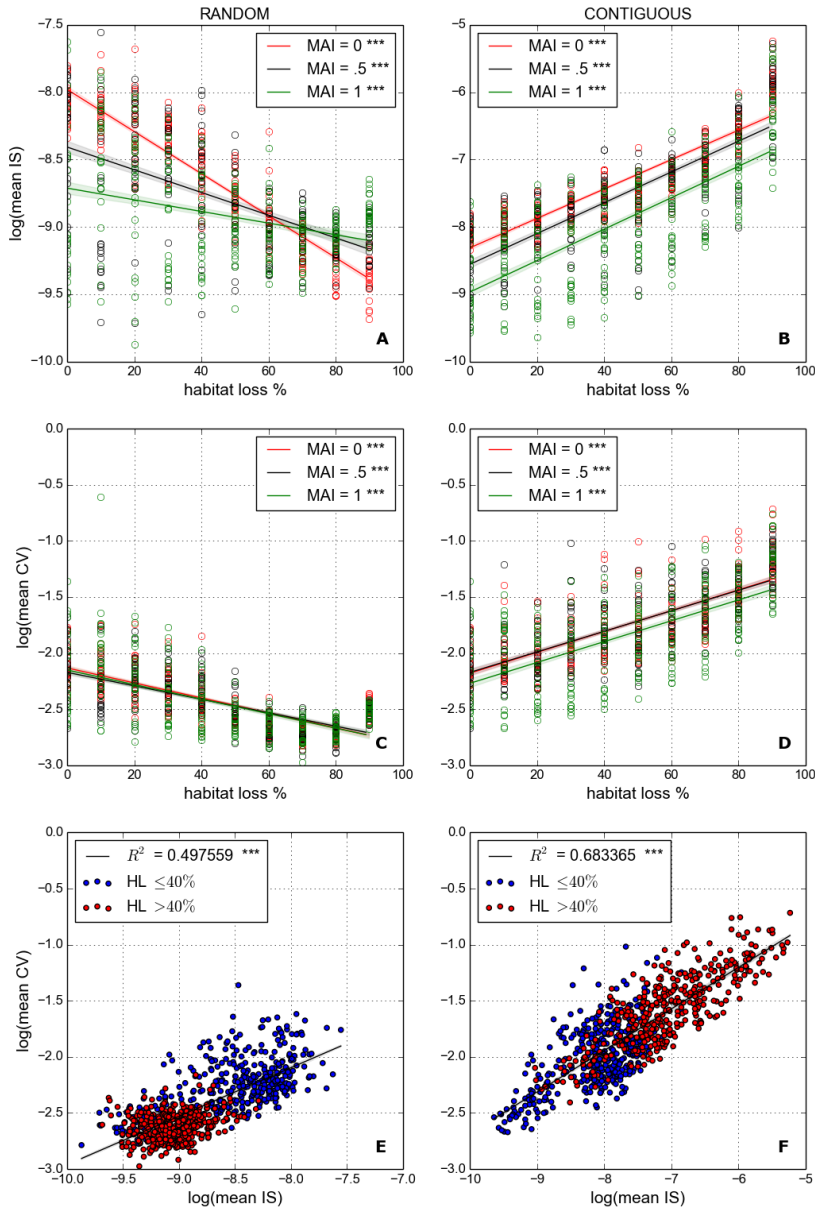


Figure 3.16: Interaction strengths and temporal variability. Both natural log-transformed to linearise trends. Panels A-B: Interaction strength metric IS (defined in section 2.8.2) averaged over all interactions in realised network. Panels C-D: mean CV, coefficient of variation in species abundances (defined in section 2.8.2) averaged over all species. Panels E-F: IS as a linear predictor for mean CV, with low and high HL communities indicated by blue and red circle respectively. All communities for MAI= 0.0, 0.5, 1.0 shown. Linear fits and p-value markers as in previous plots (see caption of figure 3.7).

individuals, number of links), or display significant changes under one scenario but not the other (e.g. population evenness). However the trends observed in variability are qualitatively opposite for the two HL scenarios. This leads us to question the mechanism behind the changes in variability.

The only metric, aside from variability, which shows trends in opposite directions under different types of HL is *interaction strength* (IS). These trends are illustrated in the top row of figure 3.16, where we again use the natural log-transform of the data. Under random HL the average interaction strength decreases, whereas under contiguous HL it increases. We also observe a dependence of interaction strength on MAI ratio, as reported in [58]. In pristine landscape higher MAI communities have weaker interaction strengths. Under contiguous HL this ordering of IS according to MAI is conserved across the HL gradient. However under random habitat loss communities with a high MAI ratio do not lose interaction strength as much as low MAI communities. The result is that beyond about 70% HL high MAI communities tend to have greater interaction strength than low MAI communities. Although only shown for three MAI ratios, the pattern described is consistent across all eleven MAI ratios. The possible explanations for the dependence of the IS response on MAI ratio are discussed in section 3.5.

The bottom row (panels E and F) of figure 3.16 shows the log-transformed values of IS plotted against the log-transformed abundance variability (mean_CV). These figures show of all the simulation repeats with MAI= 0.0, 0.5, 1.0. In both the random and the contiguous scenario there is a significant linear trend between the log-transformed interaction strength and variability. The coefficient of determination R^2 values of these linear models are, as given on the plot, ≈ 0.5 and ≈ 0.7 in the random and contiguous cases respectively. This means that, on aggregate, interaction strengths can explain at least half of the variance in temporal variability, and more than this in the contiguous case. The dependence on habitat loss is also striking. In the random case, high HL ($> 40\%$) shifts communities towards lower IS and lower variability, whilst the converse is true for the contiguous case. In both cases the linear relationship between IS and variability is consistent at low and high HL. Therefore we conclude that there is a strong correlation between IS and temporal variability, which is mediated by habitat loss. In section 3.4 we present the evidence that this correlation represents *is* a causal relationship, and that *interaction strengths are key to understanding how simulated communities respond to HL*.

We observe changes in spatial aggregation under random HL, but not under contiguous HL. Spatial aggregation is measured at the local and global scales using the metrics *Moran's I* (MI) and *Geary's C* (GC) respectively (section 2.8.3). These metrics are averaged over all species in the community. Figures 3.17 and 3.18 show that, across the board, species are not highly aggregated on average. The observed values of MI and GC are close to 0 and 1 respectively, which are indicative of random distributions in space. Also higher MAI communities are found to be more aggregated than low MAI communities. As argued in [58], this is caused by an increase in the aggregation of plant species due to reduced herbivory pressure and increased local reproduction.

3.3. RESULTS

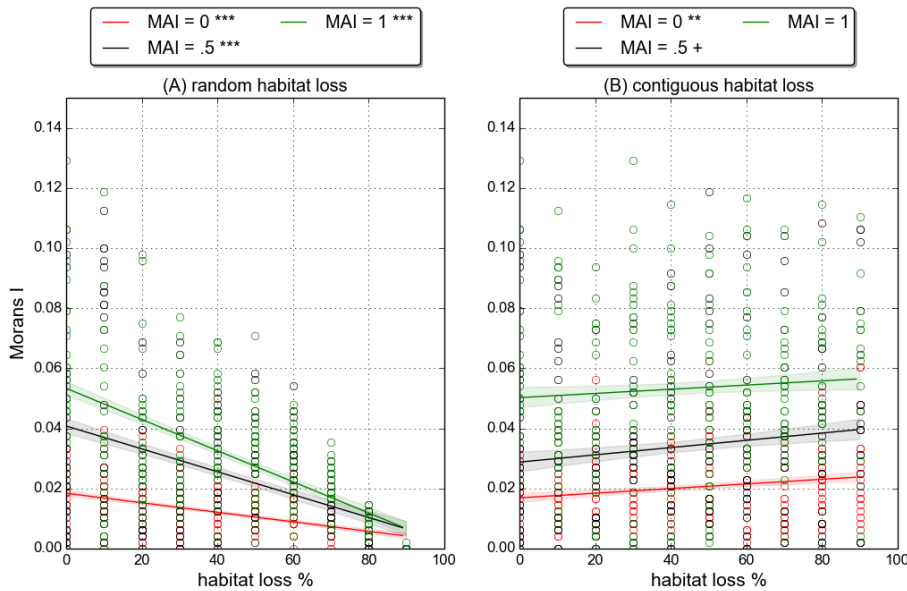


Figure 3.17: **Moran's I** metric for global aggregation (defined in section 2.8.3, averaged over all species. Linear fits and p-value markers as in previous plots (see caption of figure 3.7).

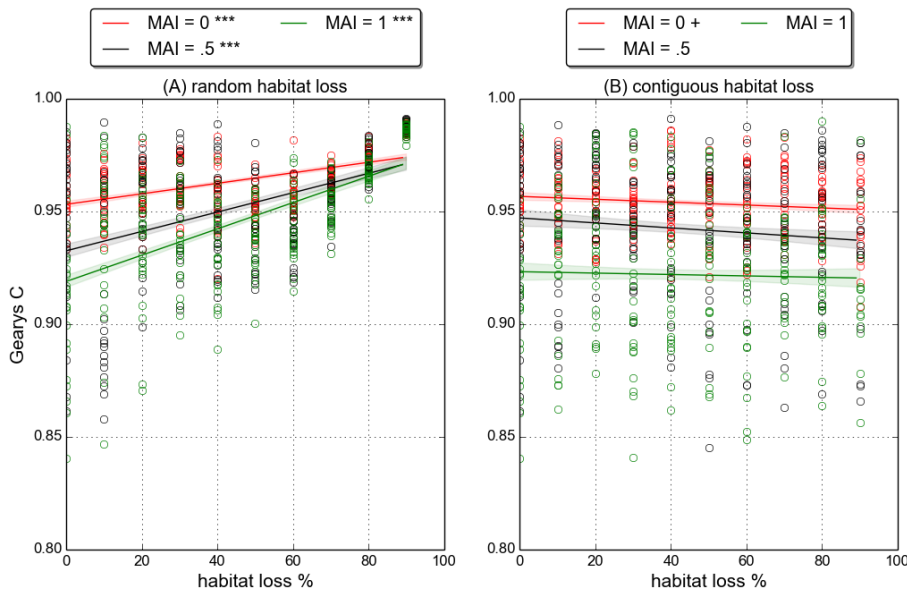


Figure 3.18: **Geary's C** metric for local aggregation (defined in section 2.8.3, averaged over all species. Linear fits and p-value markers as in previous plots (see caption of figure 3.7).

The increase in plant aggregation cascades up to higher trophic levels, where species thrive close to aggregations of food resource. In response to random HL, species on average become less aggregated in space at both the local and global scales. This is expected because the way in which habitat is destroyed creates a patchy landscape which acts against aggregation. Conversely there is some evidence that contiguous HL leads to a slight increase in aggregation. However the only significant linear trend is in MI at MAI= 0.0 (figure 3.17B). Therefore we conclude that contiguous HL does not create significant and robust changes in aggregation. This may be linked to the reduction in stability, since dynamics become more variable it may be harder for species to form local aggregations in space.

3.3.4 Invariability

The alternative stability metrics defined in section 2.8.2.1 are based on *invariability*. These include minimum invariability, population invariability, ecosystem invariability and ecosystem synchrony. Here we demonstrate that the first three of these metrics respond in the same way to HL as the *variability metrics*, giving more weight to our previous conclusions regarding stability. The fourth metric, ecosystem synchrony, gives us a new piece of evidence about how the dynamics of the communities change in response to HL.

Figure 3.19 shows the response of minimum invariability to HL. We use the natural log-transform of the data, as in section 3.3.3, because of the apparent exponential nature of the trends in the raw data. From the figure we see that minimum invariability increases in response to random HL, whereas it decreases in response to contiguous HL. The trends are the same for population and ecosystem invariability, and statistically significant at all MAI ratios (results not shown). These changes in invariability are in agreement with the results of the previous section - community dynamics becomes less variable under random HL, and more variable under contiguous HL. The interpretation of these metrics in [59] lends support to the conclusion that the observed changes in temporal variability are also associated with changes in the stability of the community in a dynamical systems sense (see section 2.8.2.1). Specifically the changes in minimum invariability likely to correspond to similar changes in the asymptotic resilience (derived from the system Jacobian) that governs the rate of return to equilibrium.

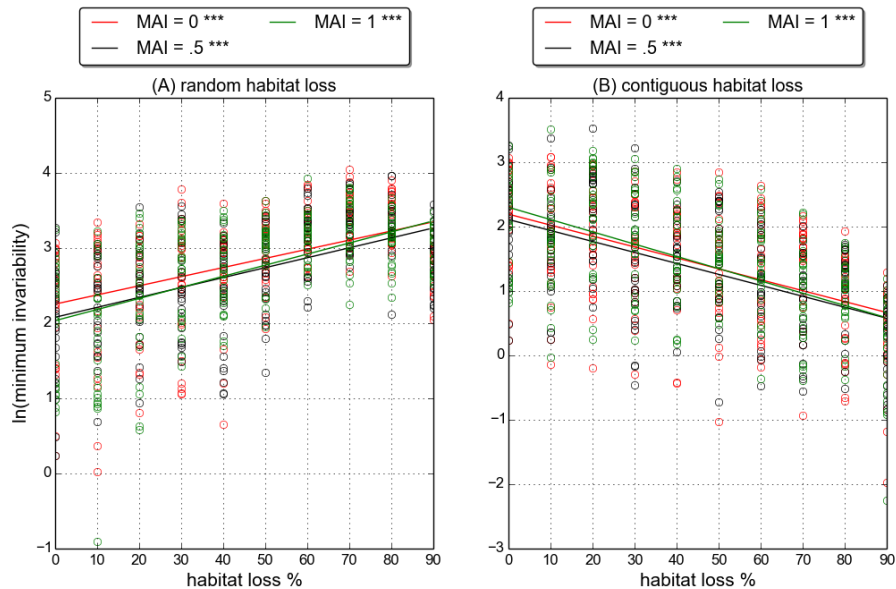


Figure 3.19: **Minimum invariability** as defined in section 2.8.2. Linear fits and p-value markers as in previous plots (see caption of figure 3.7).

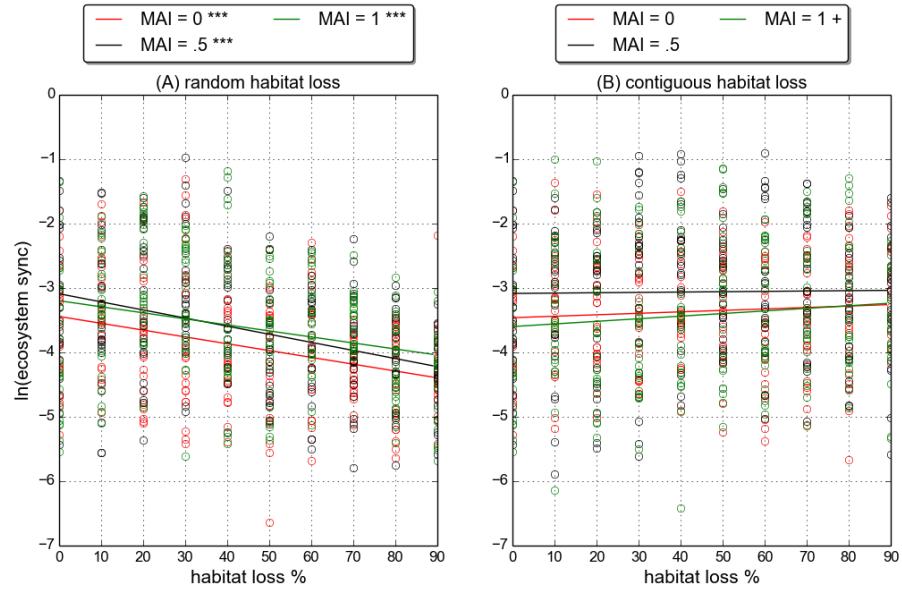


Figure 3.20: **Ecosystem synchrony** as defined in section 2.8.2. Linear fits and p-value markers as in previous plots (see caption of figure 3.7).

Figure 3.20 shows linear fits to the ecosystem level synchrony for the two HL scenarios. In the random case there is a significant decrease in synchrony, whereas in the contiguous case there is no significant change. Also in all cases the synchrony is relatively low. Perfectly synchronised dynamics for all species would give a log-synchrony value of 0. Therefore all communities are well below perfect synchrony. This is expected from trophic dynamics, since it is well known the predator-prey dynamics leads to a phase lag between the population of predator and prey. However it is important to note that trophic dynamics should also lead to some level of synchrony, as species tend to respond in the same way to fluctuations in a shared resource or predator. Therefore it may be that the change in synchrony under random HL is a signature that the trophic component of the population dynamics is reduced, relative to the stochastic component. This would agree with the observed reduction in interaction strengths shown in figure 3.16.

3.4 Synthesis

In this section we summarise the results presented in section 3.3, and attempt to synthesise them into a coherent explanation of the main mechanisms driving community responses to HL. Under contiguous HL communities displayed fewer changes than under random HL. *In the contiguous scenario* we saw that the number of individuals, the frequency of interactions, and to a lesser extent, the number of links, all decreased with HL. However the mean interaction strength and temporal variability increased, representing a reduction in dynamic stability. There were no robust trends in network properties, diversity, evenness, relative abundance by functional group or spatial aggregation, under contiguous HL. *In the random scenario*, as in the contiguous, the number of individuals, the frequency of interactions, and the number of links, all decreased. Unlike the contiguous case, the mean interaction strength and temporal variability decreased, representing an increase in dynamic stability. Under random HL communities became more diverse and more even; displayed a shift in relative abundance towards basal species; and became less aggregated in space. There was also an increase in quantitative vulnerability; a decrease in quantitative generality; and an increase in the interaction diversity of the mutualistic sub-network.

In section 3.3.3 we demonstrated that there is a significant correlation between mean interaction strength and temporal variability. Theoretical population dynamics, in general, suggests that strong inter-specific interactions are destabilising in antagonistic systems [48, 49, 158–160], and there have been some empirical observations of this effect [51]. In a simple predator-prey model, such as the Lotka-Volterra model, it can be shown that increasing the strength of the coupling between species leads to larger amplitude oscillations and may, in certain models, *may* lead to the extinction of species due to over-predation. This consequence of strong interactions is intuitive since the stronger the coupling, or interaction, between species, the greater the effect that one has on the other. In 1972 May showed [48] that for large assemblages of species, with random interactions, the probability of stability is reduced by strong interactions. Together the body of work cited represents a general consensus that antagonistic dynamics are destabilised by strong interactions. Less is known about the dynamics of mutualistic systems, especially when they are embedded in a larger trophic system [40, 58]. However, in some studies mutualisms have been found to play a destabilising role [160, 161]. Again this consequence of mutualisms is intuitive, since an interaction which provides mutual benefaction to both parties can easily lead to a destabilising positive-feedback. In the IBM we model mutualisms as trophic interactions. The animal mutualist consumes resource from its plant partner in addition to providing the reproduction service. Therefore it is not clear whether the net result of mutualistic interactions on the plant population as a whole is positive *or of* negative. However in either case it can be argued that stronger mutualistic interactions will be destabilising. *Therefore we assert that the observed changes in interaction strengths are driving the changes in temporal variability under HL (figure 3.16).*

In section 3.3.2 we argued that *changes in the distribution of species abundances can explain how the quantitative network properties respond* under the two HL scenarios. In particular we explained how the evenness of species abundances affects interaction frequencies. Since evenness changes in the random but not in the contiguous scenario, this is able to explain why quantitative network properties are observed to respond to one type of HL but not the other. However we have yet to explain the differential response of species relative abundances under the two scenarios. Therefore we are left with two main questions: what is driving the change (or lack therefore) in the distribution of species abundances? And, what is driving the change in interaction strengths? In what follows we show that the two are closely related.

We first address the question of interaction strengths. In both HL scenarios the total number of individuals and the total number of interactions decreases. However in the random and contiguous scenarios mean interaction strengths decrease and increase respectively. Figures 3.21 and 3.22 show that these changes in mean interaction strength are due to the entire distribution of IS shifting in opposite directions. Distributions are plotted for MAI= 0.0 and MAI= 1.0, showing the same shifts in both cases. We focus on the MAI= 0.0 case because the pattern is clearer (panel A in these two figures). Under random habitat loss the distribution of IS shifts left, towards weaker interactions. The spread also decreases slightly, suggesting less variance in interaction strengths. Under contiguous habitat loss the distribution shifts towards higher interaction strengths, and also becomes much flatter, such that there is a greater spread in interaction strengths. Importantly we see that conclusions based on the mean value of IS were not misleading, for example due to a highly skewed distribution. In fact the majority of interactions in a contiguous landscape are stronger than the the majority of interactions in a randomly destroyed landscape, for a given level of HL. However we know, from figure 3.1, that the total number of individuals is similar in either landscape. Since IS is calculated by dividing the interaction frequency by the abundance of the two interacting species, it must be the case that interaction frequency is lower for a given number of individuals in a randomly destroyed landscape than a contiguous one. Indeed we saw evidence in figure 3.10 that species interact less frequently in the random scenario than the contiguous, despite comparable total numbers of individuals.

Why would species with the same abundance interact more frequently in a contiguous landscape compared to a landscape with random HL? The answer is simply that randomly destroyed cells present a barrier to the motion of individuals. To demonstrate this we conduct a series of simulation experiments, using the following procedure. We place a single individual randomly in a 200×200 landscape. The individual moves according to the same rules that the animal individuals follow in the IBM (defined in section 2.4), but without the bioenergetic constraints. We record what fraction of the available (i.e. not destroyed) landscape cells the individual visits during 5000 time steps. The experiment is repeated 100 times for each level of HL, and for both HL scenarios, to obtain the *expected range of motion* of an individual in each

3.4. SYNTHESIS

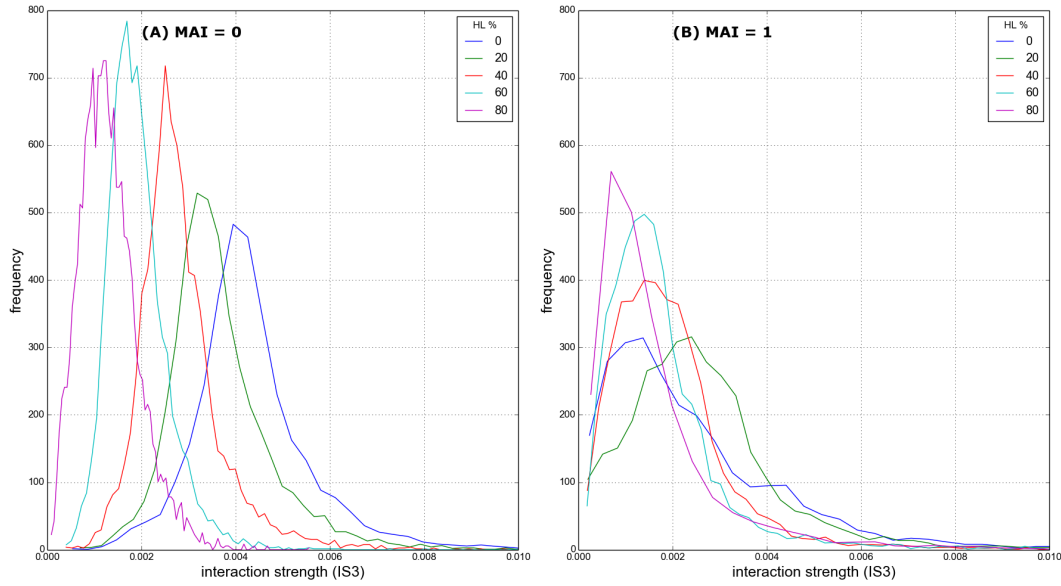


Figure 3.21: **Interaction strength distributions (IS) under random HL.** Panel A: MAI= 0.0. Panel B: MAI= 1.0. IS values for all interactions in each of 25 replicate simulations at the given MAI and HL value, frequency in 100 bins of equal width.

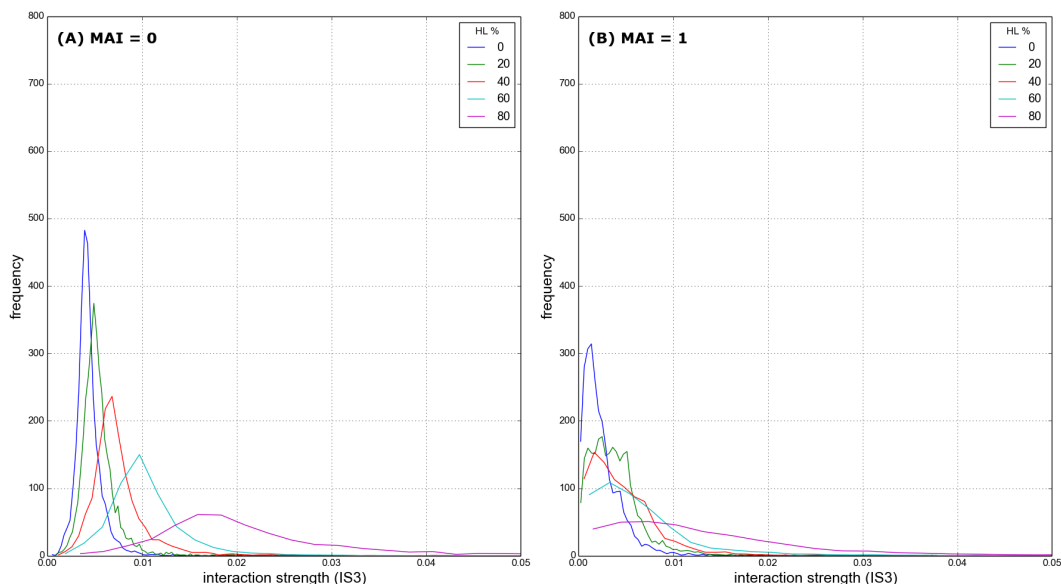


Figure 3.22: Similar to figure 3.21, but for **contiguous HL**.

type of landscape. The results are shown in figure 3.23. Panel A shows an example trajectory of an individual over 5000 time steps in a pristine landscape. Panel B shows the same, but for a landscape at 40% random HL. It is clear that the range of motion is severely restricted by the destroyed cells. In the contiguous case at 40% HL, depicted in panel C, we see that an individual does not experience such barriers to motion (except at the edges of the available habitat). Therefore an individual has the same dispersal ability, but a smaller space to search. The result is that the percentage of available landscape that an individual can explore during 5000 time steps increases under contiguous HL, but decreases under random HL. This explains the observed changes in interaction strength. If an individual is less mobile it is harder for it to find interaction partners, even if the potential partners are present in the landscape at the same abundance. The converse is true for individuals with increased mobility.

Another consequence of the reduced mobility of individuals is that, *ceteris paribus*, it decreases the probability of intra-specific interactions. These interactions are required for the sexual reproduction of non-basal species since individuals must encounter a member of the same species in space in order to create offspring. Intra-specific interactions are not recorded during the simulations, but the total number of births and total number of immigrations for each species [are is](#) recorded. In figure 3.24 we plot the proportion of total births during a simulation that are due to immigration. Here total births includes all new individuals that are created due to immigration, sexual reproduction, mutualistic reproduction, and wind dispersal of plants. From the figure it is clear that immigration is the main source of new individuals contributing over 50% of new individuals in almost all simulations. We also see that the relative contribution of immigration is roughly constant under contiguous HL, whereas immigration becomes more important under random HL. We can attribute the differing contribution of immigration, in part, to the changes in mobility illustrated in figure 3.23. In the random scenario it becomes harder for individuals to find a mate and therefore reproduce, shifting the balance in favour of immigration. In the contiguous case we may expect the opposite i.e. a reduced contribution from immigration due to individuals' increased ability to find a mate. However such an effect is not present and the contribution of immigration is constant under contiguous HL. It must be that any increase in sexual reproduction due to increased mobility is offset by some other mechanism. A candidate mechanism is increased predator mobility, meaning that prey species are more likely to be consumed before they can find a mate. This effect may be compounded by the high relative abundance of predator species in the contiguous scenario, even at high levels of HL. Indeed relative abundance and mobility of predators here suggests a strong predation pressure, which is supported by the high inter-specific interaction strengths.

This leads us to the second question posed above, regarding the distribution of species abundances. We propose that the contribution of immigration to total births explains the observed changes in species relative-abundance and spatial distributions. The immigration mechanism is a *levelling influence* on the communities, both spatially and between species. All species are equally

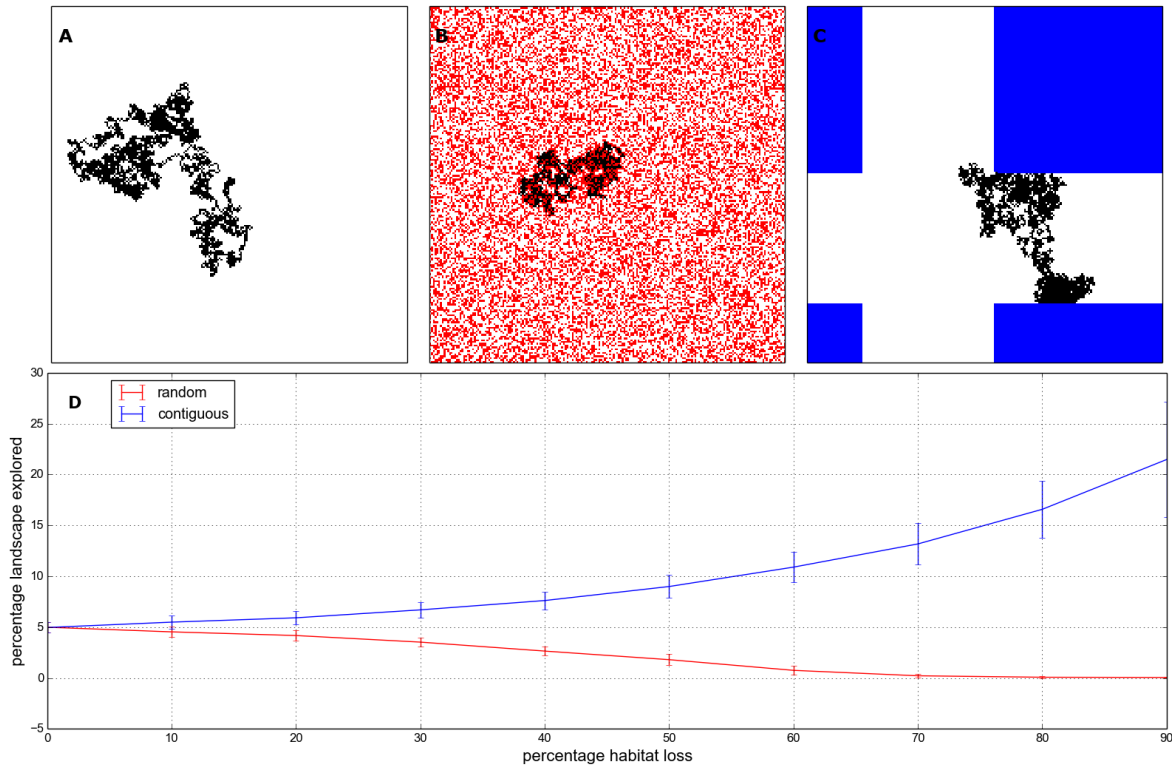


Figure 3.23: An individual's range of motion in different habitat conditions. Top row: example trajectory for a single individual over 5000 time steps in (A) pristine landscape; (B) 40% random HL; (C) 40% contiguous HL. Pristine landscape cells shown in white, destroyed cells in red and blue for random and contiguous destruction respectively. Bottom row (D): Percentage of the pristine landscape cells explored by an individual during 5000 time steps. Solid lines indicate mean over 100 repeat runs; errorbars indicate ± 1 standard deviation.

likely to immigrate, with no dependence on their abundance or distribution in the landscape. Also all empty cells are equally likely to receive an immigrant at each time step. Therefore, although there is no spatial preference built into the immigration mechanism, areas of space with a high density of individuals will be locally less likely to receive immigrants than those areas with a low density, simply due to the number of available cells. Therefore immigration, in isolation, acts to make the distribution of individuals more even between species and throughout space. These are both changes that we observe in the random scenario and not the contiguous, and therefore we attribute them, at least in part, to the increased dependence on immigration to supply new individuals.

Another important change, observed in the random but not the contiguous scenario, is the shift in relative abundances of the functional groups. The greatest changes are the increase and decrease in relative abundance of basal and top-predator species respectively. However there is also a decrease in the relative abundance of species in the second trophic level (herbivores and mutualistic-animals). Only primary predator species display no change in relative abundance. We

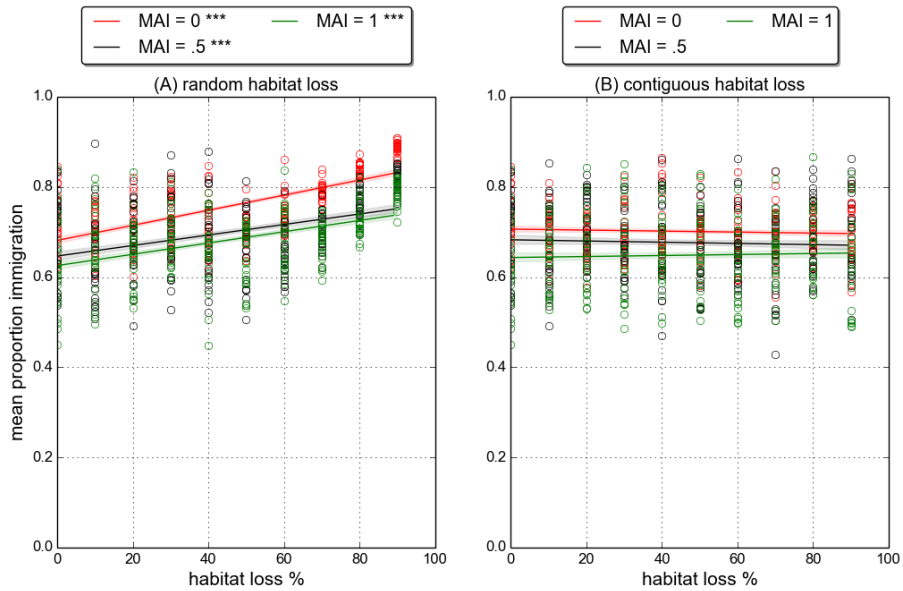


Figure 3.24: Number of immigrants as a fraction of the total number of new individuals created over the course of a simulation. Linear fits and p-value markers as in previous plots (see caption of figure 3.7).

assert that all of these changes in relative abundance can be explained by the change in mobility and its knock on effect on interaction strengths, reproduction and dependence on immigration.

As previously discussed, the reduction in mobility makes it harder to find prey and therefore reduces interaction strengths. The result is an overall decrease in predation. So species lower in the food chains benefit from reduced predation pressure, whilst species higher in the food chains suffer because less energy is being transferred up the trophic pathway. In addition reduced mobility makes it harder for animal species to find partners with which to reproduce. This negatively affects all animal species and mutualistic plants. However mutualistic plants, although they may be reproducing less frequently, receive the incidental benefit of losing less energy to their mutualistic partners. (Although this effect is present in the model it is worth noting that it may be unrealistic, since the energy investment involved in becoming a mutualist occurs prior to any interaction. See discussion in section 7.1.) Therefore we see a shift in relative abundance towards basal species, which benefit from reduced consumption whilst all other species suffer from a reduced ability to find food and reproduction partners. Animal species in the lower trophic levels receive a compensatory benefit of lower predation pressure, which partly explains why species in the second trophic level are hit less hard than top predators. The fact that the relative abundance of primary predator species does not change must be a combination of reduced predation pressure, but also a slight quirk of the modelling framework. Due to the way the networks are constructed, there are significantly more primary predator species than any

other functional group (this an known artefact of the niche model - see section 2.3.2 and figure 2.2). Therefore, since immigrant individuals are drawn uniformly at random from all species, immigrants are most likely to be primary predators. As we have seen (figure 3.23) random HL increases the community dependence on immigration. We now understand that this benefits primary predators disproportionately. Conversely the functional group with fewest species is the top-predators. Therefore this group receives fewest immigrants, compounding the other effects detailed above. Therefore it appears that mobility, along with immigration, accounts for all observed changes in species relative abundances.

It is worth here reiterating the point about ecosystem synchrony made in section 3.3.4, where we attributed the reduced synchrony under random HL to a reduction in the trophic component of the dynamics. In this section we have shown that random HL increases the contribution of immigration to the overall number of births (figure 3.24). The creation of individuals due to immigration is a random processes. Births due to reproduction, although stochastic, are dependent on trophic and non-trophic interactions. Therefore the increased contribution of immigration represents a reduction in trophic dynamics and an increase in stochasticity under random HL. We conclude that it is indeed this shift driving the decrease in synchrony. We will return to the issue [of](#) deterministic versus random dynamics in chapter 4.

3.5 Conclusion

A key feature of the results presented in this chapter is that the community response to HL is dependent on the spatial pattern of the perturbation. This spatial dependence has been reported previously in numerous studies [12, 68–73]. In general the cited studies support the conclusion that spatially-correlated HL is less detrimental to communities than random HL because the former leaves larger areas of landscape unaffected, while the latter results in patchy and fragmented landscapes. Our findings broadly agree. However, while previous theoretical studies have focused largely on extinction thresholds, we have conducted a comprehensive analysis of community responses in the absence of extinctions.

Contiguous habitat loss was mainly found to reduce temporal stability due to increased interaction strengths. Other aspects of the communities (diversity, network properties, spatial aggregation) were generally constant across the contiguous HL gradient. As such contiguous HL resulted in communities with lower absolute abundances, confined to a smaller region of space, and displaying greater temporal variability but with the same biodiversity patterns. This leads us to speculate that there may exist a scaling of time and space under which the systems at low and high HL are equivalent. However we do not explore this possibility further.

Random habitat loss was found to induce a breakdown in the trophic structure of communities, resulting from weaker species interactions and characterised by the collapse of top-predator populations. Primary predator populations were only spared, and extinctions prevented, by the immigration mechanism. Somewhat surprisingly communities under random HL became more even in terms of species relative abundances, and the temporal dynamics became less variable. Taken in isolation these results suggest that random HL is beneficial for diversity and stability. This mistaken conclusion highlights the importance of considering multiple aspects of diversity and stability when analysing multi-trophic communities (see section 2.8.2). In other aspects random HL is clearly damaging to diversity, mainly in terms of top-predator abundance. The low abundance of top-predator species makes them potentially more vulnerable to extinction, although extinctions are prevented by immigration. Under random HL communities displayed changes in network properties, which could be understood in terms of changes in the relative abundance of species.

We predicted that MAI ratio would mediate community response to HL. In fact, in almost all cases, mutualistic communities responded in qualitatively the same way as antagonistic communities. Therefore we find no significant evidence that mutualism makes communities either more or less robust to HL. One notable difference in response was IS under random HL (figure 3.16). High MAI communities did not lose interaction strength to the same extent as low MAI communities. This effect has not been explained. We suggest that it may be due to spatial aggregation, which was higher for mutualistic communities across the HL gradient (figure 3.17). Spatial aggregation means that individuals are not homogeneously distributed through the landscape which could cause spatial effects that skew the distribution of interaction strengths.

Indeed this may explain why there is more spread in the IS distributions at $MAI = 1.0$ than at $MAI = 0.0$ (figures 3.18 and 3.17). Interestingly the fact that IS is less sensitive to random HL in mutualistic communities does not translate into different variability responses.

Nestedness and compartmentalisation showed no significant trends in response to either HL scenario. These metrics have often been associated with stability in mutualistic and antagonistic communities respectively [63]. It is interesting to note that neither metric changed, despite significant and opposite trends in temporal stability under random and contiguous HL. However we did not explicitly test for the impact of these metrics on stability. It would be possible, and potentially informative, to study whether communities with higher nestedness/compartmentalisation responded differently to other communities.

Crucially we have found that, in the default parameter regime, the effects of HL are governed largely by interaction strengths and immigration. In particular interaction strengths are responsible for changes in temporal variability, and to some extent biodiversity patterns. In subsequent chapters (especially chapter 6) we will return to the role of interaction strengths. Immigration has been shown to be a stochastic influence on the dynamics, and a levelling influence between species and throughout space. Also immigration was found to prevent species extinction, allowing communities to persist in the face of high levels of HL. In this sense the communities modelled in this chapter represent *open systems* with a high rate of influx from an external source. In the ecological context, although the local landscape is almost entirely destroyed there is sufficient immigration from surrounding sources to maintain diversity. In what follows we will consider what happens when the immigration rate is varied. We begin chapter 4 with a study of *closed-communities* ($IR = 0.0$). In chapter 5 we investigate how communities respond to HL over a range of immigration rates.

CHAPTER



COMMUNITY DYNAMICS UNDER VARIABLE IMMIGRATION RATE

4.1 Introduction

In the chapter 3 we analysed in detail how simulated communities responded to two habitat loss scenarios. These simulations used the *default parameter values* for the IBM model, as published in [58]. An important feature of these simulations was that they exhibited almost no species extinctions, even up to 90% habitat loss (HL). This due to a high immigration rate ($IR = 0.005$), providing a rescue effect for all species. In nature the destruction or degradation of habitat often leads to a loss of species [7, 8]. Therefore we also intend to use the IBM to investigate the regime where habitat loss causes extinctions. The obvious way to do this is to reduce the IR. Since immigration proved to be a key driver of the dynamics in chapter 3, in this chapter we conduct a detailed analysis into the consequences of varying the IR parameter. This is largely in preparation for chapter 5 where we will study, from a more ecological perspective, how changing IR affects the response of communities to HL. We restrict the scope of this chapter to pristine landscapes ($HL = 0$). In the first part of this chapter (section 4.2) we study *closed communities* by removing immigration from the model altogether ($IR = 0.0$). We find that *closed blue communities* are characterised by many species extinctions, and we attempt to reduce these extinctions by varying certain model parameters. In the second part of the chapter (sections 4.3 to 4.6) we address an issue that is found to arise from reduced IR, namely *increased temporal variability*. In section 4.4 we revisit the assumption made in the previous analysis, that simulations reach steady-state after 5000 time steps (see section 3.2.2). In section 4.5 we test for determinism in the simulated population dynamics, and in section 4.6 we apply different sampling regimes to compare the convergence and repeatability of our experimental results.

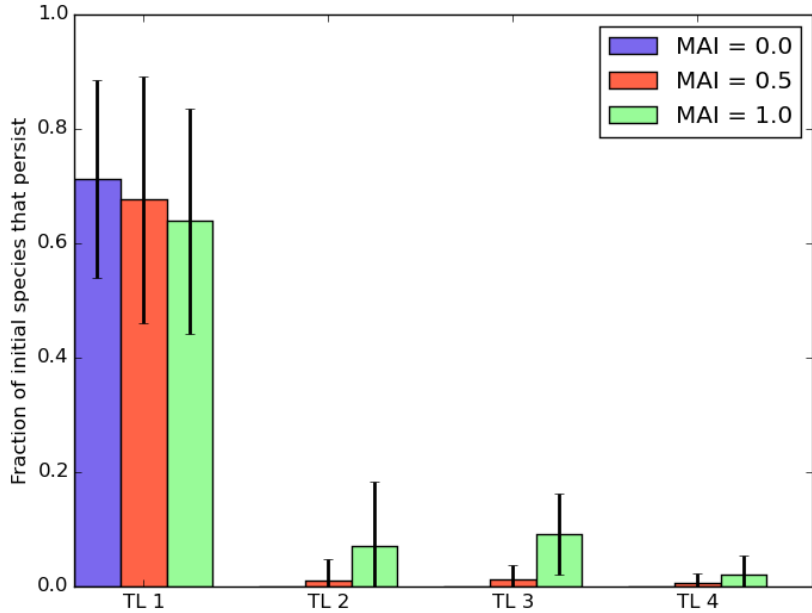


Figure 4.1: **Fractional persistence** by trophic level for three different MAI ratios, with **zero immigration** ($IR=0$). All other parameters set to default values. Fractional persistence measured by the fraction of species initially belonging to a trophic level which have not gone extinct by the end of a simulation (5000 time steps). Solid bars give the mean value over 22 repeat simulations. Error bars show ± 1 standard deviation.

4.2 Persistence in closed communities

We define a *closed-community* as one in which there is no inflow of individuals from an external source. In the model this is achieved by setting the immigration rate to zero ($IR=0$). Here we study such communities in a pristine landscape i.e. without habitat loss ($HL=0$). The simulation procedure is the same as in chapter 3. All parameters, except IR, take default values unless otherwise stated, and each simulation uses a distinct network topology generated with the method described in section 2.3. A species is said to *persist* if there is at least one individual belonging to that species present in the landscape on the final time step of the simulation. Therefore *fractional persistence* is defined as the fraction of the initial pool of species (or subset of that pool) that persist. We also use the *number of persistent species*, where absolute values are desirable. All abundance measurements given are calculated from the number of individuals belonging to each species on the final (5000th) time step of the simulation. Simulations were run with three MAI ratios ($MAI = 0.0, 0.5, 1.0$) to explore the full range between antagonism and mutualism. To reduce the number of figures we sometimes present results for only one or two MAI ratios only, but make it clear where results differ across MAI ratios.

An initial set of simulations with zero IR shows that species persistence is low (Figure 4.1). We see that for an antagonistic community ($MAI = 0$) all non-basal species go extinct, as do around 30% of basal species. Introducing mutualism into the communities slightly improves fractional persistence in the higher trophic levels. We see some persistence of non-basal species, but no more than 10% of the initial pool on average survive. Therefore, even in the *best case* at $MAI = 1.0$, we expect around 90% of non-basal species to go extinct. It is clear that, given the default parameters, immigration is a requirement for the maintenance of species richness. This is a troubling feature of the model. In nature a true closed-community may not exist, but there are systems which come close (for example remote island ecosystems). It is desirable for our model to be able to describe such systems, and for us to investigate the effects of habitat loss in this extreme case. It may also be informative to discover which factors in the IBM model contribute to persistence in closed-communities. Here we conduct a systematic review of certain model parameters and their impact on persistence. Due to the large parameter space of the model we study these parameters individually, with other parameter values held constant. We restrict the analysis to four parameters, namely: MAI ratio (section 4.2.1); reproduction rate (section 4.2.2); landscape size (section 4.2.3); and number of initial species (section 4.2.4). In addition we look at the effect of the interaction network structure on persistence (section 4.2.5). The choice of each parameter is justified in the corresponding subsections. As in chapter 3 we use linear models to detect trends in persistence in response to the parameter values varied. Again the *p-value* of the fit is used to test for significance in any trend identified (see section 3.2.2).

4.2.1 Mutualistic-to-antagonistic interaction (MAI) ratio

In [58] it was shown that increasing the levels of mutualism (MAI ratio) in the IBM can have a stabilising effect. However in the previous chapter we saw that this stability did not translate into a greater robustness of mutualistic communities to habitat loss. From figure 4.1 we see that mutualism has a small but positive effect on fractional persistence at zero IR. An interesting feature of this effect is that it *cascades* to higher trophic levels, benefiting species other than mutualists. Here we explore the effect of mutualism on persistence in more detail.

Figure 4.2 shows the average abundance dynamics, by functional group (FG), for four different MAI ratios. These plots are produced by taking the mean abundance of each trophic level, at every time step, over 22 repeat simulations. In panel A we see that the abundance of plants rises to fill the whole landscape ($200 \times 200 = 40,000$), while the abundance of all other FGs is at or near zero. From the other panels (B-D) we see that increasing the MAI ratio particularly benefits the mutualistic-plants and mutualistic-animals. However this also appears to also confer some small benefit to primary-predators and top-predators, as their abundances are small but non-zero. Ecologically this makes sense. If mutualism strongly benefits mutualistic species, it will also benefit those species that feed on them. However the benefit may only be a transient effect as the abundance of plants in panel D is still rising, on average, at the end of the simulations.

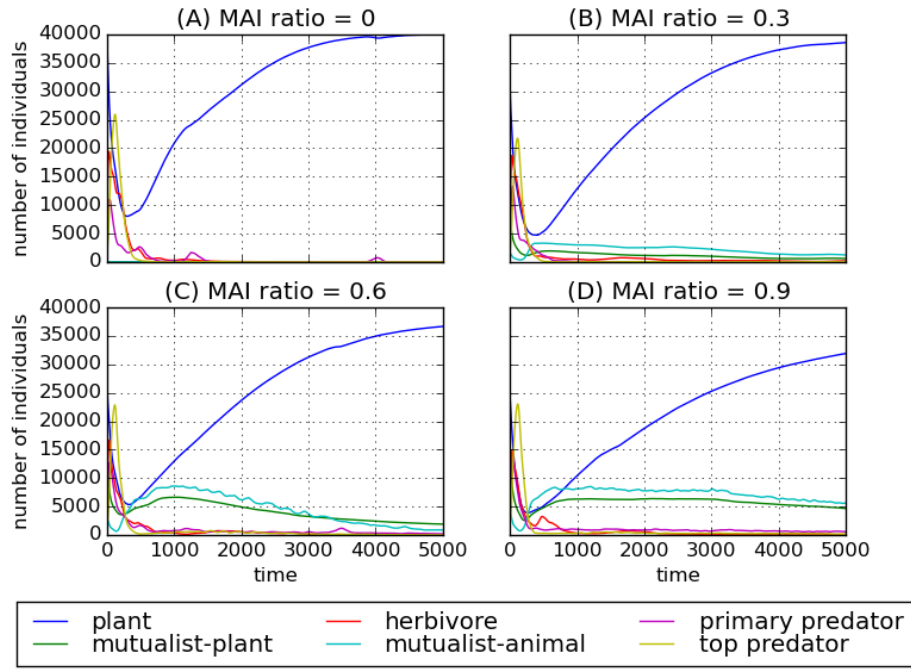


Figure 4.2: Mean dynamics by functional group for four different MAI ratios (A-D), without immigration. Lines given by number of individuals belonging to a functional group, averaged over 22 simulations. Colours indicate functional group (see legend).

Figure 4.3 shows the number of persistent species by trophic level for a range of MAI ratios. We see that increasing MAI ratio in fact has very little effect on the absolute number of persistent species in each trophic level. For example at MAI= 1.0 there are only two persistent species on average in the second trophic level. Therefore the increase in abundance seen in figure 4.2 must be due to a small number of dominant species. We conclude that mutualism has a negligible effect on overall persistence in terms of species richness.

4.2.2 Reproduction rate

The initial transience in the abundance dynamics at zero IR (figure 4.2) is characterised by a sharp decline in plant abundance (mutualist and non-mutualist), which reaches a minimum and then rises again. We hypothesise that this overconsumption of producers, and therefore limited availability of food for animal species, causes many of the extinctions. Indeed in these simulations $\sim 85\%$ of the extinctions occur during the first 500 time steps. Therefore we look at the possibility of improving persistence by increasing the reproduction rate (RR). The RR parameter defines that rate at which non-mutualist plants reproduce (via the wind-dispersal mechanism, see section 2.4). Therefore increasing this mechanism should improve the availability of plant biomass in the system, with potentially cascading effects. The RR parameter does not affect mutualistic-plants,

4.2. PERSISTENCE IN CLOSED COMMUNITIES

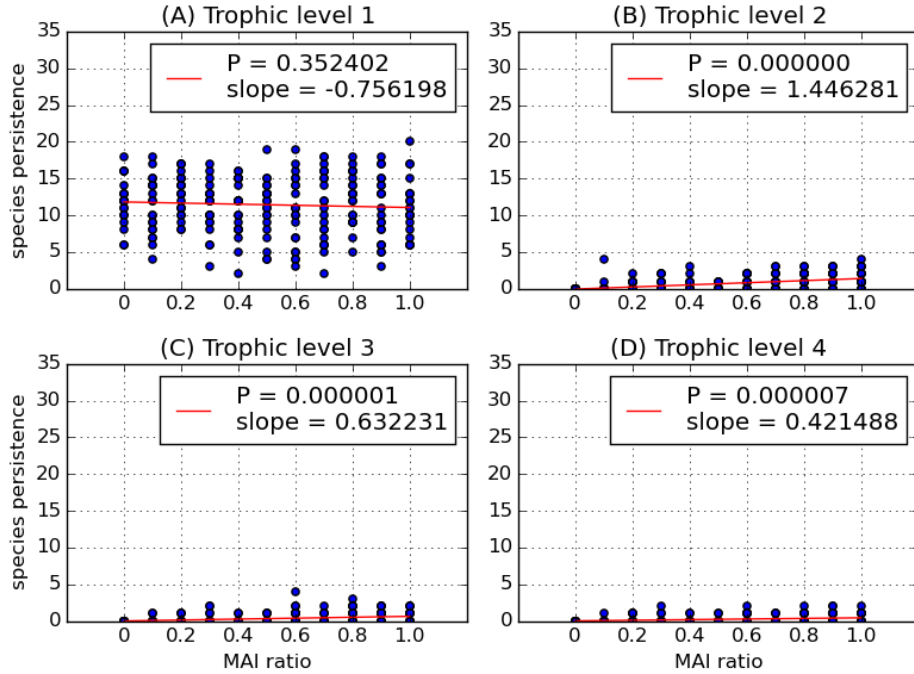


Figure 4.3: **Number of persistent species** plotted against MAI ratio, for each trophic level (A-D). Blue circles give number of persistent species, for a single simulation, on the 5000th time step. 22 repeat simulations at each MAI ratio. Red lines show linear regression fits, with slope and p-value of fit given.

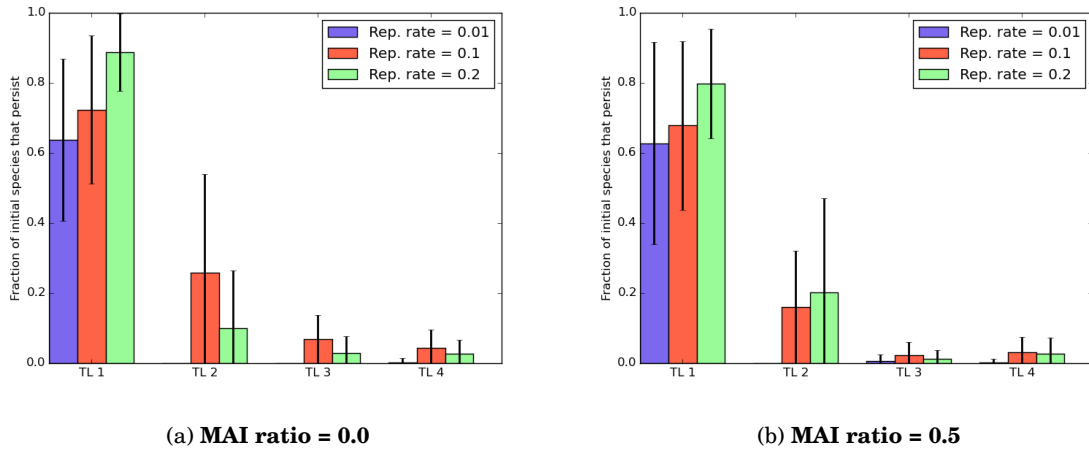


Figure 4.4: **Fractional persistence** by trophic level for three different reproduction rates (RR), at two MAI ratios (A-B). Fractional persistence measured by the fraction of species initially belonging to a trophic level which have not gone extinct by the end of a simulation (5000 time steps). Solid bars give mean value over 22 repeat simulations. Error bars show ± 1 standard deviation.

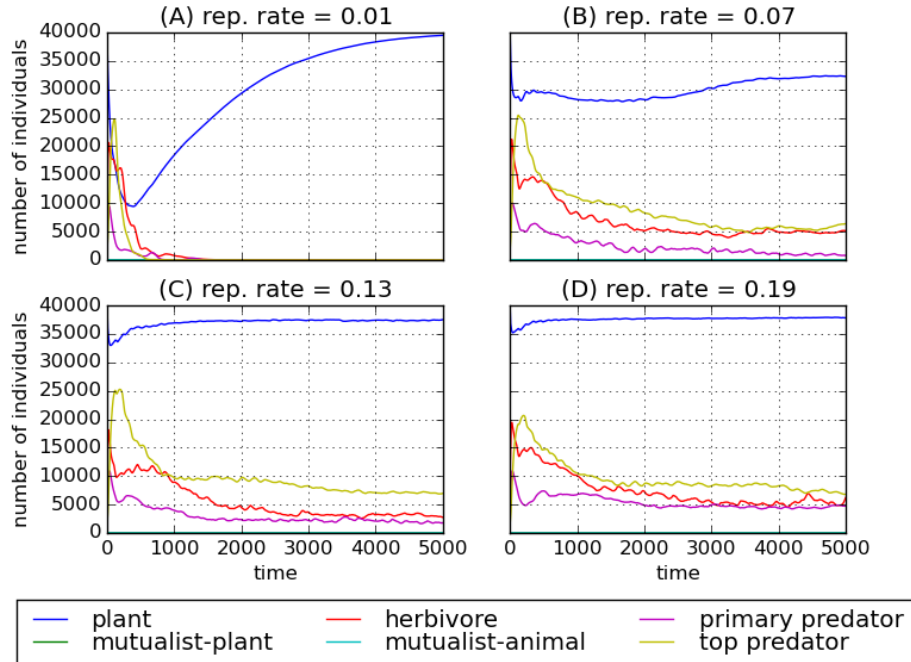


Figure 4.5: **Mean dynamics by functional group** for four different reproduction rates (A-D), at **MAI=0**. Lines given by number of individuals belonging to a functional group, averaged over 22 simulations. Colours indicate functional group (see legend).

which only reproduce via their interactions with mutualistic-animals and not via wind-dispersal. Here we vary the RR between 0.01 (default value) and 0.2 and look at the effect on persistence.

Increasing the RR improves the fractional persistence of all trophic levels, as shown in figure 4.4. This effect is greatest for the two lowest trophic levels, but has a small cascading effect on the upper two trophic levels. However, as we saw with MAI ratio, the improvement in persistence due to RR is relatively small. Even for high RRs we still find that many species go extinct. Looking at the abundance dynamics in figures 4.5 and 4.6 we see that increasing the RR reduces the severity of the decline in plant abundance during transience. The resulting increase in the availability of plants does benefit all trophic levels by increasing the number of individuals present. However, because of the low fractional persistence, it must again be the case that these communities are dominated by just a couple of species in each trophic level, with all other species going extinct. The results for MAI= 1.0 (not shown) are qualitatively similar, although these communities contain fewer plants that reproduce via wind-dispersal and can therefore benefit from increased RR. In the remaining simulations for this section, as we continue to search for improvements in persistence, we choose to use RR= 0.1 . This choice reflects the resulting improvement in abundances across trophic levels compared with the default value. It was decided that this effect, combined with changes in other parameter values may help to improve persistence further.

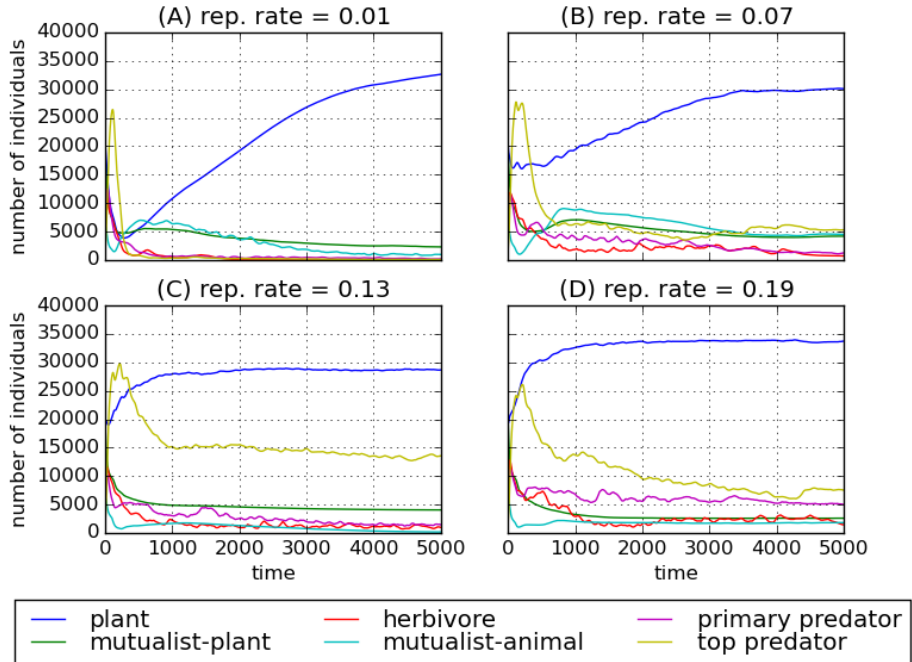


Figure 4.6: **Mean dynamics by functional group** for four different reproduction rates (A-D), at **MAI=0.5**. Lines given by number of individuals belonging to a functional group, averaged over 22 simulations. Colours indicate functional group (see legend).

4.2.3 Landscape size

One might hypothesise that competition for space is causing species extinctions, in which case increasing the size of the landscape may improve persistence. We varied the width of the square landscape between 100 and 1000 cells, running 25 repeat simulations at each width. These simulations were run for $MAI= 0.0, 0.5, 1.0$, and used the increased reproduction rate $RR= 0.1$. Figure 4.7 shows how the number of persistent species changes in response to landscape size for $MAI= 0.0$ and 0.5 (results qualitatively similar for $MAI= 1.0$). For both MAI ratios depicted there is an overall increase in species persistence up to a landscape width of 800. **We suggest that the decrease in persistence at a width of 1000 is a statistical anomaly, although this is not investigated further.** Overall, the increase in persistence is driven by small increases in the species richness of each trophic level. Beyond a width of 800 cells persistence appears to decline, although this may be a statistical anomaly and we do not explore this result further. Even with a landscape of 800×800 the results show that we should not expect more than 20 persistent species, which represents the extinction of two thirds of the initial species pool. Therefore we conclude that landscape size does not resolve the problem of extinctions. This does not rule out competition as a cause of species extinctions in the model. However the observation that increasing the available space does not remove competition pressure suggests that competition

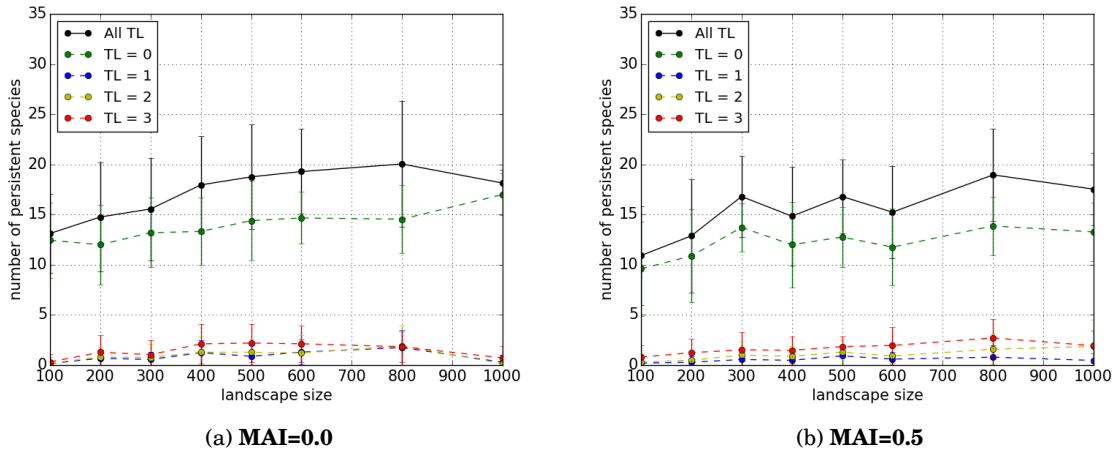


Figure 4.7: **Landscape size** against species persistence (on 5000th time step), for two MAI ratios (A,B). Total persistence, and persistence by trophic level. Points show mean value over 25 replicates. Error bars show ± 1 standard deviation.

for resources may be more significant than competition for space. Since increased space does not greatly improve persistence, further simulations in this section are run using the default landscape width of 200 which requires significantly less CPU time than for a width of 800.

4.2.4 Number of initial species

All previous simulations have been run with an interaction network consisting of 60 species. We consider the possibility that beginning the simulation with a larger network may result in a greater number of persistent species. In this way we may hope to evolve to a stable network structure as extinctions kill off species that are not viable. Here we vary the number of species in the network between 30 and 240, and look at the effect this has on persistence. As in the previous section, 25 repeat simulations are run for each number of species at all three MAI ratios (0.0, 0.5, 1.0).

Using a network of more than around 70 species causes a problem with our network generation procedure. As described in section 2.3 we use the niche model to create interaction networks, but reject those that do not satisfy the trophic constraints. With a large number of species the probability of the niche model generating a network that meets the trophic constraints becomes low enough that the procedure cannot be run within a reasonable time ($time > 2$ days on Blue Crystal for 100 species). In particular, as discussed in section 2.3.2, the niche model overestimates the number of primary-predator species, and underestimates the number of herbivores. To overcome this problem we here construct networks in two different ways: 1) we use the standard niche model with no trophic constraints; and 2) we *rewire* networks generated using the niche model iteratively updating the network until it meets the trophic constraints. The procedure

is as follows. A species is selected uniformly at random from the trophic levels that contain more than the desired number of species. This species is then moved to a trophic level that contains too few species, and is linked to other species selected at random from a pool of possible candidates. Possible candidates are defined by the new trophic level of the species that has been moved e.g. a herbivore can only eat plants, and only be eaten by species in higher levels. The number of new links created is chosen to preserve the degree of the moved species, and therefore the connectance of the network (in/out degree cannot necessarily be preserved because of the change in trophic level). The procedure is repeated, moving randomly selected species until all trophic constraints are satisfied. Mutualistic links are then introduced using the standard *link replacement* method (section 2.3.3). Here we use the same constraints as were applied in the original network generation procedure. That is the proportion of species belonging to trophic levels one, two and four must be at least 25%, 25% and 5% respectively. We refer to the networks generated using procedures 1 and 2 as *niche* and *rewired*, respectively. Simulations are run for both types of network.

Figures 4.8 and 4.9 show how the number of persistent species depends on the number of species in the initial network. For the *niche* networks we see that there is little change in species persistence. Whereas for the *rewired* networks we see a large increase in total persistence. However this increase is mainly due to plant species, with only a small change in persistence for trophic levels two, three and four. The difference between the *niche* and *rewired* network results is due to the fact that large niche model networks are dominated by *primary predators*. It appears that the primary predator species out-compete each other and therefore we do not see a large change in persistence. Conversely, for the *rewired* networks the number of species in each trophic level grows proportionally with the total number of species. The only significant benefit is to plant species, which seem to be able to coexist in larger numbers. We conclude that increasing the number of initial species is not able to generate the diverse communities that we had hoped for. However the *rewiring algorithm* developed for this analysis represents a novel modification to the niche model, which may prove useful for the generation of realistic interaction networks.

4.2.5 Network structure

A notable feature of the results presented in this section is that there is significant variation in persistence between replicate simulations. Presumably some of this variation is due to noise. However some of this variation may be due to the structure of the interaction network used. As we know (section 1.2.1) the structure of an interaction network is believed to impact on various aspects community stability. Here we conduct a simple experiment to determine whether network structure can generate systematic differences in persistence. We look at two extreme cases of network structure: one that was observed to generate low persistence in previous simulations, and another that generated comparatively high persistence. We run repeated simulations with these two networks and test for persistence. The aim is to determine whether the previous observations

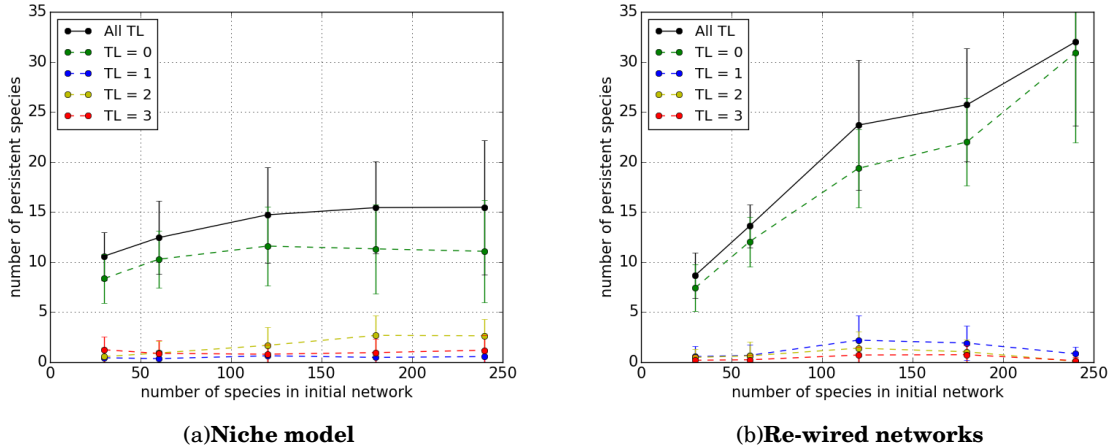


Figure 4.8: Number of initial species against species persistence at **MAI=0**, for two types of initial network: (A) Interaction network generated using standard niche model, and (B) generated using re-wired niche model topology (see text). Total persistence, and persistence by trophic level. Points show mean value over 25 replicates. Error bars show ± 1 standard deviation.

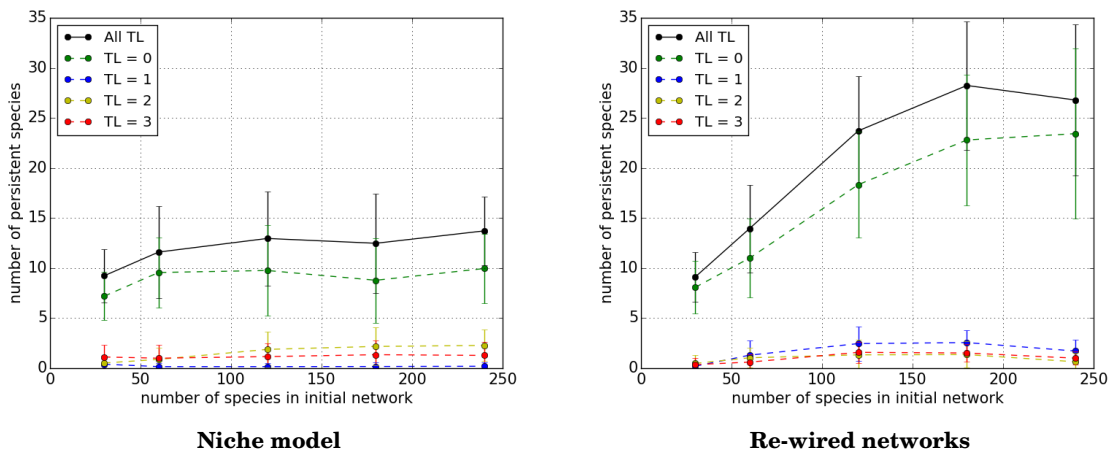


Figure 4.9: Similar to figure 4.8, but with MAI=0.5.

(low and high persistence) were due to some intrinsic property of the network structure, or were due to chance.

The two networks are chosen from the 25 repeat simulations with a *rewired* antagonistic ($MAI = 0.0$) network of 120 species (figure 4.8B). A network of 120 species is used because it generates slightly greater persistence than network with fewer species, as seen in section 4.2.4. We visually select the two networks that display the best and worst persistence profiles. The best case, giving the ‘*good*’ network, had persistent species in all trophic levels and two persistent species in each of trophic levels three and four. In contrast the worst case, giving the ‘*bad*’ network, had no species persistence in any trophic level above one. With each of these two networks we run 100 repeat simulations ($MAI = 0.0$) to test if this observed difference in persistence is repeatable and therefore due the network structure.

The *good* and the *bad* network structures are shown in panel A in figures 4.10 and 4.11 respectively. Visually there is little to distinguish the two networks. However we find that they have very different and repeatable persistence properties. Panel C of these figures shows the average number of persistent species in each trophic level. It is clear that the *good* network performs systematically better on average, in terms of persistence, than the *bad* network. The *good* network results in, on average, more than two persistent species in all non-basal trophic levels. In contrast the *bad* network results in an average of less than one persistent species in all but the basal level. Therefore the difference in persistence between these two networks is repeatable. An analysis of which network properties are associated with increased persistence is beyond the scope of this work. However such an analysis could be an interesting avenue of further work. We simply conclude that network structure does play a role in shaping simulated communities, something which had been assumed previously but not tested explicitly.

4.2.6 Summary

From the results presented in this section it appears that immigration is required in order for the IBM to generate communities with more than a handful of persistent species in the higher trophic levels. Having not exhaustively searched the parameter space we cannot be certain of this fact (see discussion in section ??). However this finding is not in disagreement with our observations of the natural world. Indeed the first laboratory experiments to produce persistent predator and prey populations in a microcosm, conducted by Gause [?], required either spatial heterogeneity (to provide refuge for the prey) or immigration in order to prevent extinctions [?]. Also, in larger systems the *principle of competitive exclusion* is expected to cause extinctions. The principle states that the number of coexistent species cannot be greater than the number of niches (or alternatively, the number of limiting resources). The reasoning is that two species competing for the same resource is unstable, such that if either species happens to gain an advantage it drives the other to extinction. The principle of competitive exclusion presents an apparent paradox in Nature because many communities exhibit species richness much greater than

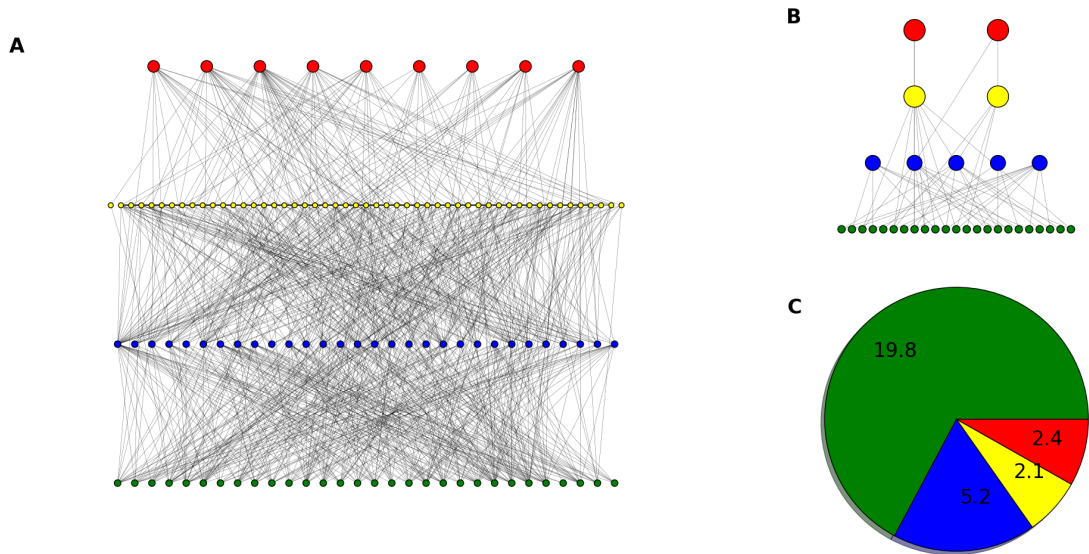


Figure 4.10: Example of a ‘**good network structure**’. Colours represent trophic level. (A) Antagonistic network of 120 species, rewired from the niche model (see text), used as input for simulations. (B) Example of ‘pruned’ network consisting of the species that persist after 5000 time steps. (C) Mean number of species belonging to each trophic level in the pruned network, averaged over 100 replicate simulations (all using A as the initial network).

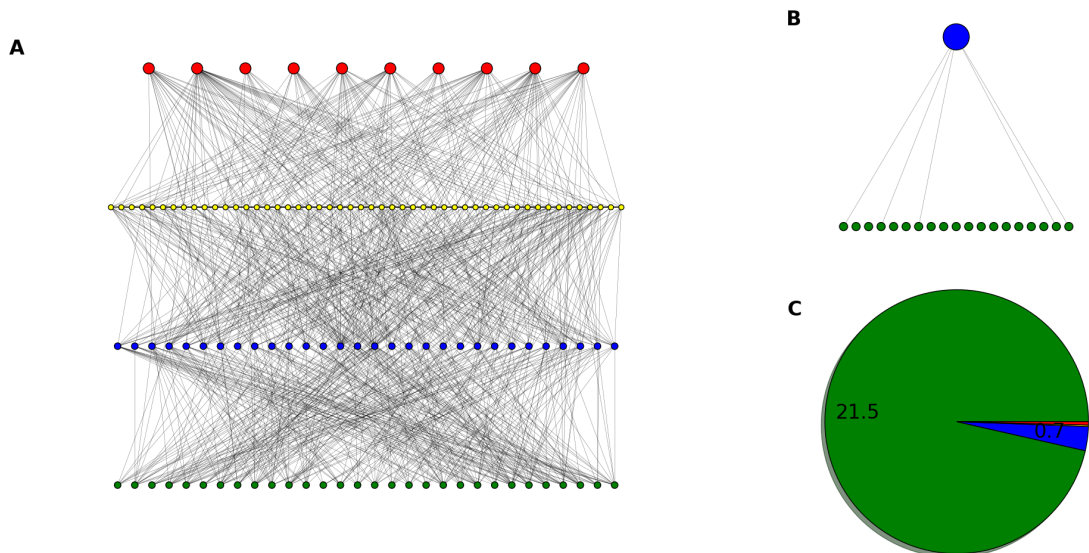


Figure 4.11: Example of a ‘**bad network structure**’. Similar to figure 4.10, but with a different initial network of 120 species used as input for the simulations.

the apparent number of limiting resources. A prime example of such communities are oceanic plankton, hence the *paradox of the plankton* [?]. One proposed solution to these paradoxes comes from meta-community theory (see section 1.2). That is, although local populations may be unstable in isolation, they exist as part of a meta-community. Various models predict that meta-community dynamics, which involves dispersal between local patches or communities, can stabilise local populations [?]. The key feature here is *dispersal*, which is not dissimilar to our immigration mechanism because it provides an external source of individuals. Therefore we propose that at least some of the extinctions we see in the IBM at zero IR are due to competitive exclusion, an effect which is reduced by the introduction of immigration.

We demonstrated in section 4.2.5 that network structure *can* have an effect on persistence, and therefore on community dynamics also. This result implies that the IBM, subsequent to this thesis, could be used to study the effect of various network properties on different aspects of stability. We also presented a novel algorithm to modify niche model networks according to desired trophic constraints. In order to justify the use of this method further investigation would be required to compare the realism of the derived topologies to empirical webs, and is also beyond the scope of this thesis.

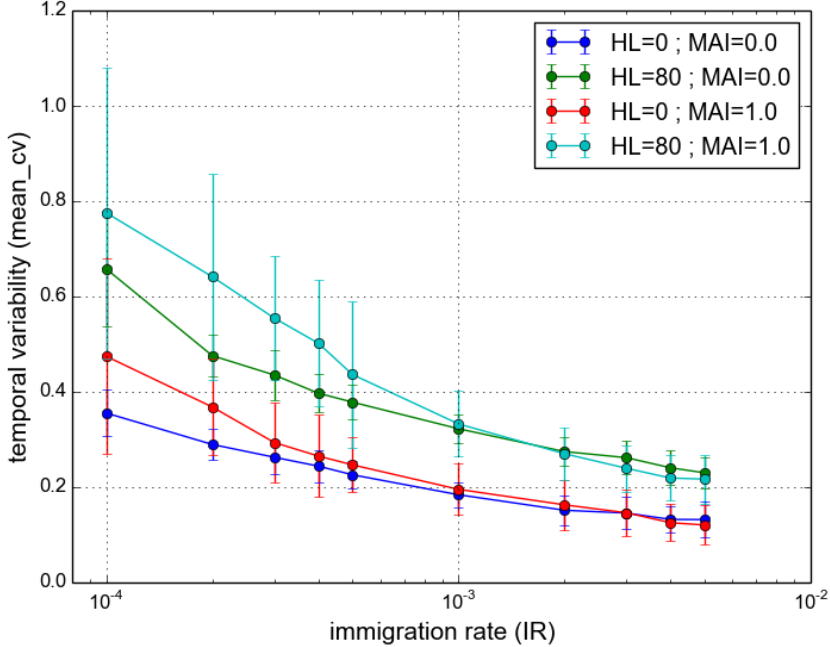


Figure 4.12: **Temporal variability** against immigration rate (IR). Variability calculated as *mean_CV* (defined in section 2.8.2). Points show mean value over 50 repeat simulations. Error bars show ± 1 standard deviation. $HL = 0$, all other parameters take *default values*.

4.3 Temporal variability and immigration

In section 4.2 we concluded that immigration is required for our model to produce persistent communities. Therefore to study communities that are persistent in pristine landscape, but exhibit HL induced extinctions, we must investigate the region between zero immigration and the *default rate* ($IR \sim 0.005$). As we began to investigate this region we found a robust feature of the model: reducing immigration rate *increases the temporal variability* of the dynamics. We again measure temporal variability using *mean_CV* (section 2.8.2), i.e. the coefficient of variation in species population dynamics, averaged over all species in the community. In the previous chapter *contiguous* habitat loss was shown to increase temporal variability, up to a average value of ~ 0.3 at $HL = 90\%$ (figure 3.16). Figure 4.12 illustrates that reducing the immigration rate can push the temporal variability well above this level, even in pristine landscape.

This increased variability may bring into question the validity of results derived from the simulation output. Implicit in our analysis so far is the assumption that the system reaches *steady-state* by the end of the simulation (see section 3.2.2). If the system is not at steady-state then our results, especially those calculated from snapshots or short samples, may not be reliable. In the high immigration regime (HIR) the steady-state assumption may be reasonable. From inspection, the HIR simulations contain transient dynamics within the first 1000 time steps,

followed by a period of relatively constant abundance (see for example figure 2.5). However the high level of temporal variability illustrated in figure 4.12 now motivates us to question whether the system does reach steady-state, especially at low IR. Therefore, in section 4.4, we conduct a detailed analysis of the *stationarity* of population dynamics generated by the IBM model. We then consider whether the increased variability is due to stochastic or deterministic effects. In section 4.5, we use *recurrence quantification analysis* to look for signatures of determinism in the simulation output. Finally we close the chapter (section 4.6) by looking at how the accuracy and reliability of our numerical results are affected by increased variability, and how sensitive the results are to the sampling regime used.

4.4 Second-order stationarity

In this section we consider the stationarity of the IBM simulation output. As discussed above, the sampling procedure employed in chapter 3 assumed that the simulations reach steady-state. By testing for stationarity we now examine that validity of this assumption. The ecological implications of stationarity are less clear. We saw in section 2.8.2 that, although stability is an important topic in the ecological literature, there is no consensus on whether natural ecosystems exist in a steady-state. This is a philosophical point, and we do not discuss it further here. However, it is important to note that there is no *a priori* requirement for stationarity imposed by ecological realism. Rather, the modelling in this section serves to shed light on the contexts in which non-stationarity may be observed in nature, and the factors contributing to it.

We introduce here three tests for second-order (or ‘weak’) stationarity in time series. Second-order stationarity may be defined as the time invariance of the first and second moments of the data. Specifically Hsu [?] states that a random process $X(t), t \in \mathbf{Z}^+$ is second-order stationary if:

$$\begin{aligned}\mathbf{E}[X(t)] &= \mu \text{ (constant)}, \\ R_X(t,s) &= \mathbf{E}[X(t)X(s)] = R_X(|s-t|),\end{aligned}$$

where $R_X(t,s)$ is the *autocorrelation* function of the process. Conceptually these conditions state that a second-order stationary time series has constant mean, and an autocorrelation dependent only on time separation. From now on we refer to a time series satisfying (4.1) and (4.2) as *stationary*. If the conditions are not met we call the time series *non-stationary*. Non-stationary time series cannot be fit to a constant distribution. Non-stationarity may be due, for example, to a trend in the data or a change in the parameters of the data generator.

In our case the data generator is the IBM model and there are several possible causes of non-stationarity. It may be that there is no steady-state equilibrium in the model. For example the number of individuals may undergo a random-walk. From previous analysis this situation seems unlikely, since we have observed what appear to be deterministic population cycles.

However randomness has not been explicitly tested for. Another possibility is that the dynamics is characterised by large amplitude oscillations in abundance, which produce non-stationarity. Again such oscillations have not been tested for. Alternatively a steady-state equilibrium may exist, but a long period of transience means it is not reached during the time frame of our simulations (5000 time steps previously).

4.4.1 Tests for stationarity

We compare three different tests of stationarity: the Kwiatkowski-Phillips-Schmidt-Shin (KPSS) [?]; the Augmented Dickey-Fuller (ADF) [?]; and the the Priestley-Subba Rao (PSR) [?] tests. These tests were chosen for their popularity in the time series literature. All three are implemented in the programming language *R* [140]. The KPSS and ADF are provided in the *tseries* package, and the PSR is in the *fractal* package. All three tests are applicable to univariate time series.

The ADF test has a null hypothesis (H_0) that the time series is non-stationary. The test models the data as an auto-regressive process, and the null hypothesis is that this process has a *unit root*. The test produces a statistic that is negative. The greater the magnitude of the test statistic the more evidence there is to reject H_0 in favour of stationarity.

The KPSS test complements the ADF test in that the null hypothesis is stationarity. The data is modelled as the sum of a random-walk and an error component, and tests the hypothesis that the variance of the random walk is zero. The test statistic is always positive, and the greater its magnitude the more evidence there is to reject H_0 in favour of non-stationarity.

The null hypothesis of the PSR test is also that the series is stationary. The test is based on the idea that non-stationary processes have power spectra that change over time [?]. These are called *evolutionary spectra*. The test, as implemented in *R*, returns several statistics. We quote the ‘p-value for T’ which can be thought of as the confidence that the estimated spectral density functions are constant in time.

4.4.2 Characterising the tests

To understand the performance of the stationarity tests (section 4.4.1) we apply them to three example time series, which we refer to as HI, RW and NS. The first series, HI, is taken from a single IBM simulation run with $IR = 0.001$, zero mutualism ($MAI = 0.0$) and otherwise default parameters (table 2.1). The series represents the total number of individuals of all species at each time step. The simulation was run for 50,000 time steps, compared with the 5000 used in previous chapters. The increased length allows more time for the simulation to reach steady-state, and allows comparison of tests applied to different sections of the series. The first 1000 time steps were discarded, since these contain clearly transient dynamics (see figure 4.15B), leaving a time series of 49,000 points. The IR used is lower than the *default value*, but an order or magnitude higher than the lowest IR used in this chapter (see figure 4.12). The rate $IR = 0.001$

was chosen because it gives slightly increased temporal variability over the default value and therefore increased chance of non-stationarity. In the context of what follows we refer to IR as high immigration (HI).

The series RW and NS are chosen as a negative and a positive control respectively. Both have the same length as HI. RW is a non-stationary series generated by a one-dimensional *random-walk*, defined as:

$$x(t) = \sum_{i=1}^{t-1} Z_i,$$

where Z_i are independent random variables that may take a value of either -10 or $+10$, both with probability half. An ensemble of such random walks was generated and a single instance was chosen with mean and variance closest to those of the HI series. RW has mean and standard deviation of 15525.2 and 1549.8 respectively, compared to 15915.8 and 1545.6 for HI. For comparison, NS is a stationary series generated by drawing each value independently from a normal distribution with mean and variance equal to that of HI. The three series are plotted in figure 4.13.

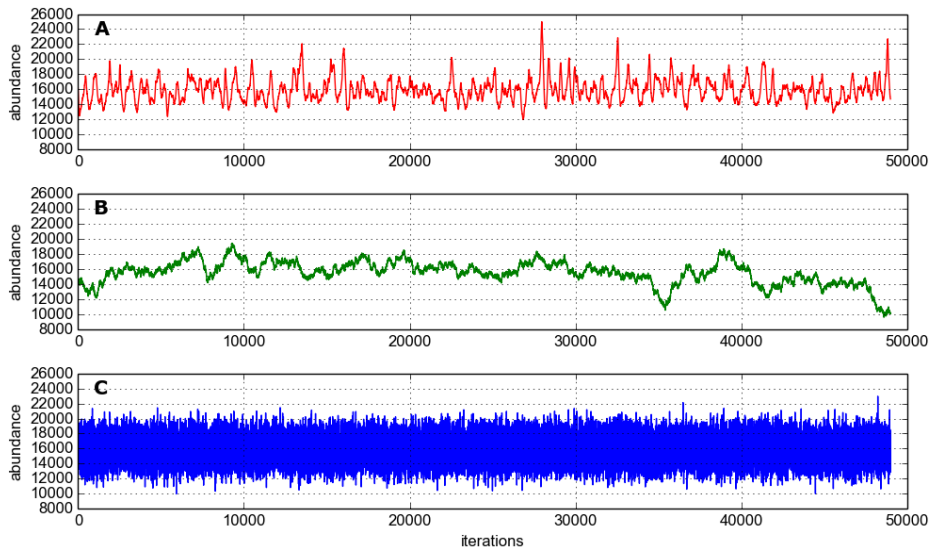


Figure 4.13: The three time series used to characterise the performance of the stationarity tests (see text for details of how they are generated). The initial 1000 points are removed such that all are 49,000 points long. **(A) HI:** total abundance dynamics of a simulation with high immigration rate; **(B) RW:** a random walk without drift; and **(C) NS:** a series generated by independent sampling from a normal distribution.

Initially we apply the three stationarity tests to the entire length of the time series. The results are shown in table 4.1. ADF finds significant evidence that all three series are stationary, at 99% confidence. We may be suspicious of this result since we know that RW is generated by

| | A.D.F. | | P.S.R. | | K.P.S.S. | |
|----|----------|---------|--------|--------------|----------|---------|
| | stat | p-value | stat | p-value | stat | p-value |
| HI | -15.401 | <0.01 | - | 0.0004782808 | 0.5395 | 0.03277 |
| RW | -4.0386 | <0.01 | - | 0.9929773 | 18.7453 | <0.01 |
| NS | -37.5348 | <0.01 | - | 0.811097 | 0.0466 | >0.1 |

Table 4.1: Results of applying the three stationarity tests to the three time series shown in figure 4.13. P-values that indicate evidence for stationarity at 95% confidence are highlighted in green. The test statistics are also given for the ADF and KPSS tests.

a non-stationary process. However RW is a particular instance of a random walk, chosen from several thousand to closely match the mean and variance of HI. Therefore this random walk is likely to appear more stationary than others in the ensemble generated. The test statistic for ADF indicates that there is most evidence for NS to be stationary, followed by HI, then RW. The KPSS test ranks the series in the same order, based on the magnitude of the test statistic. According to this test NS is clearly stationary (accept H0), and RW is clearly non-stationary (reject h0 at 99% confidence), whilst HI is borderline. For HI we would accept the null-hypothesis of stationarity at 95% confidence, but reject it at 99%.

The PSR test gives unexpected results. It concludes that RW and NS are both stationary, whilst HI is non-stationary with a high degree of confidence (p-value < 0.001). In fact, according to PSR, RW is more likely to be stationary than NS. This result contradicts what we know about the data generators that produced the time series. Therefore we do not use this test in the analysis that follows. Nevertheless the apparently erroneous result may contain interesting information about the HI series and the process that generated it.

Having discarded the PSR test, we now apply ADF and KPSS to samples of varying sizes, taken from the three series (HI,RW,NS). Sampling begins at the first point of the series and takes consecutive points up to the desired sample length. Sample lengths range from 1000 to 49,000 data points. Again, as we saw in table 4.1, the two tests perform differently. The KPSS test correctly identifies RW and NS as non-stationary and stationary respectively, for all sample sizes. This is shown in figure 4.14B. The ADF test (figure 4.14A) correctly identifies NS as stationary for all sample sizes. For short sample sizes it also correctly identifies RW as non-stationary. However, for sample sizes much above 20,000, ADF finds significant evidence that RW is stationary at 95% confidence. This is an interesting result. Although RW is generated by a non-stationary process, it appears to fool the ADF test by staying ‘stationary enough’ over many time points.

There is mixed evidence for the stationarity of HI, as shown in figure 4.14. ADF, for all sample sizes above 2000, finds significant evidence that HI is stationary. Whereas KPSS, on the whole, gives significant evidence that HI is non-stationary - There are only seven cases where there is insufficient evidence to reject the null hypothesis that the HI series is stationary, and these occur at sample sizes between 24,000 and 34,000. *From these results it appears that the KPSS test is a stricter test of stationarity, and is less sensitive to the size of the sample.* Although it

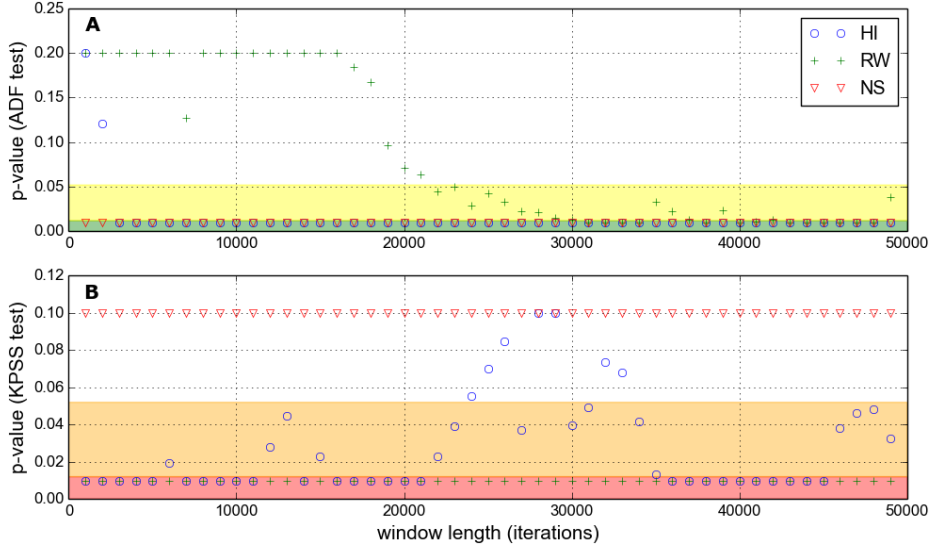


Figure 4.14: Two tests for stationarity applied to samples of varying size (window length). Samples are taken from the three time series (HI,RW,NS) shown in figure 4.13. All three time series contain 49,000 points. Sample windows begin at the first point and increase in length from 1000 to 49,000 points. Minimum p-value plotted is 0.01, actual values may be lower. (A) ADF test, with p-values capped at 0.20. The 95th and 99th percentile shaded yellow and green respectively, indicate significant evidence for stationarity. (B) KPSS test, with p-values capped at 0.1. The 95th and 99th percentile shaded orange and red respectively, indicate significant evidence for non-stationarity.

appears that the ADF test is biased in favour of stationarity, the test statistic does order the series correctly in the above examples (table 4.1) and is a useful complement to KPSS. Also it may be that the sensitivity of ADF to sample length is useful, since processes may appear stationary/non-stationary at different scales.

We consider the possibility that the method of sampling from the time series affects the results of the stationarity tests. For example samples taken near the beginning of an IBM simulation run may be more likely to give the non-stationary series because of transient dynamics. Alternatively a non-stationary data generator may produce sections of time series that appear stationary purely by chance. This sensitivity to sampling is investigated by *reversing* the time series and repeating the above analysis. For HI, RW and NS we see no qualitative change in the results presented above (therefore results not shown). We also scan sampling windows of fixed length along the series to look for time dependence in the test results. The time at which samples are taken appears to make no qualitative difference, and there is no systematic change in the results that would suggest the simulation becomes more stationary the longer it is run (again results not shown).

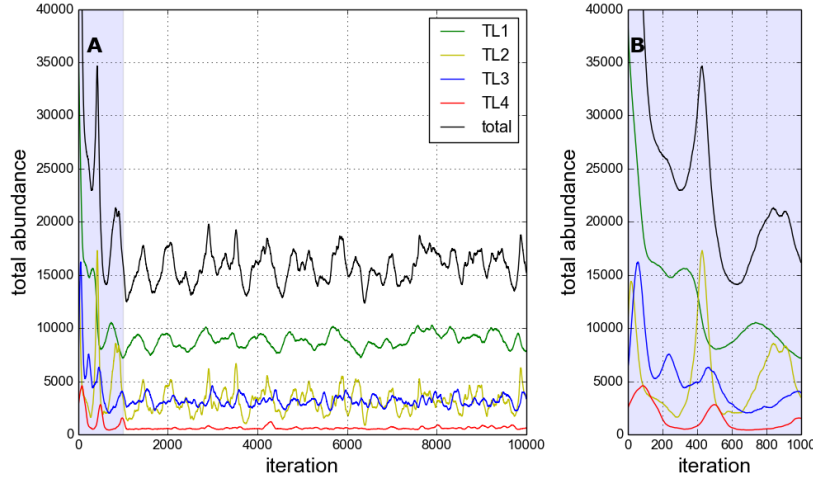


Figure 4.15: Population dynamics from HI ($IR = 0.001$) simulation: total number of individuals, and by trophic level. (A) First 10,000 time steps of simulation run (total = 50,000 time steps). (B) Enlargement of first 1000 tim steps, showing transience.

HI simulation. We now focus on the simulation data used to generate HI and look in more depth at whether this dataset can be considered stationary. We use the same two tests, ADF and KPSS, for the stationarity of univariate time series. Since our abundance vector is 60-dimensional ($N = 60$ species), it is necessary to perform some manipulation to get a time series we can test. Previously we used the total number of individuals as our time series. However simply summing over species (L1-norm) is not necessarily the most informative metric to use. One possible issue is due to the phase differences between species oscillations that we might expect due to trophic interactions. Such oscillations may mean that temporal variability is cancelled out when aggregating abundances in this way (see discussion on ecosystem synchrony, section 3.3.4). It is possible that simulations which appear stationary according to some aggregate metric (e.g. total number of species) may have non-stationary underlying dynamics. This suggests that it is most informative to consider stationarity at the species level. We also consider the stationarity of abundances by trophic level, as an alternative aggregate metric.

The dynamics of the HI simulation are aggregated by trophic level to create four new time series TL1 – 4. These *trophic dynamics* are plotted in figure 4.15, and display visibly more variability than the equivalent plot produced using the default IR (figure 2.5). The initial period of transience is expanded in panel B. As in the previous analysis this part of the time series (first 1000 time steps) is removed. The ADF and KPSS tests are applied to the four trophic series separately and the results are shown in figure 4.16. According to ADF all trophic levels are stationary for samples sizes greater than 4000. TL1 appears to be least stationary according to ADF, requiring a sample size of at least 4000 to reject the null hypothesis at 95% confidence. According to KPSS TL1 is non-stationary for all sample sizes, whilst TL2 and 3 are stationary

for samples sizes above 6000 and 1000 respectively. KPSS gives mixed results for TL4, with no clear dependence on sample size. It is hard to reconcile these results with an observation of the dynamics in figure 4.15, indicating the usefulness of the statistical tests.

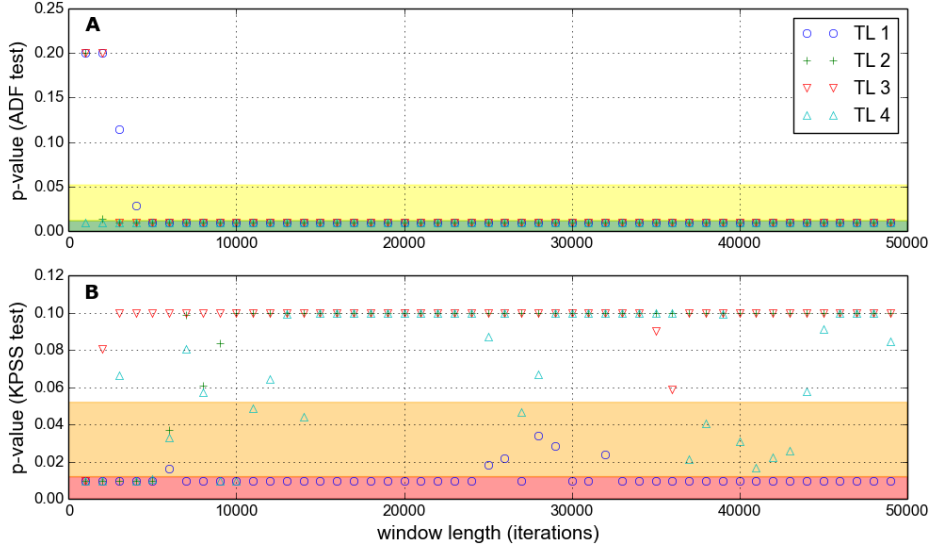


Figure 4.16: Similar to figure 4.14, but here the tests are applied separately to each trophic level of the HI simulation shown in figure 4.15.

The dynamics of all the species belonging to each trophic level are plotted in figure 4.17. It is clear here that the community is dominated by a few abundant species, mainly in the lower trophic levels, with a large number of relatively scarce species. This agrees with the rank abundance plots from chapter 3. It also appears from this figure that the more abundant species exhibit large amplitude oscillations in their dynamics. This leads us to hypothesise that the most abundant species may be non-stationary, whereas the least abundant species may be stationary. We test this hypothesis by applying the ADF and KPSS tests to the three most abundant and three least abundant species in the HI simulation. Species are selected based on their average abundances over the whole simulation (minus the initial transience).

We see from figure 4.18 that all six species are stationary according to ADF, given a sufficiently large sample size. However the sample size for all three of the abundant species to be stationary is greater (panel A: $\geq 9,000$ points) than for the three least abundant species (panel C: $\geq 2,000$ points). This suggests that the most abundant species are indeed less stationary than the least abundant species. The KPSS test supports this conclusion. KPSS finds that the three least abundant species are stationary above sample sizes of $\sim 18,000$, whereas two of the most abundant species are non-stationary for almost all sample sizes. Inspecting the dynamics in figure 4.17 we see that these non-stationary species are those with largest amplitude fluctuations in their abundances.

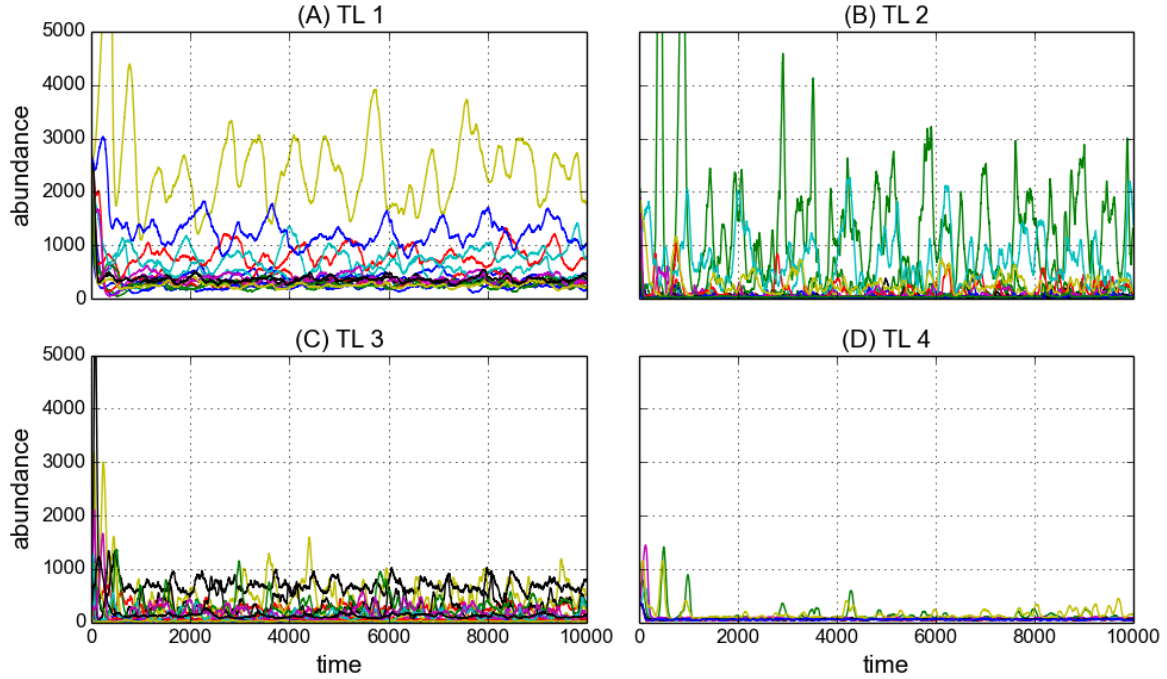


Figure 4.17: Dynamics of all species in the first 10,000 time steps of the HI simulation shown in figure 4.15. Each colour represents of different species, each panel (A-D) shows a different trophic level (TL1 – 4).

In general we conclude that the choice of metric used to generate the time series does affect the conclusions about stationarity. Overall we cannot be confident that the HI simulation is stationary, based on the results presented above for species, trophic and total abundances. This lack of stationarity is largely due to the apparent strictness of the KPSS test. We also assert that considering species dynamics individually is the most informative. It allows for the possibility that some species abundances may be more variable than others, and information is not lost due to aggregation. In the following analysis we apply stationarity tests to species dynamics individually, and calculate the number of stationary species (NSSP) as an aggregate statistic. If NSSP equals the total number of species, then the community dynamics is fully stationary according to the test used.

4.4.3 General stationarity results

We now conduct a general investigation of the stationarity of communities simulated with the IBM model. First we test the stationarity of three ensembles of new simulation runs (figure 4.19). The new simulations use default parameters, unless otherwise specified, and are run for 50,000 time steps. Two ensembles of 100 simulations each are run for high ($IR = 0.001$) and low ($IR = 0.0001$) immigration rates, which we refer to here as the HI and LI ensembles

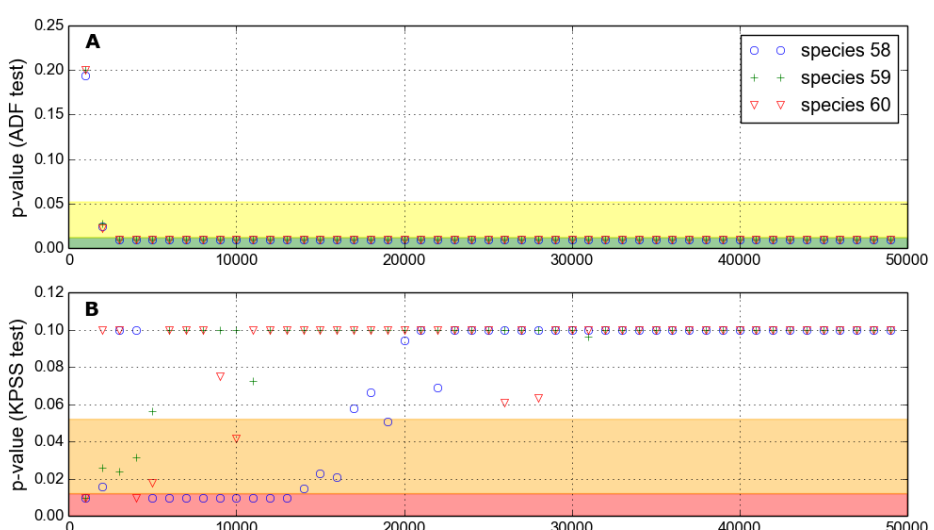
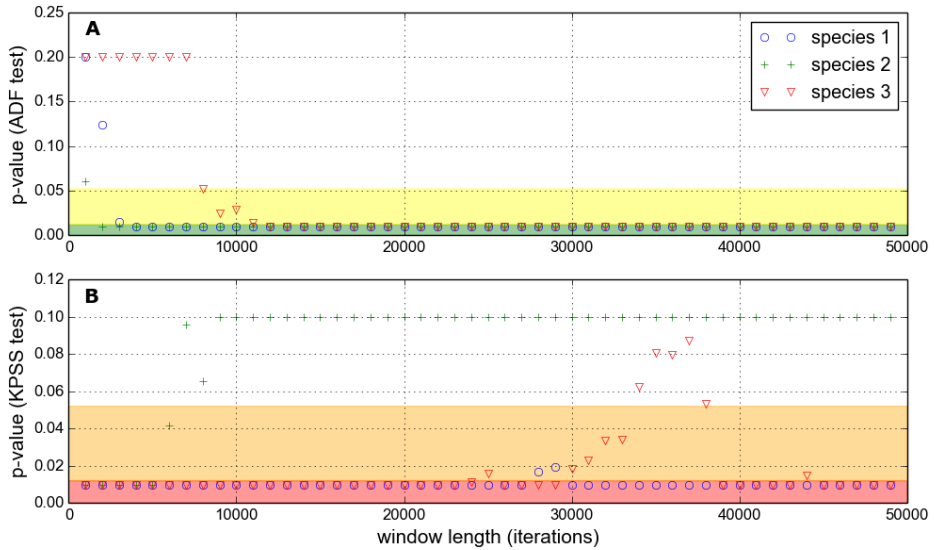


Figure 4.18: Similar to figure 4.14, but here the tests are applied separately to individual species from the HI simulation shown in figure 4.15. (A) The three species with highest long-term average abundance. (B) The three species with lowest long-term average abundance.

respectively. All networks are generated using the niche model as described in section 2.3, with zero mutualism ($MAI=0.0$), and each simulation uses a uniquely generated network. A third ensemble of 50 shorter simulations (10,000 time steps) is run, at high immigration rate, using a fixed interaction network selected at random from the HI ensemble. This third ensemble we call NM1. Stationarity testing is done using the ADF and KPSS tests characterised in section 4.4.2 above. As standard the initial 1000 time steps are discarded in an attempt to remove transience. The tests are then applied to a sample taken from the abundance time series of each species. The results presented in this section give the number of stationary species (NSSP) in the community, at the 95% confidence level.

As the length of the samples taken from the abundance time series increases, the average NSSP also increases. This is true of both tests and for all three ensembles, as we can see from figure 4.19A. According to ADF all species are stationary, on average, for sufficiently large sample length. The required length of sample is larger for the LI ensemble than for HI. For KPSS, although the NSSP does increase with sample length, it is not clear that it will asymptotically approach 60 species in the limit of many time steps. The average NSSP at 49,000 sample points is just under 40 and just over 20 for HI and LI ensembles respectively.

To check the time dependence of stationarity (i.e. are species more likely to be stationary towards the end of a simulation) samples of length 3000 were taken from different points along the time series. From figure 4.19B we can see that there is no clear trend in stationarity over 49,000 time steps. The average NSSP is almost the same whether the sample is taken from time steps 1000-3000 or 46,000-49,000. This lack of time dependence in NSSP also holds for windows of different length (results not shown).

On average we see that the LI ensemble is less stationary than the HI ensemble. This we expected based on the previous observation that reducing IR increases temporal variability. However we cannot be confident that either ensemble contains communities in which all species are stationary. This observation may be problematic for the interpretation of our results, and we discuss this further below. Interestingly the NM1 ensemble gives very similar results to the HI ensemble. It may be that stationarity of the simulation output is not dependent on the interaction network structure. Alternatively the observation may be anomalous, owing to the fact that we have accidentally chosen NM1 to closely resemble the average of this ensemble (see both panels of figure 4.19).

In chapter 5 we will explore a slice of the IBM parameter space by varying both immigration rate and habitat loss. Here we study the stationarity of the simulations that we will use in that chapter. All simulations are 5000 time steps long. The initial 1000 time steps are discarded and the ADF and KPSS tests applied, species by species, to the remaining 4000. Figure 4.20 shows the average NSSP across the region of parameter space investigated, for three MAI ratios ($MAI=0.0, 0.5, 1.0$). The results are qualitatively the same for both tests, although NSSP is higher for ADF than for KPSS as expected. On average reducing IR reduces the NSSP. A weaker, but

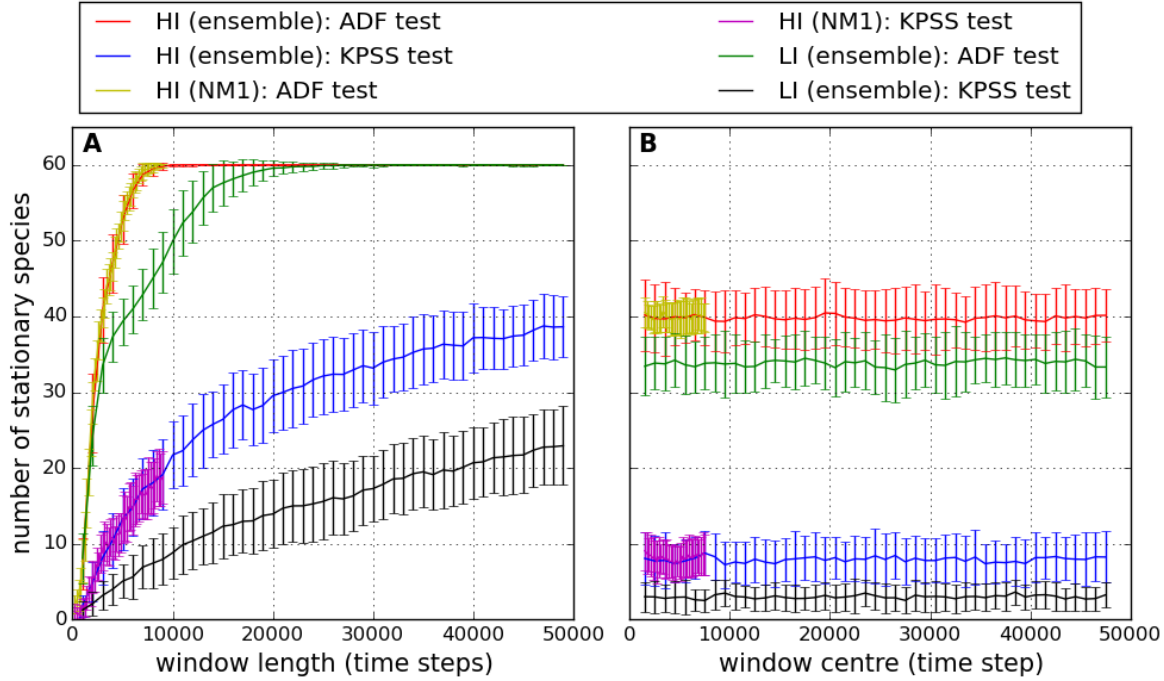


Figure 4.19: The number of stationary species (NSSP) according to the two stationarity tests (ADF and KPSS) at the 95% confidence level. Results averaged over three different ensembles of simulations: HI; NM1 (high immigration) and LI as described in the text. The first two are high immigration ensembles, whilst the latter is low immigration. Solid lines indicate mean results for the ensemble. Error bars indicate ± 1 standard deviation. (A) Each species abundance time series is sampled with a window of increasing length, as in figure 4.18. (B) Each species time series is sampled with a window of length 3000 time steps, which is scanned along the series to check for changes in stationarity over time.

still visible, effect is that increasing HL reduces the NSSP. Most striking is the effect of MAI ratio on stationarity. The average NSSP is greater across the whole parameter region at $MAI = 0.0$ than at $MAI = 1.0$, with $MAI = 0.5$ in between the two. Increasing mutualism also appears to reduce the dependence of NSSP on IR. Figure 4.21 summarises these trends using cross sections taken from the ADF heat maps (panels A,C,E) in figure 4.20, with error bars added. It is clear that there is high variability across replicate simulations, and this variability appears to be greatest for high mutualism ($MAI = 1.0$).

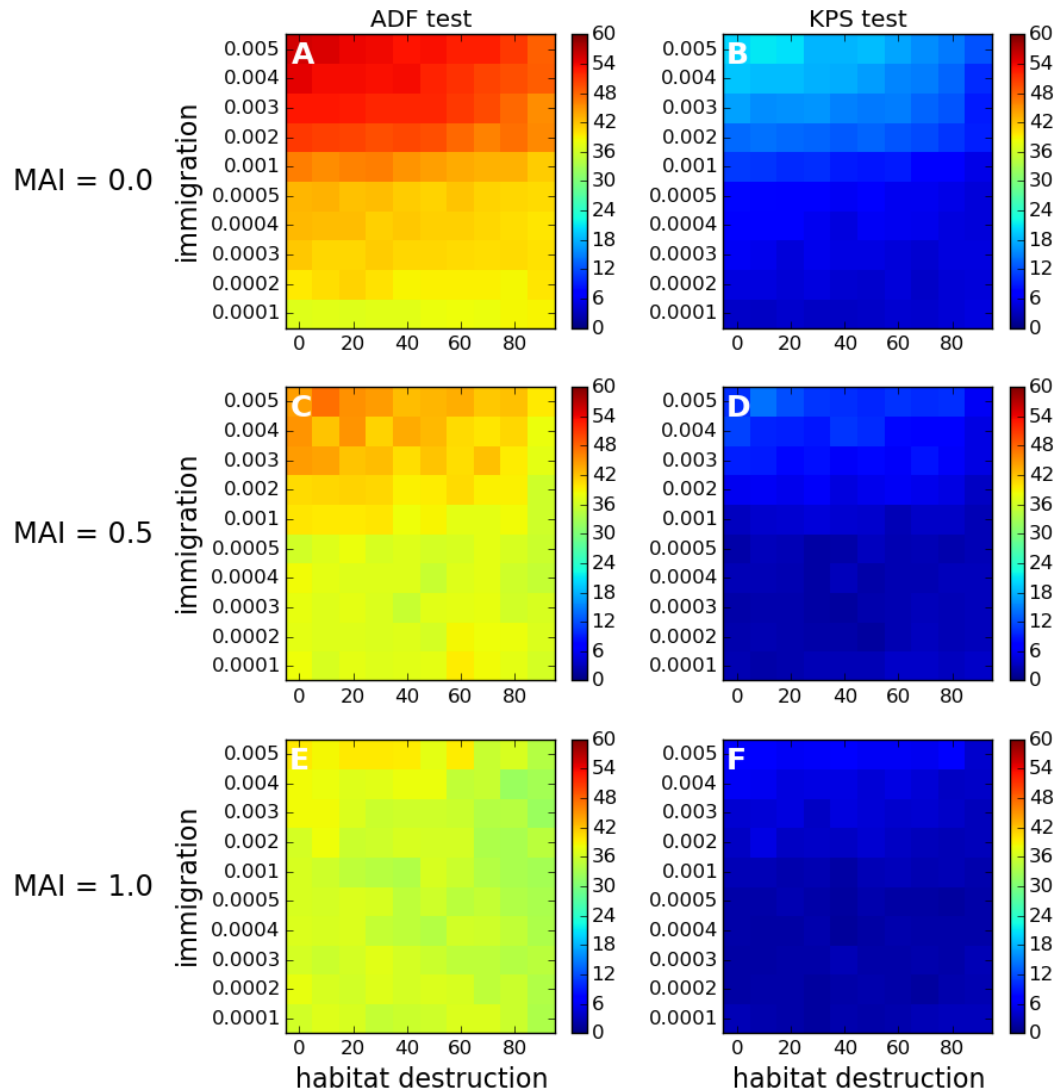


Figure 4.20: The average number of stationary species (NSSP) according to the two stationarity tests (ADF and KPSS) at the 95% confidence level. Each cell on the grid represents the mean value over 50 repeat simulations. All simulations are 5000 time steps with default parameter values. Tests are applied to the final 4000 time steps of each species abundance time series. These correspond to the simulations presented in chapter 5.

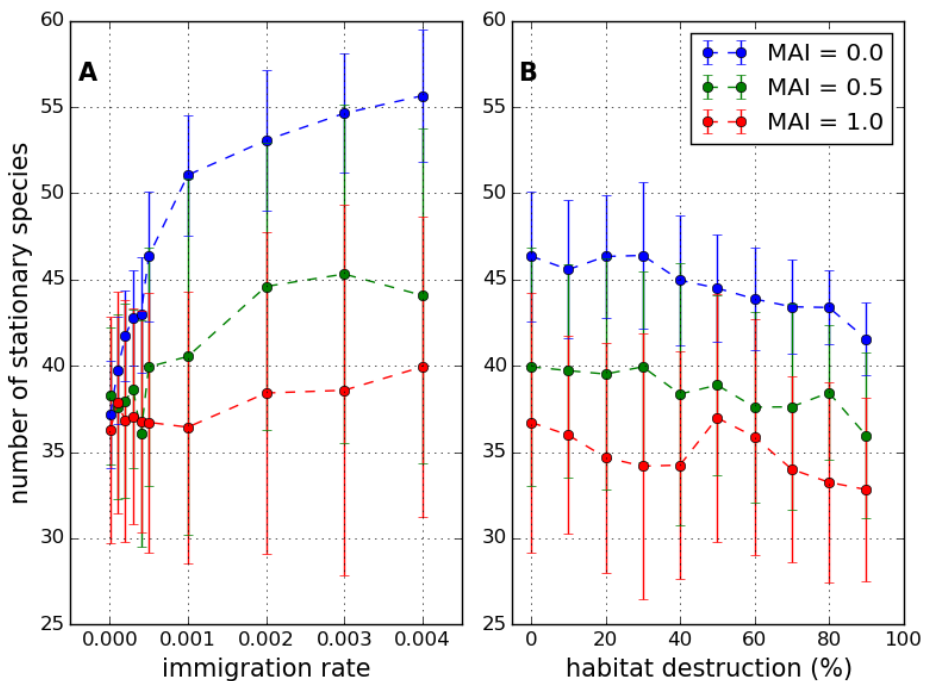


Figure 4.21: The number of stationary species (NSSP) according to the ADF test at the 95% confidence level. Points show mean value over 50 replicates. Error bars show ± 1 standard deviation. Tests are performed on the same simulations depicted in figure 4.20. (A) Plotted against immigration rate (IR), with zero habitat destruction. (B) Plotted against habitat destruction, with IR=0.001 (high immigration regime).

4.5 Testing for determinism

We have seen that population dynamics becomes highly variable, especially at low IR, and indeed may not be stationary. This leads us to speculate that in some instances the simulation output may become dominated by stochastic effects. This randomness is an interesting feature of the model, and indeed noise is ubiquitous in natural systems. However much of our analysis (chapters 3 and 5) involves interpreting the simulation results in terms of the ecological mechanisms built into the model, in particular the patterns and structures generated by species interactions. If the model output lacks determinism it may not be meaningful to conduct such analyses. Therefore we present here a test for determinism based on *recurrence quantification analysis* (section 4.5.1), which we then apply to the IBM output (section 4.5.1.1).

4.5.1 Recurrence quantification analysis

Recurrence quantification analysis (RQA) may be used to detect signatures of determinism [? ?]. The analysis is based on the idea of *recurrence* - deterministic dynamical systems tend to return to similar regions of phase space. Moreover, when they do, their trajectories tend to remain close in phase space for some amount of time. In the case of chaotic systems the trajectories will diverge, at a rate which is broadly determined by the maximal Lyapunov exponent [?]. However, even for chaotic systems, there is some tendency for neighbouring trajectories to remain close. RQA aims to detect the presence of this feature in the dynamics. The analysis is often used with univariate time series (such as in [?]), in which case time-delay embedding must be used to increase the dimensionality of the phase space. However, since we have a time series for each of the 60 species, our phase space is already high dimensional. Therefore our first step is to construct a recurrence matrix (RM). The RM is a binary matrix whose elements, for a system $x(t) \in \mathbb{R}^N$, are given by the function:

$$d_{ij} = \begin{cases} 1 & \text{if } \|x(i) - x(j)\| < r \\ 0 & \text{if } \|x(i) - x(j)\| \geq r \end{cases},$$

where r is a threshold distance that defines the measure of ‘closeness’ in phase space. Various methods have been proposed to choose the value of r . These methods are discussed in [?], but we use the method which they adopt for the results in that paper: r is chosen such that $\sim 10\%$ of the elements of the RM are equal to one.

Having constructed the RM it can be visualised as a *recurrence plot* (Figure 4.22). Such plots can be visually striking (search recurrence plots for examples), but are difficult to interpret without experience. An important feature, in the search for determinism, are *diagonal lines* - lines parallel to the leading diagonal. Such lines indicate that trajectories which find themselves ‘close’ in phase space remain close, for a period of time given by the length of the line. Visual

inspection can detect the presence of diagonal lines but it is better to use a quantitative pattern detection method. A common metric that quantifies the relative abundance of diagonal lines is the *percentage of determinism* (%DET) [? ?], and is given by:

$$(4.3) \quad \%DET = \frac{NPD}{NREC} \times 100,$$

where NREC is the number of entries in the RM equal to one; and NPD is the total number of points found on diagonal lines of length greater than or equal to two. The %DET allows quantitative comparison of the level of determinism between different RMs. In [?] they develop three statistical tests, based on %DET and two similar metrics, for the null hypothesis of pure randomness in the time series. However in the current analysis we make do with a comparison of the value of %DET between different test cases.

4.5.1.1 Results

We test for determinism in the simulation ensembles HI and LI used in section 4.4 (see for example Figure 4.19). Each ensemble consists of 100 repeat simulations with different network structures. These simulations are used because one ensemble is from the high immigration regime (HI: IR= 0.001) and one is from the low immigration regime (LI: IR= 0.0001). Therefore the temporal variability is higher on average in the LI ensemble than the HI ensemble, allowing us to study how temporal variability relates to determinism. The length of the simulations in these ensembles is 50,000 time steps, all communities are antagonistic (MAI= 0) and the landscape is pristine (HL= 0).

We construct randomised control data in two different ways. The control data is used to compare %DET results from the IBM with %DET values generated by randomness. In [?] they state a random process would generate a RM with NREC points distributed uniformly at random. We construct such matrices by randomly permuting the elements of another RM, to obtain a randomised RM with the same number (NREC) of points. The second method is to construct RMs by randomising the order of the time series of each species. This preserves the mean and variance of the population dynamics, but removes any determinism. The randomised time series are then used to construct an RM.

Figure 4.22 shows four example recurrence plots. Panels A and B show the RMs of single simulations from ensembles HI and LI respectively. Panels C and D show randomised versions of panel B generated by randomising the matrix, and by randomising the time series respectively. Panels A and B clearly have some structure, whilst the structure is lost in panel C as expected. Panel D retains some structure. In particular it contains the leading diagonal, since even the randomised time series is identically equal to itself. It also contains horizontal and vertical bands, created by points in the time series that are unusually distant (or close) to a large number of other points in the phase space. A subtle but detectable feature of panels A and B is the presence

of diagonal lines (parallel to the leading diagonal) suggesting determinism. This feature is lost in panel D, as we would expect due to the randomisation of the time series. Interestingly panel A looks very similar to figure 1(c) in [?]: an RM generated from the dynamics of a noisy chaotic Henon attractor. This leads us to speculate that the deterministic component of the dynamics may be chaotic. We do not search for signatures of chaos, partly because the presence noise severely complicates the available methods for doing so (such as estimation of the Lyapunov exponent)[?].

We calculate the %DET for each simulation in the HI and LI ensemble. In each case, for comparison, we also calculate the %DET for the dynamics of the ten most and ten least abundant species, and for the two randomised versions of the data. These results are shown in figure 4.23. The randomised data shows little variation, with a $\%DET \approx 10$ in all cases. The %DET for the least abundant species is slightly greater than for random data, suggesting some evidence of determinism but also a strong stochastic component. In both the HI and LI ensembles there is good evidence for determinism at the whole community level, with %DET consistently > 30 and > 40 respectively. It is interesting that there is more evidence of determinism in the LI ensemble than in the HI ensemble, as we were previously concerned that the high temporal variability of the LI dynamics could mean that it lacked determinism. It is also clear for these results that the deterministic component of the dynamics is dominated by the most abundant species. This, together with the results from previous sections tells us a lot about the dynamics of the model (see discussion in section 4.7). We conclude here that the analysis so far suggests that non-stationarity may be largely due to deterministic population dynamics/oscillations of the most abundant species, while the dynamics of the less abundant species are more random and more stationary, although they do have a deterministic component.

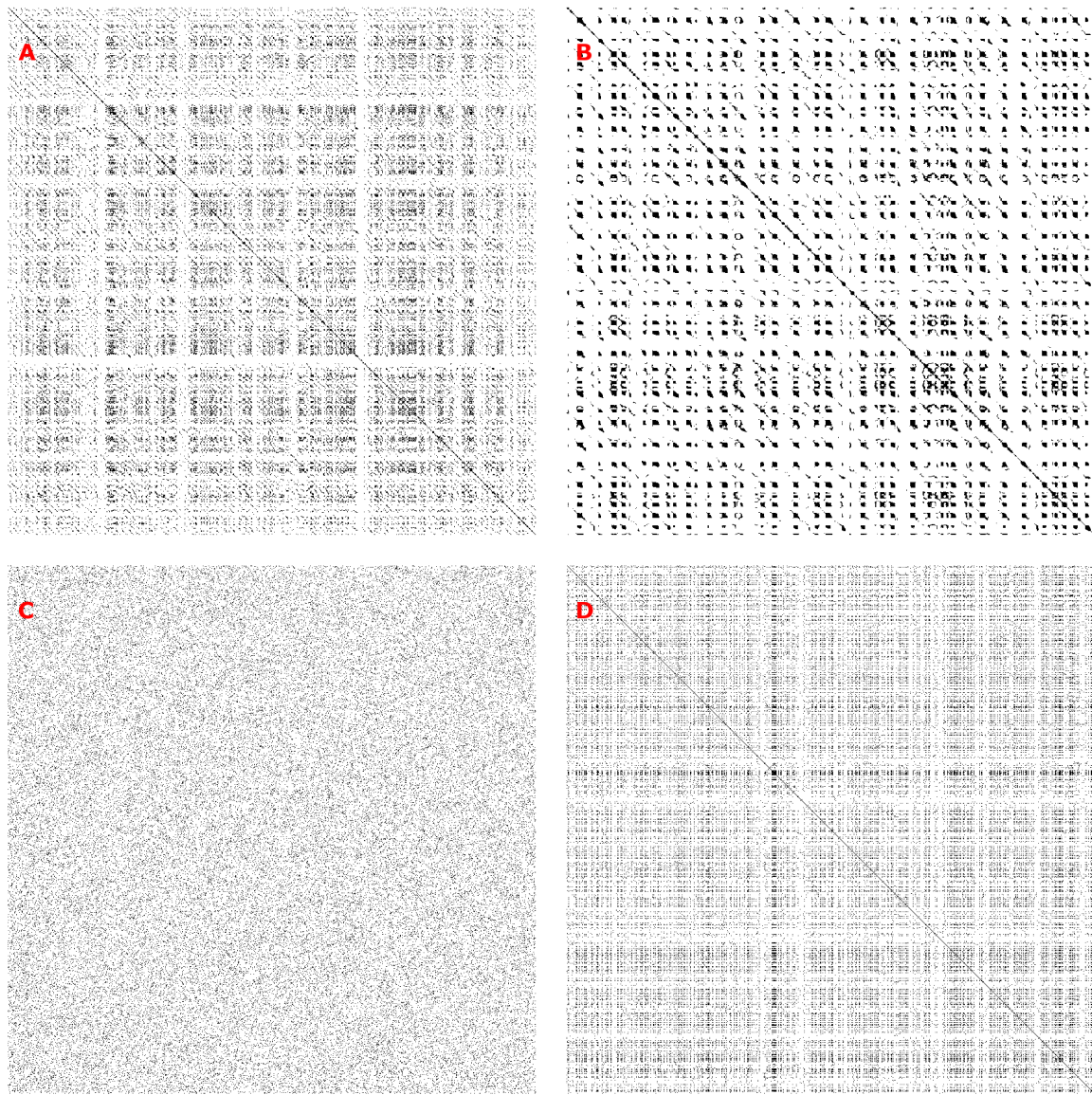


Figure 4.22: **Recurrence plots** defined by equation 4.5.1. (A) High immigration simulation ($IR=0.001$). (B) Low immigration simulation ($IR=0.0001$). (C) Randomised recurrence matrix (permutation of the elements of the matrix in B). (D) Randomised time series (permutation of species population time series from B, such that mean and variance for each species are preserved). In simulations for both A and B: $HL=0$ and $MAI=0.0$; number of time steps = 50,000; sampled every 50 time steps to construct plots.

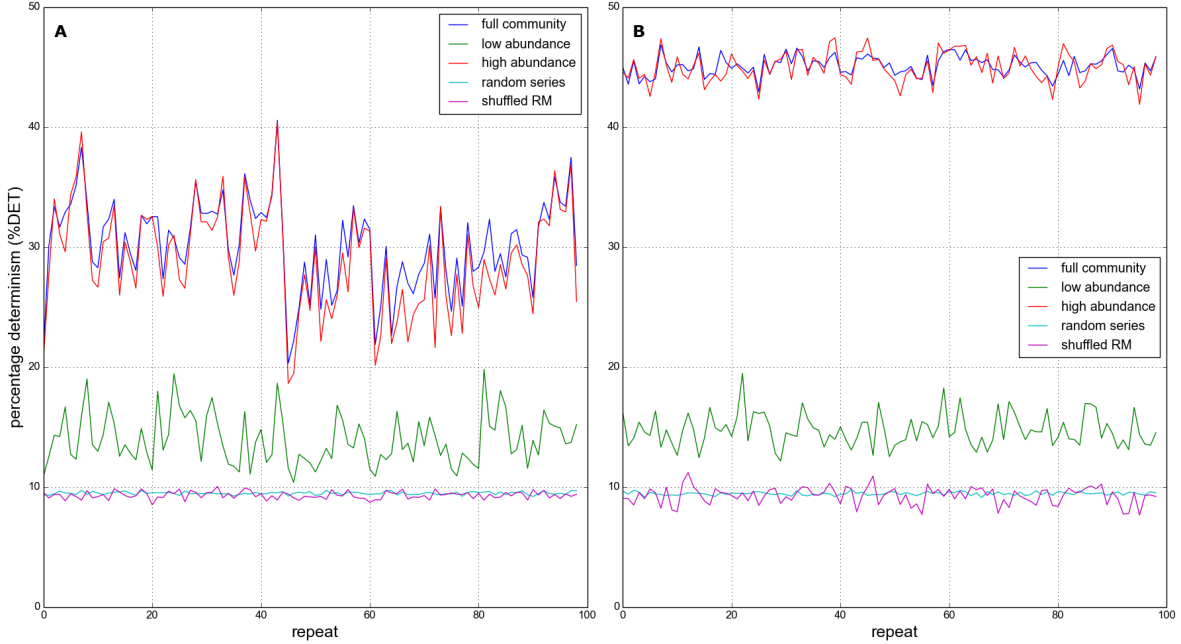


Figure 4.23: Percentage determinism (%DET) defined by equation (4.5.1). Value calculated for whole community, ten least and ten most abundant species, and for two randomised versions of the data (see text). For 100 repeat simulations at: (A) High immigration rate ($IR=0.001$); and (B) Low immigration rate ($IR=0.001$). In simulations for both A and B: $HL=0$ and $MAI=0.0$

4.6 Convergence and repeatability

In chapter 3, and at the beginning of this chapter, we used ‘snapshots’ of the simulation state to calculate species abundances. The snapshot method was justified by the assumption that simulations reached stationarity and therefore we were sampling from a steady-state distribution. However, as we saw in section 4.3, stationarity cannot be guaranteed. The results of section 4.5 suggest that this lack of stationarity is due to deterministic population dynamics, especially those of the most abundant species. With oscillatory dynamics it is clear that snapshot sampling will yield different results depending on when the measurement is taken. We make the assumption that the best way to characterise the system is to take the long-term average of the metric in question. This approach is also justified by the observation that stationarity does not increase or decrease over the course of a simulation, but remains relatively constant (figure 4.19B). In section 4.6.1 we look at how temporal variability affects the *convergence* of our results on the long term average. In section 4.6.2 we consider the *repeatability* of our results by running replicate simulations with the same network structure and parameter values.

4.6.1 Convergence

In this section we compare the performance of different estimators for species abundance. Specifically we look at estimates of abundance obtained by averaging over increasing sample lengths, and study the convergence of these estimates on the long-term average abundance. In all that follows the initial 1000 time steps are removed from the simulated time series, as has been done throughout the chapter. Therefore when we refer to a time series below, we refer to this truncated version of the time series with the initial transience removed. We define the long-term average abundance of species i as:

$$(4.4) \quad \bar{X}_i = \frac{1}{T} \sum_{t=1}^T x_{i,t},$$

where T is the number of time steps in the time series, and $x_{i,t}$ is the abundance of species i at time point t . We denote by e_i an estimator of the abundance of species i , which we compare to the long-term average abundance \bar{X}_i . The snapshot estimator e_{1i} for species i is defined as the abundance of species i on the 5000th time step. Other estimators are calculated by taking the mean species abundance over different sample lengths. Sample are always taken from the beginning of the time series.

Figure 4.24 shows three different estimators, e_1, e_2, e_3 , plotted against long-term average abundances for all the species in a community. e_1 is the snapshot estimator, while e_2 and e_3 use sample lengths of 4000 and 29,000 respectively. Results are shown for two simulations, one with high IR (0.001) and one with low IR (0.0001). The line $y = x$ is shown on all plots, giving an intuition for estimator accuracy (since a perfect estimator would lie on this line for all species). Linear regression fits to the estimator values are also plotted, with the *coefficients of determination* R^2 given. The better the estimator, the closer the value of R^2 is to one. In this way R^2 can be used as a measure of estimator quality over the community as a whole. The figure shows that, as expected, longer samples produce better estimates. The fits to e_2 and e_3 have higher R^2 than the fits to e_1 . In particular at low IR, where there is increased temporal variability, the performance of the snapshot estimator is poor ($R^2 = 0.54$ and 0.94 for e_1 and e_2).

We define another metric for estimator quality, which we call *mean relative error* MRE:

$$MRE = \frac{1}{N} \sum_{i=1}^N |\bar{X}_i - e_i|,$$

where N is the number of species, and e_i is the value of the estimator in question for species i . This metric is equal to zero for a perfect estimator. Figure 4.25 shows the performance of estimators, calculated from increasing sample lengths, applied to the HI and the LI ensembles. Performance is measured by both the R^2 value and by MRE. The performance of the snapshot estimators is poor, with MREs of around 0.3 and 0.8 for the HI and LI ensembles respectively. In all cases the estimators converge on the long term average as the sample length is increased. That is, the R^2 and MRE values converge on one and zero respectively. Convergence is slower for the LI ensemble, where even with sample lengths of 30,000 time steps the MRE is still around

0.1. However the R^2 values converge more rapidly than the MRE values. For the LI ensemble a sample length of 4000 gives an average estimator R^2 of about 0.9. From these results it appears that the snapshot estimator would introduce large errors into our results in cases where there is high temporal variability. The use of longer samples, it seems, can reduce these errors. However it is also clear that some trade-off must be made, because the length of sample required to guarantee convergence to the long-term average is very large. Based on the R^2 values it appears that samples of around 4000 time steps may be sufficient to characterise species abundances with reasonable accuracy, even in simulations with high temporal variability.

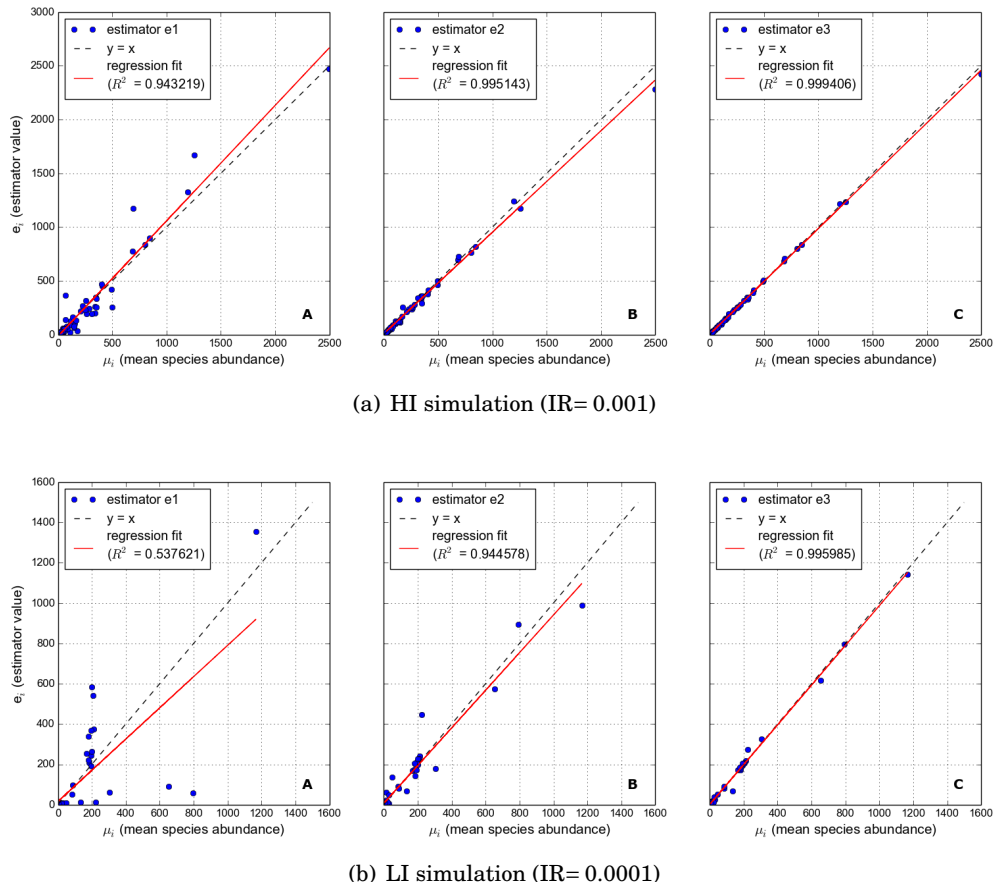


Figure 4.24: Performance of three different estimators of species abundance, applied to a (A) single HI simulation and (B) a single LI simulation. Estimator ‘e1’ is a snapshot of abundance on 5000th time step; ‘e2’ is an average over 4000 time steps; and ‘e3’ is an average over 29,000 time steps. Points are the long-term mean abundance of a species, plotted against the estimator value for that species. Red lines show linear regression fits for the estimator, and how close the estimator is to modelling the ‘true value’ of species abundances (dashed blue line).

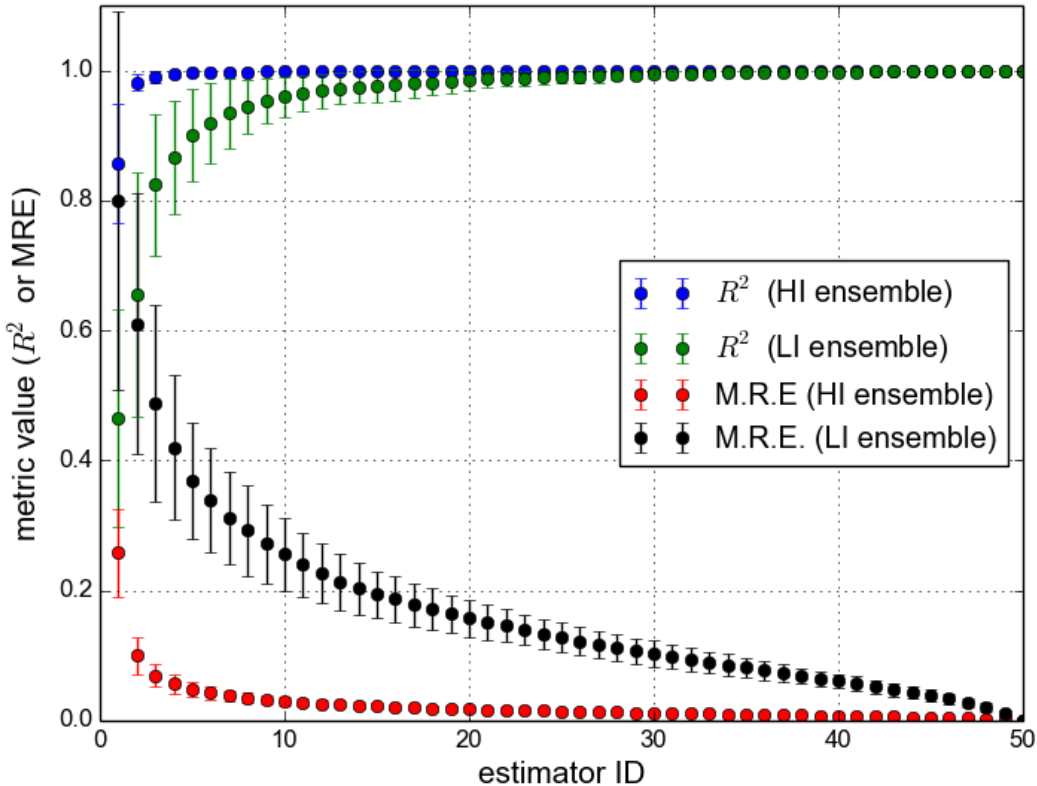


Figure 4.25: Performance of 50 different estimators for species abundance, measured by R^2 value and mean relative error MRE (see text for definitions). The first estimator (estimator ID=1) is uses ‘snapshot’ of simulation state at 5000th time step (as used in previous chapter), the remaining estimators (IDs= 2,..,50) use average abundances over sample windows ranging from length 1000 to 50,000 in steps of 1000. Points indicate mean value of metric over ensemble of simulations. Error bars indicate ± 1 standard deviation.

4.6.2 Repeatability

Here we briefly consider the issue of repeatability in our experiments. The motivation is that, given the complexity of the model, sufficient stochasticity could result in replicate simulations producing very different outputs. Various results presented in this chapter suggest that this is not the case with our model. In section 4.2.5 we saw that replicate simulations with two different network structures generated consistently different persistence profiles. Also the RQA analysis (section 4.5) revealed a strong deterministic signature in species population dynamics. The detection of determinism suggests that the local rules of the IBM successfully define mechanisms responsible for the observed patterns and dynamics, rather than simply producing randomness. As a final demonstration of repeatability we select three replicate simulations at random from the NM1 ensemble (section 4.4.3). These three simulations use the same interaction network

structure, and a high IR (0.001). As we saw in section 4.5 high immigration simulations are less deterministic, so these three replicates make a suitable check for repeatability. We compare the abundance distributions of the three replicates using *rank-abundance spectra* (RAS) [?]. RAS are a useful tool for the comparison of abundances in communities that contain the same species. Species are ranked according to their abundance in one community (as in RADs - section 2.8.1.1). The rank of each species is then fixed, giving its spectral location, which allows the comparison of the initial community with others that contain the same species. RAS are plotted for the three NM1 replicates in figure 4.26, using the long-term average abundance for each species (4.6.1). We provide no more than a qualitative description of the RAS, which clearly illustrate a high level of repeatability in the abundance distribution. There are only a few significant deviations from the rank ordering in the initial community (panel A) in the replicate communities (panels B,C). In particular the species at rank 8 has a much lower abundance in panel C than in A and B. It appears that this is may be due to competition from species in the same trophic level (ranks 38 and 54), which have a higher abundance in panels B and C than in A. The similarity of the three RAS support our conclusion that our experimental simulations are repeatable, despite the stochasticity inherent in the modelling framework.

4.7 Conclusion

In this chapter we have discovered that immigration is required for the IBM to generate persistent communities (section 4.2. In the absence of immigration the majority of species in higher trophic levels go extinct, and we have argued that this is due to competition effects (section 4.2.6). We have also demonstrated the population dynamics becomes more variable as the immigration rate is reduced (section 4.3). This may be a feature of the system passing between a regime of stable persistence at high IR into an unstable regime at low IR. Furthermore we have demonstrated that species population dynamics may be non-stationary, especially at low IR (section 4.4). However results from the recurrence quantification analysis suggest that this non-stationarity is due to deterministic population dynamics rather than stochastic effects (section 4.5). We have also shown that the dynamics of species with low abundance tend to be more stationary and less deterministic, whereas species with high abundance tend to be less stationary and more deterministic. Together these results suggest that the abundant species are undergoing larger amplitude trophic dynamics, generated by their interactions with other species. The least abundant species, we propose, are those maintained mostly by immigration (even at lower IR values) because their relative scarcity makes them less likely to interact with other species. As we argued in chapter 3, immigration is a random process. So the dependence of low abundance species on immigration would explain their lower %DET values and, together with their reduced ability to interact with other species, explains their higher stationarity.

We have addressed the impact of increased variability on our experimental results (section

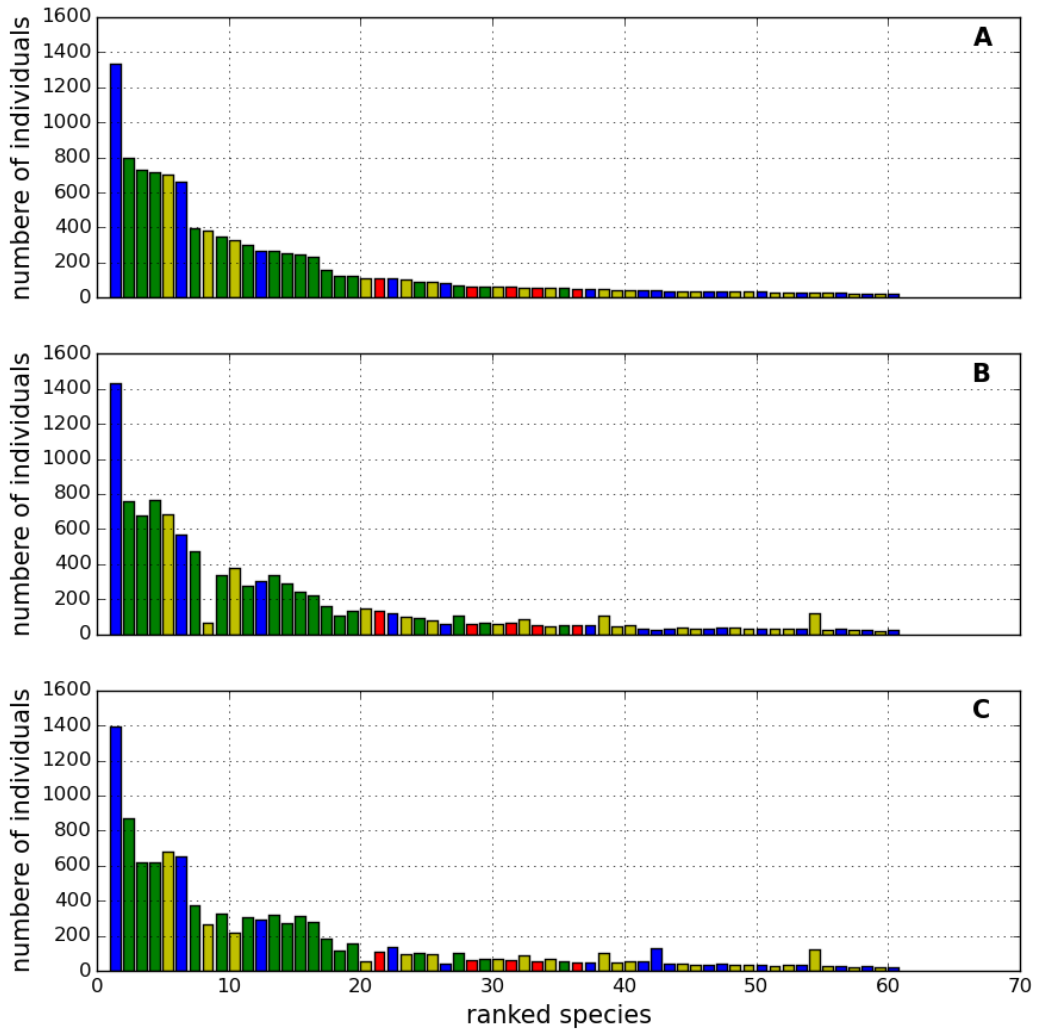


Figure 4.26: Rank abundance spectra (RAS) for three simulations from the NM1 ensemble (see text). Species abundances measured as long term average (over time steps 1000-9,000). Species are ranked according to their abundances in the first simulation (panel (A)). Ranking is retained in panels (B) and (C), which show abundances from two different simulations. Colouring of species by trophic level is consistent with previous figures.

4.6). We showed that, especially at low IR, snapshot sampling can produce abundances measures with large deviation from the long-term average. However it is also clear that, for highly variable communities, the length of sample required for the measured abundance to converge on the long term average is not practical given computational limits. Therefore we accept that increased variability may introduce random error into our results. In chapter 5 we further address this issue by comparing two different sampling regimes in the analysis. We have also briefly considered the issue of repeatability in our experimental results (section 4.6.2). In particular we saw that replicate simulations using the same interaction network produced very similar rank-abundance spectra. The reproducible rank-abundance spectra, together with the observed signature of determinism in the IBM output, give us confidence in the repeatability of our results. Although clearly the strong stochastic component requires that replicates are part of the experimental procedure, as they are throughout the thesis.

HABITAT LOSS UNDER VARIABLE IMMIGRATION RATE

5.1 Introduction

In chapter 3 we discovered that the immigration mechanism provides a *rescue effect* for all species, preventing extinctions even at high levels of habitat loss (HL= 90%). This allowed us to study community responses to HL in the absence of extinctions. However in nature it is common that HL does lead to the local loss of species [7]. Therefore we are motivated to reduce the immigration rate (IR), weakening the rescue effect, to study communities in which HL results in extinctions. In chapter 4 we found that communities at zero IR - *closed communities* - displayed many extinctions, even in pristine landscape. We concluded that some immigration is required for the IBM to produce persistent and diverse communities. Therefore in this chapter we study the response of communities to HL at IRs between zero and the *default value* ($IR = 0.005$). We expect that varying the immigration rate will cause community responses to HL to differ from those observed in chapter 3. In particular we are interested to study community responses to HL when species extinctions are allowed to occur.

In the previous analysis we have demonstrated that immigration is a key determinant of the dynamics and structure of simulated communities. In chapter 4 we saw that high IR reduces both the temporal variability and the determinism of population dynamics. In chapter 3 we demonstrated that strong immigration acts to increase the evenness in the distribution of species abundances and that this can affect network properties, for example by making interaction frequencies more even. In particular we saw that the *dependence of a community on immigration* (measured by the relative contribution of immigration to total births) could account for the different structural responses of communities under the two HL scenarios. The contiguous HL scenario did not produce significant changes in many of the metrics analysed, and it was argued

that this was due to the constant dependence of communities on immigration across the HL gradient. In contrast random HL increased community dependence on immigration, and produced significant changes in most of the metrics analysed. In this chapter we employ the same two HL algorithms (section 2.5), *random* and *contiguous*, at a range of different IRs. We anticipate that reduced IR may effectively reduce community dependence on immigration in some cases. In such cases we hypothesise that HL will make communities less even, and that there will be corresponding changes in network properties. It is most likely that such an effect will be found in the contiguous scenario, because intra- and inter-specific interactions remain strong under contiguous HL. This observation was discussed in detail in section 3.4, but the main arguments are summarised below.

Species interactions have proven to be another key driver of population dynamics and community structure, as expected. In chapter 3 strong inter-specific interactions, as measured by IS, were shown to produce high temporal variability. In chapter 4 it was demonstrated that this variability was due to deterministic oscillations, characteristic of predator-prey interactions. We have also found that the two HL scenarios have different effects on species interactions due to changes in the mobility of individuals (figure 3.23). Random HL presents a barrier to motion making both inter- and intra-specific interactions less likely. This accounts for the increased dependence on immigration in the random scenario, since sexual and mutualistic reproduction is hindered by the destroyed cells, which act as physical barriers and make it difficult for individuals to find a mate. Contiguous HL makes interactions more likely because all individuals are contained within a smaller region of space and maintain the same dispersal ability. Therefore in the contiguous scenario at low IR we may expect to see a reduced dependence on immigration, and increase in the effects associated with strong species interactions. Conversely we may expect low IR to weaken the effects of random HL, which were associated with increased dependence on immigration at the default IR value.

In general we anticipate that reducing IR will strengthen the effects associated with species interactions, and weaken those associated with immigration. In particular we expect communities to become less even and more temporally variable as IR is reduced. There may also be an increase in *ecosystem synchrony* as the stochastic component of the dynamics is reduced relative to the deterministic component. Such effects should be visible at any given HL value under both scenarios. Finally we expect that at lower IRs both HL scenarios will generate species extinctions.

In section 5.2 we detail the experimental methodology for the chapter, including an experiment to determine how to sample from the simulation output (section 5.2.1) given the increased variability expected from reduced IR (see chapter 4). Section 5.3 presents an initial analysis of certain key metrics over a slice of the IBM parameter space defined by varying IR and HL. Sections 5.4 and 5.5 develop the initial analysis further by conducting bivariate analyses at selected IR and HL values respectively. We summarise the main findings of the chapter in section 5.6, before concluding in section 5.7 with an ecological interpretation of the perspectives gained

from our simulations of the IBM.

5.2 Experimental approach

As in chapter 3 we run two ensembles of simulations, one for random and one for contiguous HL. The value of HL is varied between 0% and 90% in steps of 10%, as before. At each value of HL we run replicates at 10 different immigration rates: $IR = 1 \times 10^{-4}, 2 \times 10^{-4}, 3 \times 10^{-4}, 4 \times 10^{-4}, 5 \times 10^{-4}, 1 \times 10^{-3}, 2 \times 10^{-3}, 3 \times 10^{-3}, 4 \times 10^{-3}, 5 \times 10^{-3}$. Therefore each ensemble explores a two-dimensional slice of the parameter space, defined by the axes HL and IR. This same region of parameter space was visualised in figure 4.20 during the stationarity testing. The inclusion of variable IR increases the number of required simulations by a factor of ten, compared to the simulation ensemble of chapter 3. To reduce the computational cost we make two savings. Simulations are only run for three MAI ratios (0.0, 0.5, 1.0) instead of eleven, giving the full range between antagonism and mutualism but with lower resolution. Additionally we restrict the number of metrics that are calculated during each simulation. The spatial metrics in particular are computationally expensive. Therefore all of the metrics defined in section 2.8.3, which characterise spatial aggregation and variability, are not calculated. This speeds up the simulation run times by about a factor of five, but means that we cannot characterise spatial patterns without *post-hoc* analysis.

In section 4.6 it was shown that the increased temporal variability resulting from reduced IR can make results more sensitive to the sampling procedure. It may be desirable to run the simulations for an increased number of time steps, allowing for longer samples from which to calculate results. However it was decided that this is an unnecessary computational expense. The regression analysis of estimator quality suggested that a sample length of 4000 characterises species abundances with reasonable accuracy ($E(R^2) > 0.9$) in pristine landscape at low IR (1×10^{-4}). Therefore all simulations in this chapter were run for 5000 time steps, with the first 1000 time steps discarded before analysis (as in chapters 3, 4). In section 5.3, before presenting the main results, we further address the issue of sampling procedure by statistically comparing results obtained using two different sampling methods.

In this chapter the number of replicate simulations is increased from 25 (used in chapter 3) to 50. The use of a higher number of replicates reflects the previous observation of increased variability, and therefore a larger source of random error in the results. With 50 replicates at every value of HL, IR and MAI ratio, each ensemble contains 15,000 ($= 50 \times 10 \times 10 \times 3$) simulations. Each replicate uses a distinct interaction network generated using the same procedure as in chapter 3, that is a niche model with trophic constraints and link replacement to introduce mutualisms (details in section 2.3). The only modification is that here links between top-predators and basal species are removed from the network, so that top-predators only feed on other animal species. On average such links represented less than five percent of the total links in a network (calculated from the ensemble of simulations used in chapter 3). Therefore we not expect a qualitative change

in the main findings presented in chapters 3 and 4. As previously all simulations were run on the Blue Crystal cluster [139].

Given that we are interested in species extinctions induced by HL, in this chapter we redefine the definition of a local *extinction*. Previously a species was said to be extinct if there were no individuals belonging to that species in the landscape at the end of the simulation. However we have seen that immigration provides a *rescue effect* that is common to all species. A species may go extinct at some time in the simulation, but later recover due to immigration. For example a species may be extinct for most of the simulation and then an immigrant belonging to this species is created on the final time step. The previous definition of extinction would not count such a species as extinct. Especially at low IR we expect many species to have abundances that hover close to zero. We make the assertion that such species are effectively locally extinct because they fail to maintain a viable local population and are only sustained by immigration. Indeed, in an empirical study sufficiently rare species are unlikely to be detected and therefore do not contribute to estimates of species richness. Therefore it is felt that the previous definition of species extinction does not correctly characterise the state of the system. We propose a new definition of extinction as follows. A species is declared extinct if its population size (or average population size if sampling over a number of time steps) is lower than a specified *threshold value*. In section 5.3 we set an *arbitrary threshold* of three individuals.

5.2.1 Sampling procedure

The *Shannon equitability* metric (equation (2.2)) is calculated for all simulations using two different sampling methods. The first method uses snapshot sampling (as in chapter 3), i.e. species abundances are measured on the last time step of the simulation. The second method takes the mean species abundance over the final 4000 time steps of the simulation. Results obtained using the two sampling methods are referred to as *snapshot* and *averaged*, correspondingly. We compare the results obtained using a *two-sided t-test*, which is implemented in the *Python* package *scipy*. The test is used to compare two datasets of independent samples, testing the null hypothesis that the expected value of the two datasets are equal. If the *p-value* of the test is smaller than the confidence threshold then there is sufficient evidence to reject the null hypothesis and conclude that the means of the two datasets are significantly different. For each test we are comparing the *snapshot* and *averaged* equitability results, calculated from the 50 replicate simulations at a given HL and IR value. If the test is significant then we conclude that the two sampling methods give significantly different results in calculation of the average Shannon equitability at that value of HL and IR. We conduct tests for all HL and IR values, and all three MAI ratios, under random and contiguous HL. The *p-values* of these tests are depicted in figure 5.1.

In general figure 5.1 shows that there is strong support for the conclusion that the two sampling methods produce the same average equitability results. The worst case is random HL at MAI= 0.0 (panel A). In this case there is a region of parameter space, above HL= 60%, where

5.2. EXPERIMENTAL APPROACH

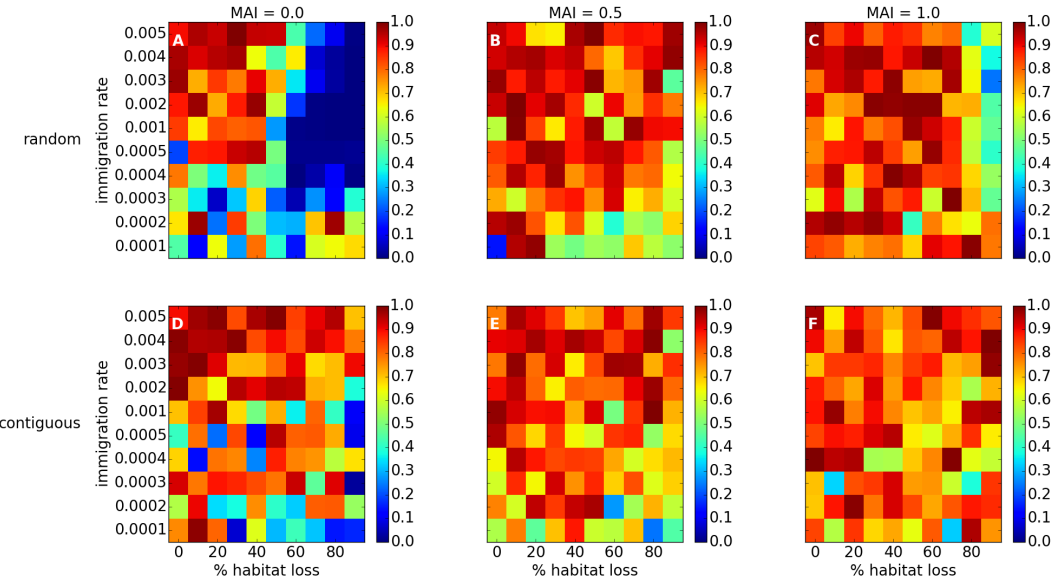


Figure 5.1: P-values for t-tests to compare the *Shannon equitability* calculated by two different sampling methods: *snapshot* and *averaged* sampling (see text for definitions). Each point in the plot represents the p-value of the test comparing the *snapshot* and *averaged* Shannon equitability results for the 50 replicate simulations at the corresponding HL and IR value. A p-value < 0.05 (i.e. dark blue) represents 95% confidence that the two sampling methods produce different average equitability results.

the p-values are significant. Therefore in this region the methods appear to give statistically different results. However, as stated, most of the tests suggest that the two methods produce statistically similar results. The similarity between the two methods is surprising given the results of the estimator analysis in section 4.6.1. In part the success of the snapshot method is likely due to averaging over 50 replicates, which effectively represent samples from the same noise distribution. It may also be that a high level of precision in the estimates of species abundances is not required to calculate community level metrics. Based on the comparison presented here we conclude that snapshot sampling is sufficient to draw general conclusions about community structure over the ensemble of simulations. This allows consistency with the analysis in chapter 3. However we acknowledge that the use of snapshot samples may introduce some error, and increased variability, into our calculations. We treat the region of parameter space in which the equitability results proved dissimilar (panel A: random HL, MAI = 0.0) with particular caution. The metrics for network properties (defined in section 2.8.4) and stability (defined in section 2.8.2) are calculated by aggregating over the final 200 time steps of a simulation, as in previous chapters. We do not provide an equivalent statistical comparison of these metrics when calculated from samples of different lengths. Given that these metrics already use a sample of length 200,

we assume that they are less sensitive than the snapshot metrics to error introduced by high variability.

5.3 Initial analysis

In this section we provide an overview of the results for both the random and contiguous scenarios, over the region of parameter space explored. Results are presented as *heat-maps* over parameter space. Each pixel corresponds to a unique pair of HL and IR values, with the temperature (colour) given by the corresponding mean value of the metric in question (averaged over the 50 replicates). In this way it is possible to gain a qualitative impression of how the various metrics respond as HL and IR are varied. In sections 5.3.1 and 5.3.2 we provide results for selected metrics associated with diversity, and variability respectively. In subsequent sections we look in more detail at key features identified from the initial analysis presented here. All results presented use the same sampling procedure as in chapter 3, i.e. snapshot samples for abundance metrics and sample lengths of 200 for variability and network metrics. The continued use of this sampling procedure is justified by the statistical analysis in section 5.2.1 above.

The top row of each heat-map corresponds to the *default immigration rate* ($IR = 0.005$). A general observation is that the results at this IR are consistent with those of chapter 3, despite the removal of the links between top-predators and basal species. We see from figures 5.2-5.5 that the trends in diversity, variability and interaction strengths, along the HL gradient at $IR = 0.005$ are qualitatively the same as those previously reported. Therefore we conclude that the removal of these links does not significantly change our results, although there may be more subtle changes in community structure and dynamics.

5.3.1 Diversity

In this section we consider three metrics associated with community diversity: *number of extinctions*, *total number of individuals* and *Shannon equitability*. The mean value of these metrics over the region of parameter space is depicted in figures 5.2 and 5.3, for the random and contiguous scenarios respectively. As discussed in section 5.2, an extinction is defined as the presence of less than three individuals in the landscape. The total number of individuals is simply the sum of all individuals in the landscape on the final time step. The Shannon equitability metric (equation (2.2)) is a measure of how evenly the number of individuals is distributed between species. The metric is normalised by the maximum Shannon diversity $\ln(S)$ for the S species present. Therefore changes in this metric are not driven by changes in species richness due to extinctions. The main features of the two figures are summarised below.

Extinctions increase as IR is reduced (panels A,D,G, both figures). On average mutualistic communities exhibit more extinctions than antagonistic communities, and contiguous HL pro-

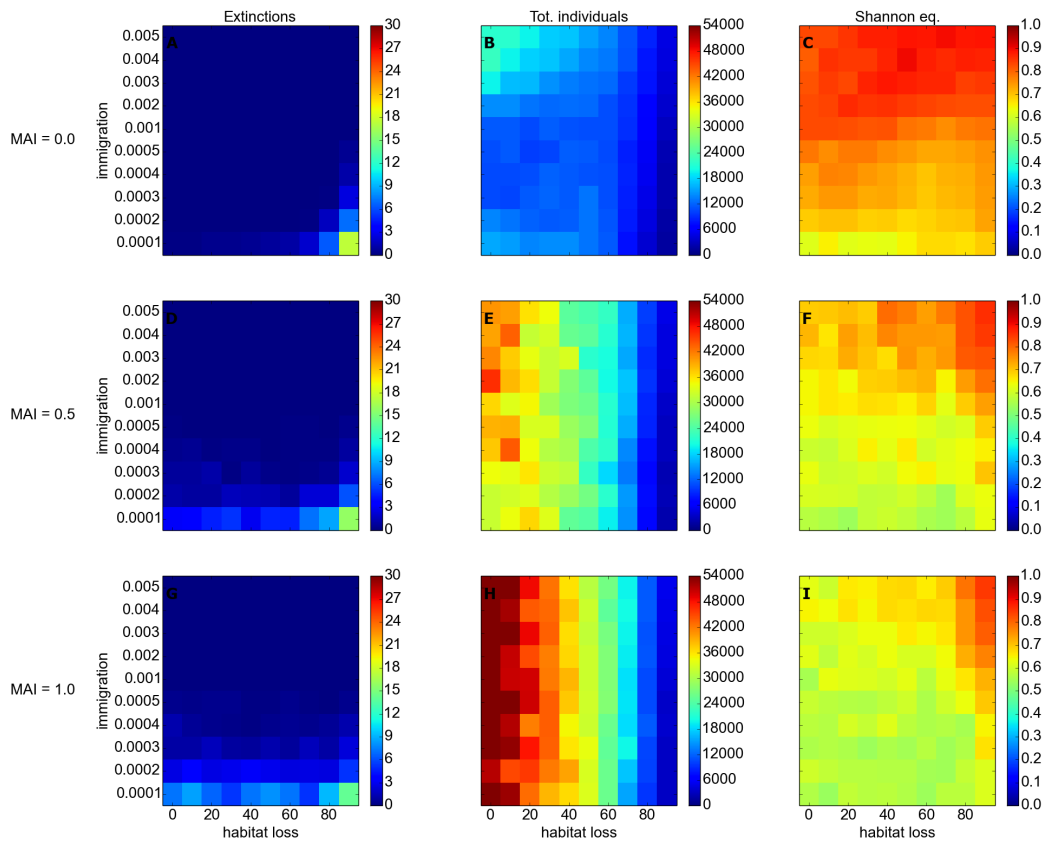


Figure 5.2: **Random HL:** Mean values of diversity metrics at each combination of HL and IR (Average over 50 replicate simulations). All metrics use snapshot sampling (see text). Each row corresponds to a different MAI ratio, as labelled. Panels A,D,G: Number of extinctions, defined as number of species with less than 3 individuals at end of simulation. Panels B,E,H: Total number of individuals in the community. Panels C,F,I: Shannon equitability metric.

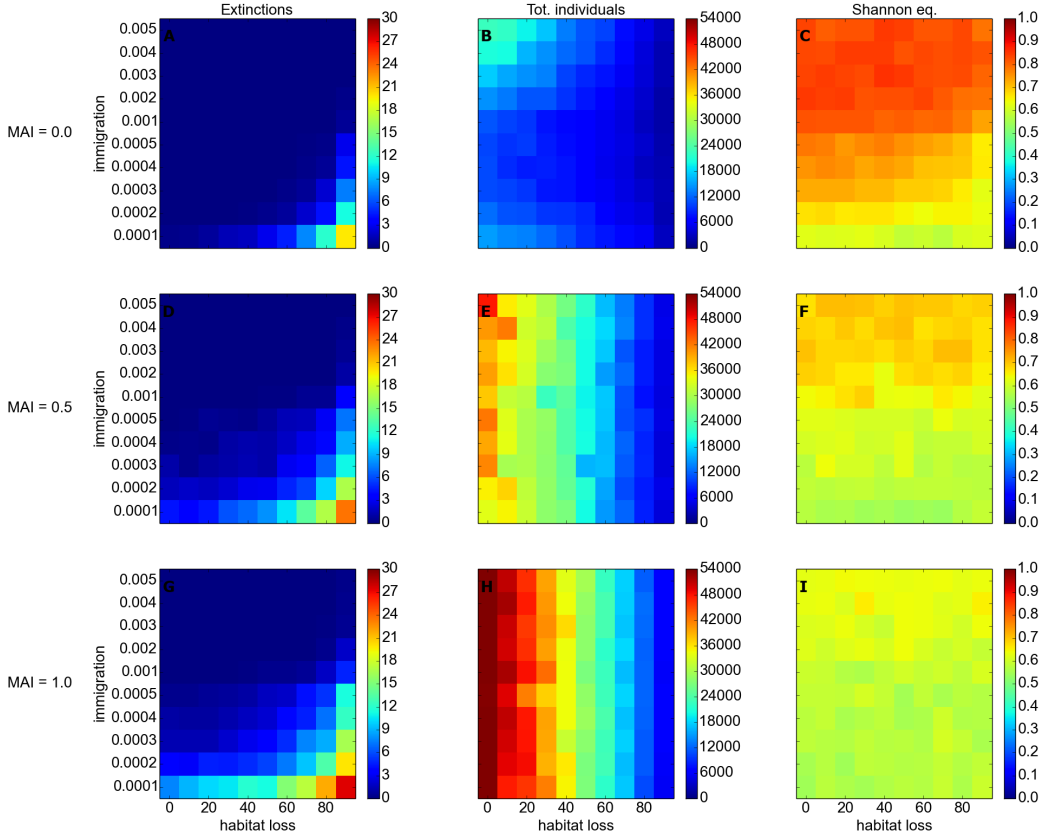


Figure 5.3: Similar to figure 5.2, but for **contiguous HL**.

duces more extinctions than random HL. In the contiguous scenario the number of extinctions increases along the HL gradient, whereas this trend is less clear in the random scenario. Under random HL the dependence of extinctions on the level of HL appears to be reduced, especially for mutualistic communities (figure 5.2, panels D,G). In agreement with the results from chapter 3 there are no extinctions at high IR, despite the change in the way extinctions are defined.

The total number of individuals decreases with HL ((panels B,E,H, both figures), which is consistent with chapter 3. In general mutualistic communities contain more individuals than antagonistic communities. Again this observation is consistent with previous findings. However here we observe that increasing mutualism changes the dependence of the total number of individuals on IR. In antagonistic communities the total number of individuals varies with IR (panel B, both figures). Initially reducing IR from the default value reduces the number of individuals, but at the lowest IR values the number of individuals increases again. In mutualistic

communities the number of individuals is less sensitive to IR (panels E,H, both figures). At MAI= 1.0 changing the IR does not appear to alter the number of individuals in either HL scenario.

The Shannon equitability decreases with IR in all cases (panels C,F,I, both figures). That is, reducing immigration causes communities to become less even. In general antagonistic communities are more even than mutualistic ones, which is consistent with chapter 3. Also consistent with previous findings is the observation that mutualistic communities (MAI= 0.5, 1.0) do not exhibit major changes in evenness under contiguous HL, but become more even under random HL. These patterns appear to hold across all IR values, although at low IR the increase in evenness due to random HL is less than at high IR. The evenness of antagonistic communities responds differently. At some IRs random HL appears to make antagonistic communities less even (IR= 0.0003 to 0.002, panel C, figure 5.2). Similarly in the contiguous scenario at certain IRs antagonistic communities become less even along the HL gradient (IR= 0.0002 to 0.003, panel C, figure 5.3). These reductions in evenness represent a departure from the results of chapter 3, and correspond to one of the predicted effects of reducing the immigration rate (section 5.1).

In summary the diversity results presented in this section confirm some of the predictions from section 5.1, but also highlight certain new and unexpected features of the model. The role of immigration in driving evenness is clear, since reducing IR reduces the Shannon equitability in all cases. As predicted there is less of a change in evenness along the random HL gradient at low IR than at high IR. Also in both HL scenarios there appear to be some cases where evenness decreases with HL. This effect was predicted for contiguous but not random HL, and is only observed for antagonistic communities. The reduced evenness is most visible between IR= 0.0003 and 0.002.

Reducing IR increases the number of extinctions due to a weaker rescue effect, as predicted. Two features of the extinction response were unexpected: that more extinctions are produced by contiguous than by random HL, and that the number of extinctions under the random scenario is less sensitive to the level of HL. These observations suggest that the mechanism behind species extinctions differs between the HL two scenarios. Based on what we saw in chapter 3 we propose that extinctions in the contiguous scenario are due to strong predation driven by high IS, whereas in the random scenario they are likely due to a collapse in the trophic structure of the community due to low IS (see section 5.4, and discussion in section 5.6).

A key unexpected feature of these results is the role of mutualism. We find that the MAI ratio plays an important role in mediating how communities respond to changes in HL and IR. This role is most clearly visible in the total number of individuals, which becomes insensitive to IR at high MAI ratios. In this sense at least mutualism can be said to confer robustness on communities in the face of variable IR. However mutualistic communities exhibit more extinctions than antagonistic ones, so in this sense mutualism is detrimental for robustness. Based on

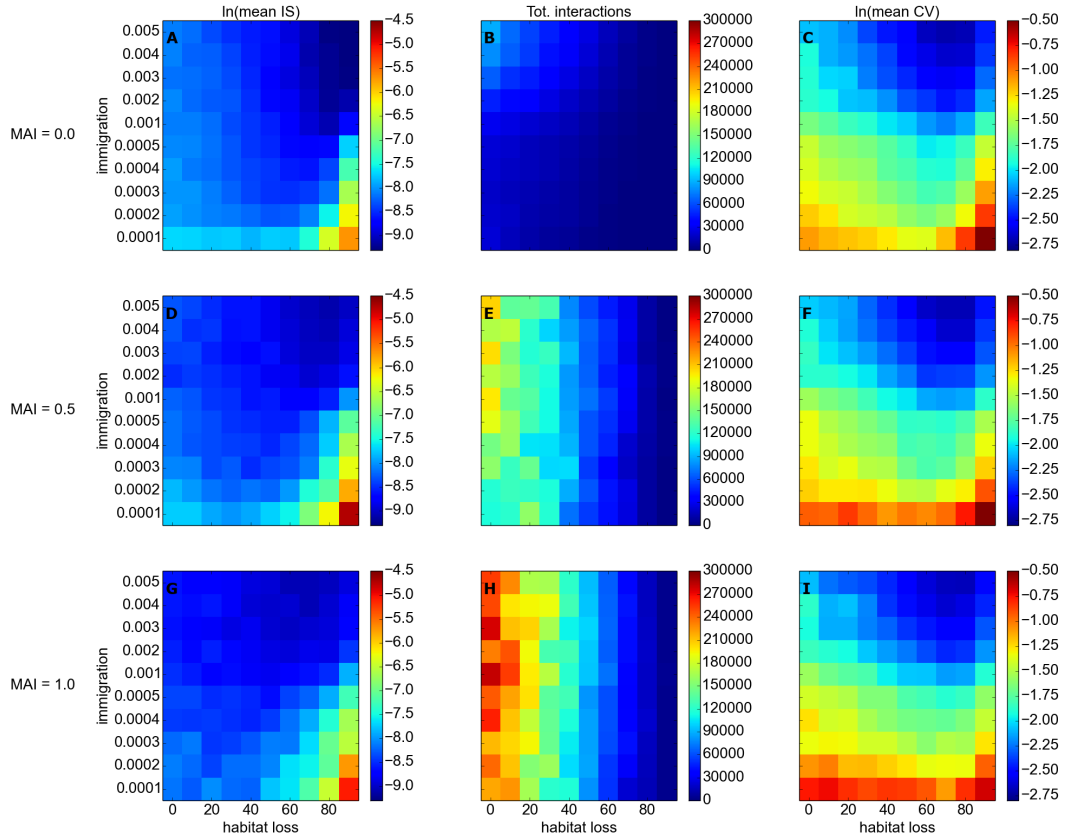


Figure 5.4: Similar to figure 5.2, but showing three different metrics: the natural logarithm of the mean interaction strength (ln(mean IS)); the total number of interactions between all species; and the natural logarithm of the mean temporal variability (ln(mean CV)). **Random HL**.

the persistence analysis in section 4.2.1, we may expect that the mutualistic communities at low IR are dominated by a small number of species in the non-basal trophic levels (see section 5.4). It is perhaps an increased dominance of these few species which accounts for the constant total abundance across the range of IR values (see section 5.5). This would be consistent with the observation that mutualistic communities become less even at low IR. Mutualism is also found to mediate the response of evenness to HL. In particular both types of HL make antagonistic communities less even at some IR values, but this effect is not present for mutualistic communities.

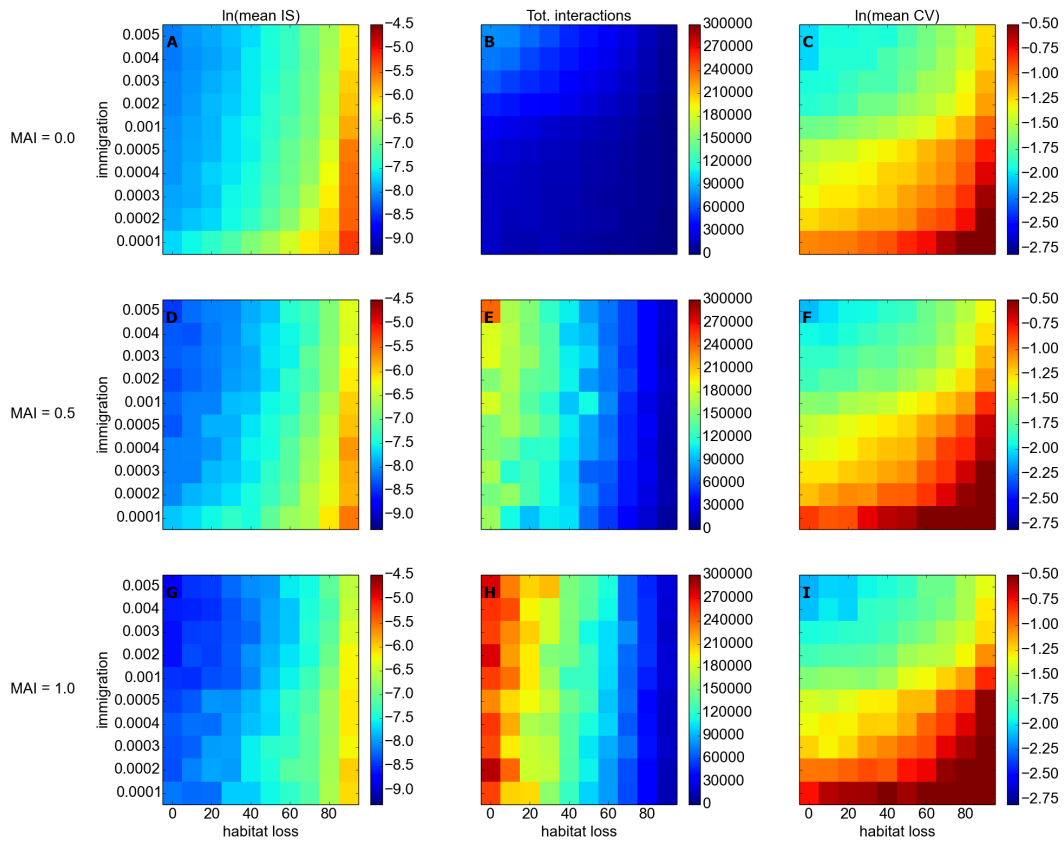


Figure 5.5: Similar to figure 5.4, but for **contiguous HL**.

5.3.2 Variability and species interactions

In this section we consider three metrics associated with variability and species interactions: *mean interaction strength* (mean IS), *total number of interactions* and *mean temporal variability* (mean CV). The mean value of these metrics over the region of parameter space is depicted in figures 5.4 and 5.5, for the random and contiguous scenarios respectively. The metric IS is the same as used previously, and is defined in section 2.8.4.3. The metric for temporal variability is the coefficient of temporal variation (CV) in species abundance, and is defined in section 2.8.2. Both IS and CV are averaged over all species in the community to give *mean IS* and *mean CV*. The natural-logarithm of these two metrics is plotted, based on the observation in chapter 3 that they vary exponentially in response to HL. The total number of interactions is the sum total of all inter-specific interaction events between individuals during the sampling period. All three metrics use a sample length of 200 time steps, taken from the end of the simulations. At the end of the section we also look at the metric for *ecosystem synchrony* (Sync), which is defined in

section 2.8.2.1. The inclusion of these metrics and its interpretation is based on findings in the previous chapter that reducing IR increases the determinism of population dynamics (section 4.5). In section 5.1 we predicted that reducing IR would increase the effects associated with species interactions, increasing both temporal variability and ecosystem synchrony. Key features of figures 5.4 and 5.5 differ according to HL type. Therefore we comment on the two HL scenarios in turn, before looking at ecosystem synchrony and summarising the results as a whole.

Contiguous HL increases both interaction strengths and temporal variability in all cases (figure 5.5, panels A,D,G and C,F,I). Therefore varying IR does not alter the direction of the response of these metrics to contiguous HL, that was observed in chapter 3. As predicted reducing IR increases temporal variability. Unexpectedly reducing IR slightly increases the mean interaction strength, an effect that is more pronounced in antagonistic communities. For antagonistic communities the number of interactions decreases with both IR and HL. For mutualistic communities the the number of interactions decreases with HL, but is less sensitive to IR. These changes broadly match the those in the number of individuals, as shown in figure 5.3, supporting the previous conclusion that interaction frequency is largely determined by species abundances (section 3.4). The one anomaly is that antagonistic communities do not display an increase in interaction frequencies at low IR, where the number of individuals is observed to increase. This suggests that the increase in number of individuals at low IR (panel B, figure 5.3) is due to an increase in the abundance of certain species which are unable to interact. The obvious explanation is that plants come to dominate antagonistic communities at low IR (see section 5.5).

The random scenario produces qualitatively the same patterns in the number of interactions (figure 5.5, panels B,E,H) as seen in the contiguous scenario. However random HL results in a slightly greater decline in interaction frequency, in agreement with the findings of chapter 3. As in the contiguous scenario reducing IR increases temporal variability, with an associated increase in interaction strength (panels C,F,I and A,D,G respectively). However the random scenario displays a more subtle interaction between variability and IS. At all IR values the gradient of increasing HL causes variability to first decrease, but then increase at extreme HL values. The role of IR is such that the *net change* in variability across the HL gradient shifts from a decrease (at high IR) to an increase (low IR). This effect holds across all three MAI ratios. Broadly these changes in variability correlate with the changes in IS, with a notable exception at the top right corner of panel A. However this corresponds to the region of parameter space identified as most sensitive to sampling error (section 5.2.1) and therefore may be a spurious result.

Ecosystem synchrony (Sync) is plotted for both HL scenarios and all three MAI ratios in figure 5.6. Sync is defined in equation (2.9), and is higher when there is some degree of synchronisation between the population dynamics at the species level. The metric approaches one for perfect synchronisation (with zero phase difference) of all species. The results shown confirm

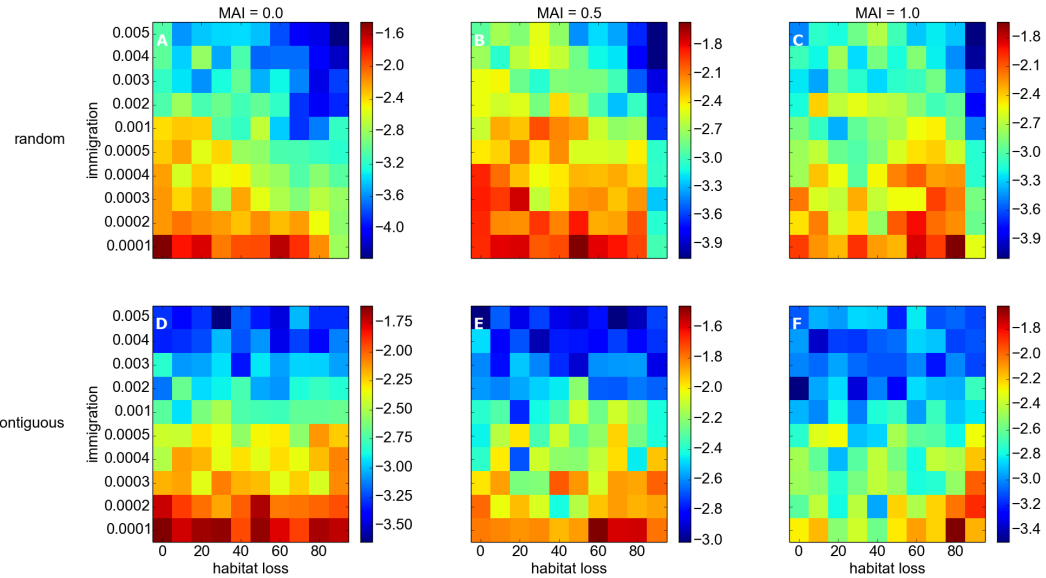


Figure 5.6: Natural logarithm of *ecosystem synchrony* ($\ln(\text{Sync})$), defined in section 2.8.2.1 for both HL scenarios, and all three MAI ratios.

our prediction that reducing IR increases synchrony of the population dynamics, in general. From the analysis in chapter 4 we can now be confident that this is due to an increase in the deterministic component (due to species interactions) relative to the stochastic component (due to immigration). Less clear from this figure is the dependence of synchrony on HL. In the random scenario HL *mainly* reduces synchrony, while in the contiguous scenario HL appears to *mainly* have no effect on synchrony. However both of these observations are less clear at MAI= 1.0.

In summary the results presented in this section are generally consistent with those of chapter 3, i.e. community responses to HL do not change when IR is varied. The notable exception to this is that at low IR random HL results in a *net increase* in temporal variability, rather than a net decrease. The increase in variability occurs at high levels of HL (> 70%), and is most visible at HL= 90% where the number of individuals is lowest. It is worth noting that the metric CV (equation (2.5)) tends to infinity as the number of individuals tends to zero. This property of the metric may explain the apparent increase in variability in highly impacted landscapes at low IR.

The results also confirm our prediction that reducing IR would increase the effects associated with species interactions. Temporal variability and ecosystem synchrony increase and decrease with IR respectively. Therefore the conclusion from chapter 4, that reduced immigration increases the determinism and variability of population dynamics, is robust across this region of parameter space under both HL scenarios. We did not anticipate an increase in interaction strengths due to reduced IR, an effect which is present in all cases. It is not clear why reducing IR increases

the mean probability of trophic interactions between species (see discussion in section 3.4 for interpretation of IS in terms of probability). We suggest that this is again due to the limit behaviour of the metric. The metric IS (equation (2.19)) tends to infinity when the number of individuals belonging to one of the interacting species tends to zero. Therefore the increase in mean IS due to reduced IR may be the result of interaction strength distributions skewed by species with very low abundance.

5.3.3 Key points and outstanding questions

The initial analysis of results presented in this section 5.3 highlights certain key features of community responses to varying IR and HL, which we explore further in the rest of this chapter. The aforementioned key features are as follows:

- Mutualistic communities exhibit more extinctions than antagonistic communities.
- The total number of individuals becomes less sensitive to IR at high MAI ratios.
- At the lowest IR values the total number of individuals increases in antagonistic communities.
- Contiguous HL produces more extinctions than random HL. Also, in the random scenario, the number of extinctions is less sensitive HL, especially for mutualistic communities.
- In certain cases the evenness of communities decrease along the HL gradient.

To investigate these features further we conduct bivariate analyses similar to those in chapter 3. The relevant metrics are plotted against either HL or IR, with the other variable held constant, and linear models are fitted to identify significant trends (see section 3.2.2). To conduct the bivariate analyses we select two perpendicular transects from the region of parameter space, one at fixed IR value and one at fixed HL value. The transect at fixed IR allows us to study trends in response to HL only (section 5.4), while the transect at fixed HL allows us to study trends in response to IR (section 5.5). In section 5.4 we select a fixed IR value of 0.0005, representing an intermediate IR at which we have observed that communities may become less even in response to HL (figures 5.2, and 5.3). This observation indicates that community responses to HL are different at this IR value from those presented in chapter 3, and are therefore of particular interest. In section 5.5 we select a fixed HL value of 40%. This represents an intermediate level of HL at which community responses may be detected (for example species extinctions at low IR), and therefore allows us to compare differences between the two HL scenarios along an IR gradient.

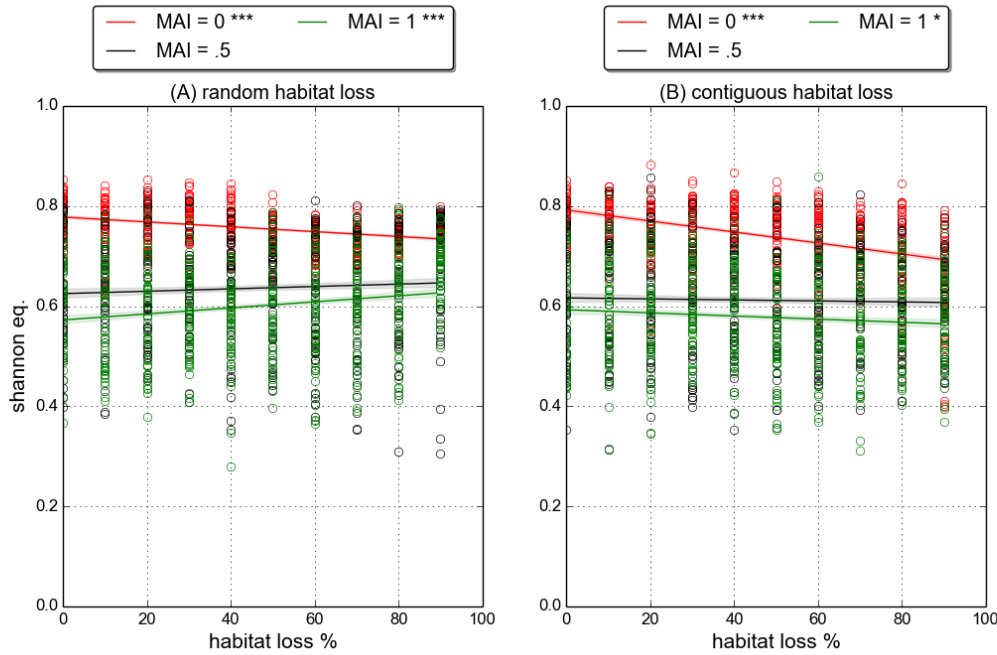


Figure 5.7: **Shannon equitability** against percentage habitat loss, for both scenarios: (A) Random HL, and (B) Contiguous HL. The format of these bivariate plots is consistent with those in chapter 3. Circles represent the metric value for a single community; lines represent a linear fit to the data and the shaded regions indicate the standard error of the mean. The markers ***, **, * and + corresponds to linear model fit p-values of < 0.001 , < 0.01 , < 0.05 and < 0.1 (marginal significance) respectively.

5.4 Bivariate analysis: fixed IR

Here we study community response to HL at $IR = 0.0005$. This IR is an order of magnitude below the *default value* of 0.005 used in chapter 3. Therefore some significant differences in community response are expected, and are anticipated from the results of section 5.3 as discussed above.

5.4.1 Evenness

Figure 5.7 shows how the *Shannon equitability* metric, calculated at the community level, changes across the HL gradient under both HL scenarios. This metric (equation (2.2)) measures how evenly abundance is distributed between all species present in the community. Maximum evenness is achieved when all species have the same abundance, in which case the metric is equal to one. From the figure we see a characteristic feature of the model, that low MAI communities are more even than high MAI communities (previously explained in chapter 3 and [58]). We also observe from the figure that communities in pristine landscape have similar evenness as those simulated with the default IR value (compare to figure 3.2). This similarity is surprising given

that we have argued previously that immigration drives evenness, and that here the magnitude of IR is an order of magnitude lower than the default value. The linear models confirm the trends in evenness, observed in section 5.3.1, that inspired this choice of IR value to study. Under both types of HL antagonistic communities ($MAI=0.0$) *become significantly less even*. Communities at intermediate MAI ratio (0.5) do not become significantly more or less even under either type of HL, while high MAI communities (1.0) respond in opposite directions. At $MAI=1.0$ communities become more even and less even under random and contiguous HL respectively, although the p-value and the slope of the trend is lower in the contiguous case. The observation that varying the level of mutualism can change the qualitative response of communities to HL is novel to this chapter.

The evenness responses are explored further by calculating the Shannon equitability within each trophic level. These results are shown in figure 5.8 for both HL scenarios. The plots reveal that there is a difference between the equitability response at the community level compared to that within trophic levels, especially under random HL. In the random scenario (panels A,C,E,G) the distribution of abundances within all trophic levels becomes more even, except for the top trophic level of antagonistic communities ($MAI=0.0$, panel G). Therefore antagonistic communities become less even on aggregate, but more even within three out of the four trophic levels. Communities at intermediate MAI ratio (0.5) become more even within all trophic levels but do not change on aggregate, whereas high MAI communities (1.0) become more even at every level. In the contiguous scenario antagonistic communities become less even within trophic levels, which is consistent with the community level response. Mutualistic communities ($MAI=0.5, 1.0$) do not exhibit changes in evenness within any trophic level. For $MAI=0.5$ this is consistent with the community level, but for $MAI=1.0$ community level evenness decreases despite constant evenness within the trophic levels.

5.4.2 Rank-abundance distributions

In this section we present rank-abundance distributions (RADs) for example communities. Each RAD plotted is for single community selected from the 50 replicates to characterise the general features of the distributions at given HL values and MAI ratios. Together the RADs help to explain the observed evenness responses from section 5.4.1, especially the discrepancy between some community level and trophic level responses. In some cases the RADs contain discontinuities (for example figure 5.9, panel C). The *Zipf* and *pre-emption* model fits to the RADs, illustrated in the plots as solid red and blue lines respectively, are unable to characterise the discontinuities. Therefore the fitted model parameters (alpha and gamma) are not used as complementary measures of community evenness, as they were in chapter 3.

Figure 5.9 shows RADs for antagonistic communities ($MAI=0.0$) under random HL. Such communities were observed (section 5.3.1) to become less even at the community level, but more even within trophic levels, in response to HL. Comparing panels A and C it is clear that the

5.4. BIVARIATE ANALYSIS: FIXED IR

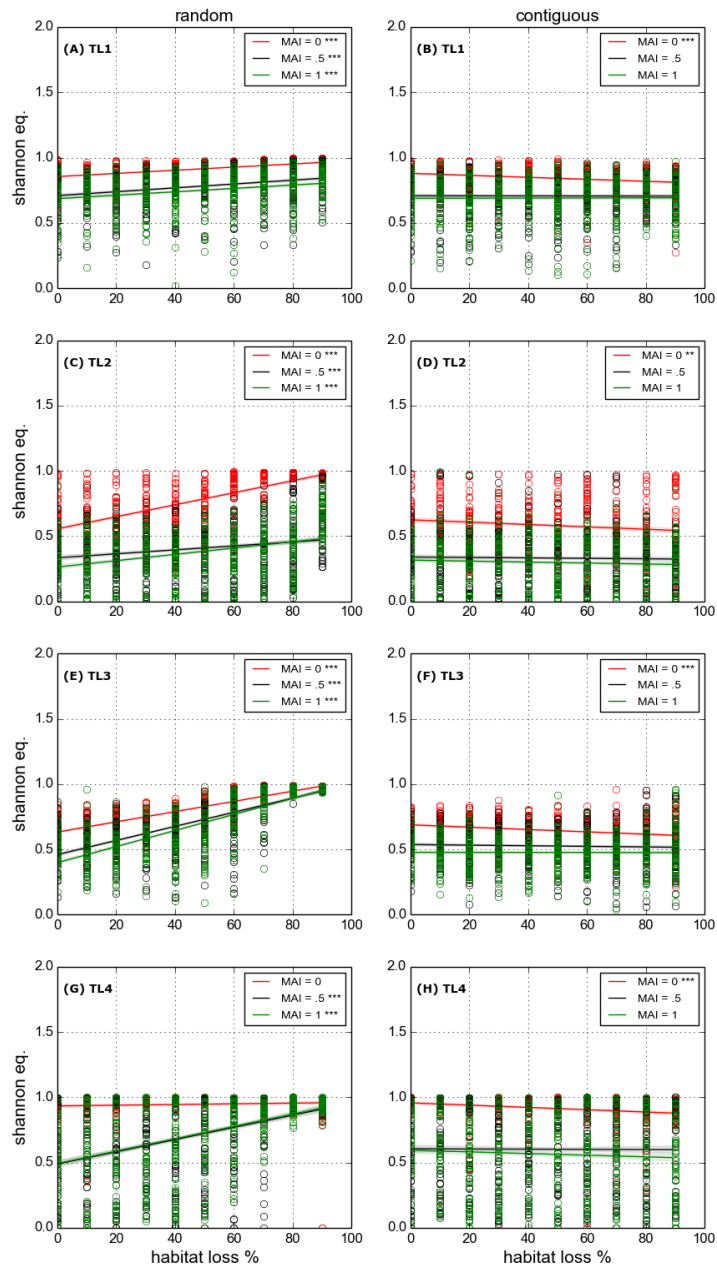


Figure 5.8: **Shannon equitability** against percentage habitat loss, for each trophic level. Left column: random HL. Right column: contiguous HL. Format of individual plots is the same as in figure 5.7.

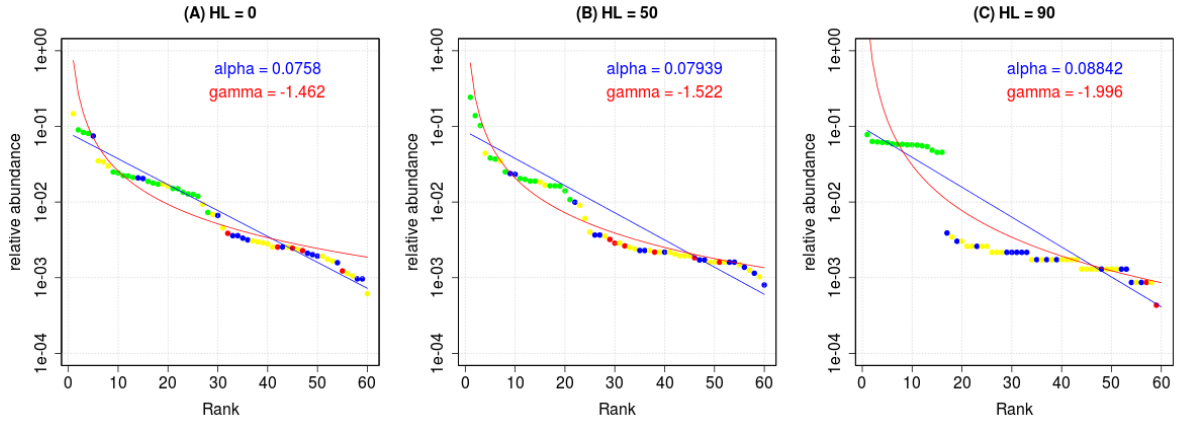


Figure 5.9: Example rank-abundance distributions (RADs) for three antagonistic communities (MAI = 0.0), under random HL, at IR = 0.0005. (A) HL = 0%, (B) HL = 50%, (C) HL = 90%. Species abundances are relative to the total number of individuals in the community, and plotted on a logarithmic scale. Circles represent species, coloured according to trophic level: green = basal; blue = herbivore/animal-mutualist; yellow = primary predator; red = top predator. Blue and red lines give the pre-emption and Zipf model fits respectively (see text in section 2.8.1.1 for definitions), best fit parameter value for each model given as annotations on plot.

decrease in community level evenness is due to an increased dominance of plant species. The RAD at **at** HL = 90% is dominated by 16 plant species, with all other species having a relative abundance of less than 0.01. The discontinuity observed here, between the groups of most and least abundant species, is characteristic of communities under random HL at this value of IR. This observation leads us to define the terms *core* and *tail* to refer to the two groups of relatively high and low abundance species. In what follows we use 0.01 as the threshold relative abundance that separates the two groups. The core and tail sections of the RAD at HL = 90% are relatively even when considered separately. Therefore the increased evenness within trophic levels one, two and three follows intuitively. In the RAD at HL = 0% species belonging to these three trophic levels are interspersed along the distribution, whereas at HL = 90% each trophic level is contained within either the core or tail section only.

Figure 5.10 shows RADs for mutualistic communities (MAI = 1.0) under random HL. Such communities were observed (section 5.3.1) to become more even at the community level, and within all trophic levels, in response to HL. Here the role of mutualism in reducing community evenness is very clear. In pristine habitat (panel A) the community is uneven with a core of ten abundant species. The difference between this mutualistic community and the equivalent antagonistic one (5.9, panel A) is striking. Here the dominance of the core species must be due to the benefit of mutualism, which is not solely conferred on species that interact mutualistically (i.e. plant and animal mutualists). The core contains species belonging to all trophic levels. In agreement with our observations at zero IR (chapter 4) some species in higher trophic levels,

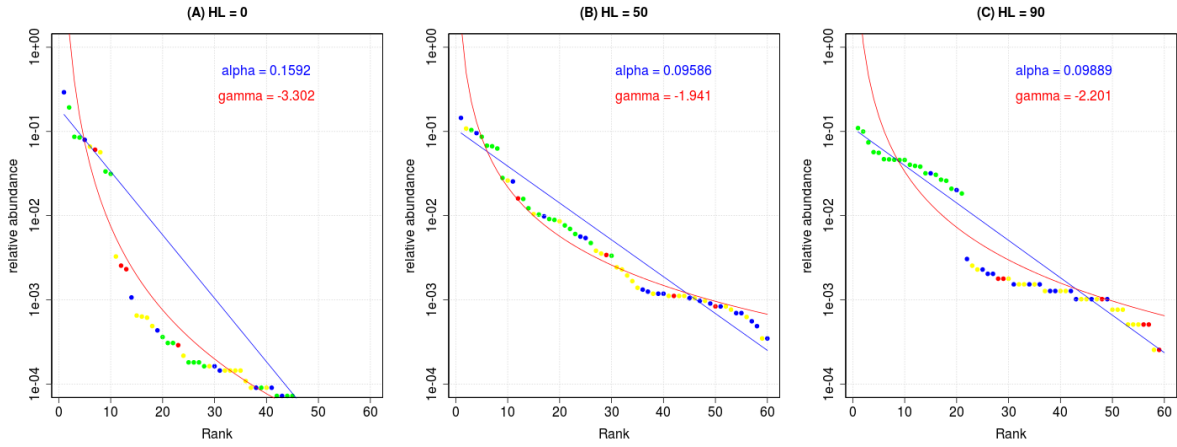


Figure 5.10: Similar to figure 5.9, but for **mutualistic communities** ($MAI = 1.0$), under **random HL**.

presumably those feeding on mutualists, benefit from the presence of mutualism in the community. However other species appear to suffer as a result of the increased fitness of their competitors. These species form a tail of low abundance resulting in a very uneven community. In fact 15 species are totally extinct (zero individuals) from this community, in a landscape without HL. Increasing HL to 50% (panel B) creates a flatter distribution with no clear distinction between core and tail, and no extinct species. The result that increasing random HL can reduce extinctions at $MAI = 1.0$ is present in some but not all replicate communities at this IR value. At $HL = 90\%$ (panel C) the RAD is more even than at 0%, although there is once again a discontinuity between core and tail. In this instance the core consists of only species belonging to trophic levels one and two. This suggests that, in highly impacted random landscapes, mutualistic-animals may still benefit directly from their mutualistic interactions, but that this benefit is no longer passed up the food chains.

Figure 5.11 shows RADs for antagonistic communities ($MAI = 0.0$) under contiguous HL. Such communities were observed (section 5.3.1) to become less even on average at both the community level and within trophic levels. Panel A is a replicate community corresponding to the same panel of figure 5.9, since $HL = 0\%$ in both cases. The RADs are qualitatively similar. From figure 5.11 the communities do appear to become less even along the contiguous HL gradient. HL is also seen to cause extinctions, which we know from figure 5.3 is a general feature of the contiguous scenario at this IR. At 90% HL two species have an absolute abundance of zero, while a number of other species have low relative abundances in discrete steps (presumably corresponding to absolute abundances of one, two, three, individuals, etc.). This pattern suggests that many species are on the border of total extinction in this community, as predicted in section 5.1. However the discontinuity that was characteristic of RADs in the random scenario is not present, such that there is no clear distinction between core and tail species (in such cases the *Zipf* and *preemption*

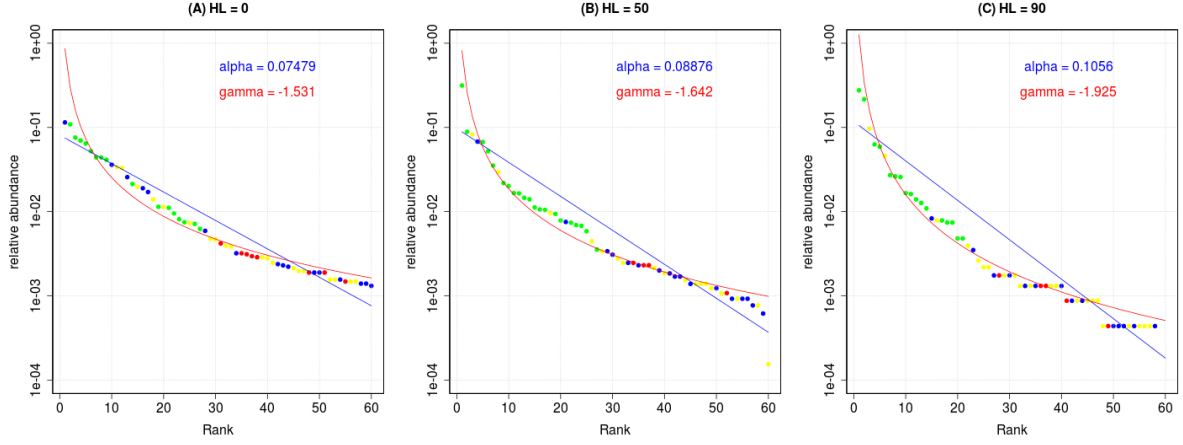


Figure 5.11: Similar to figure 5.9, but for **antagonistic communities** ($MAI = 0.0$), under **contiguous HL**.

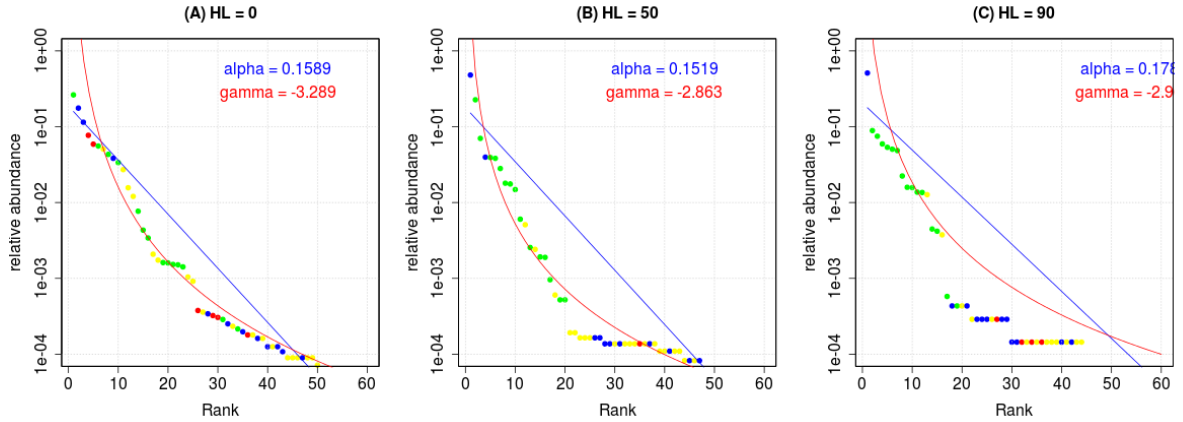


Figure 5.12: Similar to figure 5.9, but for **mutualistic communities** ($MAI = 1.0$), under **contiguous HL**.

model coefficients may be used to quantify evenness).

Figure 5.12 shows RADs for mutualistic communities ($MAI = 1.0$) under contiguous HL. Such communities were observed (section 5.3.1) to become slightly less even on average at the community level, but the evenness did not change significantly within functional groups. Panel A is a replicate of the community in the same panel of figure 5.10, since $HL = 0\%$ in both cases. In figure 5.12 there is less of a distinction between core and tail, and there are fewer extinct species, but otherwise the RADs are qualitatively similar. These mutualistic communities are less even than the antagonistic communities in figure 5.11 because of the effect of mutualism already discussed. The communities also decrease in evenness along the HL gradient, and exhibit more species extinctions than the antagonistic equivalents. We suggest that the reason evenness does not decrease within trophic levels due to HL, is partly that these communities already have

low evenness in pristine landscape. A wide range of relative abundances for all four trophic levels is visible in panel A of the figure. Once again there is not a clear discontinuity between core and tail species. However at 90% HL the tail-end of the distribution again displays discrete steps in relative abundances characteristic of species on the border of extinction.

5.4.3 Relative abundance by functional group

In this section we briefly consider how the relative abundance of the functional groups responds to HL at the same IR value (0.0005). Figure 5.13 shows the relative abundance of each functional group under random HL. The main feature of these plots is that random HL causes a shift in biomass towards the basal trophic level. The same type of shift was observed at the default IR value in chapter 3, however it is more extreme at this low IR. The only non-basal functional group which retains any appreciable abundance up to high levels of HL (90%) are mutualistic-animals. At 90% HL antagonistic communities become almost completely dominated by plants (relative abundance < 0.9), while communities with mutualism become dominated by plants (mutualistic and non-mutualistic) and mutualistic-animals. Both these observations are consistent with the RADs presented in section 5.4.2. The shift towards basal species under random HL is due to weaker trophic interactions, which in turn is related to the decreased mobility of individuals in a randomly impacted landscape (as argued in section 3.4).

At the default IR value we saw that the relative abundance of primary-predators was constant along the random HL gradient. This, it was argued, is because primary-predators are the largest functional group in terms of species and therefore receive the most input from immigration. Here we see that the relative abundance of primary-predators decreases, and we associate this difference with reduced input from immigration due to the low IR value. Also figure 5.13 reveals that in pristine landscape top-predators have a lower relative abundance than at the default IR value, while plants have a higher relative abundance (especially at MAI= 0.0, see figure 3.7 for comparison). We conclude that this difference is partly due to the removal of feeding links between top-predators and basal species, links which were not removed in chapter 3. However there may also be an effect of reduced IR. Since immigration provides a food source for all non-basal species, the reduction of IR will affect species at the top of food chain the most, whilst the reduced predation pressure will benefit basal species which do not require food.

Figure 5.14 shows the relative abundance of each functional group under contiguous HL. There is a slight decrease in the relative abundance of both predator groups at all MAI ratios (panels E and F). We know that mobility (section 3.4) and trophic interactions (figure 5.5) remain strong under contiguous HL. Despite this predator species suffer as a result of contiguous HL at this IR value, suggesting reduced resource availability and perhaps increased competition. At MAI= 0.0 and 0.5 there is an increase in the relative abundance of non-mutualistic plants, presumably due to decline in the abundance (or extinctions of) grazing species. However mutualistic-plants do not benefit, perhaps because they are grazed on by mutualistic-animals

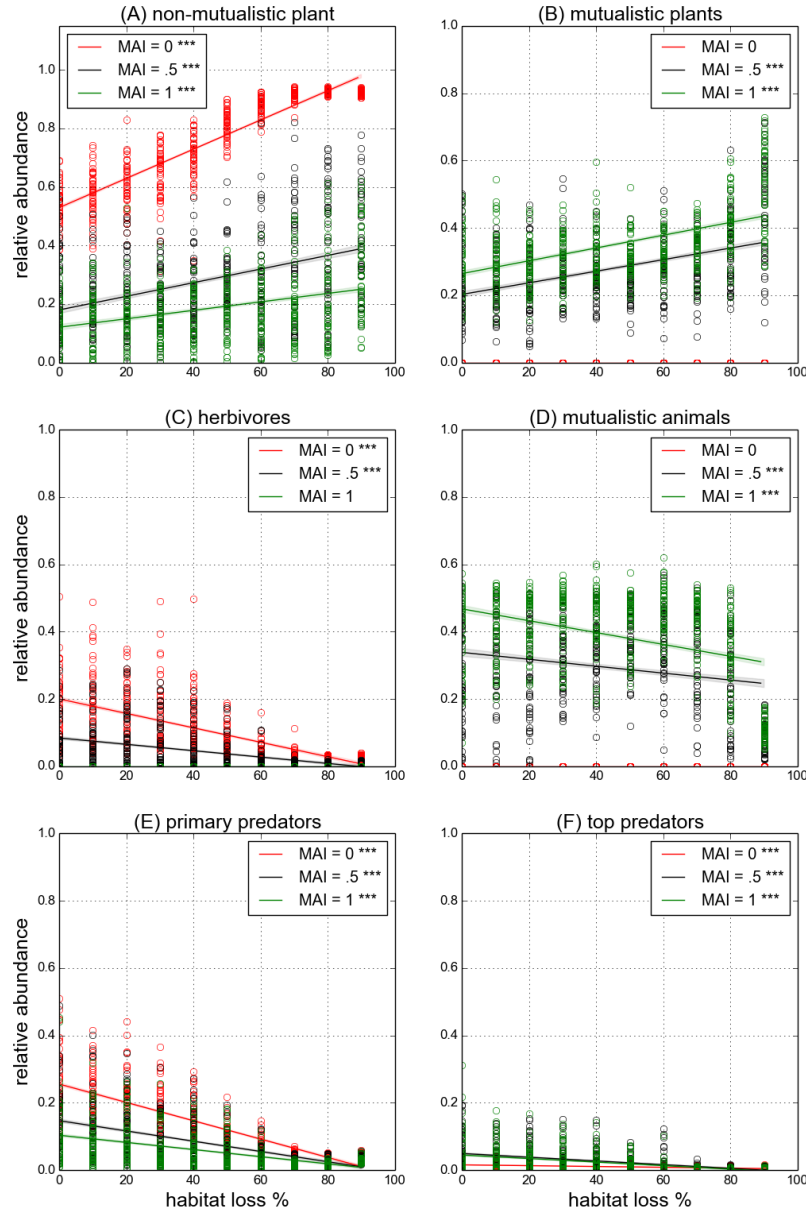


Figure 5.13: **Relative abundance** by functional group for **random HL**. Abundance relative to total number of individuals in the community. Format of individual plots is the same as in figure 5.7.

5.4. BIVARIATE ANALYSIS: FIXED IR

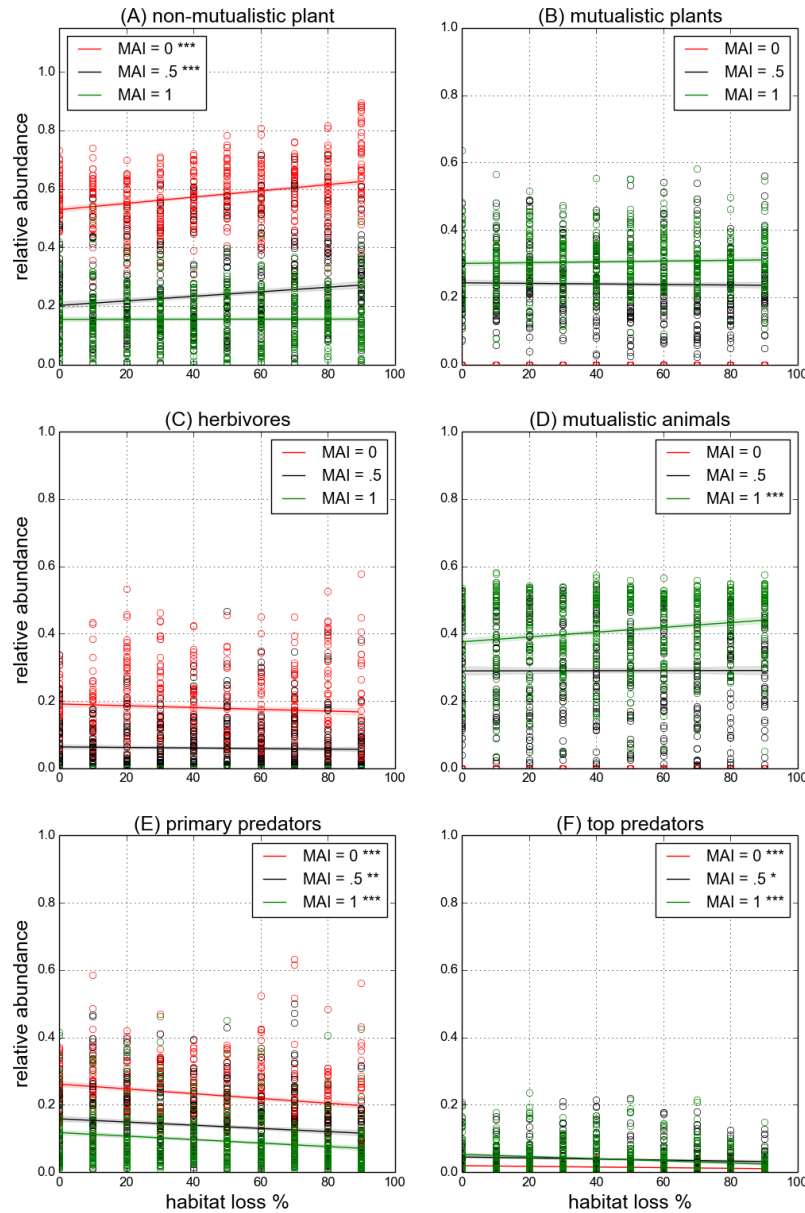


Figure 5.14: **Relative abundance** by functional group for **contiguous HL**. Abundance relative to total number of individuals in the community. Format of individual plots is the same as in figure 5.7.

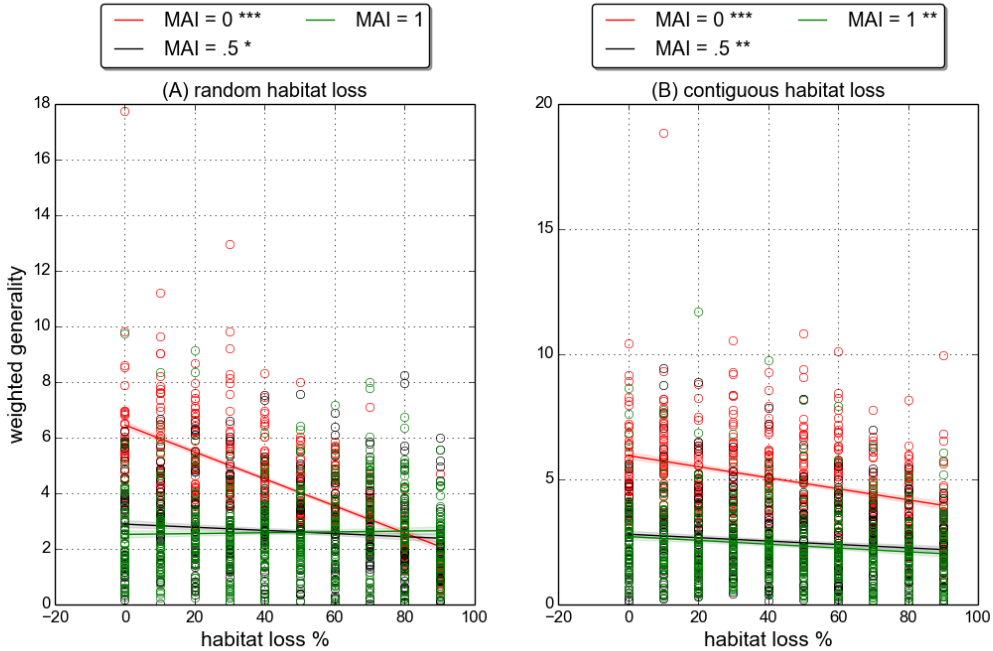


Figure 5.15: Similar to figure 5.7, but for *weighted quantitative generality* (defined in section 2.8.4). **IR= 0.0005**.

which either remain relatively abundant ($MAI= 0.5$) or increase in relative abundance ($MAI= 1.0$).

5.4.4 Network properties

We now consider changes in network properties in response to HL. For simplicity results are only presented for quantitative generality and vulnerability (defined in section 2.8.4). In chapter 3 we saw that the response of these metrics was associated with changes in the evenness of species abundances, or lack thereof. Therefore we may expect responses that correspond to the changes in evenness discussed in section 5.4.1. However the lower IR used here (0.0005) produces species extinctions, as we have seen. The loss of species may also drive changes in network properties.

Figure 5.15 shows the response of generality under random and contiguous HL. We see that generality decrease significantly in all cases, except at $MAI= 1.0$ under random HL. In general the change in generality is less for communities with mutualism, and they tend to have lower generality than antagonistic communities across the HL gradient. This difference relates to the lower evenness of mutualistic communities. A decrease in the generality metric corresponds to a drop in the *number of effective prey per predator*, which may be associated with a reduced number of *actual prey*, a reduced evenness in interaction frequencies, or both. In the random scenario we expect a drop in the actual number of prey because of the restriction on mobility presented by destroyed cells. In the contiguous scenario a drop in the actual number of prey may be produced

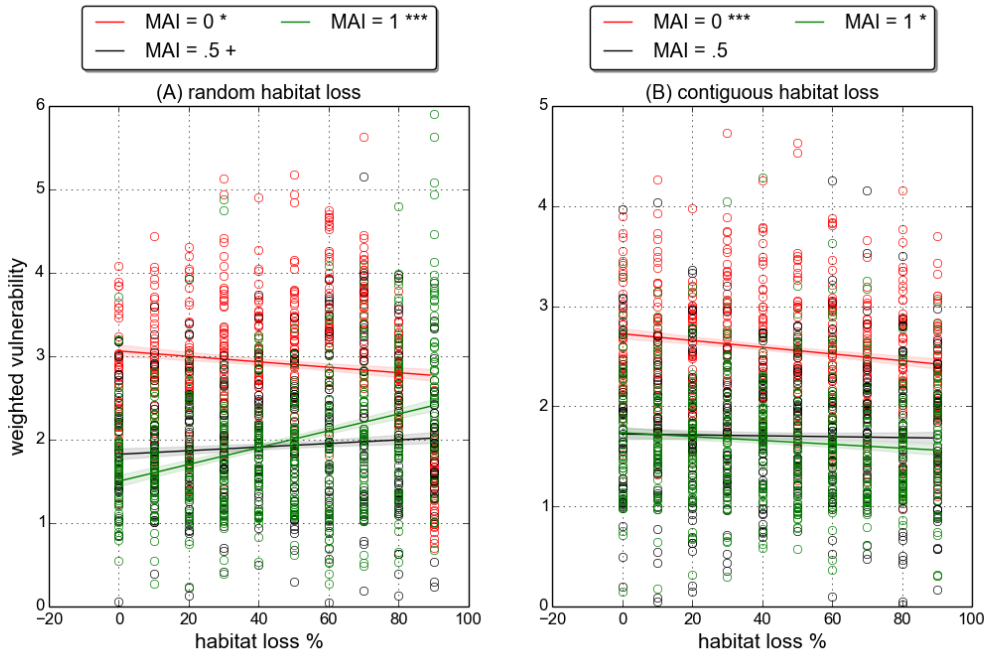


Figure 5.16: Similar to figure 5.7, but for *weighted quantitative vulnerability* (defined in section 2.8.4). IR= 0.0005.

by species extinctions or extreme scarcity. Also in some cases at this IR value we have seen that communities become less even, which acts to reduce the evenness of interaction frequencies.

Figure 5.16 shows the response of vulnerability under random and contiguous HL. A decrease in vulnerability represents a decrease in the *number of effective predators per prey*, and an increase represents the converse. At MAI= 1.0 random HL produces a significant increase in vulnerability (panel A). This corresponds to the increase in evenness observed for these communities (figures 5.7 and 5.8). In all other cases vulnerability either decreases or does not change significantly, in ways that correspond directly to the observed changes in evenness. Therefore, as in chapter 3, the results for the quantitative network metrics are consistent with the conclusion that they are predominantly driven by changes in the evenness of species abundances.

5.5 Bivariate analysis: fixed HL

In this section we study communities along a gradient of IR, at fixed HL. An intermediate HL value of 40% was selected such that *some* of the effects of habitat loss are present in the communities studied (see section 5.3.3). For an intuition of the state of the landscape at 40% HL see figure 3.23 (and the relevant animations at [138]). The analysis in this section addresses the following two observations from earlier in the chapter:

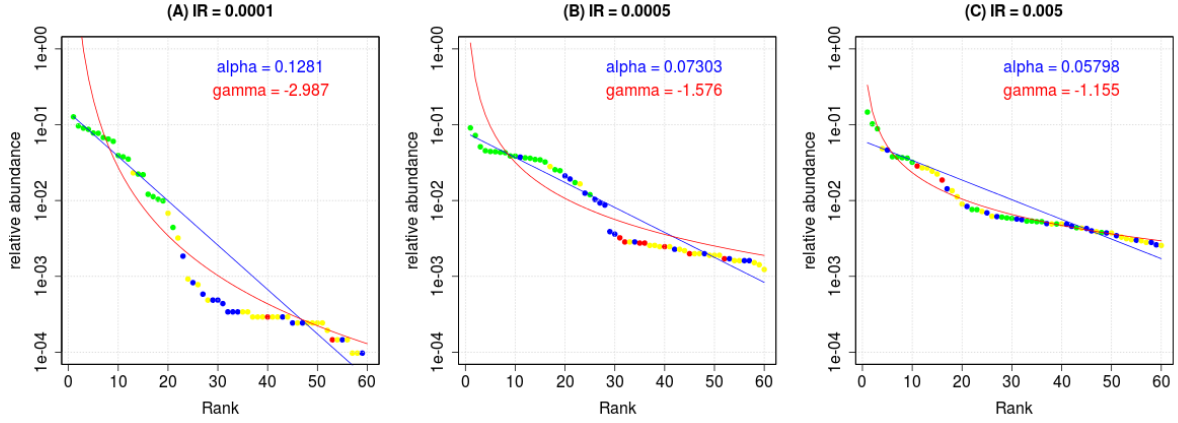


Figure 5.17: Similar to figure 5.9, but for three different IR values. In all cases **HL = 40%**. These RADs are for **antagonistic communities** (MAI = 0.0), under **random HL**.

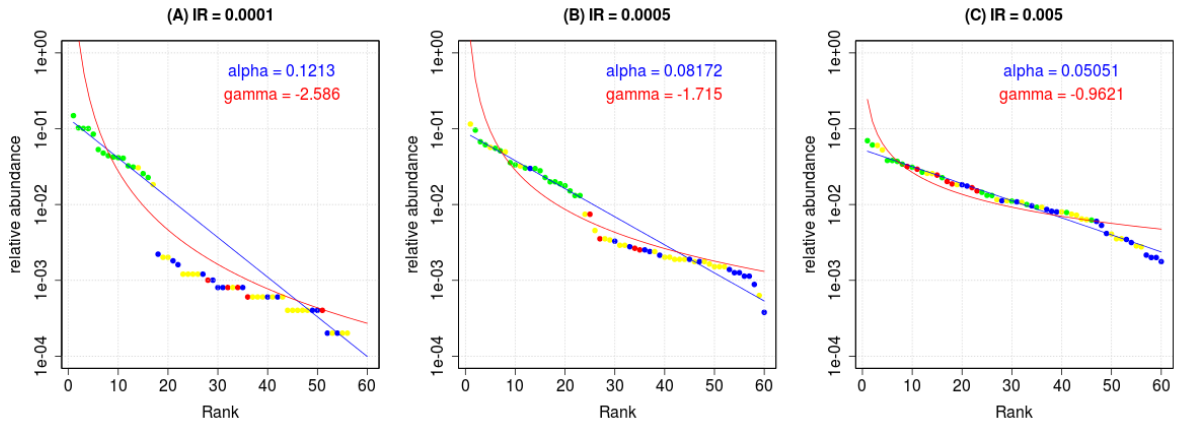


Figure 5.18: Similar to figure 5.9, but for three different IR values. In all cases **HL = 40%**. These RADs are for **antagonistic communities** (MAI = 0.0), under **contiguous HL**.

1. The total number of individuals in mutualistic communities appears to be insensitive to IR (figures 5.2 and 5.3).
2. The total number of individuals in antagonistic communities increases at the lowest IR values (section 5.3.1), but this is not matched by a corresponding increase in the total number of interactions (section 5.3.2).

Both observations can be understood by looking at rank-abundance distributions (RADs) for communities at different IR values. RADs are plotted at three IR values: the lowest IR (0.0001), the highest IR (0.005), and the intermediate IR (0.0005) which was used in the previous section. Figures 5.17 and 5.18 show RADs for antagonistic communities at 40% random and contiguous HL respectively. At the lowest IR (panel A) the RADs are uneven and discontinuous,

5.5. BIVARIATE ANALYSIS: FIXED HL

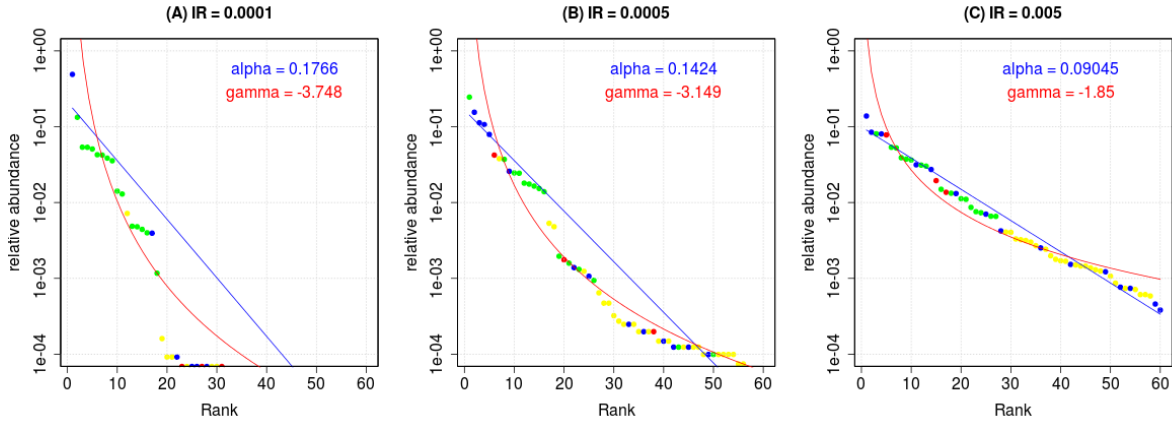


Figure 5.19: Similar to figure 5.9, but for three different IR values. In all cases **HL = 40%**. These RADs are for **mutualistic communities** (MAI = 1.0), under **random HL**.

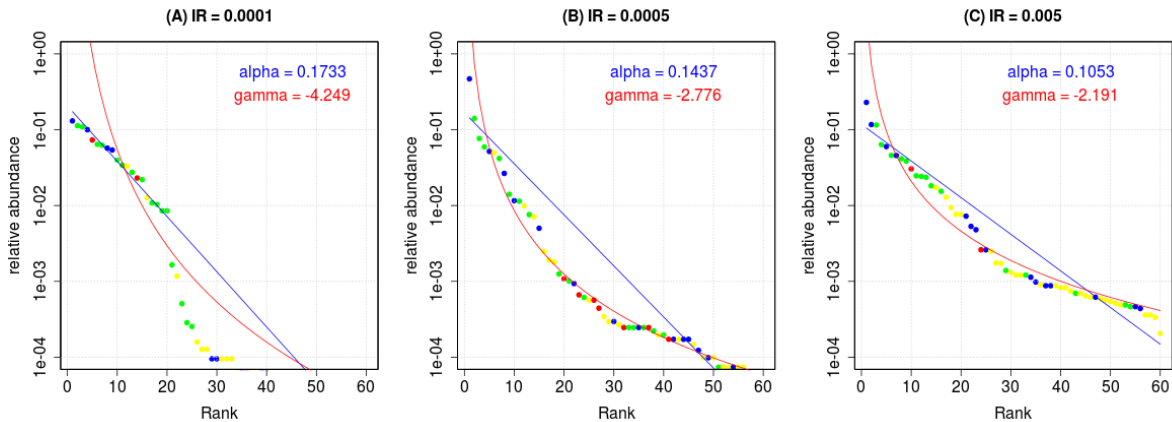


Figure 5.20: Similar to figure 5.9, but for three different IR values. In all cases **HL = 40%**. These RADs are for **mutualistic communities** (MAI = 1.0), under **contiguous HL**.

and the communities are dominated by plant species. This confirms our prediction from section 5.3.2 that the increase in abundance of antagonistic communities at very low IRs is due to an increased dominance of plants. At $IR = 0.0001$ in both types of habitat (random and contiguous), non-basal species struggle to maintain viable populations that can interact with and make use of the high availability of plant biomass. This is consistent with results from section 4.2 where it was observed that communities without immigration are characterised by mass extinctions in non-basal levels, even in pristine landscapes. Increasing the IR makes the RADs more even. At $IR = 0.0005$ (panel B) communities are still dominated by plant species, but the discontinuity between core and tail species is reduced. At $IR = 0.005$ the communities are more even still and more non-basal species are present in the lowest ranks.

Figures 5.19 and 5.20 show RADs for mutualistic communities at 40% random and contiguous HL respectively. At the lowest IR (panel A) the RADs are uneven and species persistent is low. In both types of landscape there are only around 30 species present in the community. In the random landscape the core of species consists only of plants and a single species from the second trophic level, which must be a mutualistic-animal. None of the benefit of mutualism is conferred to other species due to the nature of random HL, as we have seen previously (section 5.4.2). In the contiguous landscape the core is more diverse, with species from all trophic levels, as we would expect due to the stronger species interactions in such a landscape. In both the random and contiguous cases we again see that increasing IR makes the RADs more even, which by now is a familiar result. Despite the very different characteristics of the RADs, the total number of individuals is approximately equal in all six communities displayed (as discussed in section 5.3.1). We see that the constant number of individuals in mutualistic communities is due to the dominance of a core of species, which may or may not contain species from all trophic levels depending on the type of HL. Increasing the immigration rate serves to increase diversity by reducing the dominance of the mutualistic core, and promoting evenness in the RADs, whilst maintaining the same total abundance.

5.6 Discussion

The main goal of this chapter was to determine how community responses to the two habitat loss (HL) scenarios differed from those seen in chapter 3, when the immigration rate parameter (IR) was reduced. In particular, given that the loss of habitat in nature leads to the loss of species, we were interested to find IR values at which HL produced species extinctions. Also, given the importance of the immigration mechanism in driving structural properties such as evenness (chapter 3), and dynamical properties such as variability and determinism (chapter 4), we were motivated to study such properties systematically over a large region of parameter space. The analysis has generally furthered our understanding of communities simulated using the IBM model. We have found certain results to be consistent with those of chapter 3, and which therefore appear to represent robust features of the model. We have also presented certain new and unexpected results, which provide fresh insight into the workings of the model. The key results, falling into both of the aforementioned categories, are discussed in turn below before considering the ecological significance of these results in the conclusion (section 5.7).

Strong species interactions are associated with high temporal variability in population dynamics. This result was evident from the previous two chapters, and is robust across the region of parameter space explored here (section 5.3.2). Random HL serves to reduce species interaction strengths, and therefore reduces temporal variability. The converse holds for contiguous HL. In general reducing the IR increase temporal variability (in agreement with chapter 4), and slightly increases interaction strengths. Both the metric for temporal variability (mean CV)

and for interaction strength (IS) tend to infinity in the limit that species abundance tends to zero. This property of the metrics must be considered in situations where species abundances are low, especially given the discrete nature of the model (species abundance must be integer valued). Specifically this limit behaviour appears to be an issue for *IS* at the lowest IR value (both scenarios), and for *mean CV* at high levels of random HL.

Immigration is a key feature of the model. The roles of immigration in promoting evenness and reducing temporal variability were first observed in chapters 3 and 4. Both observations hold across this region of parameter space (sections 5.3.1, 5.3.2 and 5.4.1). The fact that immigration prevents species extinctions has also been confirmed, since lowering IR was found to produce species extinctions (section 5.3.1). However extinction patterns were found to differ between the contiguous and random scenario.

In general contiguous HL produces more extinctions than random HL (section 5.3.1). Also the number of extinctions due to contiguous HL is clearly dependent on the level of destruction, whereas under random HL this is only the case for antagonistic communities. At the reduced IR of 0.0005, random HL does result in uneven communities with discontinuous RADs (section 5.4.2). Under both types of habitat loss predator species (top two trophic levels) suffer (section 5.4.3). However, the low abundance species in the tail of the RAD are less vulnerable to extinction under random HL than contiguous. Under contiguous HL communities become less even (at the IR= 0.0005) and many species in the tail go extinct. This results from the strong trophic interactions, characteristic of the contiguous scenario, which drive species to extinction. In contrast random HL produces weak interactions, and as such rare species are subject to less predation pressure from the more abundant species.

In this chapter we have seen marked difference between mutualistic and antagonistic communities. As discussed previously mutualistic communities are less even (chapter 3 and [58]). One consequence of this is that mutualistic communities exhibit more extinctions than antagonistic ones (section 5.3.1). Under random HL at low IR these extinctions are seen even in pristine landscape, where trophic interactions remain strong, and may be reduced by the onset of HL which reduces interaction strengths. Under contiguous HL mutualistic communities only exhibit more extinctions from increased HL, since trophic interaction strengths are increased. Extending the findings of chapter 4, it is now clear that the lower evenness of mutualistic communities results from the dominance of a core group of species (section 5.4.2, 5.5). Depending on the context, this core group may contain non-mutualistic species which benefit as a by-product of mutualism. The core group is also able to maintain the total abundance of the community as a whole in the face of changing IR (section 5.3.1), by increasing its dominance (section 5.5). Increased IR serves to reduce the dominance of the core group and allow competing species to prosper.

In section 5.4.4 we saw that network properties (quantitative generality and vulnerability) may change under both types of HL at low immigration rates (IR= 0.0005). This represents a departure from the results of chapter 3, where only random HL produced significant changes in

network properties. In general the observed changes in network properties are consistent with the conclusion that they are largely driven by changes in the distribution of species abundances (characterised by *evenness*). However the species extinctions, observed at reduced IR, may also contribute to changes in network properties. Further analysis would be required in order to fully understand the mechanisms that drive changes in the structure of the realised interaction network. We do not pursue such an analysis in this thesis. We conclude that network properties may indeed change in response to HL, in ways that are related to other changes in the community. Therefore such properties represent useful indicators of the impact of HL. However sole focus on network properties may obscure some of the effects of HL. For example, network properties did not change under contiguous HL at high IR (chapter 3), despite significant changes in interaction strengths (IS) and a loss of temporal stability.

5.7 Conclusion and perspectives

In this section we summarise the main findings regarding community responses to habitat loss, and discuss them in the context of the literature introduced in chapter 1. In the following chapter we then move on to the problem of inferring species interaction strengths from population dynamics. From the analysis in this chapter, and chapter 3, it is clear that mutualism plays an important role in shaping communities, and mediating their response to HL. In general we have observed that mutualism reduces the evenness of communities, and it appears that this is due to a dominant core of species which benefit either directly or indirectly from mutualism (sections 5.4 and 5.5). Two recent empirical studies have detected a similar effect in natural systems. The presence of a *resource mutualism* between plants and root fungi was experimentally manipulated in a field study by Rudgers et al. [?], and in a mesocosm experiment by Keller [?]. Both studies determined that the presence of mutualism had negative effects on the diversity of the plant community as a whole, resulting from increased dominance of the plant mutualists. In [?] the mutualism was found to increase total plant productivity on aggregate, despite the decrease in diversity. In [?] the effect of mutualism was seen to propagate to higher trophic levels, reducing the diversity of arthropod species. Our results are in agreement with these observations. Furthermore, they suggest that the diversity-reducing effect of mutualism changes community response to habitat loss, leading to a larger number of extinctions due to the reduced fitness of non-mutualistic competitors.

Our findings support previous theoretical results that the effects of HL are mediated by the spatial pattern in which habitat is destroyed [67–73]. The most general result from the studies cited is that habitat lost in some spatially-correlated manner is less detrimental than habitat lost at random (in terms of the number of expected extinctions). The reasoning for this is that spatially-correlated loss leaves larger areas of pristine habitat in tact. We have compared two patterns of HL: random and contiguous. Our treatment represents a detailed investigation of

the matter because the modelling is spatially-explicit, individual based, and multi-trophic. The results do not entirely agree with previous modelling studies. In particular contiguous HL was found to produce more extinctions than random HL, and was also more damaging in terms of dynamic stability. In contrast random HL showed the potential to produce *trophic collapse*, because destroyed landscape cells provided barriers to motion, reducing the ability of individuals to find interaction partners. In some cases random HL produced communities that were almost entirely dependent on immigration to persist. However, because of the weak trophic interactions in these communities, even a small non-zero IR was enough to mitigate species extinctions.

The observed responses of communities under contiguous HL are consistent with those derived from a meta-community model by McCann et al. [99]. Their model showed that *spatial compression* of communities may result in strong predation by organisms in higher trophic levels, with a destabilising effect in the local communities. Perhaps the most significant difference between our model and theirs is the mechanism by which predator species are able to persist in highly impacted landscapes. In our model this mechanism is immigration (see chapter 4), in theirs it is mobility of the predator between different patches. However, the destabilising effect of predation is the same. There is some empirical evidence that increased temporal variability is present at the edge of forest fragments [88]. Gonzalez et al. [17] suggest that this effect may be due to increased interaction strengths, although they stress the need for empirical studies to confirm this hypothesis. Similarly Wang et al. [33] have demonstrated, using data from Barro Colorado Island, that temporal variability in tree biomass increases as patch size is reduced. However, it is not clear if this variability is associated with increased interaction strengths. Our findings, together with these previous studies, support the call for empirical research into the effect of habitat loss on interaction strengths.

In general our model suggests that strong trophic interactions are destabilising. This conclusion is supported by a wealth of previous theoretical studies (from [48] to [49] and [158]), and by the empirical work of O'Gorman [51]. We have seen that strong interactions produce variable population dynamics, reduce the evenness of the community, and drive species extinctions in the case of contiguous HL. There is also evidence (chapter 4) that trophic interactions drive resource competition in simulated communities. However we have not modelled competitive interactions directly. Coyte et al. have recently suggested that such interactions may be key in stabilising communities [160], and their inclusion in the IBM may present an interesting avenue for further study. In general we have not found evidence that the introduction of mutualism stabilises the dynamics of communities with strong antagonistic interactions, as suggested by Mougi et al. [43]. In fact, as discussed above, mutualism has proven to be harmful to communities in many ways.

Throughout chapters 3 to 5 immigration has been revealed as a key factor in the IBM. The immigration mechanism, as we model it, drives evenness in species abundances and their distribution across space. Immigration may also counter the effects of mutualism (by reducing the dominance of the mutualistic core), and dampen the temporal variability associated with strong

species interactions. It may also mitigate some of the effects of HL, in particular by preventing the extinction of species. However, in this chapter, we have shown that there is a subtle interplay between immigration and the response of community properties (such as evenness) to HL. In many ways the response of communities at low levels of immigration ($IR = 0.0005$) was more *realistic* than those observed at the *default IR*. Specifically, HL resulted in species extinctions; predator populations suffered under both types of HL; and evenness decreased in some cases (representing a loss of diversity). These findings suggest that the *default IR value* may be artificially high compared that of natural communities.

It is clear, from chapter 4, that some non-zero IR is required for the IBM to produce persistent and diverse communities. Such a situation may not be *unrealistic*. As discussed in section 1.2, the study of local communities in isolation from their surroundings is an abstraction of nature. In [30] Rickelfs argues that not only must we consider larger areas of space in order to understand biodiversity at a regional scale, but we must consider influence from different localities in order to understand any single local assemblage of species. Hence the popularity of the meta-community concept [34], and the associated class of models (for example [73]). The immigration mechanism of the IBM models such connectance of the local community with other parts of the landscape. Given the importance of immigration, and the simplicity of the mechanism by which we model it, this seems a natural candidate for further development of the IBM. One possibility would be to introduce differential rates of IR for species in different trophic levels (this would account for the fact that larger species tend to be more mobile). An alternative, and more computationally expensive option, would be to simulate numerous communities in parallel and allow dispersal of individuals between different landscapes. In either case, changes to the way that immigration is modelled would likely affect simulated community responses to HL.

In this chapter and chapter 3 we have seen that network properties may change in response to HL. We have argued that, in the IBM simulations, the changes in network properties are largely driven by changes in the distribution of species abundances. Therefore in this chapter we have focused more closely on properties relating to species abundances and on stability. However the ability to study network properties and how they relate to other aspects of simulated communities is a powerful feature of the IBM. Therefore further investigation on this topic represents more scope for future development. It would be informative to use statistical methods to quantify the mechanisms that drive changes in network structure. It would also be possible to ask explicit questions about the role of network structure in generating community properties (such as stability). This possibility was touched on in chapter 4. By using interaction networks with pre-defined properties (for example modularity or nestedness), or even empirically derived networks, it would be possible to gain more insight into the role different structural properties.

CHAPTER
6

TOWARDS INFERRING SPECIES INTERACTIONS FROM POPULATION DYNAMICS

6.1 Introduction

In this chapter we develop a methodology for the estimation of species interaction strengths from population dynamics data. The primary motivation for this task was provided in section 1.5. Throughout this thesis we have seen that species interactions play a key role in driving the structure and dynamics of simulated communities. In particular strong interactions have been shown to increase the temporal variability of population dynamics. They have also represented one main difference between communities under the two types of habitat loss (HL) studied: random and contiguous. Random HL has been shown to present barriers to the motion of individuals, which reduced species interaction strengths. In contrast contiguous HL was found to increase interaction strengths by compressing individuals into a smaller region of space. These changes in interaction strengths partly explained the different responses of communities to the two types of HL. For example contiguous HL produce more extinctions, and did not result in trophic collapse of communities to the same extent as random HL. The important role of interaction strengths in understanding the results of previous chapters, further motivates the study of methods to quantify them. Previously the metric IS (equation (2.19)) has been used. However this metric requires accurate knowledge of all interaction frequencies and species abundances. The method developed in this chapter requires only the latter, although abundance time series are required rather than snapshots. The method also makes explicit the connection between community dynamics and interaction strengths, by fitting a population dynamics model.

The original intention for this chapter was to obtain an empirical dataset with high resolution abundance time series *and* quantified interaction strengths. Such a dataset would provide the

ideal test of the methodology presented. However such data was not forthcoming, either in the form of experimental mesocosm data, or that sampled from a real-world community. Therefore the methodology is developed with application to simulated community dynamics. Such an approach ensures knowledge of the interactions involved in the study system, and allows detailed analysis of the results over a range of experimental conditions. Section 6.2 provides full details of the methodology, which is summarised in figure 6.1. In section 6.3 interaction strengths are inferred from two species predator-prey dynamics, simulated using ordinary differential equation models. The accuracy of the inferred results are evaluated for two different simulation models, under noise and using different sampling regimes. In section 6.4 interaction strengths are inferred from community dynamics simulated using the IBM model. Two, three, five, and sixty species communities are investigated. In section 6.5 the performance and limitations of the methodology are discussed. Finally in section 6.6 further developments are considered, including the potential for applications to empirical data. Although the focus of this chapter is on antagonistic predator-prey interactions, the intention is that this methodology could be extended to infer other interaction types (mutualism and competition).

6.2 Methodology

The methodological approach to the estimation of species interaction strengths is depicted in figure 6.1. The starting point is a *data generator* from which samples of population sizes are taken over a given period of time. The *data generator* may be a natural ecosystem, or laboratory experiment, from which we wish to determine which species are interacting and quantify the strengths of those interactions. Given that the interaction strengths between species are not known *a priori* for a natural system (hence the motivation for the current investigation), in this chapter we use computer simulations of interacting species as a *data generator* to develop the methodology. Sampling from the *data generator* produces a *data stream*, which is an N -dimensional time series $x_i(t)$ representing the population size of each of the N species sampled at discrete time points t . Examples of *data generators* and *data streams* are plotted in section 6.3.4. An *inference method* is then applied to the sampled time series, producing estimates of the strength of interactions between all pairings of the N species in the original *data generator*. The *inference method* used here involves fitting a *generalised Lotka-Volterra* (GLV) model, which is defined in section 6.2.2. The procedure used to fit the GLV to time series is adapted from work by Shandilya and Timme [118], and is detailed in section 6.2.3.

The performance of the *inference method* is evaluated by comparing its results to known properties of the *data generator*. In the first part of this chapter (section 6.3) ordinary differential equation (ODE) models are used as *data generators* to simulate population dynamics. These ODE models are defined in section 6.2.1 and are useful here because they allow analytic calculation of *a priori* interaction strengths. Therefore we are able to compare the interaction strengths estimated

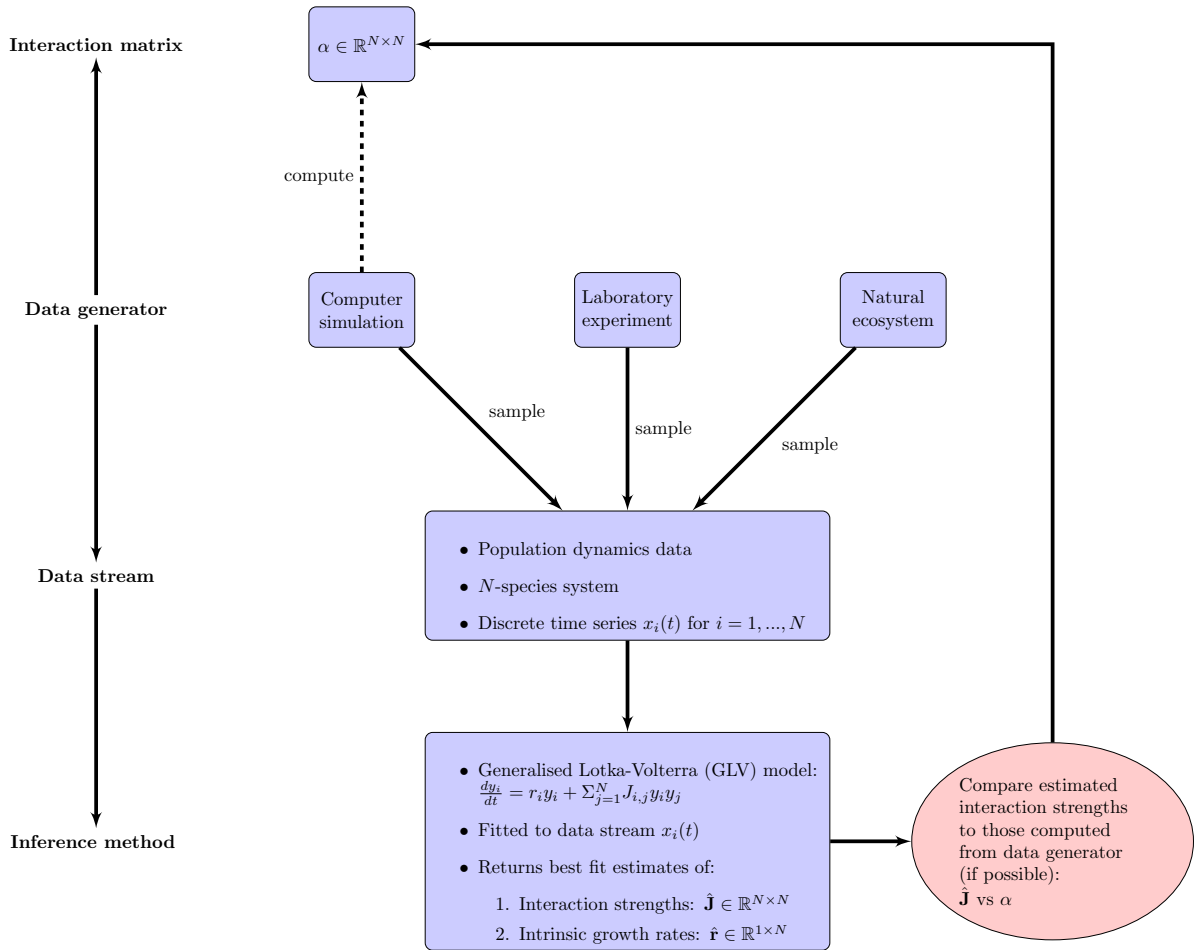


Figure 6.1: Methodological approach to estimate species interaction strengths from population dynamics, and evaluate the resulting estimates.

by the *inference method* (the GLV fit), to those calculated directly from the *data generator* (the ODE model). To calculate interaction strengths from the ODE models we use a metric called the *interaction matrix* (α) [46]. The definition of α and its interpretation are given in section 6.2.4.

Later in the chapter (section 6.4) the IBM model, familiar from previous chapters, is used as the *data generator*. Unlike the ODE models the IBM does not allow *a priori* calculation of interaction strengths. However we do know *which species interact* in the IBM, because this is specified by the underlying interaction network. Therefore one test of the *inference method* when applied to the IBM is to see if it correctly identifies which species are interacting. Also, in the IBM, interaction strengths between species emerge as a result of interactions between individuals in the landscape. We have seen previously that the strength of these species interactions can be quantified from simulation output by the metric IS (defined in section 2.8.4.3). Therefore the performance of the *inference method* can also be evaluated by comparing IS and α . More details on the use of the IBM as the *data generator* are given at the beginning of section 6.4. In the rest

of this section full details of the methodology as applied to ODE *data generators* are provided, in the order introduced above (and corresponding to the flow chart in figure 6.1).

6.2.1 Data generator: ordinary differential equation models

In section 6.3 ordinary differential equation (ODE) models are used as the *data generator*. As discussed above, this approach allows analytic calculation of *a priori* interaction strengths from the simulation models. It also enables us to investigate problems arising from non-linear functional interaction between species. The results presented in this chapter are all for *antagonistic* communities. Therefore each inter-specific interaction is modelled as predator-prey type. The ODE modelling framework defined below is specific to predator-prey systems, but may be extended to model other interaction types (e.g. competition and mutualism). For an N species predator-prey system the ODE model is defined by N coupled first-order differential equations, which take the general form

$$(6.1) \quad \frac{dx_i}{dt} = G_i(x_i) + \sum_{j=1}^N C_{ij}(x_i, x_j),$$

where x_i represents the population density (or biomass/abundance) of species i ; $G_i(x_i)$ is the intrinsic growth function of species i ; and $C_{ij}(x_i, x_j)$ is a function that defines the coupling (or interaction term) between species i and j . The form of (6.2.1) is sufficiently general that most common models from the population dynamics literature may be expressed in this way by making suitable choices for C and G . Examples of such models include those of Holling [119], Rosenzweig and MacArthur [?], Arditi [120], and Lotka-Volterra [127, 128]. In section 6.3 the results presented are for two species systems, for which the full model may be expressed as

$$\begin{aligned} \frac{dx_0}{dt} &= G_0(x_0) + a_{01}x_1 H(x_0, x_1), \\ \frac{dx_1}{dt} &= G_1(x_1) + a_{10}x_0 H(x_0, x_1) \end{aligned}$$

where species x_0 and x_1 are the population densities of the prey and the predator species respectively; and we have expressed the coupling term in terms of $H(x_0, x_1)$, the *functional response* (FR) of the predator, which is multiplied by constant coupling coefficients a_{ij} . The FR defines the per-capita rate of consumption of the predator, and is a key feature of such predator-prey models [96, 122]. The coefficients a_{01} and a_{10} are negative and positive respectively, such that the prey losses biomass, and the predator gains biomass as a result of the interaction. These coefficients may be used to introduce asymmetry into the interaction terms. For example it is common to choose $|a_{01}| > |a_{10}|$, to model the inefficiency of the predator in the conversion of biomass from the prey. For the intrinsic growth functions we use the functional forms

$$G_0(x_0) = r_0 x_0 \left(1 - \frac{x_0}{K_c}\right)$$

$$G_1(x_1) = r_1 x_1,$$

where $r_0 > 0$ and $r_1 < 0$ are the intrinsic growth rates of the prey and predator respectively; and K_c is the carrying capacity of the prey species. Therefore the predator has an exponential intrinsic mortality, whereas the prey species has logistic intrinsic growth. These use of these functional forms to model intrinsic growth was made popular by Rosenzweig and MacArthur [?]. The justification for the use of logistic growth in the prey but not the predator is that it models a finite availability of resource (be it space, light, nutrients etc.) to the prey species, whereas the resource availability to the predator (i.e. x_0) is modelled directly. However some models, especially those of marine systems, have included similar limiting terms in the intrinsic growth function of the predator species [?]. These limitations are known as *closure terms*, and they attempt to model feeding effects on the predator from species in higher trophic levels which are not modelled directly. For simplicity we choose not to include closure terms in our modelling framework.

The functional response (FR) defines the per-predator rate of consumption of prey. We focus on the forms proposed by Holling in the 1950s [119], which remain widely used in this field [?]. However it is worth noting that various other forms have been proposed and there is an ongoing debate about which form is most appropriate in different situations [96, 122] (see discussion in section 1.5). There are three types of Holling FR, referred to as types I, II, and III. These can be expressed as

$$H_I(x_0, x_1) = x_0,$$

$$H_{II}(x_0, x_1) = \frac{x_0}{x_0 + K_s},$$

$$H_{III}(x_0, x_1) = \frac{x_0^2}{x_0^2 + K_s^2},$$

where x_0 is the prey density, and K_s is the saturation constant for the predator, giving the prey density at which the per-predator consumption rate reaches half-maximum. We choose to narrow our investigation by focusing here on the first two forms: Holling type I and type II. Based on the choice of FR we obtain two distinct simulation models, which we refer to as the *type I* and *type II* models.

The type I model uses the FR given by (6.4). This is the simplest of the Holling functions. The per-predator predation rate is linear in prey-density. The full *type I* model is given by

$$\begin{aligned}\frac{dx_0}{dt} &= r_0 x_0 \left(1 - \frac{x_0}{K_c}\right) + a_{01} x_0 x_1 \\ \frac{dx_1}{dt} &= r_1 x_1 + a_{10} x_0 x_1,\end{aligned}$$

The type I model may be rescaled in order to reduce the number of parameters. This makes the local stability analysis simpler, and reduces the dimension of the search space when probing the equations numerically via simulation. We introduce the following non-negative parameters

$$\begin{aligned}\tilde{t} &= -r_1 t, \quad A = \frac{r_0}{r_1}, \quad B = \frac{a_{01}}{r_1}, \\ C &= \frac{-a_{10} K_c}{r_1}, \quad \tilde{x}_0 = \frac{x_0}{K_c}, \quad \tilde{x}_1 = x_1,\end{aligned}$$

such that equations (6.7) and (6.8) may be written

$$\begin{aligned}\frac{d\tilde{x}_0}{d\tilde{t}} &= A\tilde{x}_0(1-\tilde{x}_0) - B\tilde{x}_0\tilde{x}_1 \\ \frac{d\tilde{x}_1}{d\tilde{t}} &= -\tilde{x}_1 + C\tilde{x}_0\tilde{x}_1,\end{aligned}$$

which is the same *type I* model, but expressed in a reduced parameter space. Henceforth for simplicity we drop the *tildes* unless otherwise stated. The equilibrium population densities are given by

$$x_0^* = \frac{1}{C}, \quad x_1^* = \frac{A}{B} \left(1 - \frac{1}{C}\right),$$

such that x_0^* is always positive since $C \in \mathbb{R}^+$; and x_1^* is positive when $C > 1$. This is a requirement for physical realism, since it is not possible to have negative populations of species. In most applications it is also required that the equilibrium is stable, to allow for the coexistence of species (i.e. *persistence*, see section 4.2). The equilibrium is locally stable if the eigenvalues of the *Jacobian* matrix (\mathbb{J}) have negative real parts. The Jacobian for this model, evaluated at the equilibrium, is given by

$$(6.14) \quad \mathbb{J}_{type\ I} = \begin{bmatrix} -A/C & -B/C \\ A/B(C-1) & 0 \end{bmatrix}.$$

We use conditions on the model Jacobian to guide realistic parameter selection when simulating the model. Parameter selection is discussed further section 6.3.3.

The type II model uses the FR given by (6.5). The per-predator predation rate is a non-linear function of prey density. The type II FR models predator saturation - individuals take a certain amount of time to process and digest prey - such that the predation rate does not increase linearly as the availability of prey increases. Instead the response curve flattens out, or saturates, at high prey densities (see figure 6.2 below). The full *type II* model is given by

$$\begin{aligned}\frac{dx_0}{dt} &= r_0 x_0 \left(1 - \frac{x_0}{K_c}\right) + \frac{a_{01}x_0 x_1}{x_0 + K_s} \\ \frac{dx_1}{dt} &= r_1 x_1 + \frac{a_{10}x_0 x_1}{x_0 + K_s},\end{aligned}$$

We may perform a similar rescaling as we did with the *type I* model to reduce the number of parameters. We introduce the following non-negative parameters

$$\begin{aligned}\tilde{t} &= -r_1 t, & A &= \frac{r_0}{r_1}, & B &= \frac{a_{01}}{r_1 K_c}, & C &= \frac{-a_{10}}{r_1}, \\ D &= \frac{K_s}{K_c}, & \tilde{x}_0 &= \frac{x_0}{K_c}, & \tilde{x}_1 &= x_1,\end{aligned}$$

such that equations (6.13) and (6.14) may be written

$$\begin{aligned}\frac{d\tilde{x}_0}{d\tilde{t}} &= A\tilde{x}_0(1 - \tilde{x}_0) - \frac{B\tilde{x}_0\tilde{x}_1}{\tilde{x}_0 + D} \\ \frac{d\tilde{x}_1}{d\tilde{t}} &= -\tilde{x}_1 + \frac{C\tilde{x}_0\tilde{x}_1}{\tilde{x}_0 + D},\end{aligned}$$

which defines the *type II* model with seven instead of seven parameters. Again we drop the *tildes* unless otherwise stated. The equilibrium populations for this model are given by

$$x_0^* = \frac{D}{C-1}, \quad x_1^* = \frac{ACD(C-1-D)}{B(C-1)^2},$$

such that $x_0^* > 0$ if $C > 1$, and $x_1^* > 0$ if $C - D > 1$. These conditions provide constraints on the possible choice of parameters. Further constraints are imposed by the aforementioned conditions on the trace and determinant of the *Jacobian*. For this model the Jacobian, evaluated at the equilibrium, is given by

$$(6.21) \quad J_{type\ II} = \begin{bmatrix} A \left(\frac{-CD+C-D+1}{C(C-1)} \right) & \frac{-B}{D} \\ \frac{A(C-1-D)}{B} & 0 \end{bmatrix}.$$

Parameter selection for this model is also discussed in section 6.3.3.

6.2.2 Inference method: generalised Lotka-Volterra model

Having simulated population dynamics, using the ODE *data generators* just defined, we then sample from the simulation output to produce a discrete time series $x_i(t)$ for each species i . The time series represents the population size of that species at discrete points in time. Together the $x_i(t)$ for all species represent the *data stream*. To estimate species interaction strengths we fit a *generalised Lotka-Volterra* (GLV) model to the data stream. The GLV model is the extension of the Lotka-Volterra equations to N species, and is given by

$$(6.22) \quad \frac{dy_i}{dt} = r_i y_i + \sum_{j=1}^N J_{ij} y_i y_j,$$

where y_i is the population density of species i ; r_i is the intrinsic growth rate; N is the number of species; and J_{ij} is the coupling between species i and j . Specifically \mathbf{J} is the GLV coupling matrix, not to be confused with the *Jacobian* \mathbb{J} used in local stability analysis. All parameters here (r_i and J_{ij}) may take positive or negative values. The estimated values of J_{ij} , obtained from the model fit, give estimates of species interaction strengths. The J_{ij} values also define the type of interaction between two species. For example if $J_{ij} < 0$ and $J_{ji} > 0$, this suggests that species j predares on species i . The diagonal elements of the coupling matrix ($i = j$) give estimates of intra-specific interactions.

Our choice of the GLV model reflects its simplicity and therefore its breadth of application. As seen from equation (6.2.2) there are no assumptions about species roles built into the functional forms of the model. That is, before the model is parametrised, it does not specify if species i is a prey or a predator. Therefore when the model is fitted to a *data stream* the roles of predator and prey emerge from the fitted model parameters. This feature of the model is especially desirable for the application of our methodology to larger multi-trophic systems (section 6.4).

The *type I* model from section 6.2.1 can be expressed as a GLV model by assigning the parameters as follows

$$r_0 = A, \quad r_1 = -1, \quad J_{00} = A,$$

$$J_{01} = -B, \quad J_{10} = C, \quad J_{11} = 0.$$

Therefore the GLV model should be able to exactly fit to a *data stream* derived from the *type I* model. In this instance we would be able to recover the interaction strengths (and other model parameters) with high accuracy. In practice such ‘perfect’ results are hampered by the presence of noise and sparsity of sampling from the data generator (see results in section 6.3.5). In contrast the *type II* model cannot be expressed in GLV form because of the non-linear functional response (equation (6.5)). Therefore fitting the GLV model to a *data stream* derived from the *type II* model can at best produce approximations of the true interaction strengths and rate parameters (see results in section 6.3.6). However such a situation represents an important test of the inference method, since functional responses found in nature likely take some non-linear form [120].

6.2.3 Inference method: model fitting

To fit the GLV model to sampled *data streams* we use the numerical method developed by Shandilya and Timme [118]. We include here the derivation of their method, but slightly simplified because in their application each *node* represented a chaotic oscillator with three-dimensional dynamics. In our application each node represents a species, with one-dimensional dynamics. The method gives ‘best fit’ estimates of the GLV parameters, which were introduced in section 6.2.2. Conceptually these estimates are obtained by minimising the error between time derivatives calculated from the *data stream*, and those predicted by the model given the *data stream*. Suppose we that we are trying to fit a population model that, for each species i , takes the general form

$$(6.25) \quad \dot{y}_i = r_i f_i(y_i) + \sum_{j=1}^N J_{ij} g_{ij}(y_i, y_j),$$

where $\dot{y}_i = \frac{dy_i}{dt}$; N is the number of species in the system and i, j index the species. The r_i and J_{ij} are constants coefficients, whereas f_i and g_{ij} are known functions. This form looks familiar, indeed all of the ODE models discussed so far in the chapter may be expressed in this form. There is an intrinsic growth term, and a linear sum of pairwise interaction terms. To express the GLV model (equation 6.2.2) in this form, we let

$$\begin{aligned} f_i(y_i) &= y_i \\ g_{ij}(y_i, y_j) &= y_i y_j. \end{aligned}$$

It would be possible to use this method to fit models other than the GLV, so long as the functions f_i and g_{ij} are *known and parametrised*. Since the functions f_i and g_{ij} are known there are $N + 1$ unknowns in equation (6.2.3): r_i and $J_{i,j}$ for $j = 1, \dots, N$. Therefore, if we knew the exact values of \dot{y}_i, y_i and the y_j ’s, at $N + 1$ time points, then we could solve the equation for r_i and the $J_{i,j}$ ’s. However in any practical application our knowledge of the system is not *exact*; the system is subject to noise; and the model may be an imperfect description of the dynamics. So the equation cannot be solved exactly. We must look for an approximate solution. To do this the full *data stream* is sampled at $M + 1$ time points t_m for $m \in 1, \dots, M, M + 1$. Therefore we obtain $M + 1$ data samples $x_i(t_m)$ to which the model is fitted.

The data samples are used to construct estimates for the states (\hat{y}_i) and their time-derivatives ($\hat{\dot{y}}_i$) at M intermediate time points, for every species i . The time-derivatives are estimated to first order, taking the finite difference between samples at two consecutive time points, giving estimates

$$(6.28) \quad \hat{y}_i(\tau_m) := \frac{x_i(t_m) - x_i(t_{m-1})}{t_m - t_{m-1}},$$

where $\tau_m \in \mathbb{R}, m \in \{1, \dots, M\}$ is the midpoint of the two time-points, given by

$$\tau_m := \frac{t_{m-1} + t_m}{2}.$$

To evaluate the functions f_i, g_{ij} at these new time-points we must estimate the states $y_i(\tau_m)$ from our samples $x_i(t_m)$. We use the linear interpolation, such that

$$(6.29) \quad \hat{y}_i(\tau_m) := \frac{x_i(t_{m-1}) + x_i(t_m)}{2}.$$

So by evaluating (6.2.3) and (6.2.3) using the $M + 1$ samples, and substituting the estimates $\hat{y}_i(\tau_m)$ and $\hat{y}_i(\tau_m)$ into equation (6.2.3) we obtain M equations, one for every time point τ_m :

$$(6.30) \quad \hat{y}_i(\tau_m) = r_i f_i(\hat{y}_i(\tau_m)) + \sum_{j=1}^N J_{ij} g_{ij}(\hat{y}_i(\tau_m), \hat{y}_j(\tau_m)).$$

We now simplify the notation such that equation (6.2.3) may be written

$$\hat{x}_{im} = r_i f_{im} + \sum_{j=1}^N J_{ij} g_{ijm},$$

where the subscripts i, j indicate the species, and m indicates the time-point τ_m for which the equation holds. This system of M equations can be expressed in matrix form as

$$(6.31) \quad Y_i = J_i G_i,$$

where we have

$$Y_i = \begin{pmatrix} \hat{y}_{i1} & \hat{y}_{i2} & \cdots & \hat{y}_{iM} \end{pmatrix} \in \mathbb{R}^{1 \times M},$$

$$J_i = \begin{pmatrix} r_i & J_{i1} & J_{i2} & \cdots & J_{iN} \end{pmatrix} \in \mathbb{R}^{1 \times (N+1)},$$

$$G_i = \begin{pmatrix} f_{i1} & f_{i2} & \cdots & f_{iM} \\ g_{i11} & g_{i12} & \cdots & g_{i1M} \\ g_{i21} & g_{i22} & \cdots & g_{i2M} \\ \vdots & \vdots & \ddots & \vdots \\ g_{iN1} & g_{iN2} & \cdots & g_{iNM} \end{pmatrix} \in \mathbb{R}^{(N+1) \times M}.$$

Therefore J_i contains all the model parameters from (6.2.3) as unknowns, whilst Y_i and G_i are evaluated from the *data stream*. The system (6.2.3) has $N + 1$ unknowns (J_{ik} for $k = 1, \dots, N + 1$) and M equations. In the case when $M > N + 1$ the system is overdetermined and there is no exact solution in general. We look for an approximate solution \hat{J}_i that minimises the error between the LHS and RHS of equation (6.2.3). Therefore we seek to minimise an error function $E_i(\hat{J}_i)$ with respect to the matrix elements \hat{J}_{ik} :

$$(6.32) \quad \min_{\hat{J}_{ik}} \left\{ E_i(\hat{J}_i) = \sum_{m=1}^M \left(Y_{im} - \sum_{k=1}^{N+1} \hat{J}_{ik} G_{ikm} \right)^2 \right\},$$

To minimise this function we look for solutions for which

$$\frac{\partial}{\partial \hat{J}_{ik}} E_i(\hat{J}_i) = 0.$$

By taking the derivative of the RHS of equation (6.2.3) we have that

$$\begin{aligned} \frac{\partial}{\partial \hat{J}_{il}} E_i(\hat{J}_i) &= \frac{\partial}{\partial \hat{J}_{il}} \left[\sum_{m=1}^M \left(Y_{im} - \sum_{k=1}^{N+1} \hat{J}_{ik} G_{ikm} \right)^2 \right] \\ &= -2 \sum_{m=1}^M \left[\left(Y_{im} - \sum_{k=1}^{N+1} \hat{J}_{ik} G_{ikm} \right) G_{ilm} \right]. \end{aligned}$$

Equating this derivative to zero we have

$$\begin{aligned} 0 &= \sum_{m=1}^M \left(-Y_{im} G_{ilm} + G_{ilm} \sum_{k=1}^{N+1} \hat{J}_{ik} G_{ikm} \right) \\ &= \left(-Y_i G_i^T \right)_l + \sum_{m=1}^M G_{ilm} (\hat{J}_i G_i)_m \\ &= \left(-Y_i G_i^T \right)_l + \sum_{m=1}^M (\hat{J}_i G_i)_m G_{ilm}^T \\ &= -Y_i G_i^T + \hat{J}_i G_i G_i^T. \end{aligned}$$

Therefore we conclude that

$$(6.34) \quad \hat{J}_i = Y G_i^T \left(G_i G_i^T \right)^{-1},$$

which is the same result as derived in [118]. In our case this solution represents the analytic form for the best estimate of the parameters in the GLV equation for species i . However, without constraints on the second derivative of the error function $E_i(\hat{J}_i)$, there is no guarantee that this solution is a minimum rather than another type of stationary point. In [118] there is no justification given for the assumption that this solution represents a minimum. We do not investigate this problem analytically, instead we evaluate the resulting parameter estimates to determine the success of the estimation procedure. For an N species system, by applying equation

(6.2.3) to each species in turn, we obtain the full set of GLV parameter estimates $\hat{J} \in \mathbb{R}^{N \times N}$ and $r \in \mathbb{R}^N$.

The model fitting method described in this section was implemented in *Python* [137], with matrix multiplication using the package *numpy*. The analytic solution to the error minimisation problem makes this model fitting method computationally efficient, compared to algorithms that conduct a numerical search of parameter space. This efficiency allows us to perform many replicate calculations. However the quality of the parameter estimates produced may be lower than other, more computationally expensive, model fitting algorithms (see discussion section 6.5). Finally, it is possible to assess the goodness of fit achieved by evaluating the error function (equation (6.2.3)).

6.2.4 Interaction matrix

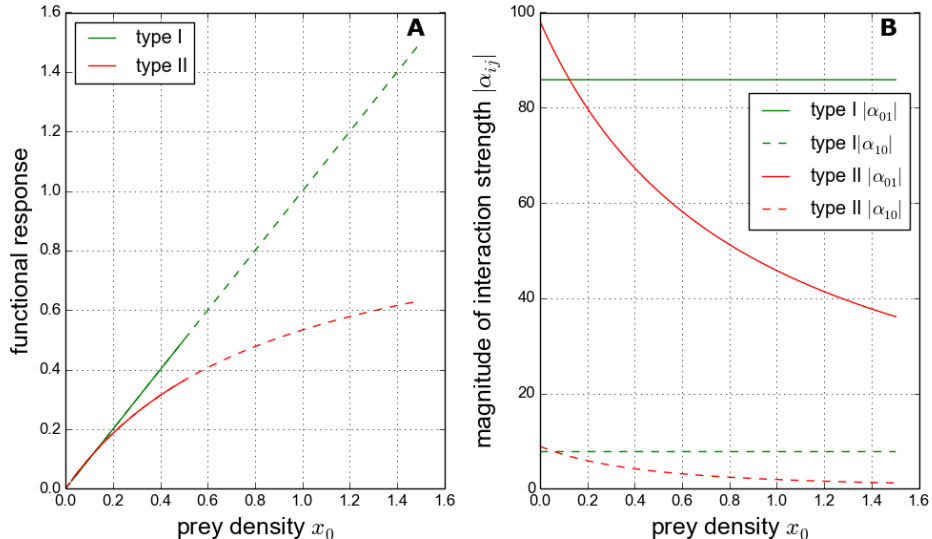


Figure 6.2: Example of (A) the functional response (FR) curve, and (B) the corresponding inter-specific interaction strengths α_{ij} for one parameter set of the *type I* model (green), and one of the *type II* model (red). The FR for the *type I* model is calculated as Bx_0 , and for the *type II* model as $Bx_0/(x_0 + D)$. Definitions for α_{ij} in the two models are given in the text. Both parameter sets have values $A = 13.58$, $B = 85.87$, 7.79 , the *type II* model has $D = 0.88$. These parameter values were selected following the procedure described in section 6.3.2.

Having estimated species interaction strengths using the inference method described above, we compare them to interaction strengths calculated directly from the *data generator*. In doing so we evaluate the performance of the inference method. As discussed in section 1.2.1 there are numerous metrics available to quantify species interaction strengths. The standard metric to quantify interaction strength from ODE population models is known as the *interaction matrix* α [54]. This metric allows direct comparison between interaction strengths calculated from different

ODE population models. The matrix element α_{ij} , quantifies the effect of a small change in the population density of species j on the per capita growth rate of species i , and is calculated by

$$(6.35) \quad \alpha_{ij} = \frac{\partial}{\partial x_j} \left(\frac{1}{x_i} \frac{dx_i}{dt} \right),$$

where x_i and x_j are the population densities of species i and j respectively. The element α_{ii} quantifies an intra-specific interaction such as the density dependent term in the intrinsic growth function (6.3). Evaluating (6.2.4) for the GLV model (6.2.2) gives

$$\alpha_{ij} = J_{ij},$$

such that the GLV coupling matrix is equal to the interaction matrix for this model. Evaluating (6.2.4) for the *type I* model ((6.11) and (6.12)) gives

$$\alpha_{type \ I} = \begin{bmatrix} -A & -B \\ C & 0 \end{bmatrix},$$

such that the *type I* model has constant interaction strengths that can be directly compared to those of the GLV model. However evaluating (6.2.4) for the *type II* model ((6.13) and (6.14)) gives

$$(6.36) \quad \alpha_{type \ II} = \begin{bmatrix} -A + \frac{Bx_1}{(x_0+D)^2} & \frac{-B}{x_0+D} \\ \frac{CD}{(x_0+D)^2} & 0 \end{bmatrix},$$

such that the three non-zero interaction strengths are functions of prey density x_0 , rather than constants. The form of the functional response (FR) curves and inter-specific interaction strengths for the *type I* and *II* models are illustrated in figure 6.2. In panel A the non-linearity of the type II FR is visible, modelling the effect of predator saturation as discussed in section 6.2.1. In panel B we see that the result of this non-linearity is interaction strengths that decrease as a function of prey density, whereas the *type I* model has constant interaction strengths. In fact the interaction strengths of the *type II* model tend to zero in the limit that prey density tends to infinity. This property may seem counter intuitive for a measure of interaction strength, since we may expect a large effect of prey on predator when the prey population is very large. Indeed for large prey populations the *biomass* flow does remain large, but the incremental effect of an increase in prey population on the predator growth rate is small.

Based on the comparison of the functional forms in figure 6.2, we expect that the ability of a model with constant interaction strengths (such as the GLV model) to approximate the dynamics of the *type II* model may depend on the extent to which the FR deviates from linearity. This hypothesis is investigated in section 6.3.6.

6.2.5 Summary of methodology

Here we summarise the methodology which is depicted in figure 6.1 and detailed in the sections above. First ODE models (section 6.2.1) are used to simulate population dynamics. This step represents the *data generator*. The population dynamics are then sampled discretely to produce a *data stream*, to which the GLV model (section 6.2.2) is fitted using the method described in section 6.2.3. The GLV fit produces constant numeric estimates of interaction strengths in the form of \hat{J} , the fitted coupling matrix. Also produced are estimates of the intrinsic growth rate parameters \hat{r}_i for each species. The fitted parameters are compared to those calculated analytically from the *data generator*. The main focus of the analysis is on the estimates of interaction strength given by \hat{J} . In particular we are interested in whether \hat{J} correctly identifies the types of interaction between species (i.e. which species eats which), and if so, how accurate are the estimated strengths of the interactions. A secondary concern is the accuracy of the estimated intrinsic growth rates \hat{r}_i . However this is related to the main question since the accuracy of all estimates is broadly determined by the *quality* of the GLV fit to the *data stream*.

6.3 Results: ODE as data generator

In this section we analyse the performance of the inference method (sections 6.2.2 and 6.2.3) in estimating interaction strengths from noisy two species predator-prey dynamics. The dynamics are simulated using the *type I* and *type II* ODE models (section 6.2.1). In section 6.3.1 we discuss how noise is modelled, and in section 6.3.2 the procedure for numerical simulation of the ODE models is given. Constraints on the parameter values used for simulations are detailed in section 6.3.3. Sections 6.3.5 and 6.3.6 present results for the *type I* and *type II* models respectively. Both sections analyse the effects of noise and sampling intensity on the accuracy of estimated interaction strengths. In section 6.3.7 the impact of non-linearity in the functional response of the predator (a feature of the *type II* model) is studied directly. We quantify the extent of this non-linearity and the effect that it has on the accuracy of results. A novel method for dealing with the non-linearity, referred to as *range sampling*, is also introduced. The focus of this section is on two species systems. In section 6.4 the analysis is extended to systems with more species.

6.3.1 Modelling noise

A key feature of the simulations is the inclusion of *noise*. Random effects are ubiquitous in natural systems and in ecological data. Therefore in developing a methodology to estimate species interaction strengths it is necessary to characterise its performance under noisy conditions. In modelling population dynamics it is common to distinguish between two different types of error: *process* and *observation* error [122?]. Process error results from randomness that is inherent to the mechanisms of the system itself. For example the IBM model used previously (section 2.4) has randomness built into the behaviour of the individuals. Similarly a natural ecosystem is

subject to demographic stochasticity resulting from numerous sources (e.g. environmental forcing, disease etc.). Observation error results from imperfect knowledge of the system being studied. Empirical sampling cannot exactly measure the state of a natural system and therefore some level of observation error is inevitable. In the current analysis we *restrict the focus to process error*, since this type of error is inherent to the system being studied and therefore cannot be reduced. Observation error, on the other hand, may be reduced by experimental design. Therefore we argue that consideration of process error is more important for the development of the methodology presented in this chapter. The exclusion of observation error is also consistent with all previous analyses of the IBM, in which exact knowledge of the system state at any given time point was assumed. Therefore treatment of observation error represents an extension to this work that lies beyond the scope of the current thesis.

In population biology it is conventional to model process error using *multiplicative noise* [122?]. One reason for this is the *postulate of parenthood* (coined by Hutchinson [?]), which states that the growth rate of a species must be equal to zero when the population size is zero. Multiplicative noise is so-named because it consists of a random variable multiplied by the population size x_i , such that the term vanishes for zero populations as required by the postulate of parenthood. It is worth noting that the postulate only pertains to *closed-systems*, where there is no external source of individuals (see section 6.4). Based on convention [122] we define a multiplicative noise term

$$(6.37) \quad \xi_{i,t} = x_{i,t} \epsilon_{i,t},$$

where $\epsilon_{i,t}$ is a random number drawn from a normal distribution with mean zero and variance $\sigma_{noise} \Delta t$. The value σ_{noise} is hereafter referred to as the *noise intensity*, and the value Δt is the size of the integration time-step used in numerical simulation of the ODE models (see section 6.3.2). For simplicity we use the same value of noise intensity for both species, although it is possible to define different noise distributions for each species in the system.

6.3.2 Simulation procedure

Simulations were run following a standard procedure that ensures consistency and allows comparison between numerical results. All simulations were run using the first-order forward Euler approximation to the deterministic ODE models. It was heuristically determined that this simple approximation produced solutions that were numerically stable for all of the two species systems simulated in this section. The Euler approximation may be defined by the stochastic difference equation

$$x_{i,t+1} = x_{i,t} + \Delta t f(X_t) + \xi_{i,t},$$

where $x_{i,t}$ is the population density of species i at time t ; Δt is the integration time step; $\xi_{i,t}$ is the noise term (6.3.1); and $f_i(X_t)$ defines the time-derivative of $x_{i,t}$ as a function of the system state $X_t \in \mathbb{R}^N$. As such $f_i(X_t) = \dot{x}_i$, which is given by equations ((6.7),(6.8)) and ((6.13),(6.14)) for the *type I* and *type II* models respectively.

All simulations used the initial condition $x_{i,0} = x_i^*/2 \quad \forall i$, where x_i^* is the equilibrium population level of species i (defined in section 6.2.1 for both models). As such the initial system state was consistently away from the equilibrium value. In the event of a stochastic extinction of either species, both population densities were reset to their initial conditions. The case with zero noise intensity ($\sigma_{noise} = 0$) is referred to as the *deterministic case*. In all of the results presented below the simulations were run with a time step $\Delta t = 10^{-4}$. All code was implemented in the language *Python* [137], and large computations were performed on the cluster *Blue Crystal* [139].

6.3.3 Parameter selection

Certain constraints are placed on the parameter values that may be chosen when simulating either ODE model. ~~ETwo requirements for ecological realism requires are~~ that the equilibrium populations given by the model are strictly positive. ~~Furthermore, in order for deterministic ODEs to produce persistent populations, the equilibrium must be locally stable. (It is worth noting that such local stability is not necessarily realistic in a natural settings - see section 2.8.2.), and that this equilibrium is stable.~~ The conditions for the first requirement were given in section 6.2.1 as $C > 1$ and $C - D > 1$ for the *type I* and *type II* models respectively. The conditions for the second requirement are determined from the Jacobian of the model, given by (6.2.1) and (6.2.1) for the *type I* and *type II* models respectively. If the eigenvalues of the Jacobian have negative real parts then the equilibrium population is locally stable. A further requirement, due to the methodology, is that the simulated dynamics contain sufficient information to fit the GLV model. If the species populations relax to the stable equilibrium too rapidly then it may not be possible to fit the model. To avoid such a problem parameters are chosen such that the deterministic solution to the model is oscillatory (see condition 1 below). Following the precedent of Jost and Arditi (from their paper [122] discussed in section 6.1) we stipulate that the deterministic trajectory given by any parameter set must complete *at least* two large amplitude oscillations en route to equilibrium (see condition 2 below). As stated in section 6.3.2, every simulation is run with the initial population densities set to half of their equilibrium value. This ensures that the system always starts away from equilibrium.

Parameters are selected uniformly at random from predefined ranges, which are given in table 6.1 for both models. These ranges allow parameter values to vary over at least three orders of magnitude so that our numerical investigation covers a large region of parameter space. Also these ranges ensure that it is possible to select from these ranges a combination of

| | A | B | C | D |
|----------------|-----------|-----------|-----------|--------|
| <i>type I</i> | 0.1 - 100 | 0.1 - 100 | 1 - 100 | N/A |
| <i>type II</i> | 0.1 - 100 | 0.1 - 100 | 1.1 - 100 | 0.1-99 |

Table 6.1: Ranges from which parameters were selected uniformly at random for the two ODE simulation models. The parameters are all allowed to vary over at least three orders of magnitude, to ensure that our investigation covers a large region of parameter space. The restrictions on parameters C and D ensure that it is always possible to achieve an equilibrium population of both species that is strictly positive.

parameter values that produces a positive equilibrium population. If the equilibrium for the selected parameters is positive, then the values are accepted providing they met the following three conditions:

1. The equilibrium is a locally stable spiral node: the eigenvalues of the Jacobian have negative real parts, and complex conjugate imaginary parts.
2. The deterministic dynamics exhibit at least two full rotations in the phase plane before relaxing to within 5% of the equilibrium: the distance of the trajectory from the equilibrium as a percentage of the distance of the equilibrium from the origin of the phase plane.
3. The population densities do not differ by more than an order of magnitude in the deterministic case dynamics.

The final conditions helps to avoid the choice of parameters which produce numerical instability in the Euler method, since such numerical instability often leads to divergent population sizes. Using the procedure described above we select a set 100 parameter values for each of the ODE models. Parameter values from these two sets are used to generate all results presented in section 6.3. Every simulation, including those with $\sigma_{noise} \neq 0$, is run for the length of time T_{2P} required to achieve two full oscillations (in the deterministic case) for that parameter set.

6.3.4 Example dynamics

Figure 6.3 shows examples of dynamics simulated for the *type I* model, with and without noise. Two parameter sets are illustrated, one in each panel. It is clear that the deterministic trajectory completes two full oscillations within the simulation time. The figure also gives an intuition for different levels of noise intensity σ_{noise} . Panel A shows a stochastic trajectory with noise intensity 20, whereas in panel B the noise intensity is 50. In the latter case the noise causes significant deviations from the deterministic trajectories. The peaks in the stochastic prey dynamics are more than double the peaks of the deterministic case. However in both cases depicted the period of oscillation is not significantly altered by noise, which is not necessarily the case in general.

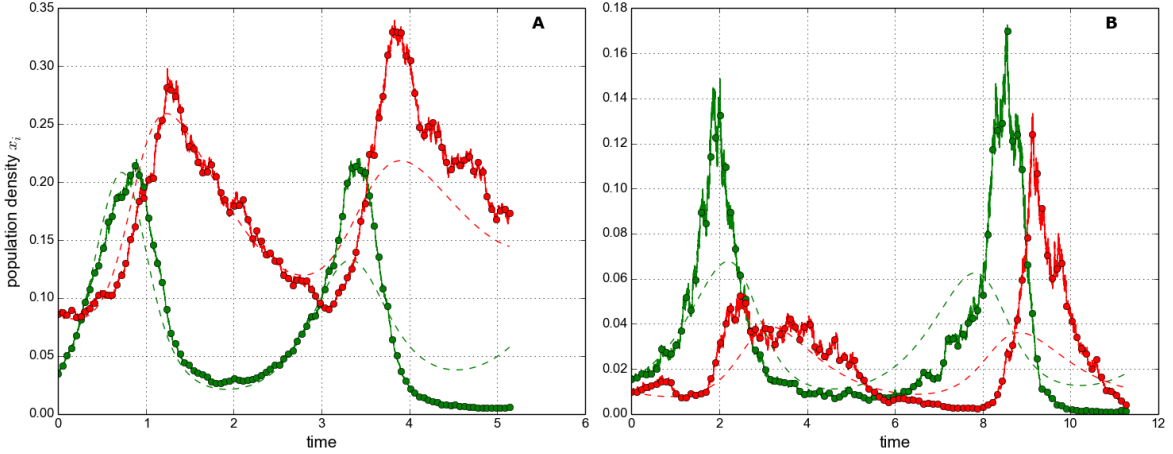


Figure 6.3: **Example dynamics of the *type I* model.** Panels A and B show different parameter sets. Green represents the prey species, and red the predator. The dashed lines show the deterministic trajectories ($\sigma_{noise} = 0$); the solid lines show a stochastic trajectory with A: $\sigma_{noise} = 20$ and B: $\sigma_{noise} = 50$. The solid circles represent the *data stream* of 100 samples, taken from the stochastic dynamics in each case.

Figure 6.4 shows examples of dynamics simulated for the *type II* model, and the corresponding time series of the inter-specific interaction strengths α_{01} and α_{10} given by (6.2.4). The stochastic dynamics illustrated in panels A and C both use $\sigma_{noise} = 20$. These dynamics demonstrate that for some parameter sets the trajectories may be more sensitive to the addition of noise than for others. We also see, from panels B and D, that for the *type II* model interaction strengths vary over the course of the simulation (in response to changes in x_0). However the extent of this temporal variation in α_{01} and α_{10} is again parameter dependent. The black solid and dashed lines in panels B and D represent the mean values of α_{01} and α_{10} respectively, over the course of the simulations. When fitting the GLV to the *type II* models the estimates interaction strengths \hat{J}_{ij} are compared to these *average values*.

6.3.5 Type I model results

In this section we characterise the performance of the inference method (section 6.2.3) for the *type I* model. Results are presented that compare the estimated GLV parameters (section 6.2.2) to those of the simulation model. The accuracy of the estimates is evaluated under different levels of noise intensity (σ_{noise}), and using *data streams* that contain different numbers of samples. As noted in section 6.2.2, the *type I* model may be expressed in GLV form. Therefore fitting the GLV to this model should produce ‘exact’ estimates of the parameter values in the deterministic case ($\sigma_{noise} = 0$). We anticipate that the accuracy of parameter estimates will be reduced at the noise intensity is increased, or as the number of samples is reduced. The noise intensity is varied between 0 (determinism) and 100 (highly stochastic), such that the dynamics depicted in panels

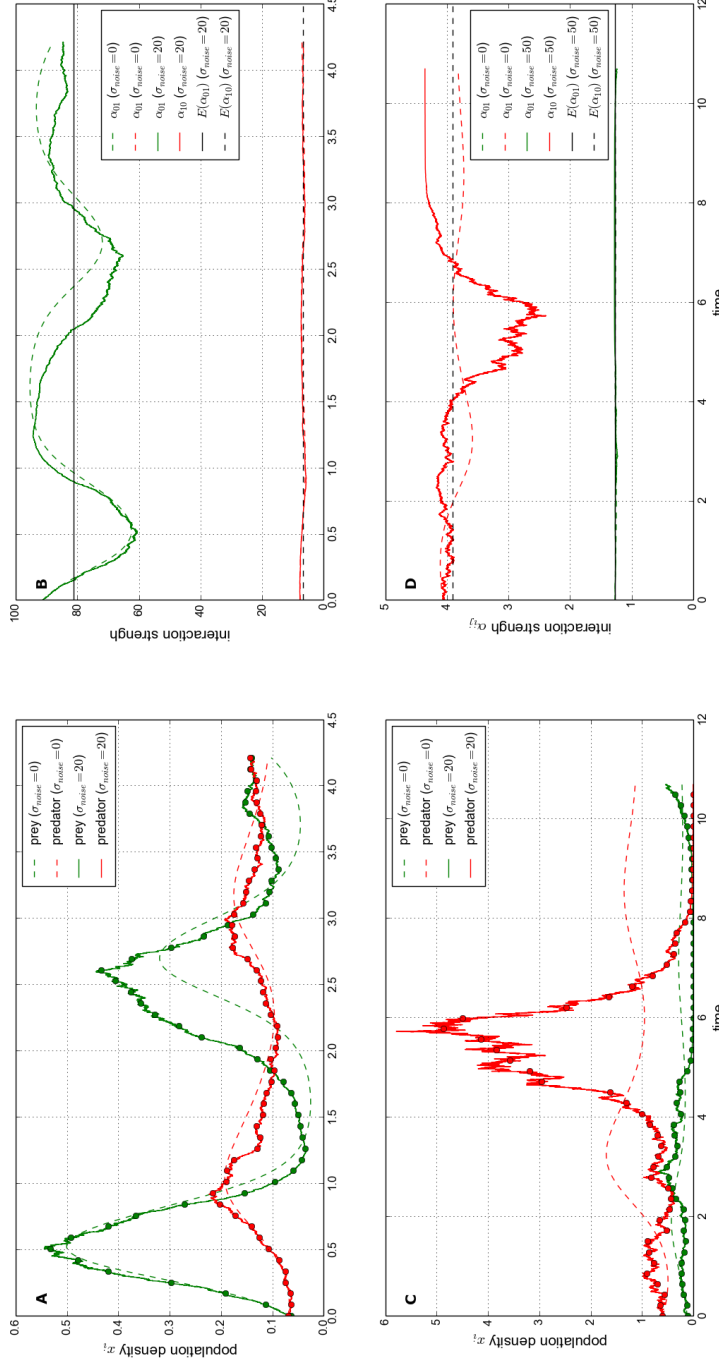


Figure 6.4: **Example dynamics and interaction strengths of the type II model.** The top and bottom rows show different parameter sets. Green represents the prey species, and red the predator. The dynamics is plotted in panels A and C, using the same format as the type I dynamics in figure 6.3. In both cases $\sigma_{noise} = 20$. Panels B and D show how inter-specific interaction strengths $\alpha_{i,j}$ vary with time, corresponding to the dynamics plotted. The black solid and dashed lines indicate the mean interaction strengths for the deterministic dynamics, as indicated in the legend.

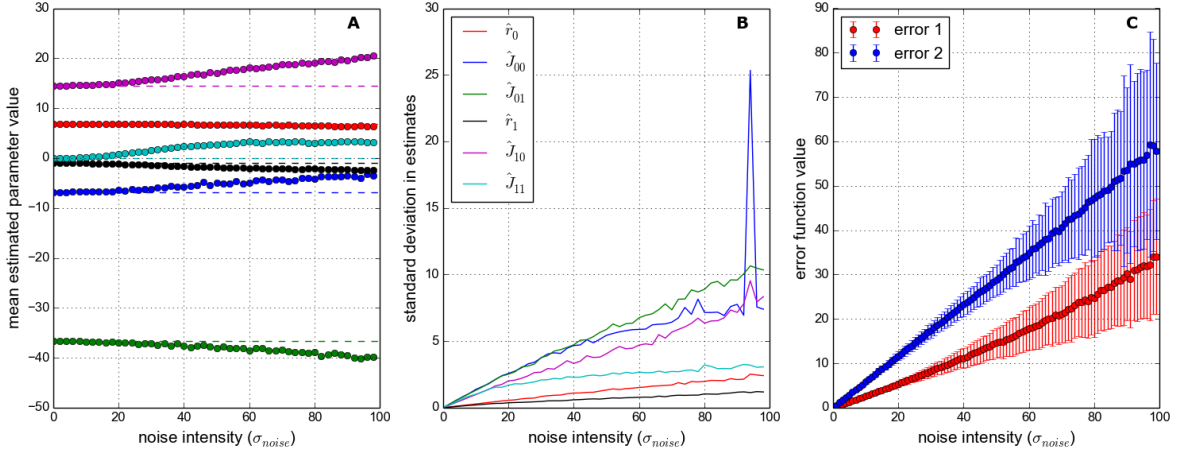


Figure 6.5: Effect of noise on parameter estimates for type I model, using a single parameter set. Parameter estimates obtained by fitting GLV model as described in sections 6.2.2 and 6.2.3. The *data stream* here consists of 100 samples from simulated dynamics, as depicted in figure 6.3. Noise intensity is varied between 0 and 100, with 1000 replicate simulations at each noise value. **Panel A:** Mean estimated parameter values (each dot representing mean over 1000 repeats). The true parameter values of the simulation model (*data generator*) are shown by dashed lines. **Panel B:** Standard deviation in the parameter estimates. **Panel C:** Value of the error functions used in the model fitting method (given by (6.2.3)), for each species. The circles show the mean error, and the bars show ± 1 standard deviation.

A and B of figure 6.3 correspond to low and intermediate levels of noise respectively. The lower limit on the number of samples that can be used is four, since the system of equations used in the error minimisation must be overdetermined (see section 6.2.3). The upper limit on the number of samples is constrained by the resolution of the simulated dynamics, which is in turn determined by Δt and T_{2P} (see section 6.3.3). It was determined that the upper limit on the number of samples that could be used with all 100 parameter sets was 10^4 .

Figure 6.5 shows the effect of increasing noise intensity on parameter estimates, for simulations run using a single parameter set (the same parameter set depicted in panel A, figure 6.3). At each value of σ_{noise} 1000 replicate simulations were run, and a *data stream* constructed by drawing 100 samples from the simulated dynamics. The GLV model was then fitted to the *data stream*. Panel A shows that, on average, the resulting estimates are close to the true parameter values for low levels of noise. As σ_{noise} increases the mean estimated parameter values diverge from the true values, such that the estimators of interaction strength become *biased*. The variability in the parameter estimates, shown in panel B, is zero in the deterministic case, and also increases with noise. It appears that some parameter values become harder to estimate than others, for this parameter set. For example the estimates of intrinsic growth rate of the prey (\hat{r}_0) remain close to the true value, and have relatively low standard deviation, even at the highest noise value ($\sigma_{noise}=100$). Comparatively the estimates of prey intra-specific interaction strength

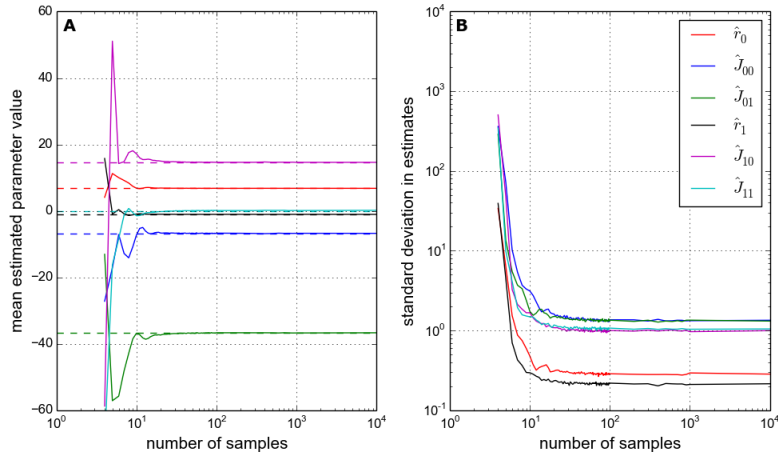


Figure 6.6: Effect of the number of samples on parameter estimates for *type I* model, using the same parameter set as in figure 6.5. Format is similar to that figure, but here 1000 replicate simulations are run at each number of samples, all using $\sigma_{noise} = 10$. **Panel A:** Mean estimated parameter values. The true parameter values of the simulation model (*data generator*) are shown by dashed lines. **Panel B:** Standard deviation in the parameter estimates.

(\hat{J}_{00}) perform poorly as noise is increased. Panel C shows the ‘best-fit’ value of the error function (6.2.3) for each species, which results from the GLV model fit. The error functions for both species increase approximately linearly with noise. Therefore it is clear that the *quality* of the GLV fit to the simulated dynamics is reduced by noise, as we expected.

Figures 6.6 and 6.7 show the effect of the number of samples on the accuracy of parameter estimates for $\sigma_{noise} = 10$ and $\sigma_{noise} = 50$ respectively. Both figures show results for the same parameter set as in figure 6.5. In general low numbers of samples (< 10) produce estimates that are not close to the true values. However as the number of samples is increased the estimates improve. In the low noise case (figure 6.6) the means of the parameter estimates converge close to the true parameter values (panel A), and the standard deviations converge to a low but non-zero value. The rate of convergence is such that there appears to be little improvement in parameter estimates for numbers of samples greater than 100. In the intermediate noise case (figure 6.7) the means of the parameter estimates approximately converge, but not necessarily on the true parameter values. In panel A we see that, even with 10^4 samples, there are a clear discrepancies between the true and the estimated values of some parameters. Additionally the standard deviations converge (panel B), but on higher values than in figure 6.6 due to the increased level of noise. As in the low noise case there appears to be little improvement in the estimates above 100 samples.

We now generalise the above results by considering an ensemble of 100 parameter sets. To quantify the accuracy of parameter estimates we define a metric for *relative error*:

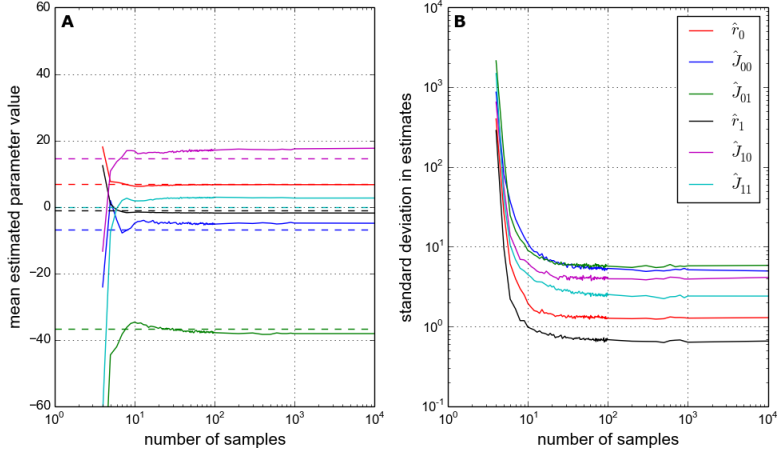


Figure 6.7: Similar to figure 6.6 but with noise intensity $\sigma_{noise} = 50$.

$$RE(p_i) = \frac{|p_i - \hat{p}_i|}{|p_i|},$$

where p_i and \hat{p}_i are the true and estimated value of parameter i respectively. As such RE is equal to zero if the estimated and true value are equal. This metric may be evaluated for any of the model parameters (unless $p_i = 0$). In the analysis that follows we focus on the inter-specific interaction strengths J_{01} and J_{10} , since quantification of these is the main motivation for the work. Also, as suggested by figures 6.5-6.7, the error in these parameters may be used as a proxy for the quality of the model fit as a whole.

Figures 6.8 and 6.9 show the effect of noise and number of samples on the relative errors $RE(J_{01})$ and $RE(J_{10})$. At each value of noise intensity, and for each number of samples, 100 replicate simulations were run for each of the 100 parameter sets. The mean and standard deviations of the RE metric over these 10,000 simulations, are plotted in panels A and B of both figures. From figure 6.8 we observe the general feature that both the mean and the variability of the error increase with noise intensity. Figure 6.9 shows that both the mean and the variability of the error are reduced by increasing the number of samples. In this case $\sigma_{noise} = 50$, and as a result the mean relative error does not converge to zero (panel A). This is consistent with our results derived from a single parameter set.

6.3.6 Type II model results

In this section we conduct a similar analysis of the inference method as in section 6.3.5, but this time using the *type II* model as the *data generator*. As we have seen (for example in figure 6.4) the interaction strengths α_{ij} in the *type II* model are not constants. They are functions of prey density x_0 , and therefore vary over the course of a simulation. In order to draw comparisons with

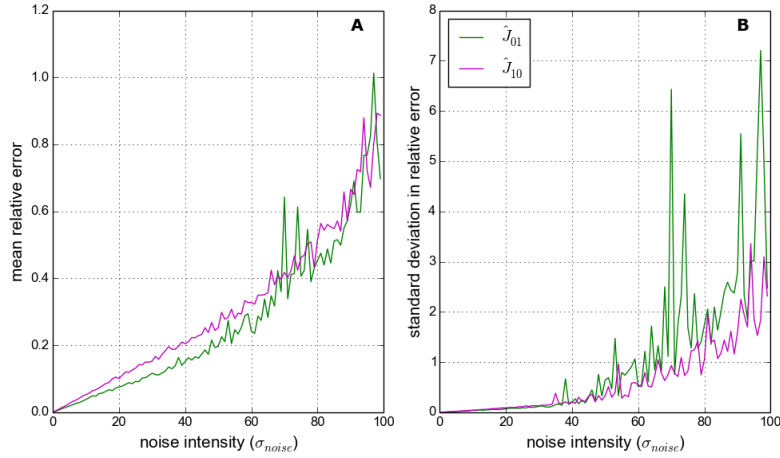


Figure 6.8: Effect of noise on parameter estimates for type I model, over 100 different parameter sets. The *data stream* here consists of 1000 samples. At each value of σ_{noise} 100 replicate simulations were run for each of the 100 parameter sets. Results shown are statistics for the full ensemble of simulations. **Panel A:** Mean relative error (defined in text) in estimates of the two inter-specific interaction strengths (\hat{J}_{01} and \hat{J}_{10}). **Panel B:** Standard deviation in these errors over all replicates.

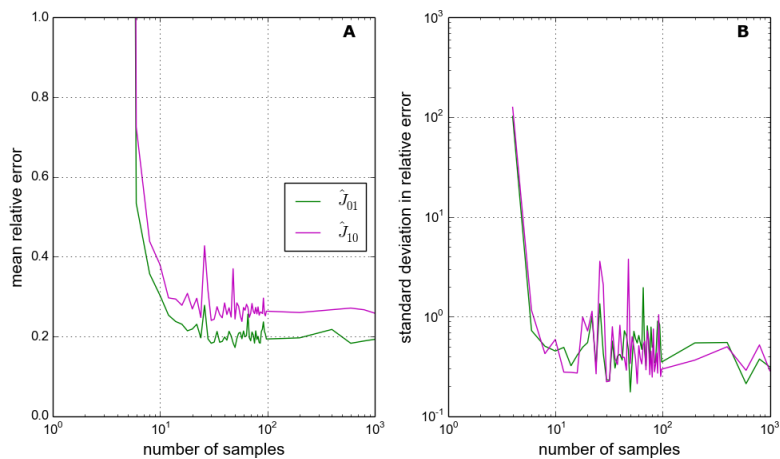


Figure 6.9: Similar to figure 6.8, but the relative errors in the estimates are plotted against number of samples. Noise intensity $\sigma_{noise} = 50$.

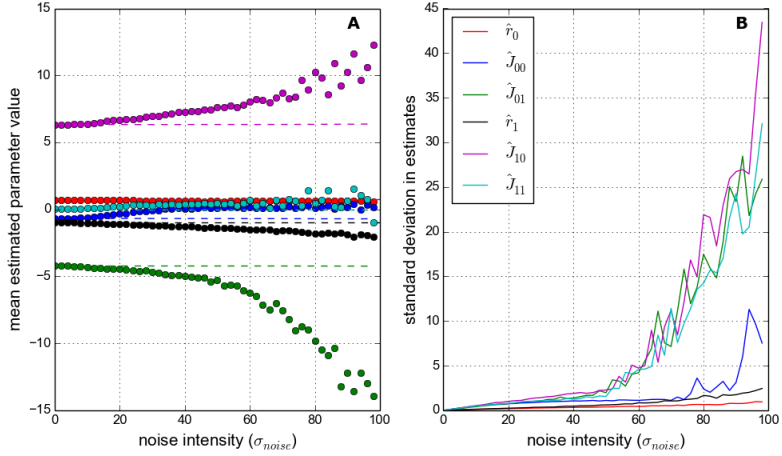


Figure 6.10: Similar to figure 6.5, but for the *type II* model, and using a *data stream* of 10,000 samples. In this case the simulation interaction strengths α_{ij} are functions of prey density. Therefore the estimates J_{ij} are compared to the mean values of α_{ij} , plotted as dashed lines.

\hat{J}_{ij} , the constant numeric estimates of interaction strength produced by the GLV fit, we take the mean values of the α_{ij} over a simulation. In the analysis below we assess whether the GLV estimates of interaction strength are close to these mean values. The intrinsic growth rates of the *type II* model are constant, and therefore may be compared directly to the GLV estimates \hat{r}_i .

Figure 6.10 show how the GLV estimates respond to increasing levels of noise, for a single parameter set. In general it was found that the estimates of interaction strength were less accurate for the *type II* model than for *type I*. This was expected since the GLV can only approximate the *type II* model, whereas it can exactly represent the *type I*. In an attempt to improve the results, the calculations shown in figure 6.10 use 10,000 samples (whereas those in figure 6.5 used 100 samples). To provide a benchmark interaction strength for this parameter set that is consistent across all simulations we use the mean values of the α_{ij} over the deterministic trajectory. These are the values displayed as dashed lines in figure 6.10. Panel A shows that, for low noise intensities, the GLV parameter estimates are close to those of the *data generator*. As the noise intensity increases the estimates diverge. Comparing figure 6.10 to figure 6.5 it appears that the estimates are more sensitive to noise in the *type II* case, despite the use of a larger number of samples. Therefore it appears that, with low levels of noise, the GLV model can well approximate the mean interaction strengths of the *type II* model, as least for this parameter set. However these estimates may become unreliable as the level of noise increases.

In order to generalise the analysis over a range of parameter values we again define a metric for *relative error*:

$$(6.38) \quad RE(p_i) = \frac{|\bar{p}_i - \hat{p}_i|}{|\bar{p}_i|},$$

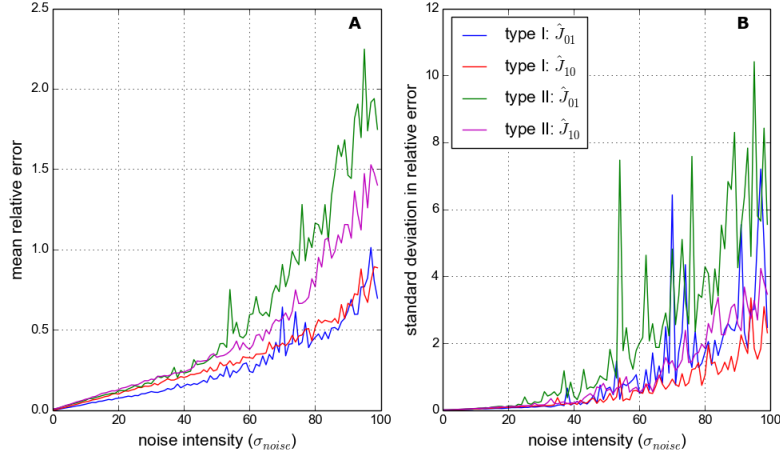


Figure 6.11: Similar to figure 6.8, but showing relative errors for both the *type I* and *type II* models. Number of samples is 1000.

which is the same as for the *type I* relative error, except that \bar{p}_i is the mean value of model parameter p_i over the simulation in question. This allows us to again draw comparisons between the accuracy of estimates obtained from simulations using different parameter values. We conduct the same analysis as for the *type I* model, with 1000 replicates for each of the 100 parameter sets over a range of noise intensities and sample numbers. Figures 6.11 and 6.12 provide a direct comparison between the relative errors for the *type I* and *type II* models. The errors for both models respond to noise and number of samples in qualitatively the same way. However the mean errors, and often the variability in the errors, are larger for the *type II* than for the *type I* model. For example the mean relative errors for the *type I* model converge on value between about 0.2 and 0.3 for high number of samples, whereas they converge on values between about 0.3 and 0.4 for the *type II* model (figure 6.12).

6.3.7 Quantifying non-linearity

The observation that the errors in the estimates of interaction strength are larger for the *type II* model than for the *type I* is related to the form of the functional response (FR). The *type II* model has a non-linear FR, which results in variable interaction strengths that can only be approximated by the GLV. This leads us to propose that the quality of estimates obtained from the dynamics of the *type II* model may depend on the extent of the non-linearity in the FR. The more linear the FR, the better we expect the GLV approximation to be. In order to test this hypothesis we develop a method for quantifying the extent of the non-linearity in the *type II* FR. This method is depicted in figure 6.13.

Panels A and B of figure 6.13 show the *type II* FR for two different parameter sets. The FR is defined by $Bx_0/(x_0 + D)$. The red lines indicate the region of the FR that is explored by the

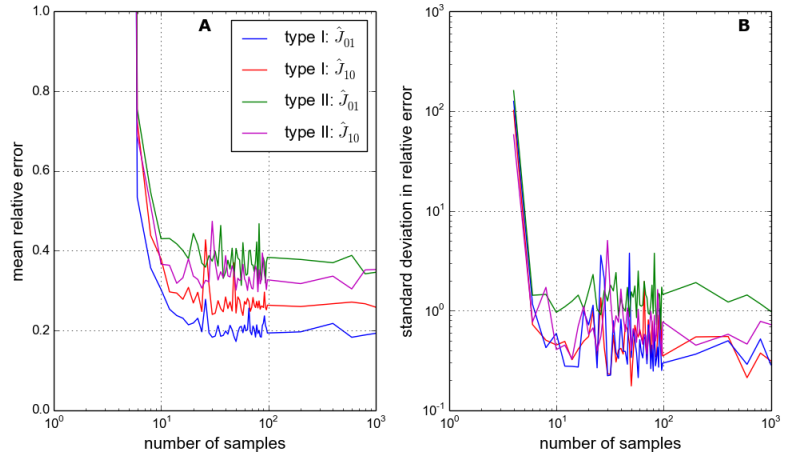


Figure 6.12: Similar to figure 6.9, but showing relative errors for both the *type I* and *type II* models. $\sigma_{noise} = 50$.

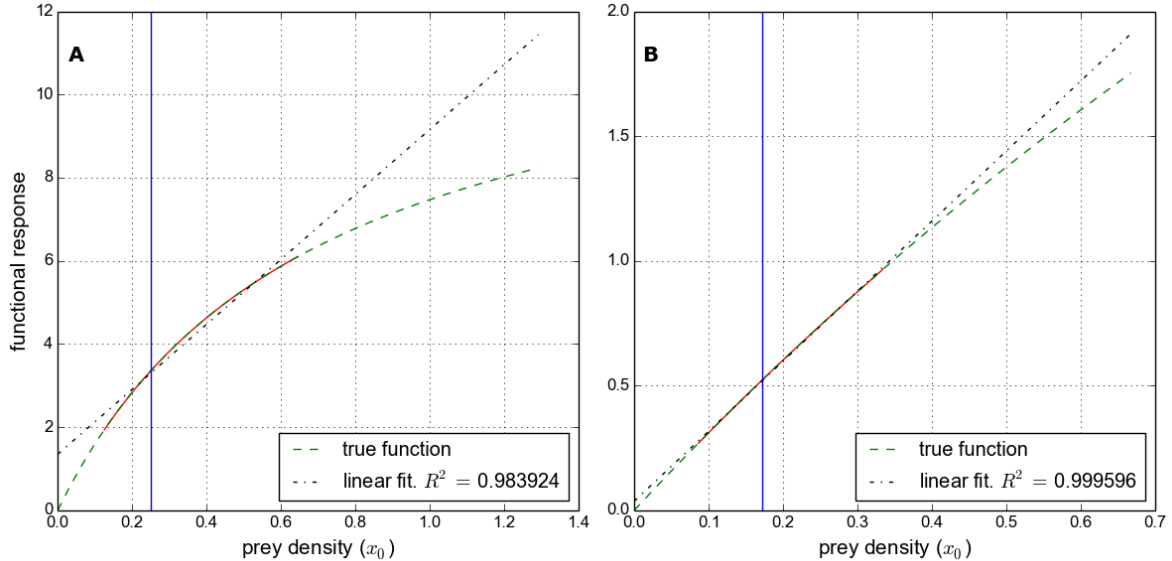


Figure 6.13: **The functional response (FR) of the predator** for two different parameter sets. The FRs plotted are given by $Bx_0/(x_0 + D)$. The green dashed line shows the analytic form of the function, the red line shows the region of the function explored during a deterministic simulation with those parameters. The black dashed line shows a linear regression fit to the explored FR (red line). The R^2 value of this fit can be used to quantify how well the FR is approximated by linearity, in the region explored by the dynamics. The blue vertical line indicates the prey equilibrium population x_0^* . **Panel A:** The least linear (lowest R^2) FR from the 100 parameter sets investigated. **Panel B:** The most linear (highest R^2) FR from the same 100 parameter sets.

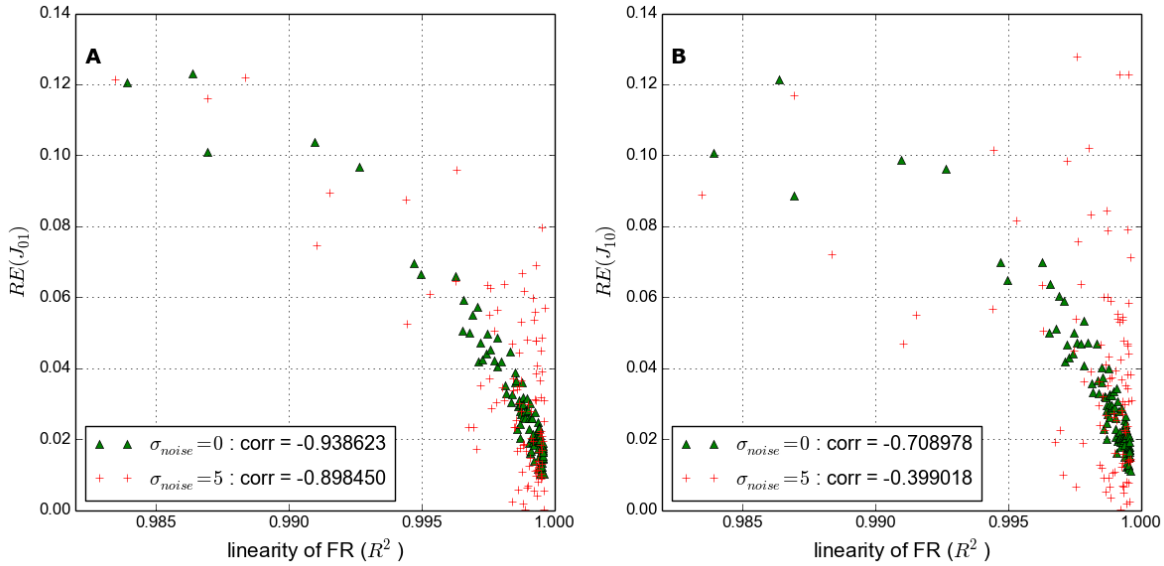


Figure 6.14: Linearity of FR as a predictor for estimate quality. One simulation for each parameter set at each noise value: $\sigma_{noise} = 0$ (green triangles), and $\sigma_{noise} = 5$ (red crosses). Linearity of the FR is measured by the R^2 of the regression fit, as in figure 6.13. The R^2 value is plotted against the relative error (RE) in the estimates of inter-specific interaction strength. The correlation coefficient between the two variables is given in the legends. **Panel A:** Prey interaction strength \hat{J}_{01} , **Panel B:** Predator interaction strength \hat{J}_{10} .

deterministic trajectory when dynamics are simulated with these parameter values. A linear regression model is fitted to this region of the FR, and the R^2 value of the fit is to quantify how good the linear approximation is. If the FR were completely linear in this region then the R^2 value would be one. The lower the R^2 value, the further the deviation of the FR from linearity. Panels A and B show the least and most linear FRs, according to the R^2 values, from the 100 parameter sets chosen for the *type II* model (i.e. same parameter sets used to generate figure 6.12).

Using this R^2 measure for linearity in the FR, we then investigate the correlation between linearity and the relative error (RE) in the estimates of interaction strength. The same RE metric (6.3.6) is used to quantify the error in the estimates \hat{J}_{01} and \hat{J}_{10} . The relative errors are plotted against R^2 for each of the 100 parameter sets in figure 6.14. There are two simulations for each parameter set, one for $\sigma_{noise} = 0$ (green triangles) and one for $\sigma_{noise} = 5$ (red crosses). In general we observe that the relative error is higher for parameter sets with less linear FR (lower R^2), as predicted. The correlation is weakened by noise, especially for the predator interaction strength J_{10} . At $\sigma_{noise} = 5$ the correlation between $RE(J_{10})$ and R^2 is only 0.40, compared to 0.71 at $\sigma_{noise} = 0$. This reduction in correlation suggests that, although the linearity of the FR is significant at low (or zero) noise values, the introduction of noise represents a source of error in the estimates which is not dependant on linearity. Indeed the extent to which noise produces error

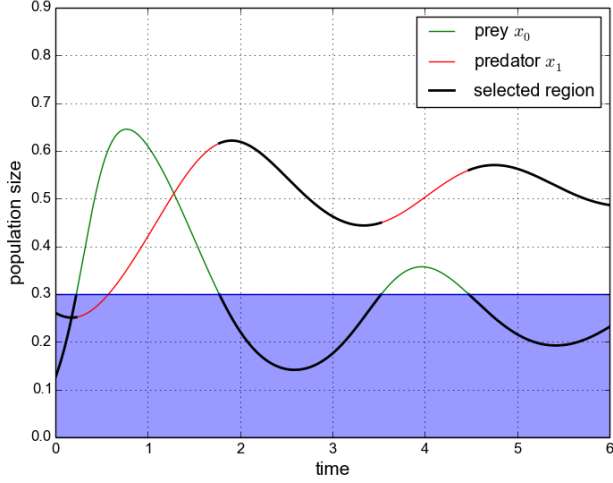


Figure 6.15: **Demonstration of range sampling** from dynamics, in order to perform a piece-wise fit of the GLV. The dynamics shown is from the *type II* model. The dynamics is split into two ranges according to prey density x_0 such that half of the time points fall into one range and half into the other. The region of prey density that defines the lower range is shaded in blue, and the portions of the dynamics that fall into this range are highlighted in black.

in the estimates is likely to depend on the sensitivity of the dynamics to stochastic perturbations. As we saw in figure 6.4, the same level of noise can cause the dynamics to deviate to different extents from the deterministic trajectory, depending on the parameter values. This sensitivity to noise can be studied analytically using stability concepts such as *reactance* and *resilience* [60]. However we do not pursue this line of investigation here.

From figure 6.14 we observe that most of the parameter sets investigated have FRs that are approximately linear (R^2 values close to one) within the region of phase-space explored by the deterministic dynamics. This is an unintended feature of the parameters sets, resulting from the constraints imposed in parameter selection. The approximate linearity of the FR in many cases leads us to question if a signature of non-linearity can be detected using our methodology. Previous work by Jost and Arditi [122] has attempted to detect the presence of different forms of functional response from population dynamics data. Their approach was to fit ODE models with different forms of FR, selecting the model that produced the ‘best fit’. As discussed in section 1.5 this approach produced mixed results. Here we propose an alternative approach that involves fitting the GLV model piece-wise to subsets of the population dynamics.

The proposed method is referred to as *range sampling*, since it involves fitting the GLV to subsets of the dynamics sampled from different ranges of prey density. The sampling procedure is illustrated in figure 6.15. We define a number of ranges R , with boundaries distributed according to prey density x_0 such that an equal number of time points falls within each range. In the case depicted there are two ranges, and the boundary between them is approximately $x_0 = 0.3$. For

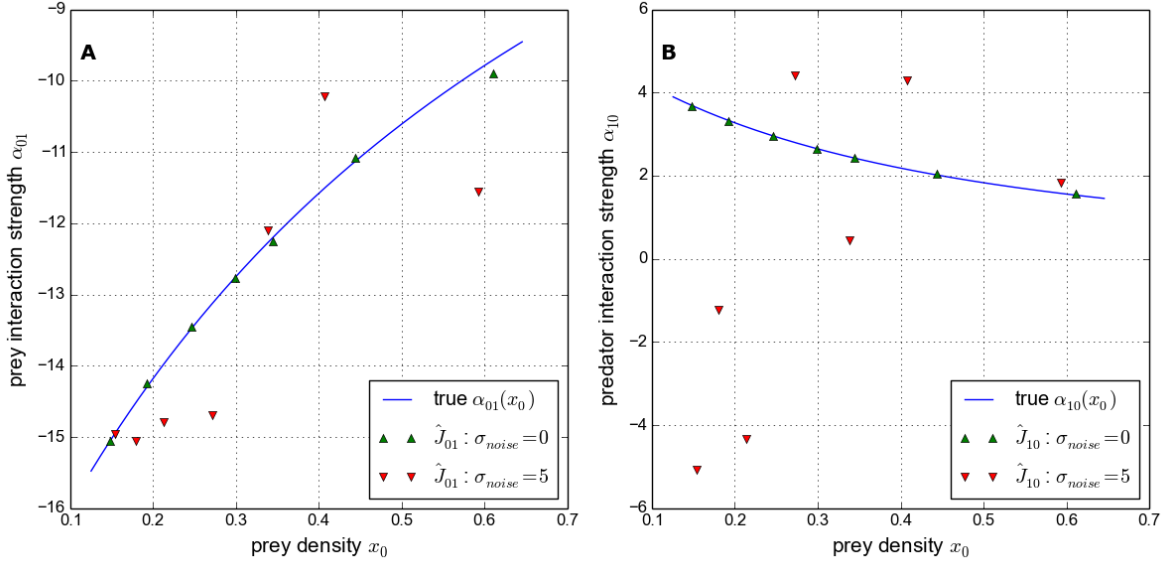


Figure 6.16: Range sampling results for the parameter set depicted in panel A of figure 6.13. The dynamics is split into seven ranges using the same procedure illustrated in figure 6.15. The GLV is then fitted separately (piece-wise) to these seven ranges, producing estimates of the interaction strength within each range. Results are calculated from single simulations, one with $\sigma_{noise} = 0$ (green triangles), and one with $\sigma_{noise} = 5$ (red triangles). Also plotted, as a blue line, is the analytic form of the interaction strength calculated from the *type II* model using (6.2.4). **Panel A:** Prey interaction strength α_{01} , **Panel B:** Predator interaction strength α_{10} .

half of the time series the prey density is lower than this boundary, and for the other half it is greater than it. Therefore the ranges define two subsets of the dynamics. The GLV model is then fitted to a *data stream* sampled from within these ranges, using the same model fitting method (section 6.2.3). The result is an estimate of the interaction strengths (and growth rate parameters) within each range of prey density. Increasing the number of ranges reduces their size, and therefore improves the approximation that the FR is linear within each range. However the more ranges there are, the fewer data points each contains to which the GLV can be fitted. If the estimates of interaction strengths vary between ranges, this represents evidence of functional dependence of the interaction strength on prey density, which we have seen previously results from non-linearity in the FR.

Figure 6.16 shows the estimates of interaction strength resulting from range sampling with $R = 7$. The results are calculated for a single parameter set (same as panel A in figure 6.13), from one simulation with $\sigma_{noise} = 0$ (green triangles), and one simulation with $\sigma_{noise} = 5$ (red triangles). The analytic forms for the interaction strengths α_{01} and α_{10} are shown as blue lines. In the deterministic case the estimates of interaction strength lie close to the analytic form. Not only can we detect functional dependence of the interaction strengths on prey density x_0 , but we are able to approximate the functional form of the interaction strengths $\alpha_{01}(x_0)$ and $\alpha_{10}(x_0)$.

However the addition of a moderate amount of noise ($\sigma_{noise} = 5$) produces significant error in the range sampling estimates. In panel A, a dependence of the estimates \hat{J}_{01} on prey density is still clear, although the estimates are scattered about the analytic function. The estimates of predator interaction strength \hat{J}_{10} show greater sensitivity to noise. At low prey densities the estimates are so far from the analytic function that they take the wrong sign (negative estimates \hat{J}_{10} suggesting that the predator is being eaten by the prey). Consequently the correct dependence of $\alpha_{10}(x_0)$ cannot be identified. In general we found that the range sampling approach is highly sensitive to noise. At values of σ_{noise} much greater than 10 all evidence that interaction strengths are functionally dependent on x_0 is lost (results not shown). Therefore we conclude that the range sampling approach, in its current form, is not practically useful for the detection of non-linear functional responses from population dynamics data.

6.3.8 Summary

In general we conclude that the inference method works well for a single prey and predator species. When applied to dynamics governed by stochastic differential equations the method accurately recovers the inter-specific interaction strengths. The parameter estimates converge as the number of samples in the *data stream* is increased. Variability in the estimates is increased by the addition of noise, which may also produce systematic error in the estimates. In the case of non-linear FR the GLV fit can approximate the interaction strengths. However this approximation is sensitive to noise and the extent of the non-linearity in the FR. A novel method for detection of non-linearity in the FR was presented. This method was shown to be successful in the deterministic case, but sufficiently sensitive to noise as to not be useful in its current form.

6.4 Results: IBM as data generator

In this section we apply the inference method to population dynamics simulated using the IBM model. Here the dynamics is not explicitly governed by differential equations, and so this represents a more realistic test of the method. The analysis is extended to systems with three and five species, which significantly increases the complexity of the problem. In particular these systems have missing links, i.e. potential interactions between species which do not actually occur. We investigate if the inference method can detect these missing links. All simulations run using the IBM have the initial 2000 time steps removed unless otherwise stated. Similar to previous chapters this removal ensures that the initial period of transience, as the system relaxes from the initial conditions, is not included in our analysis. Before presenting the results of the inference method we introduce an extension that allows the fitting of the GLV with topological constraints (section 6.4.1). We also analyse certain properties of the IBM output, in order to justify the fitting of the GLV model to its dynamics (section 6.4.2).

6.4.1 Topological constraints on the GLV

Fitting the full GLV model to population dynamics never produces estimates of interaction strength that are exactly equal to zero. Therefore in some cases it is desirable to constrain the interaction topology which is used to fit the dynamics, in order to compare how the GLV fit performs without certain links. The method for conducting this constrained fit is outlined here. We reproduce the analytic solution for the GLV fit to species i (equation 6.2.3):

$$\hat{J}_i = Y G_i^T \left(G_i G_i^T \right)^{-1},$$

where the matrices are defined as

$$Y_i = \begin{pmatrix} \hat{y}_{i1} & \hat{y}_{i2} & \cdots & \hat{y}_{iM} \end{pmatrix} \in \mathbb{R}^{1 \times M},$$

$$\hat{J}_i = \begin{pmatrix} r_i & J_{i1} & J_{i2} & \cdots & J_{iN} \end{pmatrix} \in \mathbb{R}^{1 \times (N+1)},$$

$$G_i = \begin{pmatrix} f_{i1} & f_{i2} & \cdots & f_{iM} \\ g_{i11} & g_{i12} & \cdots & g_{i1M} \\ g_{i21} & g_{i22} & \cdots & g_{i2M} \\ \vdots & \vdots & \ddots & \vdots \\ g_{iN1} & g_{iN2} & \cdots & g_{iNM} \end{pmatrix} \in \mathbb{R}^{(N+1) \times M}.$$

We can constrain the species j with which species i is allowed to interact in the fitted model. By removing the element \hat{y}_{ij} from Y_i , and the j^{th} row from G_i , we effectively remove the j^{th} species from the error minimisation. In this case we obtain an estimate $\hat{J}_i \in \mathbb{R}^{1 \times (N)}$ (rather than $\mathbb{R}^{1 \times (N+1)}$). As many species as required can be removed from the error minimisation, and when the full estimated interaction matrix \hat{J} is reconstructed we insert zeros into the corresponding matrix entries.

6.4.2 Properties of the data generator

Before applying the inference method to *data streams* derived from IBM simulations, we consider certain properties of the IBM. This model has yet to be used to simulate communities with a small number of species. In previous chapters we have studied simulated communities of no less than 30 species. The simulation of smaller communities requires some parameter adjustment in order to obtain dynamics that are amenable to our goal of estimating the strength of species interactions. We also consider the functional forms generated by the model, in order to determine

the appropriateness of fitting a GLV model to the dynamics. Specifically we study the intrinsic growth functions of basal and non-basal species, and the functional response of non-basal predators.

Unlike the ODE models used as the *data generators* in section 6.3, the IBM does not allow us to calculate analytic forms for the interaction strengths (using the metric α , defined in section 6.2.4). Rather the interaction strengths in the IBM emerge from the local interactions between individuals during the simulation. In this sense the use of the IBM as *data generator* represents a step towards *realism* in testing the inference method. However, the unavailability of analytic forms for the interaction strengths raises the question of how to evaluate the performance of the inference method. The simplest check, and the most fundamental concern, is to determine if the fitted GLV parameters correctly identify which species are prey, which species are predators, and which species interact. That is, does the method identify the correct interaction network topology. Further to this we are interested in determining how accurate the GLV estimates of interaction strength are, compared to some other measure of interaction strength derived from the IBM output. One possibility is to use the metric IS (equation (2.19)), which has been used hitherto in the thesis. However this metric only quantifies the per-capita effect on the prey population, per-capita of the predator. Therefore IS is analogous to the GLV estimate \hat{J}_{01} . In section 6.4.3 we develop an alternative metric that allows us to quantify the accuracy all the inferred GLV parameters (including inter-specific interaction strengths, and the intrinsic parameters for each species).

Figure 6.17 shows the dynamics of the IBM model, simulated with two species, for various parameter values. One species is a plant, the other is a herbivore which feeds on the plant. Throughout this section IBM simulations use a value of 1.0 for the parameter *HERB_FRACTION*, rather than the default value of 0.7. This parameter defines the fraction of the energy/resource of a plant individual that is taken when it is fed on by a consumer. The use of the value 1.0 means that any feeding interaction results in the death of the plant individual, simplifying the interpretation of the modelling and the calculation of interaction strengths. Further to this parameter adjustment, we compare the effects of changing the immigration rate parameter (IR), and the reproduction rate parameter (RR), on two species dynamics.

The immigration parameter IR represents a source of noise in the dynamics. This fact, although intuitive, was revealed explicitly by *recurrence quantification analysis* in chapter 4. As we saw in section 6.3, the performance of the inference method can be highly sensitive to noise, especially when the functional response of the predator is non-linear (see below). However the noise introduced by immigration is slightly different from the noise modelled in section 6.3. In the ODE models multiplicative noise was used, such that the noise term vanished for zero populations and the *postulate of parenthood* was not violated (section 6.3.1). In the IBM immigration represents a source of individuals that is not dependent on species populations in the landscape, and therefore net immigration does not fall to zero when no individuals are

6.4. RESULTS: IBM AS DATA GENERATOR

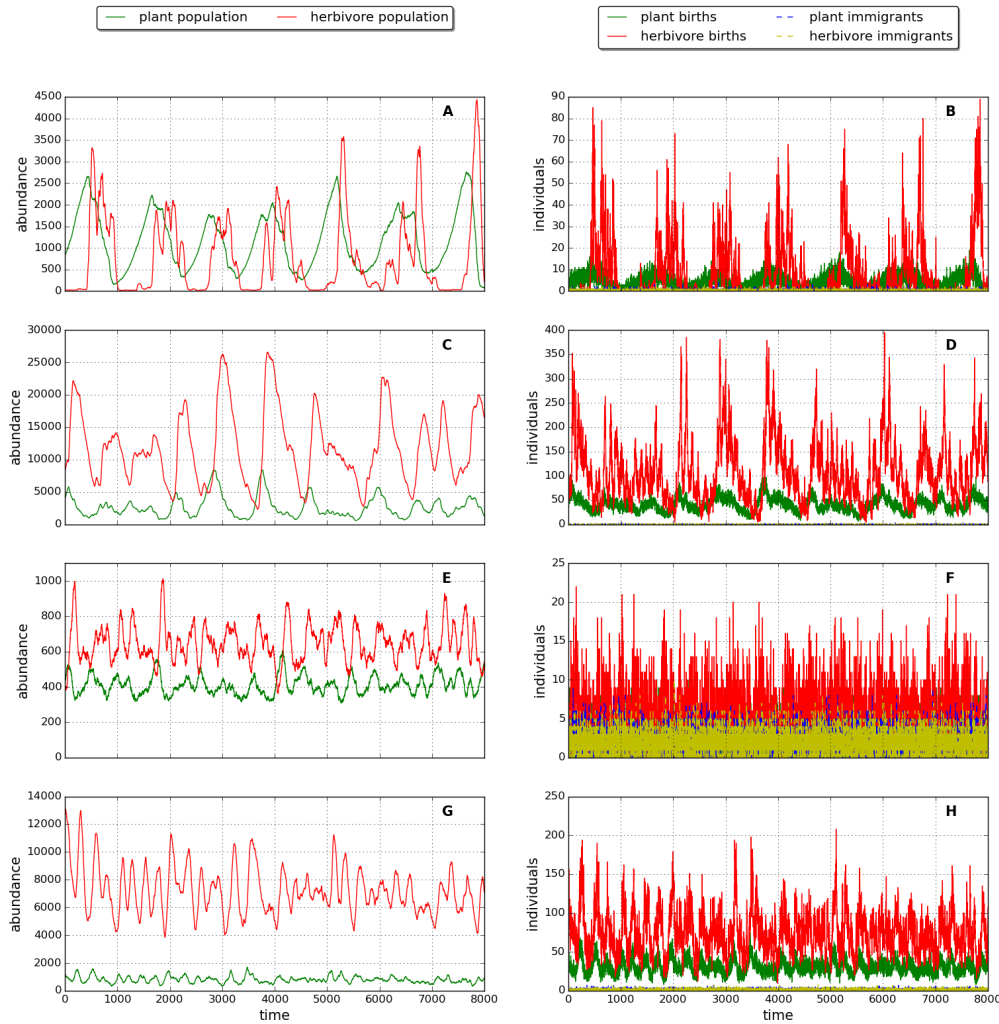


Figure 6.17: **Example dynamics of the IBM for two species** with different reproduction rates (RR) and immigration rates (IR). Here low and high RR are 0.01 and 0.1 respectively. Low and high IR are 10^{-4} and 10^{-5} respectively. **Left column:** Population dynamics of the two species. **Right column:** Time series of births and immigrations for both species. **First row:** low RR and low IR. **Second row:** high RR and low IR. **Third row:** low RR and high IR. **Fourth row:** high RR and high IR.

present. The IBM with non-zero IR violates the *postulate of parenthood*. However we argue that the noise introduced by immigration is still likely to cause systematic error in the estimates of interaction strengths. Importantly there is another source of noise resulting from the fact that the dynamics of the IBM are inherently stochastic. Individuals move around, interact and reproduce at random. It is not clear at this stage which source of noise is more significant. In an attempt to reduce the error introduced by immigration we use IR values that are low compared to those used in chapter 5. For *zero IR* we determined that the two species IBM dynamics was unstable. The herbivore species invariability went extinct (results not shown), which is consistent with results from chapter 4. Therefore two non-zero IRs were selected: 10^{-4} and 10^{-5} . The former value is equal to the lowest IR studied in chapter 5, but in the context of this chapter is referred to as the *high IR*. The latter value is an order of magnitude smaller, and therefore is referred to as the *low IR* in what follows.

The top two rows of figure 6.17 show dynamics simulated with the *low IR*, and the bottom two rows with the *high IR*. The left column shows the population dynamics, while the right column shows the number of immigrants and individuals born for both species on each time step. Panels A and E show dynamics that use the *default reproduction rate* ($RR=0.01$). In the low IR case (panel A) we see that the populations display *relaxation-type* oscillations, with the herbivore population falling close to zero for different periods of time with intermittent spiking. Such oscillations are sensitive to noise because a small stochastic increase in population during the relaxation phase can induce spiking. It was experimentally determined that the presence of such oscillations hampered attempts to infer species interaction strengths (results not shown). By increasing RR the decline in the plant population, which causes the crash in predator population, is softened (a similar argument was used in section 4.2.2). Panels C and G show dynamics with an increased RR of 0.1. In the low IR case (panel C), although there are still large amplitude oscillations, the herbivore population no longer relaxes close to zero. In all simulations that follow we use the value $RR=0.1$ in order to avoid relaxation-type oscillations.

Another consequence of increasing RR is that it increases the population levels of both species, on average. However, as we see from panels C and G, most of this benefit is conferred on the herbivore rather than the plant. Presumably the reason for this is strong predation by the herbivore, which regulates the plant populations. There is no predation pressure on the herbivore, only the effects of intrinsic mortality. The increased species abundances under high RR reduce dependence on immigration. In panels D and H the number if immigrants is barely visible, compared to the number of parented-births for both species. This observation suggests in this parameter regime that the contribution of noise resulting from immigration is low, compared to the inherent stochasticity of the IBM dynamics.

The dynamics in panels C and G in figure 6.17 correspond to the parameter values (low and high IR respectively) which we will use in section 6.4.3 to study two species systems. In later sections, where we study larger systems, the same parameter values are also used. Figure 6.2

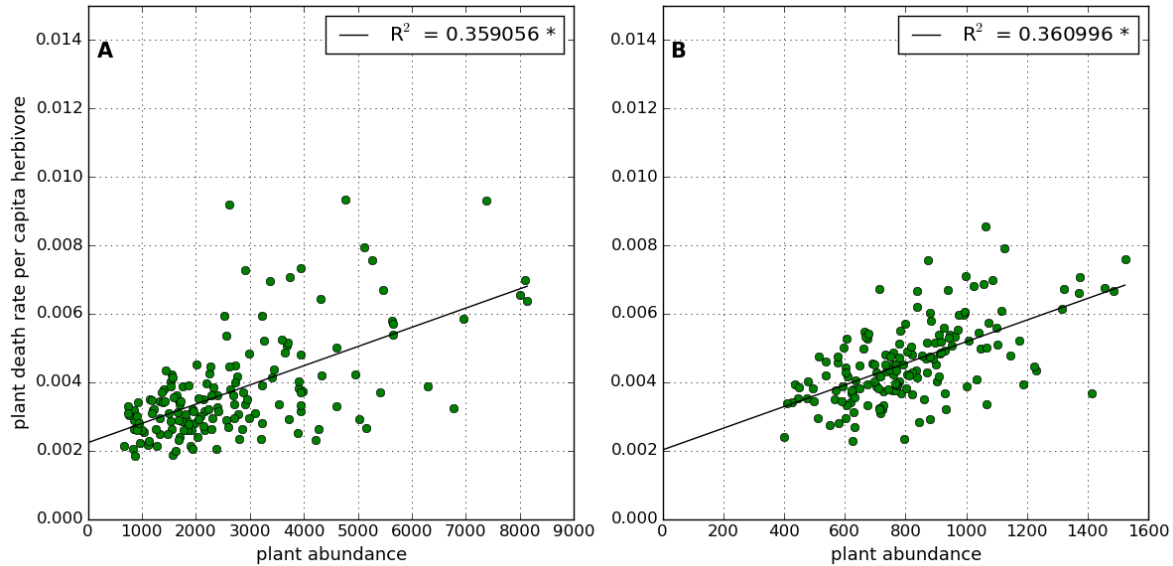


Figure 6.18: Functional response (FR) of the herbivore at two different immigration rates (IR), experimentally derived from two IBM simulations. Both simulations are of two species plant-herbivore systems, with reproduction rate (RR) 0.1 and run for 10,000 time steps. Each green circle represents the number of plants consumed during a window of 50 time steps, divided by the mean herbivore abundance during that window, plotted against the mean plant abundance during the window. The black lines represent linear regression fits to the data. R^2 values for the fits are given in legends, and significance at 95% confidence is indicated by *. **Panel A:** Low immigration rate ($IR = 10^{-5}$). **Panel B:** High immigration rate ($IR = 10^{-4}$).

shows the functional response (FR) of the herbivore at both low and high IR values. The FR is the same concept as introduced in the context of ODE modelling (section 6.2.1). It defines the rate of prey consumption per-capita of predator. Here the FR is derived from the IBM simulation output by counting the number of plants consumed during a window of 50 time steps, and dividing that count by the mean herbivore abundance during the window. The plots in figure 6.2 show the resulting FR values over the course of two simulations (panel A: low IR, panel B: high IR). From these plots we see that the FR appears to be approximately linear in plant abundance, with some deviation from linearity resulting from noise. Linear regression fits to the FRs indicate slightly less deviation from linearity at the high IR value (panel B). This observation is counter-intuitive based on results from previous chapters, where we have seen immigration act as a source of randomness in community dynamics.

Figure 6.19 shows equivalent plots of the herbivore *numerical response* (NR). NR is a similar concept to FR, but defines the per-capita birth rate of a predator as a function of its prey population [?]. The NR is evaluated from the IBM simulation output in a manner analogous to that just explained for the evaluation of the FR. From the figure we observe that the NR is approximately linear. There is visibly more deviation from linearity in the low IR case (panel A),

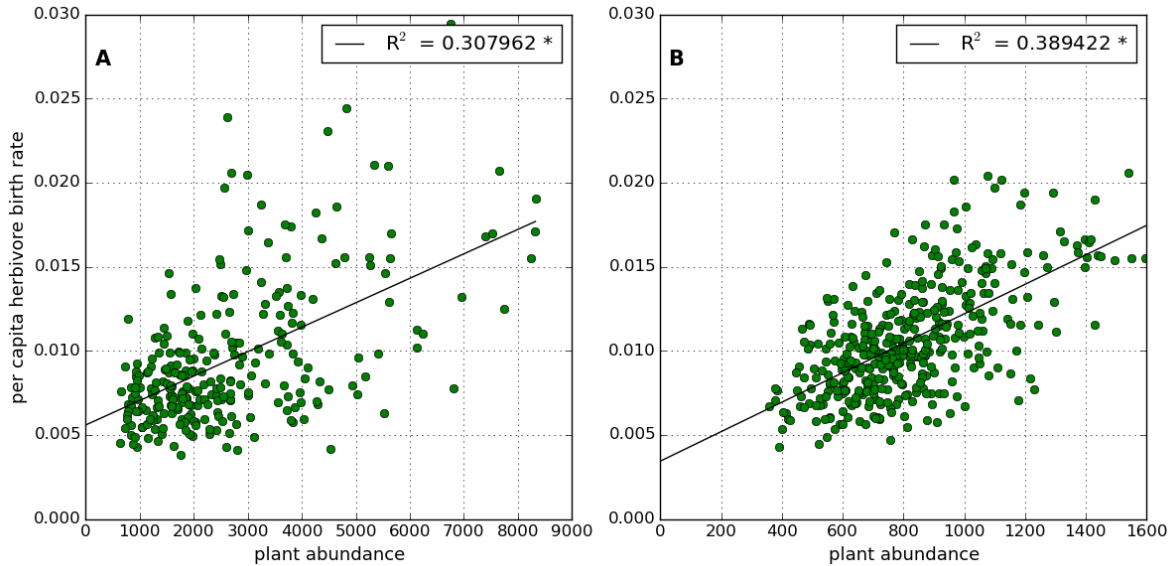


Figure 6.19: Similar to figure 6.18, but for the **numerical response (NR) of the herbivore**. Each green circle represents the number of herbivores born during a window of 50 time steps, divided by the mean herbivore abundance during that window, plotted against the mean plant abundance during the window.

than in the high IR case (panel B). This observation is confirmed by the R^2 values of the linear regression fits. Therefore we conclude that noise resulting from stochasticity of the dynamics is more likely to be a source of error in the GLV fit, than is any non-linearity in the herbivore interaction functions. Indeed given that we do not model prey handling times in the IBM, it is reasonable that no signature of predator saturation is detected [119]. Furthermore it appears that stochastic effects are greater at high IR (10^{-4}) than at low IR (10^{-5}).

Figure 6.20 shows experimentally derived forms of the intrinsic growth and mortality functions of the plant (panel A) and herbivore (panel B). These results were obtained by simulating landscapes with different starting abundances of a single species, without any individuals of the other species. In all cases $IR=0.0$, such that the only new individuals are due to reproduction. The intrinsic growth of the plant (panel A) is the classic *logistic-type* sigmoidal shape that we expect when modelling a basal species. At low population densities the growth is near exponential, but at high population densities the growth rate is curtailed as the species approaches carrying capacity. In the case of plants the carrying capacity is equal to the number of landscape cells (40,000), since plant individuals may only occupy the *inhabitant space* in each cell (see section 2.4). The herbivore mortality function (panel B) is approximately sigmoidal. The initial conditions of the IBM are such that each individual begins with a random amount of energy. Therefore herbivores initially reproduce and the population level increases. However, the population (for the experiments depicted) never reaches the herbivore carrying capacity, which is twice the number

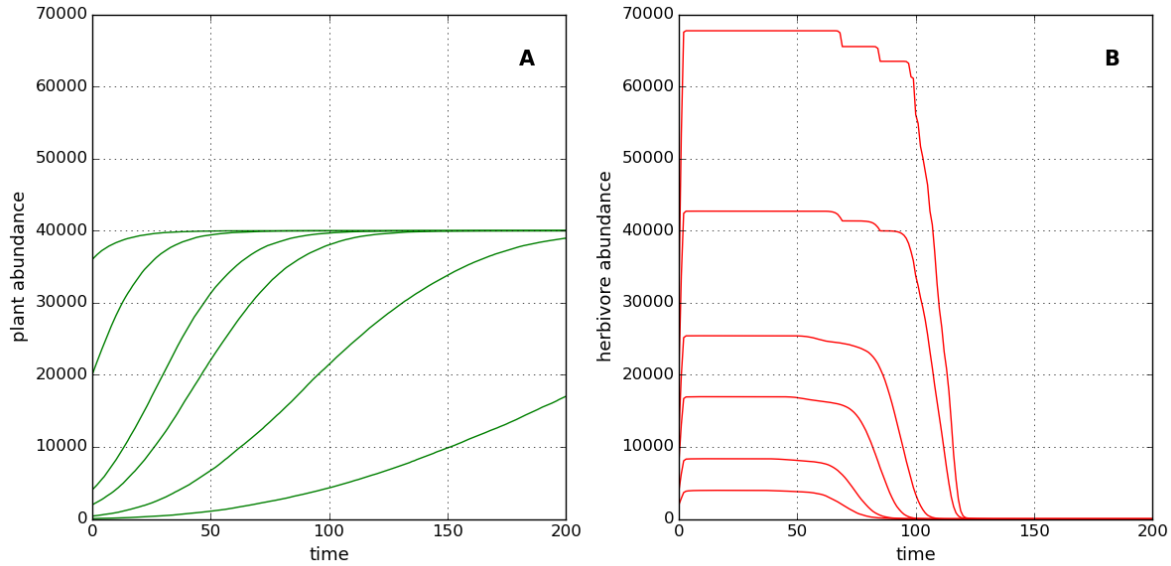


Figure 6.20: Intrinsic growth and mortality functions derived experimentally from two species IBM simulations. **Panel A:** How the plant population grows from different initial abundances, in the absence of any herbivores. **Panel B:** How the herbivore population declines from different initial populations, in the absence of any plants.

of landscape cells (80,000) because non-basal individuals may occupy both the *inhabitant* and *visitor* spaces in a cell. The plateau in herbivore population is below carrying capacity because there is a finite amount of energy in the system. The decline in the population from the plateau is sharp, but displays evidence of density-dependence similar to that observed for plant growth. The discrete steps visible at high population levels are possibly due to herbivores, which started with the same amount of energy, running out of energy at the same time. This feature suggests the possible existence of a *time delay* in the herbivore response to changes in the availability of food. (This time delay may be thought of as an *extinction debt*.) However, the main features of the intrinsic functions depicted, together with the near-linear functional forms seen in figures 6.2 and 6.19, suggest that an attempt to fit the GLV model to the IBM dynamics is valid.

6.4.3 Two species results

In this section results are presented for application of the inference method to *data streams* derived from two species IBM simulations. In all cases the simulations contain one plant and one predator species, and the parameters used are those described in the previous section. Therefore we compare the case of low IR (10^{-4}) with high IR (10^{-5}). We first demonstrate the convergence of the GLV parameter estimates under different sampling conditions, and then develop a method for quantifying the accuracy of the estimates. All simulations were run for 10,000 time steps, and the initial 2000 time steps were discarded to remove the initial transience (in accordance with

previous chapters).

Figure 6.21 shows how the GLV parameter estimates vary with sample length and sampling frequency in the case of *low IR*. As in section 6.3 sample length is varied by taking samples of increasing length from the beginning of the population dynamics, using all consecutive time points. Sampling frequency is defined as the total number of samples F , which are drawn at equal intervals from the full length of the dynamics. We compare the fits of two models, M_0 and M_1 . M_0 is the GLV model with the constraint that intra-specific interactions are equal to zero (see section 6.4.1). M_1 is the full GLV model without topological constraints. Each model is fitted to 25 replicate simulations, so we can compare the mean and variability in estimated parameter values. In general we observe that the parameter estimates converge as the both sample length and sampling frequency are increased. This convergence is more rapid for increasing sampling frequency, suggesting that it is better to use samples drawn from the full length of the dynamics. That is, for a given number of samples, low resolution sampling of the full dynamics performs better than high resolution sampling of a subset. We also observe that the introduction of intra-specific interactions (M_1) does not significantly affect estimates of prey interaction strength (\hat{J}_{01}), whereas it does affect estimates of predator interaction strength (\hat{J}_{10}). The estimates of \hat{J}_{10} are also more variable than those of \hat{J}_{01} .

Figure 6.22 shows the equivalent convergence plots for the *high IR* case. Here the convergence of the estimates with sampling frequency is slower. From panels B and D we conclude that at least 1000 samples, distributed along the full length of the dynamics, are required to produce convergence of the estimates. As in the low IR case, we see that there is less variability in the estimates \hat{J}_{01} , than in \hat{J}_{10} , and that the latter estimates are more affected by the inclusion of intra-specific interactions. Note the scale on the y-axes of panels A and B are an order of magnitude larger than those in figure 6.21. The magnitudes of the estimates of inter-specific interaction strength (\hat{J}_{01} and \hat{J}_{10}) are larger in the high IR case than in the low IR case. This observation is not consistent with results from chapter 5, where it was seen that reducing the IR increased the mean value of IS for the community as a whole. However the observation is consistent with the argument that reducing IR reduces the probability of interaction between individuals, because there are fewer individuals present in the landscape. We suggest that the disparity between these results and those of the previous chapter is due to the limit behaviour of the IS metric (as previously argued), which biases the community level result as some populations approach zero. However it may also be the case that the GLV parameter estimates converge on values which are incorrect (i.e. do not faithfully represent the interaction strengths of the system).

One possible way to determine the accuracy of the GLV parameter estimates is to simulate the GLV model using the fitted values, and compare the simulation to the original *data stream*. In figure 6.23 we use this method to compare the fits of M_0 and M_1 to a single *low IR* simulation. Both fits use a *sampling frequency* of 1000, based on the convergence results discussed above. In

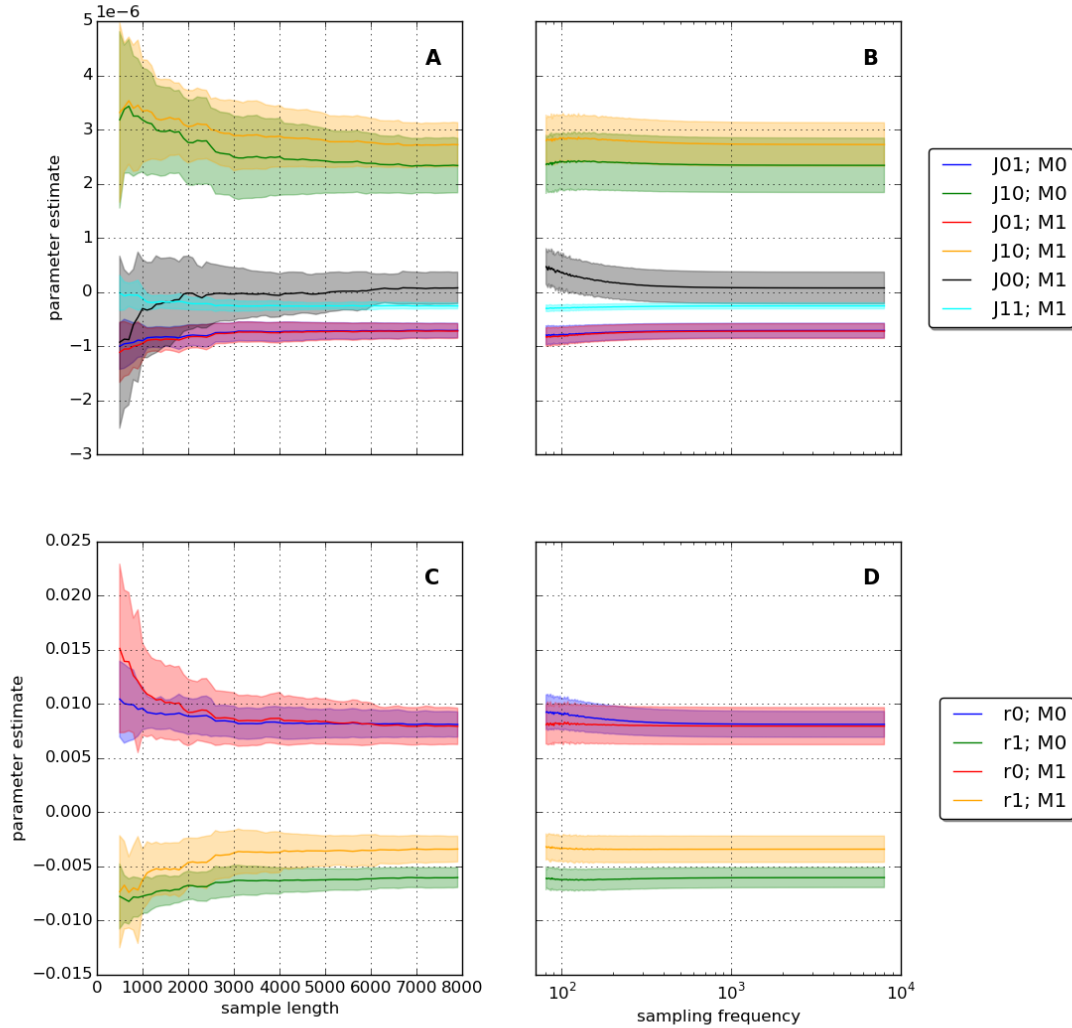


Figure 6.21: Convergence of parameter estimates for low immigration rate ($IR = 10^{-5}$). Solid lines represent mean values, shaded areas represent ± 1 standard deviation, over 25 replicates. M0 indicates GLV model fit without intra-specific interactions ($J_{ii} = 0$). M1 indicates GLV model fit without constraints on topology (see text). **Top row:** interaction strength estimates. **Bottom row:** growth rate estimates. **Left column:** convergence as sample length increased. **Right column:** convergence as sampling frequency increased.

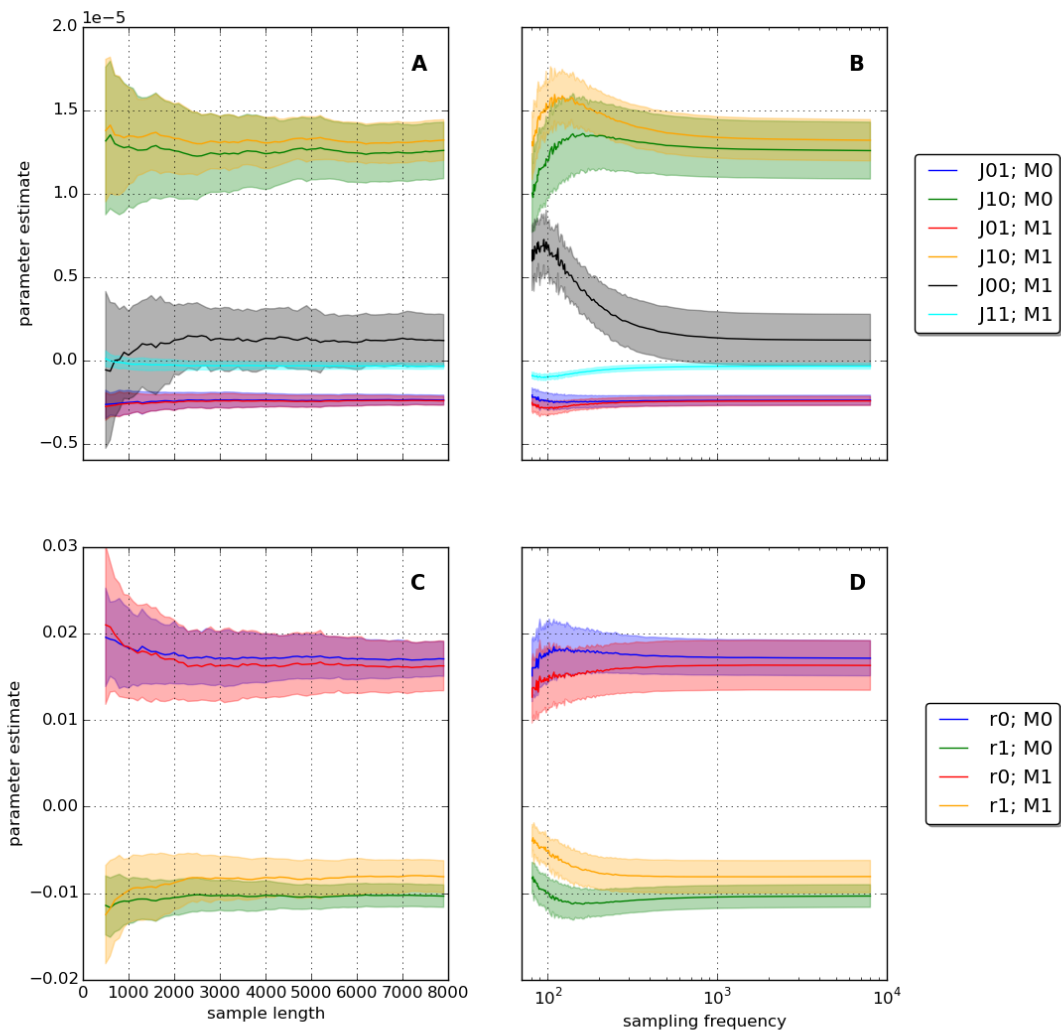


Figure 6.22: Similar to figure 6.21, but for **high immigration rate** ($IR = 10^{-4}$).

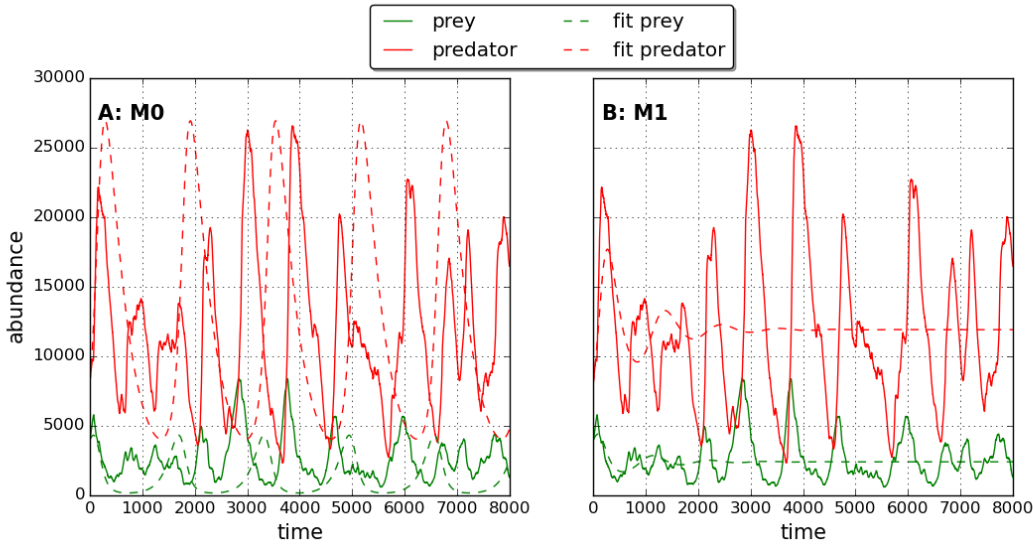


Figure 6.23: Comparison between true and fitted dynamics for two different fitted models: M0 and M1. Solid lines represents the simulated IBM dynamics at **low IR** (10^{-5}). Dashed lines indicate a deterministic simulation of the fitted GLV, from the same initial conditions as the IBM time series. **Panel A:** M0 is GLV model with constraint that $J_{ii} = 0$ (no intra-specific interactions). **Panel B:** M1 is full GLV with no constraints.

panel A we see that the simulated M0 fit produces oscillatory dynamics of comparable amplitude and period to those in the *data stream*. In panel B we see that the introduction of intra-specific interactions dampens the oscillations in the fitted model (M1). However stochastic forcing may induce oscillations in a system with a stable equilibrium, such as this M1 fit. Therefore, under the correct noise conditions, the M1 fit may produce dynamics the are similar to the *data stream*. Furthermore the shapes of the intrinsic functions, seen in section 6.4.2, suggest the presence of intra-specific effects in the IBM. Therefore we conclude that simulating the fitted GLV is not an appropriate way to determine to accuracy of the fit.

Rather than simulating the fitted GLV model, we assess the predictions that the fitted model makes about the birth and death rates of both species. To compute these predictions the relevant parameters of the GLV are multiplied by some combination of the species population vectors. For example the prediction for *predator births* is given by $\hat{J}_{10}X_0X_1$, where X_0 and X_1 are the true populations of the two species from the IBM simulation. The full set of definitions for the predicted rates of the fitted models are given in table 6.2. The GLV model fit without intra-specific interactions is named M0, as before. The GLV fit with intra-specific interactions raises the question of whether intra-specific interactions contribute to the birth or death rate of a species. Therefore the models labelled M1 and M2 refer to the same GLV fit, but M1 has the intra-specific terms added to the birth rate predictions, where M2 has them added to the death rate predictions. All rate predictions are plotted in figure 6.24 for a low IR simulation, and in figure 6.25 for a high

IR simulation. The model fits in all cases us a sampling frequency of 1000. The true birth and death rates for both species are plotted in green, for visual comparison with the predictions.

| model | M0 | M1 | M2 |
|-----------------|------------------------|---|---|
| prey births | $\hat{r}_0 X_0$ | $\hat{r}_0 X_0 + \hat{J}_{00} X_0^2$ | $\hat{r}_0 X_0$ |
| predator births | $\hat{J}_{10} X_0 X_1$ | $\hat{J}_{10} X_0 X_1 + \hat{J}_{11} X_1^2$ | $\hat{J}_{10} X_0 X_1$ |
| prey deaths | $\hat{J}_{01} X_0 X_1$ | $\hat{J}_{01} X_0 X_1$ | $\hat{J}_{01} X_0 X_1 + \hat{J}_{00} X_0^2$ |
| predator deaths | $\hat{r}_1 X_1$ | $\hat{r}_1 X_1$ | $\hat{r}_1 X_1 + \hat{J}_{11} X_1^2$ |

Table 6.2: The way in which the various demographic rate predictions are calculated from the fitted model parameters, based on the observed populations. The vectors X_0 and X_1 are the full abundance time series of the plant and herbivore species respectively. Multiplication of these vectors is *element-wise*.

From figures 6.24 and 6.25 we make the following observations. The periods of oscillation in the predicted rates match those of the true values closely. This is no surprise given that the predictions are calculated using the true population time series. However, in most case the predictions are also of comparable magnitude to the true values. Therefore the GLV fit can produce reasonable predictions of all demographic rates at any time point, given the abundance of both species. In the predictions of prey births and deaths there is little different between models M0, M1 and M2 (panels A and C, both figures). In the predictions of predator births and deaths, M1 clearly gives inferior results at low IR (panels B and D, figure 6.24). At high IR a difference is visible between the estimates of the three models (panels B and D, figure 6.25) but it is hard to tell which model produces the best predictions. In order to quantify the performance of the different models in predicting species births and deaths we define a *relative error metric*

$$(6.39) \quad \langle RE \rangle = \frac{1}{T} \sum_{t=1}^T \left(\frac{|b(t) - p(t)|}{|b(t)|} \right),$$

where T is the number of time steps in the dynamics, $b(t)$ is the true number of births or deaths on time step t , and $p(t)$ is the number of births or deaths predicted by the fitted model. This metric quantifies the mean relative deviation of the predictions from the true values over the full time series.

Figure 6.26 summarises the relative error in the predicted births and deaths over an ensemble of 25 replicate simulations at low IR. The models are fitted to the simulated dynamics using a sampling frequency of 1000, as before. The fitted model parameters are then used to predict the

6.4. RESULTS: IBM AS DATA GENERATOR

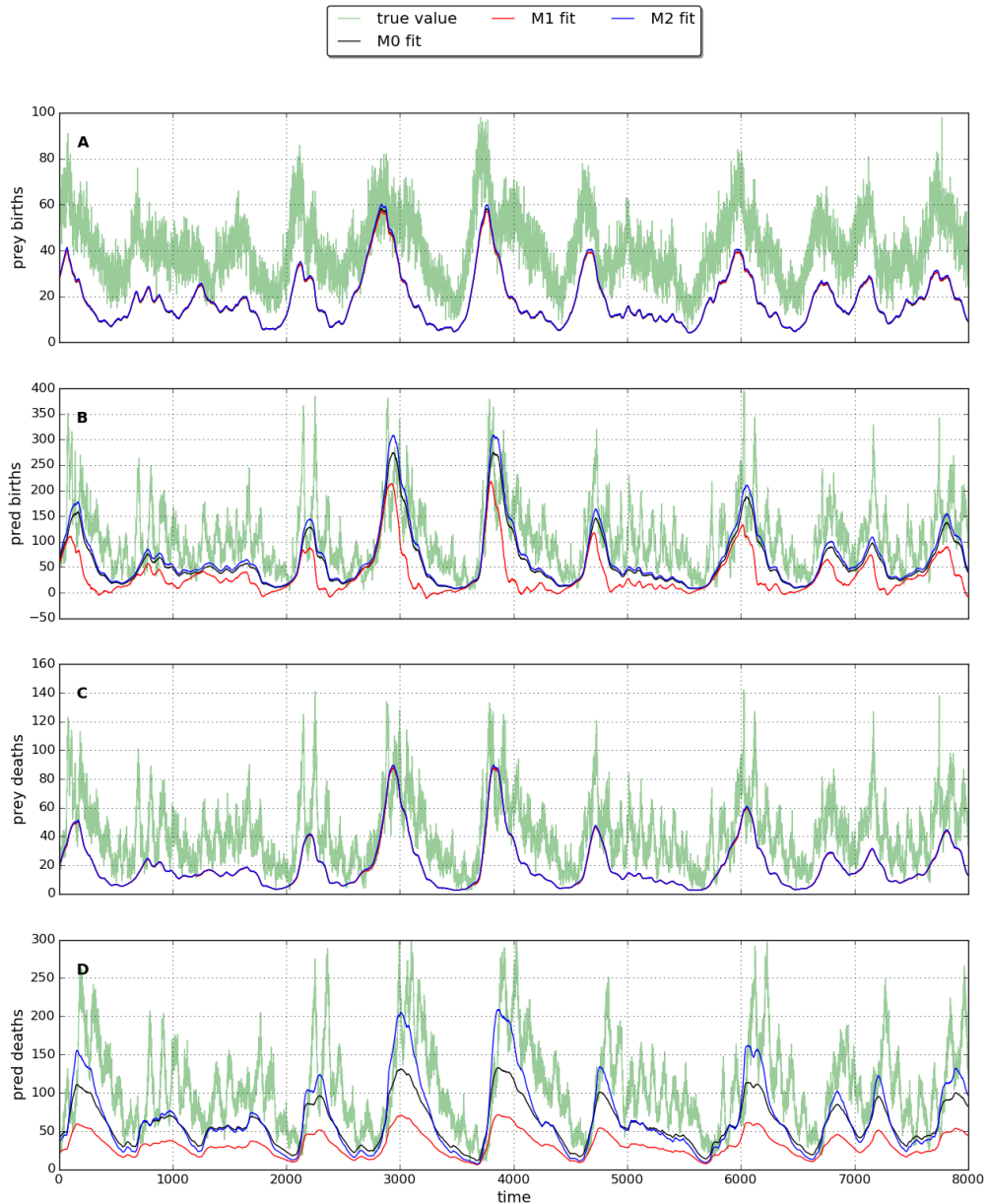


Figure 6.24: Births and deaths predicted by three different model fits: M0, M1, M2 (see text for model definitions). Green line is the true number of births and deaths for each species on each time step, recorded from the IBM simulation. Coloured lines represent model predictions of the number of births and deaths, based on the true population level of both species at each time step (see text for further details). The simulation was run using **low IR** (10^{-5}).

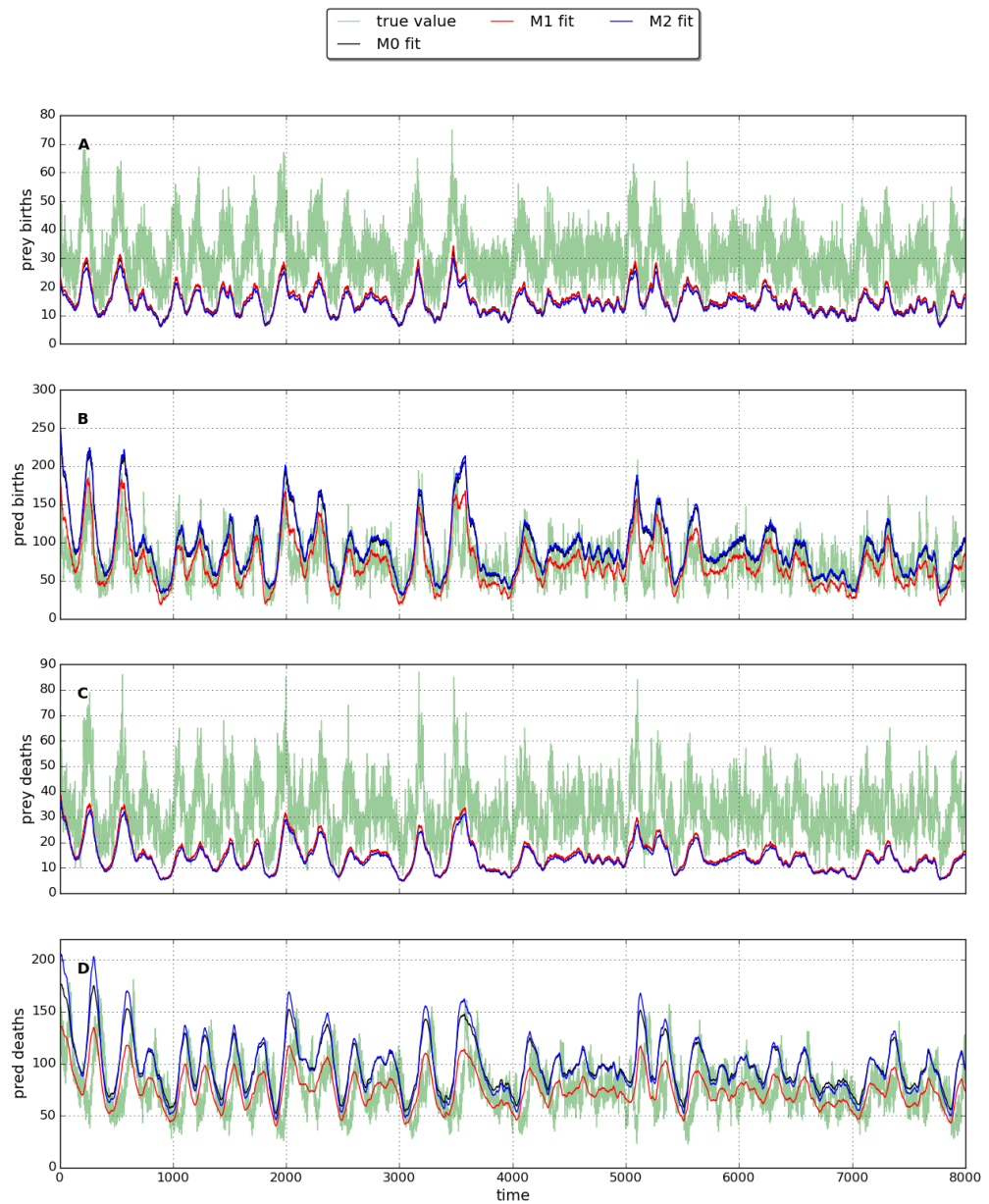


Figure 6.25: Similar to figure 6.24, but for an IBM simulation at **high IR** (10^{-4}).

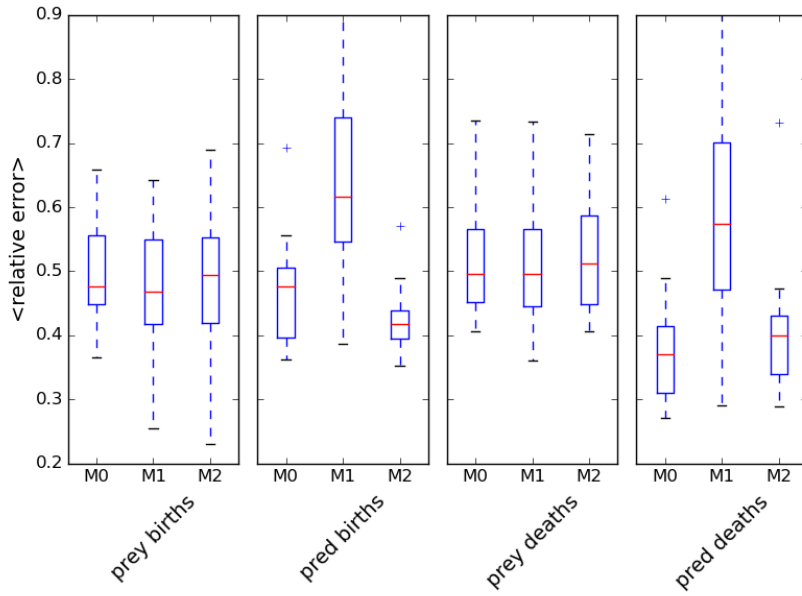


Figure 6.26: **Relative error in the rate estimates** displayed in figure 6.24 (prey and predator births/deaths). The relative error metric is defined in equation (6.4.3). The relative error statistics illustrated are derived from model fits to 25 replicate IBM simulations at **low IR** (10^{-5}). Boxes extend to the first and third quartiles of the data, and the red line indicates the median. Whiskers extend to show the range of the data, up to a maximum of 1.5 times the inter-quartile distance beyond which points are shown as outliers.

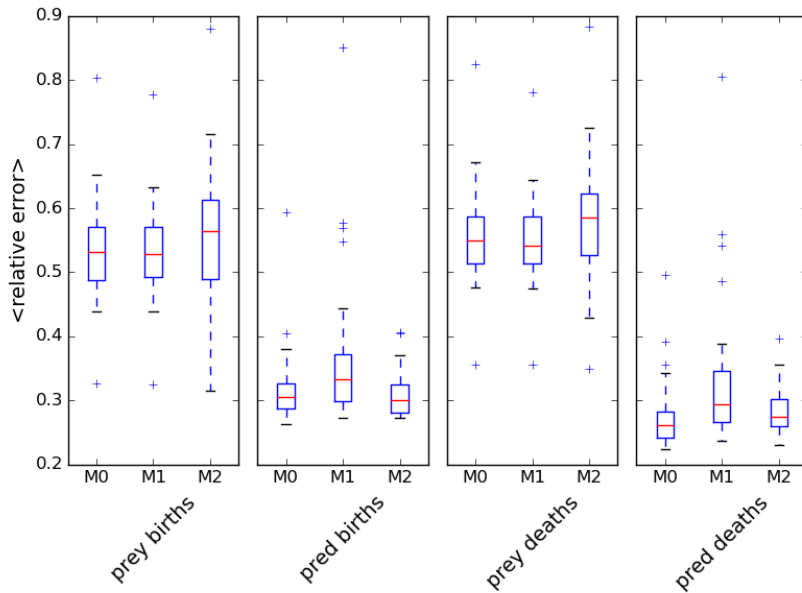


Figure 6.27: Similar to figure 6.26, but for results of model fits to 25 replicate IBM simulations at **high IR** (10^{-4}).

births and deaths of both species, and the relative errors (RE) calculated as just described. For prey births and deaths there is little difference between the three models. Based on the median RE (red lines), the model M1 produces the best estimates by a narrow margin. For the predator estimates M1 clearly has higher errors, while M2 and M0 perform best for births and deaths respectively. Figure 6.27 shows the equivalent results for 25 simulations at high IR. The prey estimates have similar, or slightly higher, errors than in the low IR case, whereas the predator estimates show significantly lower errors. In the high IR case M2 performs the worst for the prey estimates, and M1 performs the worst for the predator estimates. Comparing across both low and high IR it appears that M1 is the correct model for the prey, while M2 is the correct model for the predator. However the inclusion of intra-specific interactions does not necessarily improve the rate predictions over those of M0. The use of M1 for prey predictions, and M2 for predator predictions, is consistent with the intrinsic functions derived in section 6.4.2. That is, intra-specific interactions contribute to prey growth rates, but to predator mortality rates.

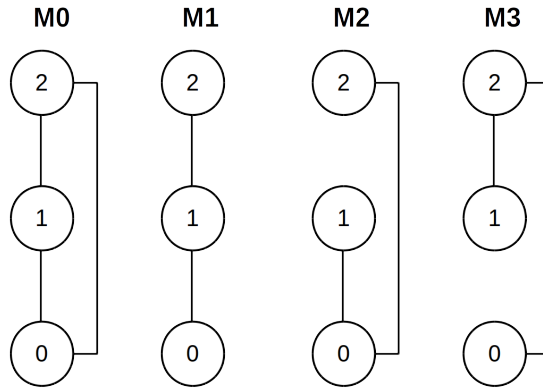


Figure 6.28: The four candidate models investigated in this section. M0: fully connected. M1, M2, M3: one links removed. M1 is the ‘correct’ model i.e. the food chain simulated by the IBM, to which the models are fitted. All four models include intra-specific interactions (self-loops), although these are not drawn.

6.4.4 Three species results

In this section results are presented for fitting to 3 species IBM simulations of a *food chain*. Each simulation contains a single plant species, a single herbivore species, and a single predator species which feeds only on the herbivore. This scenario represents the first test of the inference method in correctly identifying the interaction network topology. There is a potential link, between the plant and predator species, that is not present in the underlying interaction network. We investigate whether the method can detect the absence of this link. In all cases the GLV is fitted *with* intra-specific interactions. According to the analysis in the previous section such interactions are taken to contribute to plant births, and to the deaths of the other two (non-basal) species, when rate predictions are made. We investigate the fitting of four candidate models (M0-3) with different constraints on interaction topology. These topologies are shown in figure 6.28, and are the only four possibilities that are connected (i.e. no isolated species). All models are subsets of M0, with M1 representing the true food chain that is simulated.

Figure 6.29 shows the convergence of parameter estimates with sample length for models M0 (right column) and M1 (left column), at high IR. The results at low IR are similar, and therefore not shown. The convergence depicted here is less convincing than in the two species case. In particular the estimates \hat{J}_{10} , \hat{J}_{12} and all r_i , do not settle down as sample length is increased. A further concern is that, for all sample lengths, $\hat{J}_{02} > 0$ and $\hat{J}_{20} < 0$. These parameters correspond to the spurious link (not present in the true network), and the signs quoted are indicative of the *plant species consuming the predator species*. It is worth noting that, when fitting M0, parameter that correspond to missing links will never be estimated as *exactly* equal to zero. The hope is that either the model fit reveals that such parameters are of small magnitude, or that there is some other means by which to determine to correct topology.

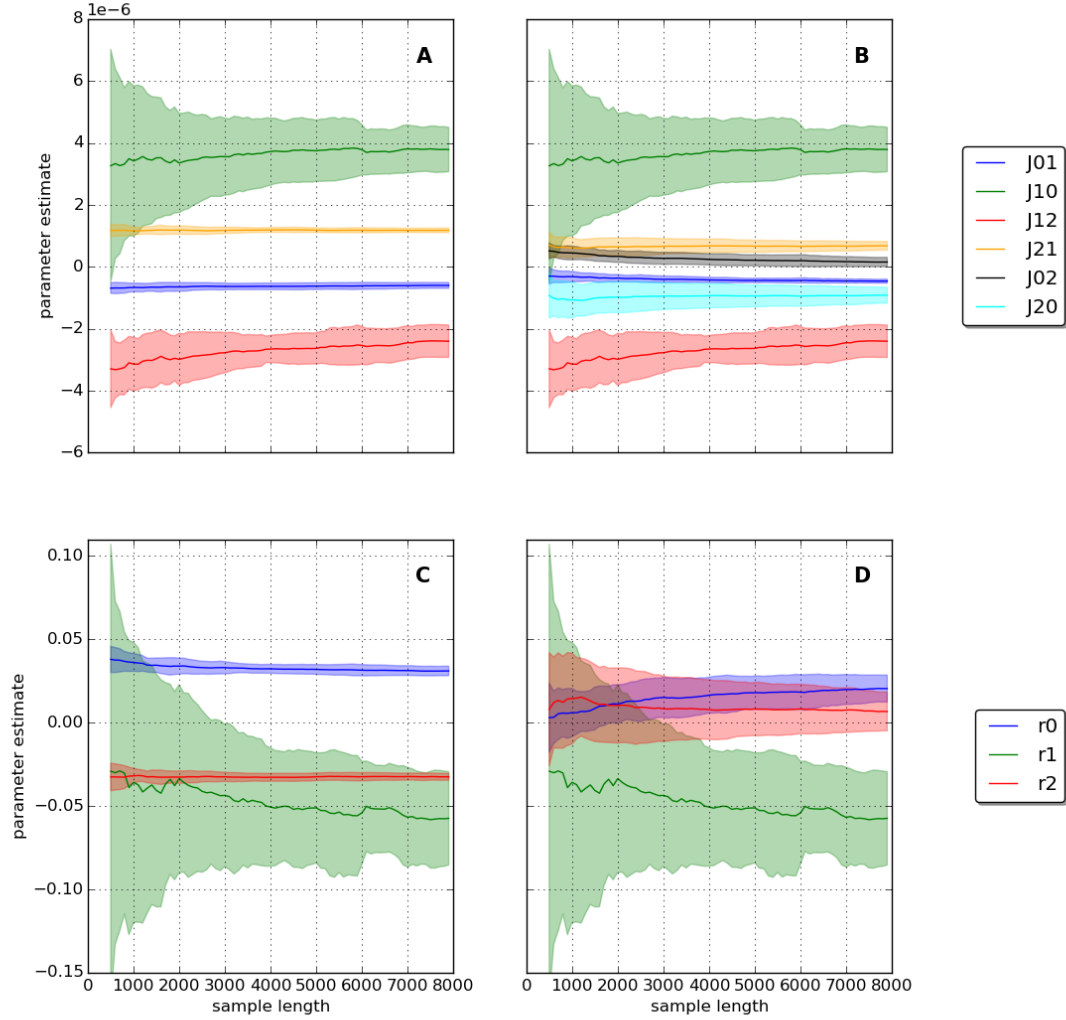


Figure 6.29: Convergence of parameter estimates with sample length for high immigration rate ($IR = 10^{-4}$). Two different models fitted to three species food chain dynamics. Inter-specific interactions (top row), and intrinsic parameters only (bottom row). Solid lines represent mean values, shaded areas represent ± 1 standard deviation, over 25 replicates. Panels A and C show fits of model M1. Panels B and D show fits of the model M0. These models are illustrated in figure 6.28. Intra-specific interactions are included in the fits, but are not plotted for simplicity.

6.4. RESULTS: IBM AS DATA GENERATOR

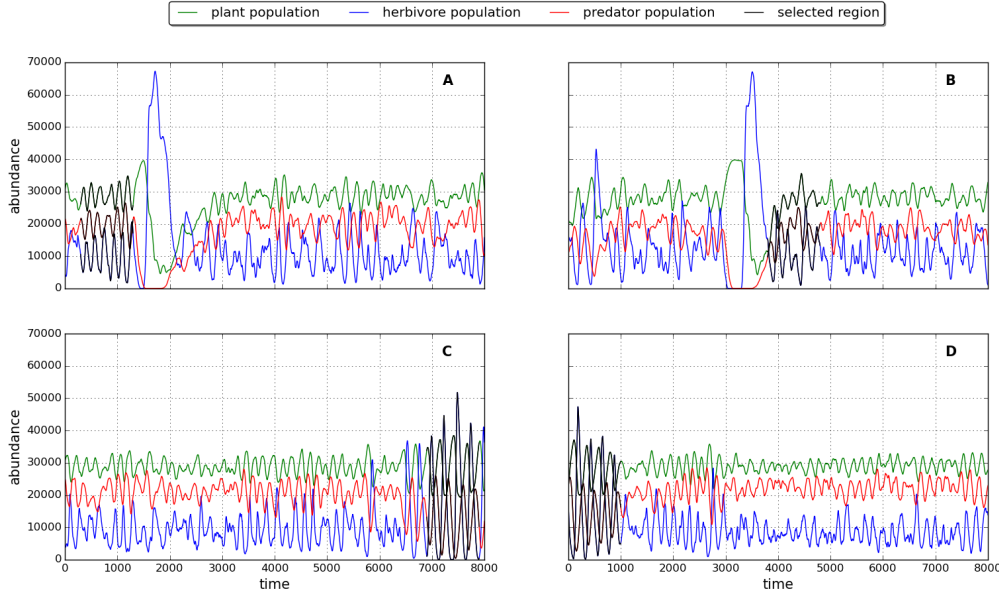


Figure 6.30: Example dynamics of 3 species IBM food chain, four different simulations (panels A,B,C,D). Top row: low IR (10^{-5}). Bottom row: high IR (10^{-4}). Regions plotted in black are those selected as *data streams* for GLV fit (see text for details of how selected).

Looking at the simulated food chain dynamics in figure 6.30, we speculate that the lack of convergence, and possibly the spurious interaction, may result from features of the dynamics. The dynamics shown are highly variable and appear *quasi-periodic*. It may be that the GLV struggles to fit to large regions of such dynamics. In an attempt to overcome this problem we employ a method to select the optimum region of the dynamics for fitting the GLV. The selection method consists of scanning a sampling window of length 1000 time steps along the full dynamics. The model M0 is fitted to the dynamics within the window and the error functions (equation (6.2.3)) of the three species are summed. We then select the window with the minimum total error in the fit. These selected regions are plotted in black for the four simulations shown in figure 6.30. The regions appear to share the common feature that they display oscillations of a relatively constant amplitude and period, compared to the rest of the dynamics. This observation supports our belief that the complexity of the dynamics negatively affects the GLV fit. In the analysis that follows all models are fitted to regions of the dynamics selected in the way just described.

Figures 6.31 and 6.32 show birth/death predictions of the fitted models to a single three species simulation at low IR and high IR respectively. Here we see significant difference between the quality of the predictions made by the different models. Note that for each species there is always a model (M1-3) that is equivalent to model M0 for that species. This is because in each of the models M1-3 one species is allowed to interact with both of the others, as they all are in model M0 (see figure 6.28). For most of the predictions at both IR values M3 (yellow) visibly performs

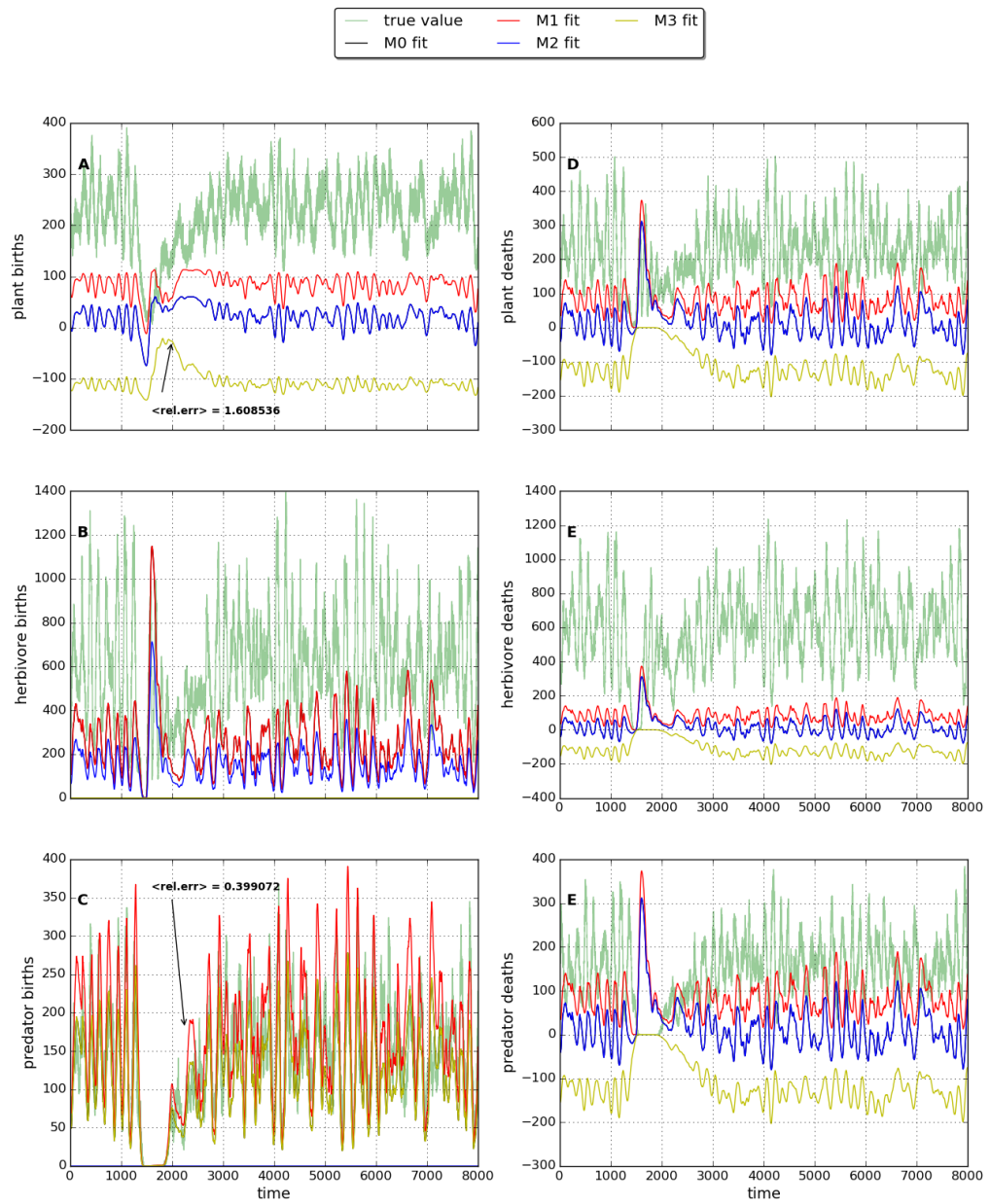


Figure 6.31: Similar to figure 6.24, but with different models fitted to a three species simulation at **low IR**. The simulation is the same as that in panel A of figure 6.30. The models M0-3 are depicted in figure 6.28. Arrows indicate the value of the relative error metric (RE) for two example model predictions.

6.4. RESULTS: IBM AS DATA GENERATOR

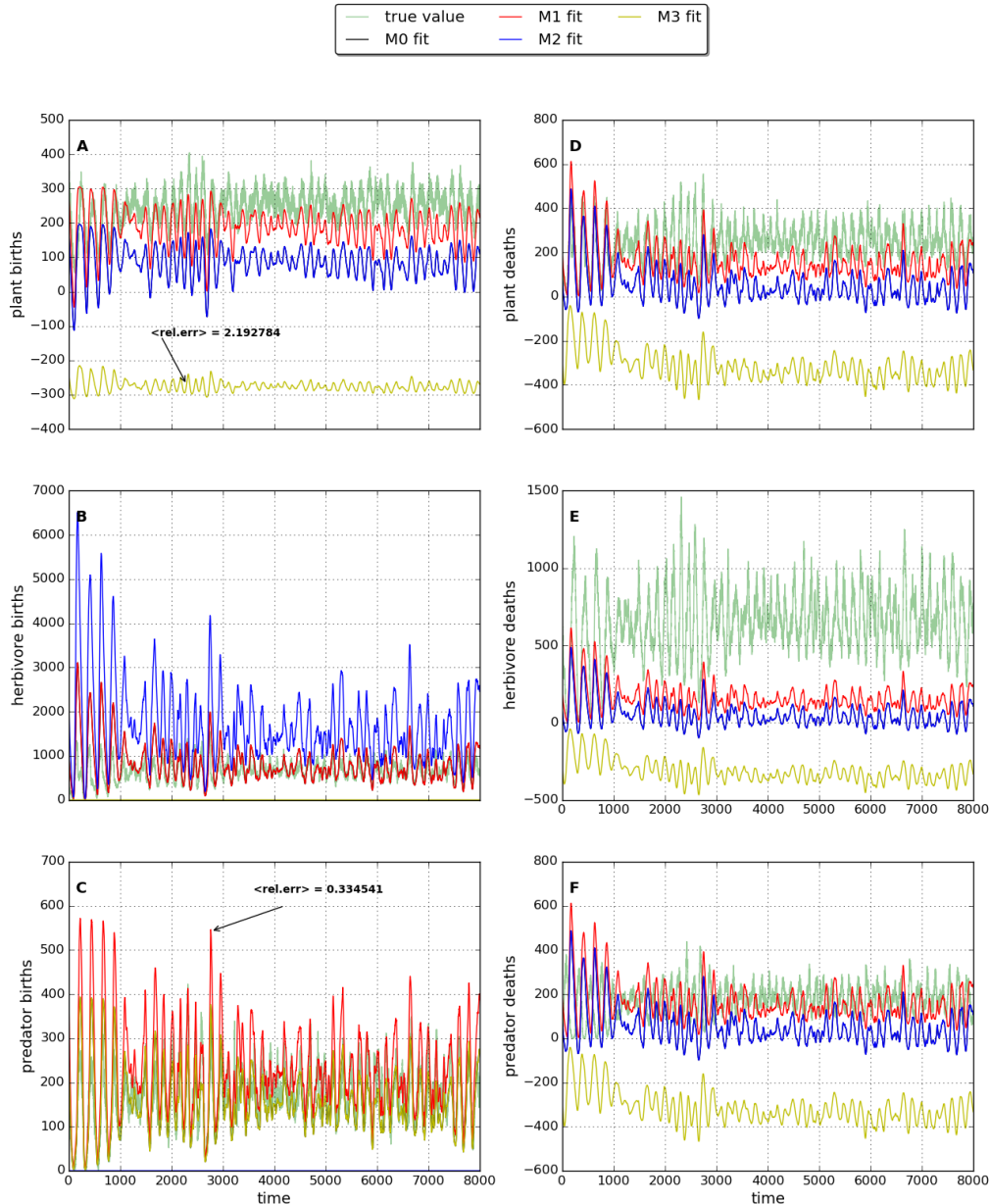


Figure 6.32: Similar to figure 6.31, but for **high IR**. The simulation is the same as that in panel C of figure 6.30.

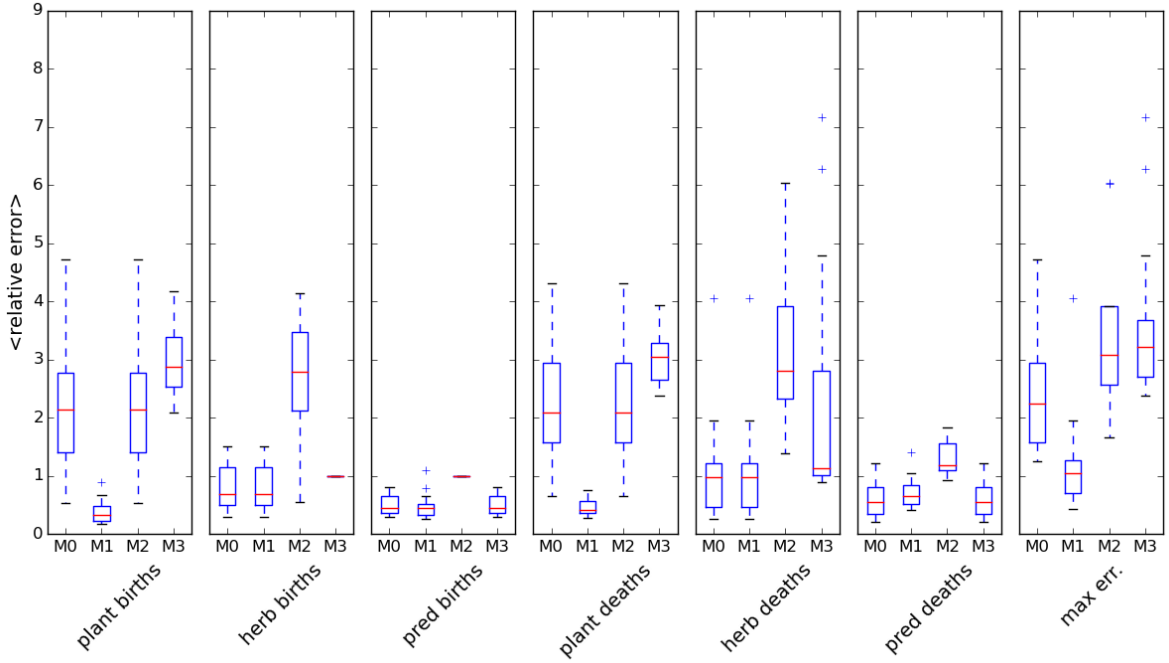
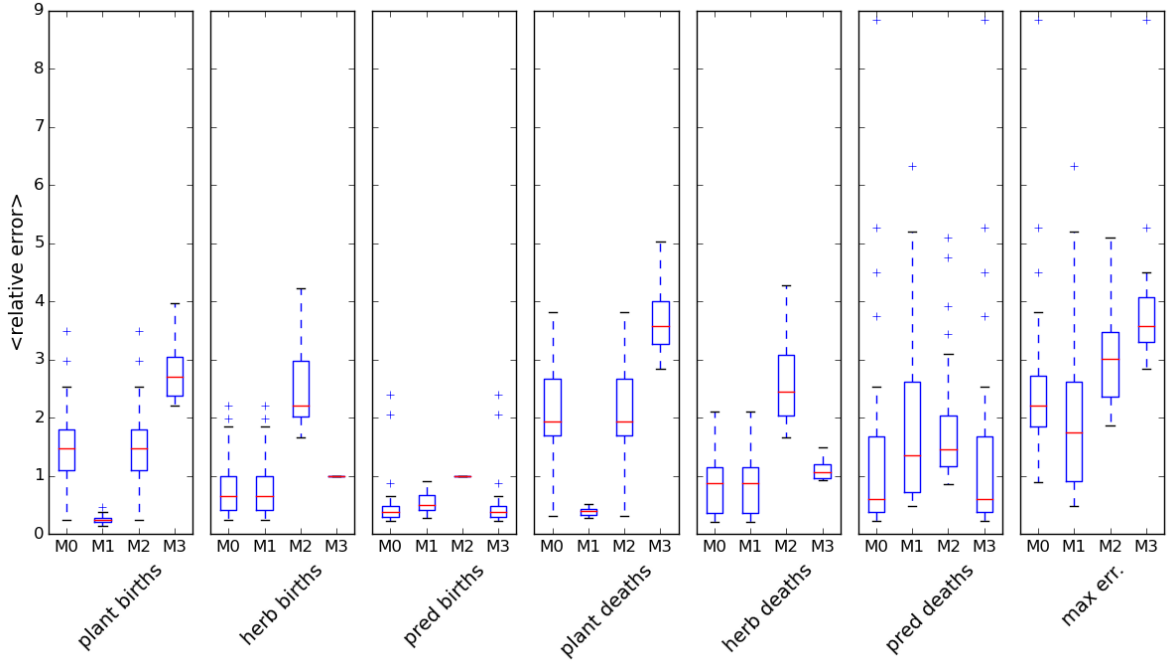


Figure 6.33: Similar to figure 6.26, but with different models fitted to 25 three species simulations at **low IR**. This figure includes an additional statistic labelled *max err.*, which is the maximum relative error in any prediction for a given simulation.

the worst. This is the model with the link between plant and herbivore removed. Also M2 appears to perform worse than M1 in most cases. M2 is the model with the link between herbivore and predator removed. It is reassuring that the removal of links which are present in the true network results in predictions that are worse than those of M1. To confirm the repeatability of this observation we employ the relative error metric (6.4.3) from the previous section, the determine the accuracy of model predictions over ensembles of 25 replicate simulations.

Figures 6.33 and 6.34 show the relative errors in birth/death predictions for the ensembles of simulations at low and high IR respectively. We see that the predictions of M1 perform better than those of M2 and M3 in almost all cases (according to the median and the range of RE). Furthermore M1 performs at least as well as M0, the unconstrained GLV fit, is most cases. The exceptions to these observations are in the predator deaths at low IR, and both predator births and deaths at high IR. In these cases models M0 and M3 perform at either better than, or equally as well as M1. We conclude that the inclusion of the spurious link between plant and predator species improves the prediction of the demographic rates of the predator by the fitted model. We also reiterate that when this link is included the parameter estimates \hat{J}_{02} and \hat{J}_{20} suggest that the predator is being eaten by the plant (see for example figure 6.29). We return to this strange feature of the results in section 6.4.7. In the final panel of figures 6.33 and 6.34 we include the statistic *maximum error*, which is the largest relative error out of all rate predictions for a given


 Figure 6.34: Similar to figure 6.33, but for 25 simulations at **high IR**.

simulation. For example, in figure 6.32, the maximum relative error for M3 is in the prediction of plant births. The error takes a value of 2.19, which is indicated by the arrow. The *maximum error* statistic allows us to determine which model fit provides the best predictions across all demographic rates. In both the low and high IR cases M1, the model with the correct topology, performs the best.

The correct model (M1) may produce the best rate predictions, but without knowledge of the true rates we cannot use this fact to identify the correct topology. We now attempt to identify which model (M0-4) represents the correct topology using only knowledge of the fitted models, and information about the IBM population dynamics (i.e. no knowledge of true demographic rates). We conduct three checks on the fitted models. First we evaluate the Jacobian of the model and determine if the equilibrium is locally stable (see section 6.2.1). Secondly we calculate the relative error between the model equilibrium and the long term average of the population dynamics for each species. Thirdly we compute the error function of the model fit $E(\hat{J}_i)$ for each species i (equation (6.2.3)), normalised by the sum of the first derivatives of the population dynamics of species i . The results of these three checks are summarised in figures 6.35 and 6.36 for the low and high IR ensembles respectively. At low IR, M1 does not perform consistently better than the competing models in terms of either equilibrium or error function values. At high IR, M1 performs best in terms of the predicted equilibrium values for all species, although the predator equilibrium results are comparable to those of M3. However M1 again does not display the lowest error function value for any species. In both the low and high IR cases the fitted M1

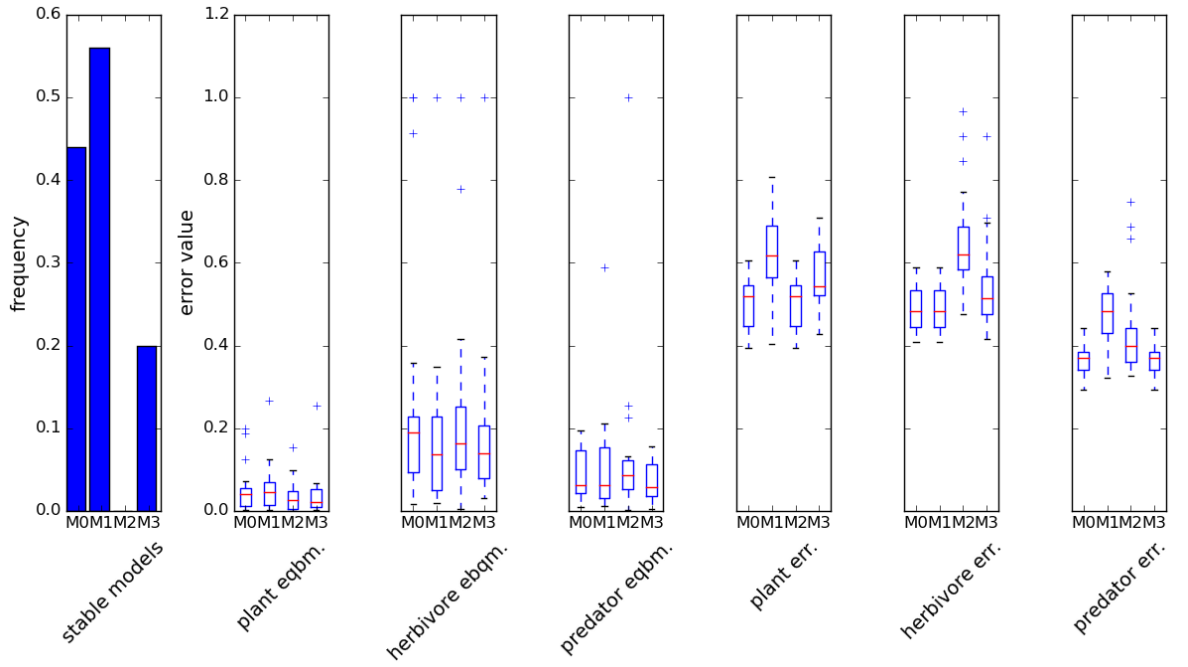
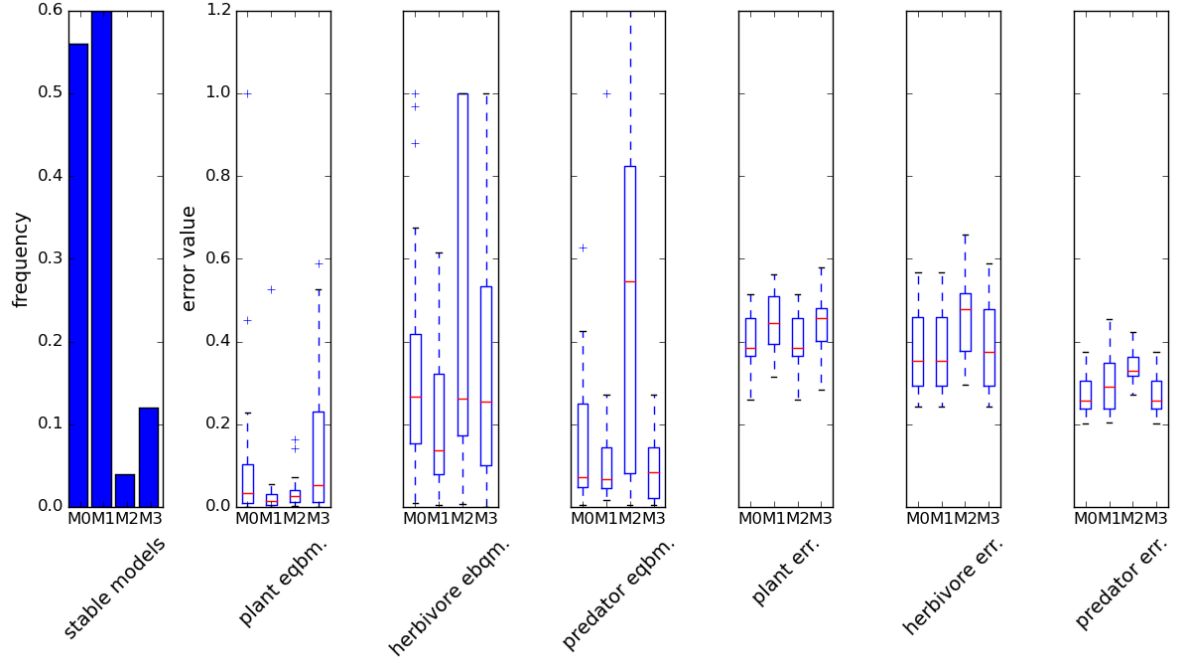


Figure 6.35: Evaluating the performance of the different model fits over 25 replicate simulations at **low IR**. Stability (panel 1) is determined from the Jacobian of the fitted model (see text). The errors in the equilibrium of each species (panels 2-4) represent the relative error between the equilibrium population of the fitted model and the long term average of the species population dynamics. The final three errors (panels 5-7) are the normalised error function of the model fit for each species (see text).

model is stable more frequently than any other. M0 is also stable with relatively high frequency, compared to M2 and M3 which are usually unstable. If presented with a single *data stream* of three species from which to infer the correct interaction topology, it may be possible to do so with reasonable confidence based on these results (with particular focus on stability). However no conclusive method for doing so emerges from the three checks presented. We concluded that the identification of the correct topology from three species food chain simulations remains an open problem. In section 6.6 we suggest improvements to the methodology, including the use of prior knowledge, that may facilitate the reliable identification of topology. We also argue that the method may prove useful regardless of topology identification, in particular in its ability to predict demographic rates and biomass flows.

6.4.5 Five species results

In this section we briefly consider the application of the inference method to a five species system. The step from three to five species significantly increases the complexity of the problem. Given the difficulty of identifying the correct interaction topology for three species, we may anticipate


 Figure 6.36: Similar to figure 6.35, but for **high IR**.

that it is not possible with five. However, based on the three species results, we may expect reasonable predictions of demographic rates, especially when the fitted model is constrained to the correct topology (this constrained model is again called M1). With five species there are a total of ten possible inter-specific interactions. This fully connected topology is shown as M0 in figure 6.37. There are a combinatorially large number of subsets of M0, depending on how many links L are included. For a network with L links there are $\binom{10}{L}$ distinct interaction topologies. For the IBM simulations we choose a symmetrical network with four links, shown as M1. It was experimentally determined that the symmetry of this network promoted stability in the population dynamics (results not shown). For example the introduction of the link \hat{J}_{03} to M1 makes the network asymmetric, benefiting species 3 over species 1 (two feeding links versus one), and benefiting species 2 over species 0 (one predator versus two). The network M1 contains two plants (species 0 and 2), two herbivores (species 1 and 3) and a single predator (species 4).

Five species IBM dynamics with interaction topology M1 are shown in figure 6.38. Panels A and B show dynamics at low IR, which are more variable than the high IR dynamics shown in panels C and D. In what follows we focus on the high IR case based on previous observations that it is easier to fit to dynamics that are less complex. This choice reflects an attempt to slightly simplify the challenge posed by the inference of interactions from the 5 species system. We again select the optimum region of 1000 time steps from the dynamics to use as the data stream. The regions are selected in the same way as in section 6.4.4, and are illustrated in figure 6.38. In this analysis we focus on the seven models depicted in figure 6.37. M0 is the full unconstrained GLV

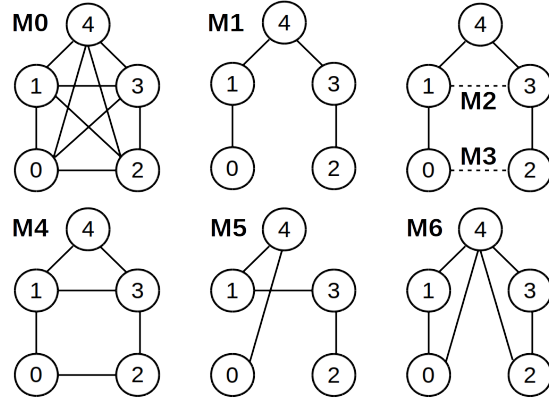


Figure 6.37: Seven candidate 5 species models. M0: fully connected. M1: the true topology of the IBM simulations to which the GLV is fitted. M2 and M3: One link added to M1, as indicated. M4-6: Different but plausible topologies. All models include intra-specific interactions (self-loops), although these are not drawn.

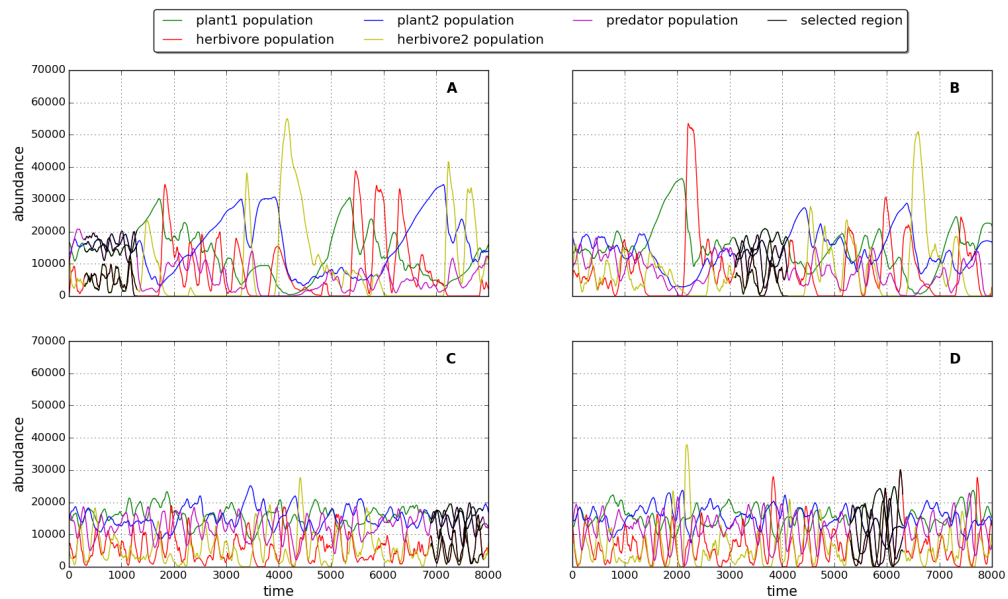


Figure 6.38: Similar to figure 6.30, but for five species simulations of the IBM with interaction topology M1 (shown in figure 6.37). Panels A and B: low IR. Panel C and D: high IR. The regions plotted in black represent selected *data streams* to which the GLV is fitted (selected using same criteria as in section 6.4.4).

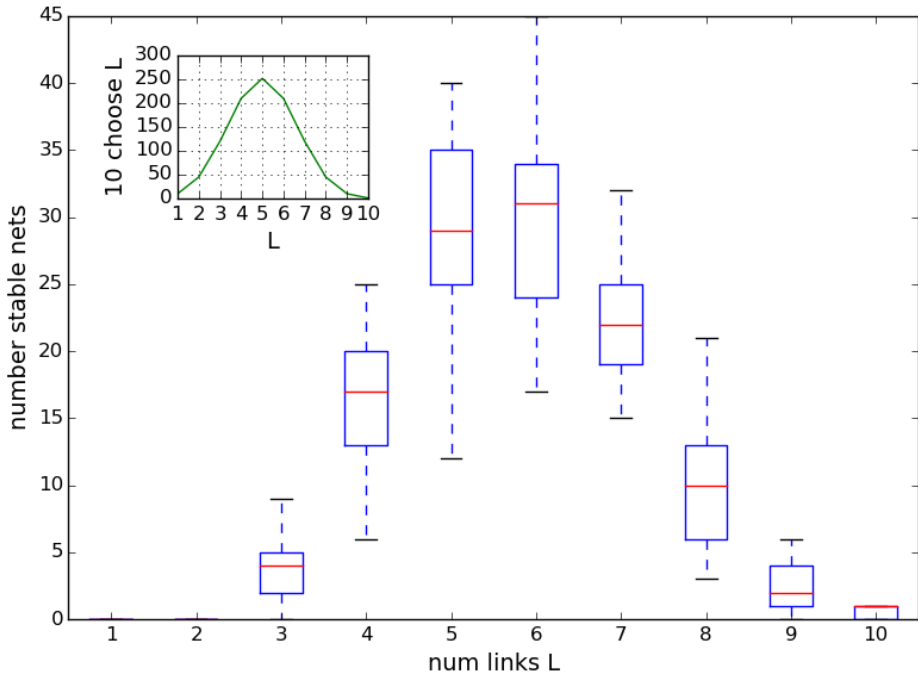


Figure 6.39: **The number of stable 5 species topologies** with L inter-specific interactions, when fitted to 25 replicate IBM simulations at **high IR**. The IBM simulations use topology M1 (figure 6.37), which has $L=4$. The inset shows the total number of possible networks with L links, all were tested. Stability is defined as the local stability of the equilibrium of the fitted model.

topology, while M1 is the true topology as discussed. The other models are selected as plausible alternatives to M1. In particular, the models M2-4 represent the true topology with the addition of one or two links between species in the same trophic level. These additions are plausible given the evidence of competition for space that we have seen previously (chapter 4). As such we may expect these additional interactions to represent competitions (see section 6.4.6).

Given the large number of possible topologies we first study the stability properties of all the potential competing models. Figure 6.39 summarises how many stable models exist at each value of L , for all 25 repeat simulations. Stability is again defined by the Jacobian of the fitted models. The number of stable models varies with L in a manner that approximately matches the total number of possible models (shown as an inset in the figure). However the most possible models exist at $L = 5$, whereas the greatest number of stable models exist at $L = 6$. The true model M1 contains four links. At this value of L there are $\binom{10}{4} = 210$ possible models, of which only between 5 and 25 are dynamically stable. This raises the question as to whether M1 belongs to the stable set of models with $L = 4$. Figure 6.40 shows the frequency with which each model M0-6 is stable over the 25 replicates. We see that M1 is stable in all 25 cases, as are M2, M3 and M4. The latter models represent M1 with addition of either one or two links between species in the same trophic level (plant-plant, herbivore-herbivore, or both). We discuss the frequent stability of these three

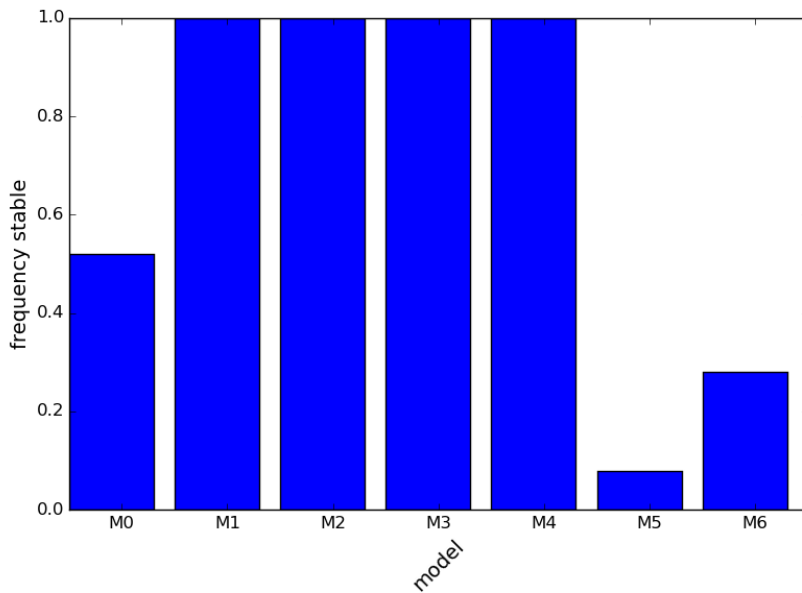


Figure 6.40: **The frequency with which each model (M0-6) is stable** when fitted to 5 species dynamics at **high IR** (25 replicate simulations). Stability is defined as the local stability of the equilibrium of the fitted model. The models M0-6 are shown in figure 6.37.

models further in section 6.5. Model M0 is stable in around half of the simulations, while models M5 and M6 are rarely stable. Therefore it appears that focus on dynamics stability can indeed reduce the search space for identification of the correct topology, especially if the number of links in the true network is known.

Figure 6.41 summarise the relative errors in the demographic rate predictions for the seven models M0-6, and an additional two models. These models, M7 and M8, are selected on a case by case basis from the set of stable models with $L=4$ and $L=5$ respectively. The models are selected such that the maximum relative error in any rate prediction is minimised. Therefore the topology of these models can vary between simulations. From the figure we observe that, on aggregate, the predictions of M1, M3 and M5 are of comparable quality. The models M6-8 perform better, but only slightly. All models have a median maximum relative error (bottom panel) that is approximately equal to or greater than one. Therefore none of the models give accurate rate predictions for all species. We acknowledge that some information is lost by the use of the maximum relative error metric. For example a model may produce very accurate predictions in all but one of the rates. Additionally we note that the use of greater L values increases the number degrees of freedom, and therefore is likely to improve fit of the constrained GLV. Therefore further analysis should employ more sophisticated techniques for model comparison, such as the *Akaike information criterion* (AIC) [?], or *Approximate Bayesian Computation* (ABC) [?]. In general we conclude that the true model (M1) performs favourably compared to competing alternative models in terms of stability and rate predictions. However no consistent criteria for the selection of the correct

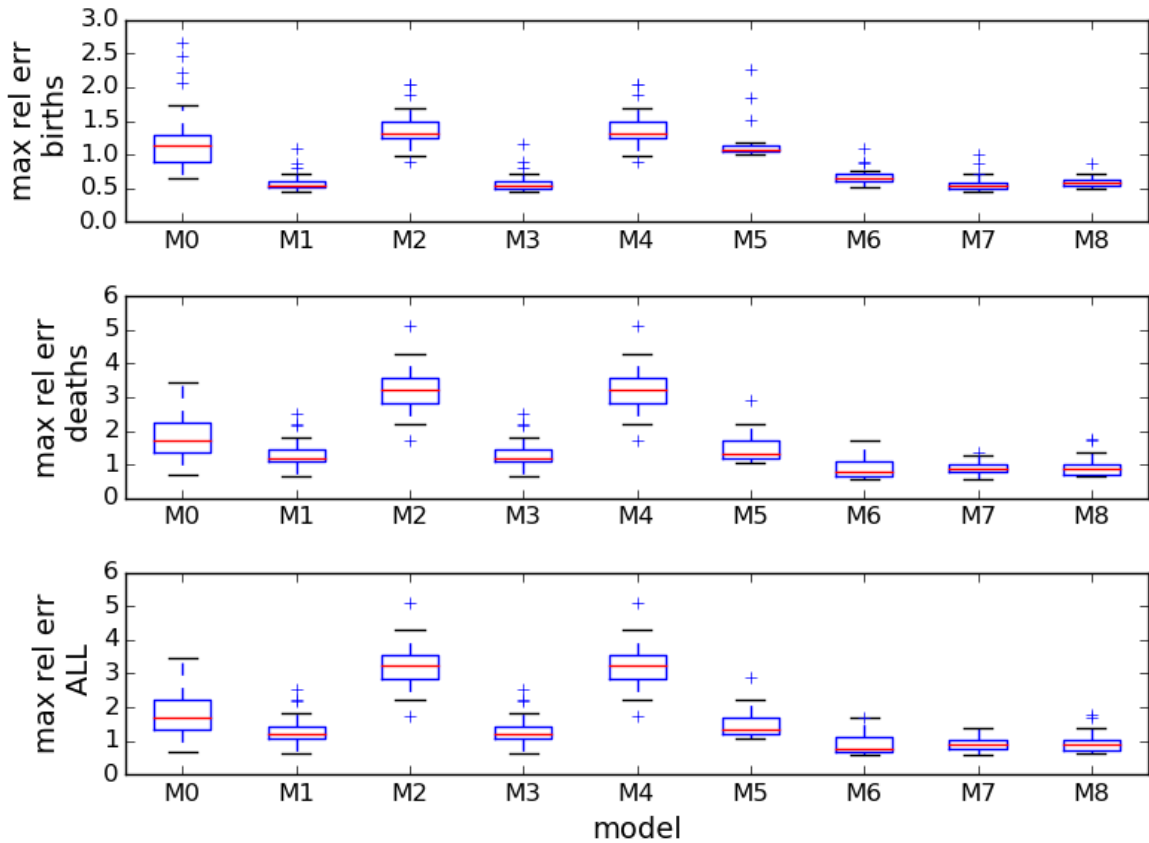


Figure 6.41: **Relative errors in the demographic rate predictions** of the models M0-6 (figure 6.37), plus two additional models: M7 and M8. M7 is selected as the model in the set of stable models with four links ($L=4$) that has the lowest relative error. M8 is the same but for $L=5$. As such the topologies of M7 and M8 are not fixed. The errors shown are the maximum relative error in the predicted births (top row) and predicted deaths (middle row) for each simulations, and the maximum relative error in all rate predictions (bottom row). Relative error is defined in equation (6.4.3), and example rate predictions for three species are illustrated in figure 6.31.

network topology have been identified.

6.4.6 Inferred topologies

We now explicitly consider the accuracy of the inferred topologies when fitting the full (unconstrained) GLV model to data generated by the IBM model. That is, we ask whether the inferred interaction strengths correctly identify which species are interacting and how they are interacting. Here we plot the inferred topologies, and compare them to the true interaction networks used in the IBM simulations. We analyse a 5 species system, and 60 species systems with and without mutualism. In the case of 60 species the complexity of the problem is reduced by aggregating the population dynamics. The time series for all species belonging to each functional group are summed. As such the 60 species system without mutualism produces four groups: one for each trophic level. The 60 species system with mutualism produces six groups: two in the lowest two trophic levels, and one in the top two levels. The GLV model is then fitted by treating each of the groups as a single *species*. In all the results presented the GLV is fitted to a sample of 1000 time steps, selected as before by scanning the time series for the region which produces the lowest error function value. We perform $K = 25$ replicate simulations for each system and take the average value of the estimated interaction strengths $\langle \hat{J}_{ij} \rangle = \sum_{k=1}^{25} \hat{J}_{ijk} \quad \forall i, j$.

Figure 6.42 shows the results for the same 5 species system studied in section 6.4.5, which was simulated here with $IR = 0.001$. Panel A shows the interaction network used for the simulations, while panel B shows the average inferred topology obtained by the GLV fits. An inferred trophic link from species i to species j is identified as one for which $\hat{J}_{ij} < 0$ and $\hat{J}_{ji} > 0$. Such links are plotted in black, with the thick end of the line indicating the consumer. Competitive links are those for which both $\hat{J}_{ij} < 0$ and $\hat{J}_{ji} < 0$. Such links are plotted in red. All links are weighted by the logarithm of the average interaction strength, multiplied by a scaling factor: $\ln(\gamma \times (\hat{J}_{ij} + \hat{J}_{ji})/2)$. Comparing panels A and B we see that the trophic links which *are present* in the system, are correctly identified by the GLV fit (0-1, 2-3, 1-4, 3-4). Additionally the GLV identifies competitive interactions between the pair of plant species (0-2), and between the two herbivore species (1-3). Since we have previously seen evidence of competition for space in the IBM (chapter 4), we may be confident that these inferred competitive interactions are meaningful. However the method also identifies four spurious interactions. Namely the plants are seen to consume all three non-basal species. Two of these links are weak (0-3, 1-2), but the other two are relatively strong (0-4, 2-4). We conclude that the method works well in this case, on average, other than the two strong trophic links from top-predator to the basal species. We return to this feature in section 6.4.7.

Figure 6.43 shows results for a 60 species system without mutualism ($MAI = 0$). Again 25 replicate simulations were run, this time using the *default parameter values*. These values were used to deliberately ensure a significant amount of noise was present in the simulations, resulting from the high immigration rate ($IR = 0.005$). The nodes here represent the four functional groups: plants, herbivores, primary predators, and top predators. Panel A indicate the true interactions

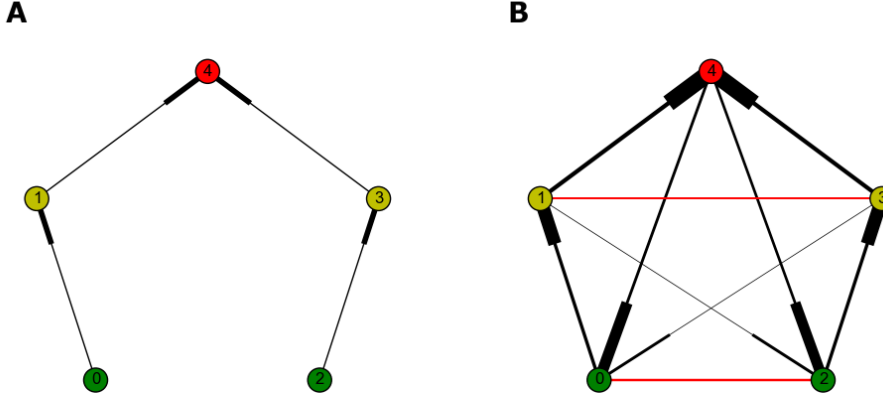


Figure 6.42: Five species system at high IR (0.001). Panel A: The topology of the interaction network used for simulations. The links displayed are all of equal weight, since we do not specify interaction strengths prior to simulation, only the topology. Panel B: The average inferred topology over 25 replicate simulations. For each simulation the full GLV model is fitted to the optimum region of 1000 time steps (see text). We take the average value of each element of the inferred interaction matrix \hat{J} , over the 25 replicates. The links are coloured by the type of inferred interaction. If $\hat{J}_{ij} < 0$ and $\hat{J}_{ji} > 0$ this indicates a trophic link from resource i to consumer j , plotted in black with the thick end towards the consumer. If both $\hat{J}_{ij} < 0$ and $\hat{J}_{ji} < 0$ the link is competitive and plotted in red. If both $\hat{J}_{ij} > 0$ and $\hat{J}_{ji} > 0$ the link is mutualistic and plotted in blue. All links are weighted by the average interaction strength: $(\hat{J}_{ij} + \hat{J}_{ji})/2$.

structure, and we see that here top predators can feed on plants (as in chapter 3). Panel B shows the average inferred network. We see that all trophic links are correctly identified, except for the link between herbivores and primary-predators (1-4). This link is inferred as competitive, which may be a reasonable inference to make. Not all primary-predators consume herbivores, and not only do these two groups compete for space, but some species within these groups also compete for resources. Figure 6.44 shows results for the same 60 species system (MAI=0), but this time with the links between basal and top-predator species removed (as in chapter 5). Again all trophic interactions are inferred correctly. The removed link (0-5) is identified as competitive, although it is weaker than the trophic links. There is no reason to think that basal species compete with top-predators. Therefore we conclude that this link is spurious.

Figure 6.45 shows results for a 60 species system with mutualism (MAI=0.5). By including mutualism the number of functional groups is increased from four to six. In the bottom trophic level there are non-mutualistic (0) and mutualistic (2) plants. In the second trophic level there are herbivores (1) and mutualistic-animals (3). The green link in panel A indicates the mutualism

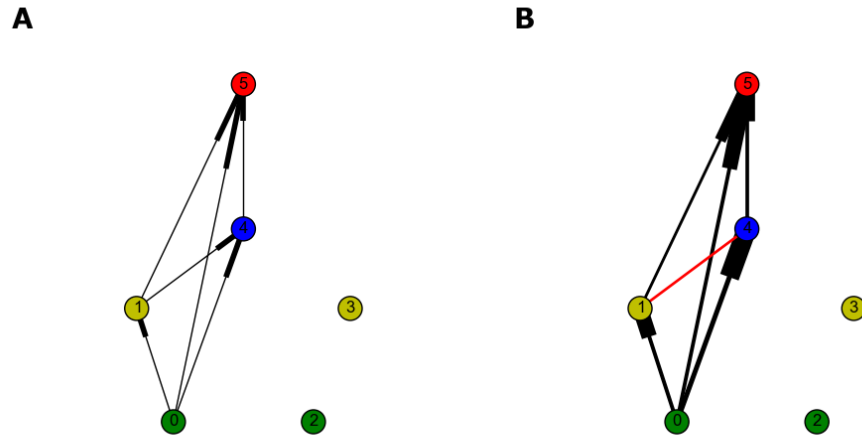


Figure 6.43: Similar to figure 6.42, but for **60 species with MAI=0**. IR= 0.005. Here each node represents a functional group. 0: Non-mutualistic plants. 1: Mutualistic plants. 2: Herbivores. 3: Mutualistic-animals. 4: Primary predators. 5: Top predators. Trophic links in black, competitive links in red, mutualistic links in blue.

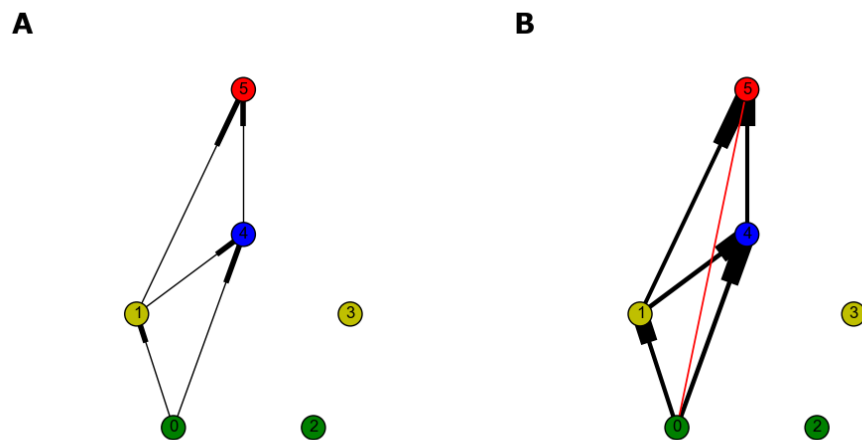


Figure 6.44: Similar to figure 6.43, but for **60 species at MAI=0, without links between basal species and top-predators**.

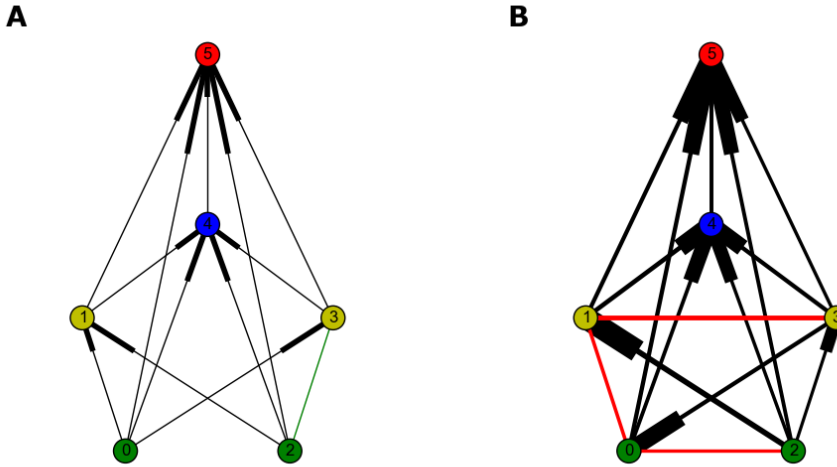


Figure 6.45: Similar to figure 6.43, but for **60 species at MAI=0.5**.

between groups 2 and 3. From panel B we see that the feeding relationships of the top two trophic levels (groups 4 and 5) are inferred correctly. However there is some confusion at the base of the food web. Specifically the plant-herbivore interaction (0-1) is inferred as competitive, and the non-mutualistic plants are inferred to consume the mutualistic animals. The mutualistic interaction (2-3) is identified as a trophic link, rather than a mutualism. However, this is not necessarily wrong since energy does flow along this pathway. As with the five species system, the method identifies competition between groups in the same trophic level (0-2 and 1-3). Figure 6.46 shows results for the same 60 species system, but with the links between basal and top-predator species removed. This removal significantly affects the results, and numerous spurious interactions are identified. In particular, all but one of the inferred top-predator interactions are incorrect. The method does detect a strong signal of mutualism between groups 2 and 3. However, given the high level of error overall, this is not particularly encouraging.

6.4.7 Phase space analysis

One feature of the inference method, emerging from the analysis of systems with more than two species, is its tendency to detect spurious types of interaction between plant and predator species. In the three species case the estimated model parameters suggested that the predator was being eaten by the plant (figure 6.29). In the five species case the same phenomenon was observed (figure 6.42), and in the 60 species systems with mutualism the plants appeared to consume the mutualistic-animals (figures 6.45 and 6.46). In this section we propose an explanation for why the inference method produces these spurious results.

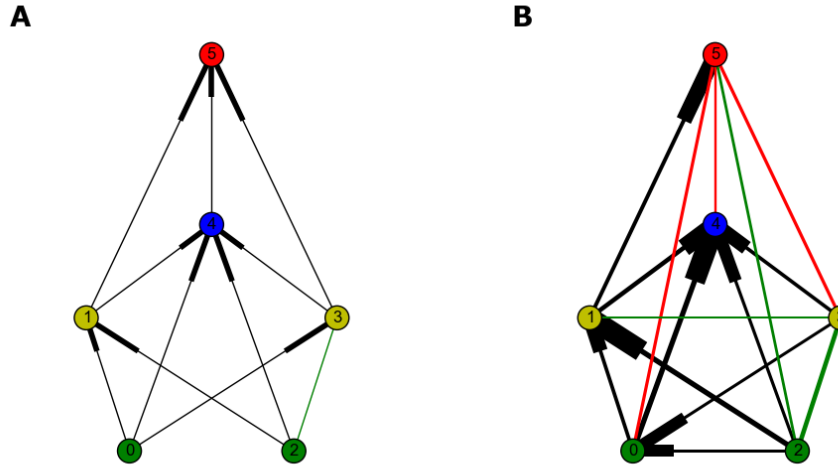


Figure 6.46: Similar to figure 6.43, but for **60 species at MAI=0.5, without links between basal species and top-predators.**

A robust feature of predator-prey dynamics, such as those modelled by the GLV, is that the oscillations of the predator population lag behind those of the prey population. This phase lag results in trajectories with anti-clockwise rotation in the phase plane, when the prey population is plotted on the x-axis, and the predator on the y-axis. This feature has been used previously in attempts to infer predation interactions. For example Sandvik et al. [113] developed a method to quantify the direction and extent of this rotation, in order to detect signatures of predation from empirical population dynamics. However in certain situations the phase relationship may be reversed. For example Gilpin showed that certain sections of the famous Hudson Bay hare-lynx time series display clockwise rotation in the phase-plane. This led to the playful title of his publication: ‘*Do hares eat lynx?*’ [112]. Various models have managed to produce predator-prey dynamics that display such clockwise rotation, for example by including *time-delay* [?], or rapid evolution [?]. However it could be that the clockwise rotation results from other factors. The hare-lynx system is embedded in a larger food web [?]. It may be that trophic interactions with other species are enough to disrupt the usually robust anti-clockwise rotation. Alternatively the dynamics may be disrupted by environmental forcing, which Mutshida et al. [116] suggest has a stronger effect on population dynamics than trophic interactions in natural systems.

In figure 6.47 we employ a simplified version of Sandvik’s method [113] to study the dynamics of the 3 species IBM in the phase plane. We use the portion of low IR dynamics from panel A of figure 6.30 that was used to fit the GLV model in that case (region plotted in black). The dynamics is standardised by subtracting the mean, and dividing each species population time series by its standard deviation. As such the trajectories are centred on the origin when projected in each

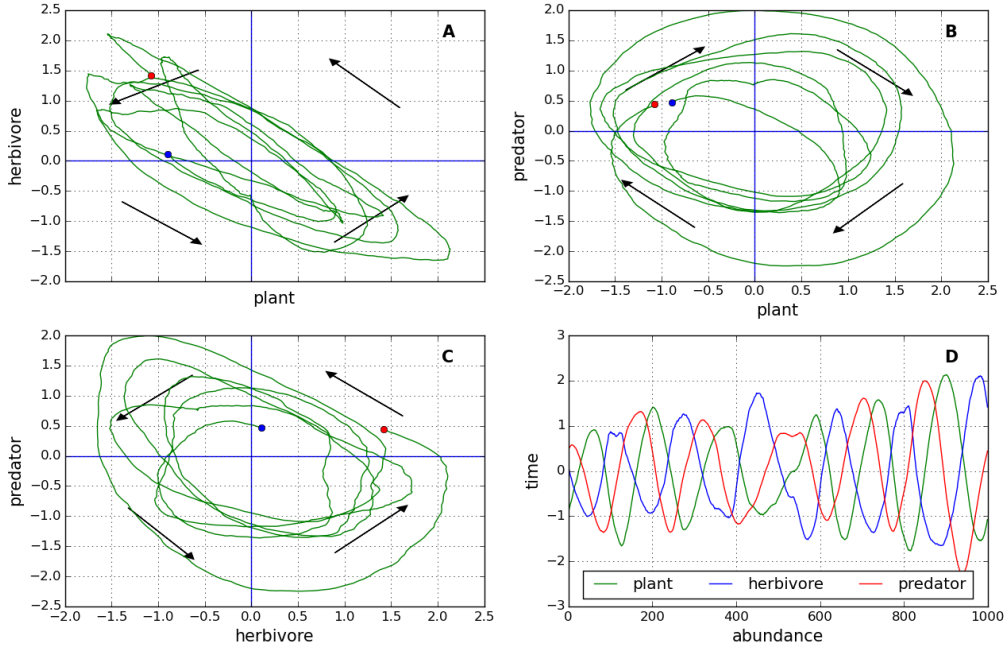


Figure 6.47: Phase plane projections of 3 species food chain dynamics of the IBM model. Anti-clockwise rotation in the phase plane is characteristic of the species on the x-axis being the prey. Dynamics are standardised as described in the text. Panels A-C: projections onto phase plane defined by the three pairs of species. Arrows indicate average direction of trajectories in each quadrant. Blue and red circles show begging and end of trajectories respectively. Panel D: The standardised three species dynamics. This is the same dynamics as the black region in panel A of figure 6.30 (i.e. low IR).

phase-plane. The average direction of the trajectories in each quadrant are then calculated. The figure reveals anti-clockwise rotation in the plant-herbivore (panel A) and herbivore-predator (panel C) phase plane. As discussed these rotations are the standard characteristic of the trophic interactions involved between these two pairs of species. However the plant-predator phase plane (panel B) displays clockwise rotation, which is characteristic of the plant eating the predator. We suggest that such phase relationships are the cause of the spurious links detected by the GLV fit. It may be that the robust phase relationship between plant and predator is the result of some underlying feature of the IBM dynamics, which the GLV does not model (for example time delay). Alternatively it may simply be the result of the incremental phase lags produced by the two interactions depicted in panels A and C. In either case this result represents a simple proof that reliance on phase relationships for the detection of species interactions in multi-trophic communities is unwise. The implications of this result for our inference method are discussed

further in the next section (6.5).

6.5 Discussion

In this section we summarise the main results of the chapter, and discuss the successes and limitations of the methodology. For two species systems the methodology works well, for data generated with both the ODE and IBM models (sections 6.3 and 6.4.3). The GLV fit is able to identify which species is the prey and which is the predator, and recovers the interaction strengths with a high level of accuracy in the presence of noise. The method was seen to provide reasonable estimates of the average interaction strengths, derived from simulations using a non-linear functional response (section 6.3.6). The extent of the non-linearity in the FR was found to be a source of error, with the GLV better able to approximate dynamics that were generated with an FR that was close to linearity. However, noise appeared to be a greater source of error than non-linearity in the FR, at least for the parameter values investigated. Multiplicative noise of sufficient magnitude was found to induce systematic errors in the estimates of interaction strength, even when long samples were used for inference (section 6.3.5 and 6.3.6). It was demonstrated that the mean estimates of interaction strength converged with sample length. In the presence of noise a sample length on the order of 1000 was required in order to produce convergence. Therefore high resolution time series would be required for empirical application of the method (see section 6.6). In the absence of noise we demonstrated that *range sampling* could not only identify non-linearity in the FR, but accurately characterise the interaction strength functions for both species. However this result was highly sensitive to noise.

The species intrinsic and interaction functions emerging from the IBM simulations were determined experimentally (section 6.4.2). Their forms suggested that the IBM dynamics may be well approximated by the GLV model. The sigmoidal forms of the intrinsic growth and mortality functions were taken as evidence of density dependence (intra-specific interactions). In fitting the GLV to two species IBM dynamics we saw further evidence of this density dependence. The inclusion of intra-specific interactions in the model fit improved the prediction of demographic rates given by the fitted model (section 6.4.3). The inclusion of intra-specific interactions was also found to stabilise the equilibrium of the fitted model, to the extent that a comparison between the IBM *data stream* and the deterministic fitted dynamics was not useful in assessing the quality of the fit (figure 6.23). Instead we decided to use a metric to assess the quality of the estimated GLV parameters, based on the accuracy of the demographic rate (birth/death) predictions they produced.

The inference method was then tested on three species food chain dynamics, simulated using the IBM (section 6.4.4). The GLV model was fitted to the dynamics with different constraints on the topology. It was shown that the fit using the correct topology (M1) produced statistically better demographic rate predictions than the other fits (including the unconstrained GLV fit).

However, without prior knowledge of the system, there was no way to guarantee identification of the correct network topology. The correct model fit (M1) did not show significantly lower values in the error functions, or in the errors of the equilibrium populations, compared to the competing models (M0,M2,M3). The correct fitted model was linearly stable with the highest frequency, suggesting that stability considerations may present a way forwards in topology identification.

The complexity of the problem was increased when fitting to five species dynamics because there exist a large number of potential topologies, which represent competing models (section 6.4.5). The correct topology (M1) was found to produce a model fit that was linearly stable for all replicates. Additionally the topologies (M2-4), which included links between species of the same trophic level, were stable for all replicates. These links were included to account for possible competitive interactions between such species. However, there were always a number of competing models, with incorrect topologies, that were stable. It was not possible to reliably distinguish the correct topology from the set of stable models. Furthermore, there was always a stable model which gave rate predictions that were at least as accurate as those of the correct model, if not better. In general then, the inference method applied to the five species system is not successful.

Since we were not able to reliably identify the correct topology for three and five species systems, we studied the average inferred topologies when the full (unconstrained) GLV was fitted (section 6.4.6). For the five species system most interactions were inferred correctly, with trophic interactions between all predator-prey pairs and competitive interactions between species in the same trophic level. However the method detected a strong signal that the plant species consume the top-predator (something that was also seen in the three species case). This represents a significant problem with the methodology, since no such interaction is present in the IBM. In section 6.4.7 we demonstrated that the detection of such spurious links may result from pairwise phase relationships between non-interacting species, that emerge as a result of other interactions. The results for 60 species systems appear to support this conclusion (section 6.4.6). The inference method performed better (in terms of the inferred topology) when direct interactions were included between basal and top-predator species. This difference was especially visible for the mutualistic 60 species systems. We propose that spurious phase relationships are more likely to emerge when the dynamics of pairs of species are not constrained by the presence of a direct trophic link.

The tendency to detect spurious interactions is a major limitation of the inference method. It is not clear to what extent this limitation results from either the model fitting method, or from the use of the GLV model itself. There may be some issues with the ability of the GLV to approximate the dynamics of the IBM. In section 6.4.2 we saw some evidence of a time delay in the response of the herbivore population. Additionally, there is some level of delay built into the mechanism for mutualistic interaction. (After a mutualistic interaction, the animal moves away from the plant for some distance before producing the offspring.) Such time delays are

not included in the GLV model, and therefore may represent a source of error in the inference. The GLV also does not model immigration. Instead we have treated immigration as a source of noise, although as we saw it represents a type of noise that violates the postulate of parenthood, unlike the multiplicative noise modelled in section 6.3. It may be possible to include a term in the GLV that models immigration directly, and that this would improve the performance of the method. However, neither of these possible issues with the GLV appear to address the main concern: that plants seem to eat predators. We argue that this may be an issue with the model fitting method. The GLV model is fitted by optimising the parameters to minimise the error in instantaneous rates of change (section 6.2.3). An alternative approach would be to optimise the parameters via repeated simulation of the GLV. One such method has been used by Jost and Arditi [122] to fit ODE models to two species dynamics. Although such numerical optimisation is more computationally expensive (especially for larger systems), it would be informative to investigate if it can improve the inference of species interactions.

6.6 Further work

In this section we consider further developments of the methodology, and the scope for application to empirical data. In terms of the analysis, there may be other methods to compare the quality of inferred parameters between competing models. In section 6.4 we used the mean relative error in demographic rate predictions for this purpose. However it would be informative to employ a statistical procedure for model selection, such as the Akaike information criterion (AIC). Such a method may tell us more about the quality of inferred parameters, and provide improved ability to distinguish the correct interaction topology. In terms of the inference method itself, it may be possible to improve the results by using it with complementary techniques. In the context of inferring gene regulatory networks (see section 1.5), Marbach et al. [109] have shown that no single inference method (out of 30 tested) performs optimally in all cases. They suggest that the best practice is to use complementary methods for network detection to allow cross-validation. We propose that the same may be true for inferring species interactions. Therefore a fruitful direction for future work may be the integration of several currently available methods (see section 1.5). For example a method by Harris [111] uses spatial co-occurrence data to determine which direct and indirect interactions are likely to be present. Such a method could be used to constrain the topology prior to fitting the GLV. The IBM model would be well suited to conduct future studies of this type.

The ultimate goal of the research in this chapter is application to empirical population dynamics data. Our investigation has made certain simplifying assumptions that would need to be addressed prior to this application. We have neglected seasonality and environmental forcing. However, these factors play a significant role in driving real-world population dynamics [116]. The IBM model currently neglects further features of the real-world, such as spatial heterogeneity

and prey-handling times (which induce non-linear FRs). In general, the IBM model could be extended to include some of these features, perhaps with application to a specific study system in mind. Candidate empirical systems include the plankton food webs of Lake Constance [?] and Helgoland [?]. High resolution long-term time series data is available for both these systems. Knowledge about the structure of these food webs is speculative at best, because of the near impossibility of directly observing the interactions in the wild. Therefore, methods for inferring species interactions have potential to advance our knowledge about such systems. A focused empirical application would guide future development of the methodology. For example, nutrient limitation is a well known feature in plankton dynamics, and would therefore need to be included in the modelling.

In some ways the use of the method presented [in](#) this chapter represents a naive treatment of the subject. We assumed no *a priori* knowledge about the *data generator* that produced the dynamics. In empirical applications the ecologist would have access to some information about the system. Therefore, the results could be improved by taking an informed approach to inferring species interactions. In the example of a marine plankton community, it may not be clear which species are interacting, but approximate species roles (e.g. autotroph versus heterotroph), and trophic positions, may be known. Therefore, some constraints could be placed on the GLV fit. Additionally the results of the inference method can be compared with previous knowledge, in order to determine plausibility. For example, we have seen that there are often only a small number of stable competing topologies (for five species). Therefore a reasoned comparison of these topologies may reveal which one is most likely to be correct. Furthermore, we have seen that, in some cases, the GLV fit was able to produce reasonable predictions of demographic rates. In empirical application, it would be possible to predict the biomass flows through the food web, and compare these predictions to prior knowledge about biomass flows in marine systems.

CHAPTER



CONCLUSION

All results have been previously summarised and discussed in detail in the conclusions of the individual chapters. Particularly, sections 5.7 and 6.5 provide discussions of the results regarding habitat loss, and the inference of species interactions respectively. In this chapter we reiterate the main findings from each of the research chapters (sections 7.1 - 7.4), before summarising the main avenues for further work that have been revealed throughout the thesis (section 7.5).

7.1 Habitat loss with high immigration rate

In [this chapter 3](#) we discovered that the default immigration rate ($IR = 0.005$) was sufficiently high as to prevent the local extinction of species, even in landscapes where 90% of the cells were destroyed. This feature allowed us to study changes in simulated communities in the absence of extinctions. Empirical studies have indicated that habitat loss can cause structural changes to communities without the loss of species [11, 14, 16]. The results of this chapter are a relevant contribution towards understanding those structural changes.

Communities responded differently to the two types of habitat loss: random and contiguous. Random HL reduced the temporal variability in species population dynamics, and reduced the average strength of species interactions. Random HL also increased the evenness in species abundance distributions, with associated changes in network properties, and made communities less aggregated in space. All of these changes, it was argued, could be understood as resulting from an increased dependence of communities on immigration. The random distribution of destroyed cells throughout the landscape provided a barrier to the motion of individuals, meaning that it was harder to 1) find food, and 2) find a mate. As a result, immigration became the dominant source of new individuals in the landscape.

In contrast, contiguous HL increased the temporal variability in species population dynamics, due to an increase in species interaction strengths. The increased probability of interaction resulted from the confinement of individuals, with the same level of mobility, into smaller contiguous regions of habitat. Since trophic interactions remained strong, immigration did not come to dominate these communities. The structure of communities under contiguous HL, including network properties, was mainly unchanged.

An unrealistic feature of the IBM emerged from the results presented in this chapter. In section 3.4 it was observed that mutualists which lack interaction partners, although unable to reproduce, benefit by losing less energy to the interaction. In reality the energy investment involved in becoming a mutualist occurs regardless of any interaction. For example, a flowering plant produces fruit whether or not there are seed-dispersers to consume it. We propose there should be a minor amendment to the way that mutualism is modelled in future work, although we would not expect a significant departure from the results presented.

7.2 Community dynamics under variable immigration rate

Having established, in chapter 3, the importance of immigration in mediating community responses to HL, we then studied community *dynamics* under different immigration rates. This chapter focused on the effect of changing the immigration rate in the absence of habitat loss. We saw that, without any immigration ($IR = 0.0$), many species go extinct when all other parameters take the default values. For antagonistic communities all non-basal species went extinct, while mutualistic communities displayed persistence of a few non-basal species (facilitated by the mutualism). Parameter adjustment was able to slightly improve species persistence, but in general communities were unstable without immigration. We concluded that competition between species in the IBM was strong, and partly responsible for the extinctions. Such an effect is not surprising given the simplified homogeneous landscape of the IBM. It is well known that landscape heterogeneity can reduce competition between species with differential traits, and promote coexistence [? ?]. We note here, that it would be possible to conduct a more sophisticated exploration of the parameter space, using *boosted regression trees* [?] to determine the relative contributions of each parameter towards improving persistence. Significantly, it emerged from the analysis in this sectionIt appears that immigration reduces the effects of competition, and is a requirement for the IBM to produce persistent diversity. It is possible that the introduction of landscape heterogeneity would reduce this dependence on the immigration mechanism.

Reducing the immigration rate was found to increase temporal variability in population dynamics, resulting in more species with non-stationary long term distributions. Employing recurrence quantification analysis, we determined that reducing the immigration rate increased the signature of determinism in the population dynamics. In general, high abundance species were found to have dynamics that was less stationary and more deterministic, while low abundance

species were more stationary and less deterministic. Taken together, these results developed a picture of the relative contributions of species interactions and immigration to the dynamics. Immigration represents a random mechanism, but one that suppresses temporal variability. Whilst species interactions contribute to high temporal variability via deterministic non-stationary fluctuations.

At the end of this chapter we considered the effect that high temporal variability has on the accuracy of our results. We compared species abundance measurements, calculated from samples of increasing length. It was determined that short samples produced significant errors when temporal variability was high, but that infeasibly long samples ($> 40,000$ time steps) were required in order to guarantee convergence on the long term average. This poor convergence is likely due to non-stationarity, as previously discussed, and highlights the need for a trade-off between accuracy and computational expense when sampling from the IBM simulations. In this chapter we also demonstrated a high level of repeatability between simulations, when using the same network structure.

7.3 Habitat loss under variable immigration rate

In chapter 5 we returned to study the effects of habitat loss, this time under different immigration rates. The same two types of habitat loss were used: random and contiguous. Community responses were largely consistent with those observed at high IR in chapter 3. In particular, contiguous HL increased interaction strengths, resulting in more variable dynamics. The converse was observed for random HL. These results held across most of the region of parameter space explored, but not at some extreme values of IR and HL.

Certain new results were observed as the immigration rate was changed. Most notably, at lower immigration rates species extinctions were observed. Here we saw more extinctions under contiguous HL than random HL, and more extinctions in mutualistic communities than antagonistic ones. These differences were unexpected. Previous modelling studies suggested that random HL should produce more extinctions (see section 1.3.1), and prior intuition suggested that mutualism may confer some benefit on the wider community that would mitigate extinctions. Contiguous HL resulted in more extinctions because of strong trophic interactions and highly variable dynamics. Mutualistic communities displayed more extinctions because mutualism acts to make communities uneven, with a dominant core of species out-competing the others. The observed effects of mutualism, and contiguous HL on species extinctions find some support from empirical studies (see section 5.7). Further field work is required to determine the role of species interaction strengths in these cases.

The total number of individuals in communities with high levels of mutualism was insensitive to changes in IR. However, as IR was reduced, such communities became less *even* as the mutualistic core became more dominant. Therefore we see that, in the IBM, immigration serves

to reduce the damaging effects of mutualism on the wider community. In general, we observed a subtle interplay between immigration rate, mutualism and habitat loss, in determining community evenness. For example, at $IR = 0.0005$, antagonistic communities tended to become less even under random HL, while mutualistic communities became more even. Different changes in evenness were observed at different immigrations rates, but not studied in detail.

7.4 Towards inferring species interactions from population dynamics

In chapter 6 we developed a novel method for inferring species interactions from population dynamics. The method was adapted from [118]. The task was explained as the *inverse* of the research undertaken in the previous chapters, where we modelled low level mechanics and studied the high level properties that emerged. In this chapter we attempted to work back from the high level properties to recover the underlying structure of the system. The approach was met with limited success. Accurate inference of interaction strengths was possible for two species systems. For three and five species systems, the method produced reasonable predictions of demographic rates, but it was not possible to reliably infer the correct interaction topology. The method was hampered by a sensitivity to emergent phase relationships between non-interacting pairs of species, resulting in the identification of spurious interactions. The application of the method to infer interactions between functional groups of species in larger systems showed some promise. However further development of the method is required.

7.5 Further work

The results from the habitat loss simulations represent an important contribution to the field. However, given the complexity of the IBM model, it will be necessary to undertake a sensitivity analysis prior to publication. Specifically, we propose the use of *latin hypercube sampling* [?] to determine the sensitivity of the main results presented in this thesis to variations in parameter values. Such an analysis would ensure that the conclusions presented are robust. Furthermore, much of the analysis in this thesis rests on conceptual arguments and qualitative interpretations of the results. Although we are confident in the conclusions reached, we suggest that further statistical analysis would improve the weight of these conclusions. One potential approach would be to use *structural equation modelling* (SEM) to quantify the pathways of influence that drive changes in community properties. SEM is a type of graphical modelling the allows the user to quantify correlations between multiple variables that are connected by a hypothesised causal structure. Significant correlations indicate support for the hypothesis of causality. This type of analysis is becoming increasingly popular in the biological sciences, where it is often necessary to determine the relationships between multiple interconnected variables [??]. We propose that

this approach could be used in the future to test our conclusions regarding community responses to habitat loss (and to changes in other variables such as MAI and IR).

Any theoretical results regarding community dynamics and structure require empirical confirmation. With this in mind, it is worth considering the ways in which the modelling assumptions of the IBM may produce different results from those observed in natural communities. The relevant features of the model that represent simplifications of reality include: the simplicity of the immigration mechanism; the spatial homogeneity of the landscape; the random-walk motion of individuals (which is a constant across all non-basal species); the absence of prey-handling times; the neutrality of species within trophic levels; and the binary nature of habitat loss (cells are either destroyed or pristine, rather than displaying a gradient of degradation). Extension of the IBM to alleviate all of these limitations would greatly increase its complexity. A pragmatic approach would be to develop the modelling framework in conjunction with field studies. It may be possible to identify which limitations are most significant when modelling a specific study system, and to update the model accordingly. A primary candidate for further model development is the immigration mechanism, as discussed in section 5.7.

In chapter 4 we confirmed that network structure does play a role in shaping the simulated communities. Although we have studied changes in network structure in response to habitat loss, we have not explicitly investigated the inverse. It would be informative to determine how certain structural properties directly effect community responses to habitat loss. For example, *itif* would be possible to create networks with high and low modularity, and test for differences in their response to HL. Fortuna and Bascompte [74] have suggested that empirically derived network structures are more robust the HL than randomly assembled networks. It would also be possible to test this hypothesis by using empirical food webs as input to the IBM.

Avenues for further work in the area of inferring species interactions were discussed in section 6.5, including the scope for application to empirical data. Plankton food webs were identified as possible systems to which the methodology could be applied. In any empirical application, the study system will likely comprise of more than five species. The approach taken in section 6.4, when applying the method to 60 species systems, was to aggregate the dynamics by functional group. This aggregation resulted in either four or six *functional species*, depending on the inclusion of mutualism. However, aggregating in this way requires prior knowledge of the functional groups. It also results in loss of information. If the populations of the species within a functional group are not synchronised, then summing their dynamics will result in some cancellation of population variability. Furthermore, there is the problem of diversity of interaction types between any two functional groups. For example, some primary-predator species may feed on herbivores, while others mainly compete with them. Therefore it is unlikely that the use of functional groups is a good way to aggregate the species. We suggest that further work could investigate better methods for aggregation, based on properties of the dynamics alone (i.e. not requiring any prior knowledge). A natural approach would be to use the invariability metric for

synchrony (section 2.8.2). Species that share a high level of synchrony in their dynamics could be grouped, minimising the loss of information in time series summation. Finally, we note that a useful feature of the inference method is its ability to detect competitive interactions (section 6.4.6). Competition is hard to detect empirically because it cannot be observed directly. Further work is required in this area to develop methodologies that can reliably infer species interactions. The investigation in chapter 6 highlights some of the problems that need to be solved.

BIBLIOGRAPHY

- [1] C. Darwin and W. F. Bynum, *The origin of species by means of natural selection: or, the preservation of favored races in the struggle for life.*
AL Burt, 2009.
- [2] M. E. Assessment, *Ecosystems and human well-being: biodiversity synthesis.*
Island Press, 2005.
- [3] J. E. Lovelock and L. Margulis, “Atmospheric homeostasis by and for the biosphere: the gaia hypothesis,” *Tellus*, vol. 26, no. 1-2, pp. 2–10, 1974.
- [4] R. Pachauri and L. Meyer, eds., *Climate Change 2014: Synthesis Report. Contribution of Working Groups I, II and III to the Fifth Assessment Report of the Intergovernmental Panel on Climate Change.*
Geneva, Switzerland: IPCC, 2014.
- [5] A. Staudt, N. Huddleston, and S. Rudenstein, “Understanding and responding to climate change,” *The National Academy of Sciences*, vol. 14, 2007.
- [6] G. Ceballos, P. R. Ehrlich, A. D. Barnosky, A. García, R. M. Pringle, and T. M. Palmer, “Accelerated modern human–induced species losses: Entering the sixth mass extinction,” *Science Advances*, vol. 1, no. 5, p. e1400253, 2015.
- [7] J. A. Foley, R. DeFries, G. P. Asner, C. Barford, G. Bonan, S. R. Carpenter, F. S. Chapin, M. T. Coe, G. C. Daily, H. K. Gibbs, *et al.*, “Global consequences of land use,” *science*, vol. 309, no. 5734, pp. 570–574, 2005.
- [8] T. Newbold, L. N. Hudson, S. L. Hill, S. Contu, I. Lysenko, R. A. Senior, L. Börger, D. J. Bennett, A. Choimes, B. Collen, *et al.*, “Global effects of land use on local terrestrial biodiversity,” *Nature*, vol. 520, no. 7545, pp. 45–50, 2015.
- [9] S. Kéfi, E. L. Berlow, E. A. Wieters, S. A. Navarrete, O. L. Petchey, S. A. Wood, A. Boit, L. N. Joppa, K. D. Lafferty, R. J. Williams, *et al.*, “More than a meal: integrating non-feeding interactions into food webs,” *Ecology letters*, vol. 15, no. 4, pp. 291–300, 2012.

BIBLIOGRAPHY

- [10] C. Fontaine, P. R. Guimarães, S. Kéfi, N. Loeuille, J. Memmott, W. H. Van Der Putten, F. J. Van Veen, and E. Thébaud, “The ecological and evolutionary implications of merging different types of networks,” *Ecology Letters*, vol. 14, no. 11, pp. 1170–1181, 2011.
- [11] J. M. Tylianakis, T. Tscharntke, and O. T. Lewis, “Habitat modification alters the structure of tropical host-parasitoid food webs,” *Nature*, vol. 445, no. 7124, pp. 202–205, 2007.
- [12] R. V. Sole and J. M. Montoya, “Ecological network meltdown from habitat loss and fragmentation,” *Ecological Networks: Linking Structure to Dynamics in Food Webs*, pp. 305–323, 2006.
- [13] E. Laliberté and J. M. Tylianakis, “Deforestation homogenizes tropical parasitoid-host networks,” *Ecology*, vol. 91, no. 6, pp. 1740–1747, 2010.
- [14] M. Albrecht, P. Duelli, B. Schmid, and C. B. Müller, “Interaction diversity within quantified insect food webs in restored and adjacent intensively managed meadows,” *Journal of Animal Ecology*, vol. 76, no. 5, pp. 1015–1025, 2007.
- [15] B. J. Spiesman and B. D. Inouye, “Habitat loss alters the architecture of plant-pollinator interaction networks,” *Ecology*, vol. 94, no. 12, pp. 2688–2696, 2013.
- [16] M. Hagen, W. D. Kissling, C. Rasmussen, D. Carstensen, Y. Dupont, C. Kaiser-Bunbury, E. O’Gorman, J. Olesen, M. De Aguiar, L. Brown, *et al.*, “Biodiversity, species interactions and ecological networks in a fragmented world,” *Advances in Ecological Research*, vol. 46, pp. 89–120, 2012.
- [17] A. Gonzalez, B. Rayfield, and Z. Lindo, “The disentangled bank: how loss of habitat fragments and disassembles ecological networks,” *American Journal of Botany*, vol. 98, no. 3, pp. 503–516, 2011.
- [18] J. Ladyman, J. Lambert, and K. Wiesner, “What is a complex system?,” *European Journal for Philosophy of Science*, vol. 3, no. 1, pp. 33–67, 2013.
- [19] J. P. Crutchfield and K. Young, “Inferring statistical complexity,” *Physical Review Letters*, vol. 63, no. 2, p. 105, 1989.
- [20] C. Norris, *Quantum theory and the flight from realism: Philosophical responses to quantum mechanics*. Routledge, 2002.
- [21] J. G. Sanderson and S. L. Pimm, *Patterns in Nature: The Analysis of Species Co-Occurrences*. University of Chicago Press, 2015.

- [22] D. W. Purves, S. W. Pacala, D. Burslem, M. Pinard, S. Hartley, *et al.*, “Ecological drift in niche-structured communities: neutral pattern does not imply neutral process.,” *Biotic interactions in the tropics: their role in the maintenance of species diversity*, pp. 107–138, 2005.
- [23] S. P. Hubbell, *The unified neutral theory of biodiversity and biogeography (MPB-32)*, vol. 32. Princeton University Press, 2001.
- [24] I. Volkov, J. R. Banavar, S. P. Hubbell, and A. Maritan, “Neutral theory and relative species abundance in ecology,” *Nature*, vol. 424, no. 6952, pp. 1035–1037, 2003.
- [25] P. Staniczenko, M. J. Smith, and S. Allesina, “Selecting food web models using normalized maximum likelihood,” *Methods in Ecology and Evolution*, vol. 5, no. 6, pp. 551–562, 2014.
- [26] N. Blüthgen, J. Fründ, D. P. Vázquez, and F. Menzel, “What do interaction network metrics tell us about specialization and biological traits,” *Ecology*, vol. 89, no. 12, pp. 3387–3399, 2008.
- [27] T. M. Knight, M. W. McCoy, J. M. Chase, K. A. McCoy, and R. D. Holt, “Trophic cascades across ecosystems,” *Nature*, vol. 437, no. 7060, pp. 880–883, 2005.
- [28] W. J. Ripple and R. L. Beschta, “Trophic cascades in yellowstone: The first 15years after wolf reintroduction,” *Biological Conservation*, vol. 145, no. 1, pp. 205–213, 2012.
- [29] K. N. Marshall, D. J. Cooper, and N. T. Hobbs, “Interactions among herbivory, climate, topography and plant age shape riparian willow dynamics in northern yellowstone national park, usa,” *Journal of Ecology*, vol. 102, no. 3, pp. 667–677, 2014.
- [30] R. E. Ricklefs, “Disintegration of the ecological community,” *The American Naturalist*, vol. 172, no. 6, pp. 741–750, 2008.
- [31] R. J. Whittaker, K. J. Willis, and R. Field, “Scale and species richness: towards a general, hierarchical theory of species diversity,” *Journal of Biogeography*, vol. 28, no. 4, pp. 453–470, 2001.
- [32] M. L. Rosenzweig, *Species diversity in space and time*. Cambridge University Press, 1995.
- [33] S. Wang and M. Loreau, “Ecosystem stability in space: α , β and γ variability,” *Ecology letters*, vol. 17, no. 8, pp. 891–901, 2014.
- [34] M. A. Leibold, M. Holyoak, N. Mouquet, P. Amarasekare, J. Chase, M. Hoopes, R. Holt, J. Shurin, R. Law, D. Tilman, *et al.*, “The metacommunity concept: a framework for multi-scale community ecology,” *Ecology letters*, vol. 7, no. 7, pp. 601–613, 2004.

BIBLIOGRAPHY

- [35] J. B. Logue, N. Mouquet, H. Peter, H. Hillebrand, M. W. Group, *et al.*, “Empirical approaches to metacommunities: a review and comparison with theory,” *Trends in ecology & evolution*, vol. 26, no. 9, pp. 482–491, 2011.
- [36] C. Klausmeier, “Habitat destruction and extinction in competitive and mutualistic meta-communities,” *Ecology Letters*, vol. 4, no. 1, pp. 57–63, 2001.
- [37] J. Bascompte, “Networks in ecology,” *Basic and Applied Ecology*, vol. 8, no. 6, pp. 485–490, 2007.
- [38] J. Bascompte and P. Jordano, “Plant-animal mutualistic networks: the architecture of biodiversity,” *Annual Review of Ecology, Evolution, and Systematics*, pp. 567–593, 2007.
- [39] A. J. Vanbergen, M. Baude, J. C. Biesmeijer, N. F. Britton, M. J. Brown, M. Brown, J. Bryden, G. E. Budge, J. C. Bull, C. Carvell, *et al.*, “Threats to an ecosystem service: pressures on pollinators,” *Frontiers in Ecology and the Environment*, vol. 11, pp. 251–259, 2013.
- [40] A. Sauve, C. Fontaine, and E. Thébault, “Structure–stability relationships in networks combining mutualistic and antagonistic interactions,” *Oikos*, vol. 123, no. 3, pp. 378–384, 2014.
- [41] D. M. Evans, M. J. Pocock, and J. Memmott, “The robustness of a network of ecological networks to habitat loss,” *Ecology letters*, vol. 16, no. 7, pp. 844–852, 2013.
- [42] D. Montoya, M. Yallop, and J. Memmott, “Functional group diversity increases with modularity in complex food webs,” *Nature communications*, vol. 6, 2015.
- [43] A. Mougi and M. Kondoh, “Diversity of interaction types and ecological community stability,” *Science*, vol. 337, no. 6092, pp. 349–351, 2012.
- [44] L.-F. Bersier, C. BanasÅåek-Richter, and M.-F. Cattin, “Quantitative descriptors of food-web matrices,” *Ecology*, vol. 83, no. 9, pp. 2394–2407, 2002.
- [45] N. Blüthgen, F. Menzel, and N. Blüthgen, “Measuring specialization in species interaction networks,” *BMC ecology*, vol. 6, no. 1, p. 1, 2006.
- [46] E. L. Berlow, A.-M. Neutel, J. E. Cohen, P. C. De Ruiter, B. Ebenman, M. Emmerson, J. W. Fox, V. A. Jansen, J. Iwan Jones, G. D. Kokkoris, *et al.*, “Interaction strengths in food webs: issues and opportunities,” *Journal of animal ecology*, vol. 73, no. 3, pp. 585–598, 2004.
- [47] M. Devoto, S. Bailey, and J. Memmott, “The ‘night shift’: nocturnal pollen-transport networks in a boreal pine forest,” *Ecological Entomology*, vol. 36, no. 1, pp. 25–35, 2011.
- [48] R. M. May, “Will a large complex system be stable?,” *Nature*, vol. 238, pp. 413–414, 1972.

- [49] K. McCann, A. Hastings, and G. R. Huxel, “Weak trophic interactions and the balance of nature,” *Nature*, vol. 395, no. 6704, pp. 794–798, 1998.
- [50] T. Gross, L. Rudolf, S. A. Levin, and U. Dieckmann, “Generalized models reveal stabilizing factors in food webs,” *Science*, vol. 325, no. 5941, pp. 747–750, 2009.
- [51] E. J. O’Gorman and M. C. Emmerson, “Perturbations to trophic interactions and the stability of complex food webs,” *Proceedings of the National Academy of Sciences*, vol. 106, no. 32, pp. 13393–13398, 2009.
- [52] A. Eklöf and B. Ebenman, “Species loss and secondary extinctions in simple and complex model communities,” *Journal of animal ecology*, vol. 75, no. 1, pp. 239–246, 2006.
- [53] C. N. Kaiser-Bunbury, S. Muff, J. Memmott, C. B. Müller, and A. Caflisch, “The robustness of pollination networks to the loss of species and interactions: a quantitative approach incorporating pollinator behaviour,” *Ecology Letters*, vol. 13, no. 4, pp. 442–452, 2010.
- [54] J. T. Wootton and M. Emmerson, “Measurement of interaction strength in nature,” *Annual Review of Ecology, Evolution, and Systematics*, pp. 419–444, 2005.
- [55] R. M. Thompson, U. Brose, J. A. Dunne, R. O. Hall, S. Hladyz, R. L. Kitching, N. D. Martinez, H. Rantala, T. N. Romanuk, D. B. Stouffer, *et al.*, “Food webs: reconciling the structure and function of biodiversity,” *Trends in ecology & evolution*, vol. 27, no. 12, pp. 689–697, 2012.
- [56] N. Rooney and K. S. McCann, “Integrating food web diversity, structure and stability,” *Trends in ecology & evolution*, vol. 27, no. 1, pp. 40–46, 2012.
- [57] C. Banašek-Richter, M.-F. Cattin, and L.-F. Bersier, “Sampling effects and the robustness of quantitative and qualitative food-web descriptors,” *Journal of Theoretical Biology*, vol. 226, no. 1, pp. 23–32, 2004.
- [58] M. Lurgi, D. Montoya, and J. M. Montoya, “The effects of space and diversity of interaction types on the stability of complex ecological networks,” *Theoretical Ecology*, pp. 1–11, 2015.
- [59] J. Montoya, J. Arnoldi, and M. Loreua, “Resilience, invariability, and ecological stability across levels of organization,” 2016, in press.
- [60] J.-F. Arnoldi, M. Loreau, and B. Haegeman, “Resilience, reactivity and variability: A mathematical comparison of ecological stability measures,” *Journal of theoretical biology*, vol. 389, pp. 47–59, 2016.

BIBLIOGRAPHY

- [61] Y. Wang, T. Joshi, X.-S. Zhang, D. Xu, and L. Chen, “Inferring gene regulatory networks from multiple microarray datasets,” *Bioinformatics*, vol. 22, no. 19, pp. 2413–2420, 2006.
- [62] D. B. Stouffer and J. Bascompte, “Compartmentalization increases food-web persistence,” *Proceedings of the National Academy of Sciences*, vol. 108, no. 9, pp. 3648–3652, 2011.
- [63] E. Thébault and C. Fontaine, “Stability of ecological communities and the architecture of mutualistic and trophic networks,” *Science*, vol. 329, no. 5993, pp. 853–856, 2010.
- [64] C. van Altena, L. Hemerik, and P. C. de Ruiter, “Food web stability and weighted connectance: the complexity-stability debate revisited,” *Theoretical Ecology*, pp. 1–10, 2016.
- [65] V. A. Jansen and G. D. Kokkoris, “Complexity and stability revisited,” *Ecology Letters*, vol. 6, no. 6, pp. 498–502, 2003.
- [66] S. Allesina, “Ecology: the more the merrier,” *Nature*, vol. 487, no. 7406, pp. 175–176, 2012.
- [67] R. V. Solé and J. Bascompte, *Self-Organization in Complex Ecosystems*, vol. 42. Princeton University Press, 2006.
- [68] H. I. Jager, E. A. Carr, and R. A. Efroymson, “Simulated effects of habitat loss and fragmentation on a solitary mustelid predator,” *Ecological Modelling*, vol. 191, no. 3, pp. 416–430, 2006.
- [69] C. Dytham, “The effect of habitat destruction pattern on species persistence: a cellular model,” *Oikos*, pp. 340–344, 1995.
- [70] M. Hill and H. Caswell, “Habitat fragmentation and extinction thresholds on fractal landscapes,” *Ecology Letters*, vol. 2, no. 2, pp. 121–127, 1999.
- [71] J. Travis, “Climate change and habitat destruction: a deadly anthropogenic cocktail,” *Proceedings of the Royal Society of London B: Biological Sciences*, vol. 270, no. 1514, pp. 467–473, 2003.
- [72] K. A. With and A. W. King, “Extinction thresholds for species in fractal landscapes,” *Conservation Biology*, vol. 13, no. 2, pp. 314–326, 1999.
- [73] O. Ovaskainen, K. Sato, J. Bascompte, and I. Hanski, “Metapopulation models for extinction threshold in spatially correlated landscapes,” *Journal of Theoretical Biology*, vol. 215, no. 1, pp. 95–108, 2002.
- [74] M. A. Fortuna and J. Bascompte, “Habitat loss and the structure of plant–animal mutualistic networks,” *Ecology Letters*, vol. 9, no. 3, pp. 281–286, 2006.

- [75] C. J. Melián and J. Bascompte, “Food web structure and habitat loss,” *Ecology Letters*, vol. 5, no. 1, pp. 37–46, 2002.
- [76] A. Dobson, D. Lodge, J. Alder, G. S. Cumming, J. Keymer, J. McGlade, H. Mooney, J. A. Rusak, O. Sala, V. Wolters, *et al.*, “Habitat loss, trophic collapse, and the decline of ecosystem services,” *Ecology*, vol. 87, no. 8, pp. 1915–1924, 2006.
- [77] D. H. Janzen, “The deflowering of central America,” *Nat. Hist.*, vol. 83, pp. 48–53, 1974.
- [78] M. A. Fortuna, A. Krishna, and J. Bascompte, “Habitat loss and the disassembly of mutualistic networks,” *Oikos*, vol. 122, no. 6, pp. 938–942, 2013.
- [79] J. E. Duffy, “Biodiversity loss, trophic skew and ecosystem functioning,” *Ecology Letters*, vol. 6, no. 8, pp. 680–687, 2003.
- [80] D. Raffaelli, “How extinction patterns affect ecosystems,” *Science*, vol. 306, no. 5699, pp. 1141–1142, 2004.
- [81] Y. Gavish, Y. Ziv, and M. L. Rosenzweig, “Decoupling fragmentation from habitat loss for spiders in patchy agricultural landscapes,” *Conservation Biology*, vol. 26, no. 1, pp. 150–159, 2012.
- [82] R. M. Ewers, R. K. Didham, L. Fahrig, G. Ferraz, A. Hector, R. D. Holt, V. Kapos, G. Reynolds, W. Sinun, J. L. Snaddon, *et al.*, “A large-scale forest fragmentation experiment: the stability of altered forest ecosystems project,” *Philosophical Transactions of the Royal Society of London B: Biological Sciences*, vol. 366, no. 1582, pp. 3292–3302, 2011.
- [83] N. M. Haddad, L. A. Brudvig, J. Clobert, K. F. Davies, A. Gonzalez, R. D. Holt, T. E. Lovejoy, J. O. Sexton, M. P. Austin, C. D. Collins, *et al.*, “Habitat fragmentation and its lasting impact on earth’s ecosystems,” *Science Advances*, vol. 1, no. 2, p. e1500052, 2015.
- [84] J. Rybicki and I. Hanski, “Species–area relationships and extinctions caused by habitat loss and fragmentation,” *Ecology letters*, vol. 16, no. s1, pp. 27–38, 2013.
- [85] L. R. Tambosi, A. C. Martensen, M. C. Ribeiro, and J. P. Metzger, “A framework to optimize biodiversity restoration efforts based on habitat amount and landscape connectivity,” *Restoration Ecology*, vol. 22, no. 2, pp. 169–177, 2014.
- [86] J. Fischer and D. B. Lindenmayer, “Landscape modification and habitat fragmentation: a synthesis,” *Global Ecology and Biogeography*, vol. 16, no. 3, pp. 265–280, 2007.
- [87] L.-l. Chen and C. Hui, “Habitat destruction and the extinction debt revisited: The allee effect,” *Mathematical Biosciences*, vol. 221, no. 1, pp. 26–32, 2009.

BIBLIOGRAPHY

- [88] R. M. Ewers and R. K. Didham, “Continuous response functions for quantifying the strength of edge effects,” *Journal of Applied Ecology*, vol. 43, no. 3, pp. 527–536, 2006.
- [89] L. Fahrig, “Effects of habitat fragmentation on biodiversity,” *Annual review of ecology, evolution, and systematics*, pp. 487–515, 2003.
- [90] G. Valladares, A. Salvo, and L. Cagnolo, “Habitat fragmentation effects on trophic processes of insect-plant food webs,” *Conservation Biology*, vol. 20, no. 1, pp. 212–217, 2006.
- [91] R. Kaartinen and T. Roslin, “Shrinking by numbers: landscape context affects the species composition but not the quantitative structure of local food webs,” *Journal of Animal Ecology*, vol. 80, no. 3, pp. 622–631, 2011.
- [92] S. Osorio, X. Arnan, E. Bassols, N. Vicens, and J. Bosch, “Local and landscape effects in a host-parasitoid interaction network along a forest–cropland gradient,” *Ecological Applications*, vol. 25, no. 7, pp. 1869–1879, 2015.
- [93] M. R. Rossetti, E. González, A. Salvo, and G. Valladares, “Not all in the same boat: trends and mechanisms in herbivory responses to forest fragmentation differ among insect guilds,” *Arthropod-Plant Interactions*, vol. 8, no. 6, pp. 593–603, 2014.
- [94] J. Memmott, R. Gibson, L. Carvalheiro, K. Henson, R. Heleno, M. Lopezaraiza, S. Pearce, and S. Pearce, “The conservation of ecological interactions,” *Insect Conservation Biology. The Royal Entomological Society, London*, pp. 226–44, 2007.
- [95] A. Valiente-Banuet, M. A. Aizen, J. M. Alcántara, J. Arroyo, A. Cocucci, M. Galetti, M. B. García, D. García, J. M. Gómez, P. Jordano, *et al.*, “Beyond species loss: the extinction of ecological interactions in a changing world,” *Functional Ecology*, vol. 29, no. 3, pp. 299–307, 2015.
- [96] F. Barraquand, “Functional responses and predator–prey models: a critique of ratio dependence,” *Theoretical ecology*, vol. 7, no. 1, pp. 3–20, 2014.
- [97] O. P. Judson, “The rise of the individual-based model in ecology,” *Trends in Ecology & Evolution*, vol. 9, no. 1, pp. 9–14, 1994.
- [98] V. Grimm and S. F. Railsback, *Individual-based modeling and ecology*. Princeton university press, 2013.
- [99] K. McCann, J. Rasmussen, and J. Umbanhowar, “The dynamics of spatially coupled food webs,” *Ecology Letters*, vol. 8, no. 5, pp. 513–523, 2005.
- [100] U. Brose, R. J. Williams, and N. D. Martinez, “Allometric scaling enhances stability in complex food webs,” *Ecology letters*, vol. 9, no. 11, pp. 1228–1236, 2006.

- [101] S. L. Pimm, “Complexity and stability: another look at macarthur’s original hypothesis,” *Oikos*, pp. 351–357, 1979.
- [102] M. Loreau and N. Mouquet, “Immigration and the maintenance of local species diversity,” *The American Naturalist*, vol. 154, no. 4, pp. 427–440, 1999.
- [103] M. W. Cadotte, “Dispersal and species diversity: A meta-analysis,” *The American Naturalist*, vol. 167, no. 6, pp. 913–924, 2006.
- [104] N. Mouquet, P. Leadley, J. Mériguet, and M. Loreau, “Immigration and local competition in herbaceous plant communities: a three-year seed-sowing experiment,” *Oikos*, vol. 104, no. 1, pp. 77–90, 2004.
- [105] C. E. Zartman and H. E. Nascimento, “Are habitat-tracking metacommunities dispersal limited? Inferences from abundance-occupancy patterns of epiphylls in amazonian forest fragments,” *Biological Conservation*, vol. 127, no. 1, pp. 46–54, 2006.
- [106] B. L. Foster, T. L. Dickson, C. A. Murphy, I. S. Karel, and V. H. Smith, “Propagule pools mediate community assembly and diversity-ecosystem regulation along a grassland productivity gradient,” *Journal of Ecology*, vol. 92, no. 3, pp. 435–449, 2004.
- [107] D. Ai, P. Desjardins-Proulx, C. Chu, and G. Wang, “Immigration, local dispersal limitation, and the repeatability of community composition under neutral and niche dynamics,” *PloS one*, vol. 7, no. 9, p. e46164, 2012.
- [108] W. Zhao, E. Serpedin, and E. R. Dougherty, “Inferring gene regulatory networks from time series data using the minimum description length principle,” *Bioinformatics*, vol. 22, no. 17, pp. 2129–2135, 2006.
- [109] D. Marbach, J. C. Costello, R. Küffner, N. M. Vega, R. J. Prill, D. M. Camacho, K. R. Allison, M. Kellis, J. J. Collins, G. Stolovitzky, *et al.*, “Wisdom of crowds for robust gene network inference,” *Nature methods*, vol. 9, no. 8, pp. 796–804, 2012.
- [110] I. Volkov, J. R. Banavar, S. P. Hubbell, and A. Maritan, “Inferring species interactions in tropical forests,” *Proceedings of the National Academy of Sciences*, vol. 106, no. 33, pp. 13854–13859, 2009.
- [111] D. J. Harris, “Inferring species interactions from co-occurrence data with markov networks,” *bioRxiv*, p. 018861, 2015.
- [112] M. E. Gilpin, “Do hares eat lynx?,” *The American Naturalist*, vol. 107, no. 957, pp. 727–730, 1973.

BIBLIOGRAPHY

- [113] G. Sandvik, C. M. Jessup, K. L. Seip, and B. J. Bohannan, “Using the angle frequency method to detect signals of competition and predation in experimental time series,” *Ecology Letters*, vol. 7, no. 8, pp. 640–652, 2004.
- [114] S. Froda and A. Zahedi, “Simple testing procedures for the holling type ii model,” *Theoretical Ecology*, vol. 2, no. 3, pp. 149–160, 2009.
- [115] A. Ives, B. Dennis, K. Cottingham, and S. Carpenter, “Estimating community stability and ecological interactions from time-series data,” *Ecological monographs*, vol. 73, no. 2, pp. 301–330, 2003.
- [116] C. M. Mutshinda, R. B. O’Hara, and I. P. Woiwod, “What drives community dynamics?,” *Proceedings of the Royal Society of London B: Biological Sciences*, vol. 276, no. 1669, pp. 2923–2929, 2009.
- [117] T. Saitoh, N. Chr, and O. N. Bjornstad, “Density dependence in fluctuating grey-sided vole populations,” *Journal of Animal Ecology*, pp. 14–24, 1997.
- [118] S. G. Shandilya and M. Timme, “Inferring network topology from complex dynamics,” *New Journal of Physics*, vol. 13, no. 1, p. 013004, 2011.
- [119] C. S. Holling, “Some characteristics of simple types of predation and parasitism,” *The Canadian Entomologist*, vol. 91, no. 07, pp. 385–398, 1959.
- [120] R. Arditi and L. R. Ginzburg, *How species interact*. Oxford, UK: Oxford University Press, 2012.
- [121] T.-W. Hwang, “Global analysis of the predator–prey system with beddington–deangelis functional response,” *Journal of Mathematical Analysis and Applications*, vol. 281, no. 1, pp. 395–401, 2003.
- [122] C. Jost and R. Arditi, “Identifying predator–prey processes from time-series,” *Theoretical population biology*, vol. 57, no. 4, pp. 325–337, 2000.
- [123] O. Sarnelle and A. E. Wilson, “Type III functional response in daphnia,” *Ecology*, vol. 89, no. 6, pp. 1723–1732, 2008.
- [124] D. Schenk and S. Bacher, “Functional response of a generalist insect predator to one of its prey species in the field,” *Journal of Animal Ecology*, vol. 71, no. 3, pp. 524–531, 2002.
- [125] G. Englund, G. Öhlund, C. L. Hein, and S. Diehl, “Temperature dependence of the functional response,” *Ecology letters*, vol. 14, no. 9, pp. 914–921, 2011.

- [126] A. Zamani, A. Talebi, Y. Fathipour, and V. Baniameri, “Temperature-dependent functional response of two aphid parasitoids, *aphidius colemani* and *aphidius matricariae* (hymenoptera: Aphidiidae), on the cotton aphid,” *Journal of Pest Science*, vol. 79, no. 4, pp. 183–188, 2006.
- [127] A. J. Lotka, “Elements of physical biology, reprinted 1956 as elements of mathematical biology,” 1924.
- [128] V. Volterra, “Fluctuations in the abundance of a species considered mathematically,” *Nature*, vol. 118, pp. 558–560, 1926.
- [129] R. J. Williams and N. D. Martinez, “Simple rules yield complex food webs,” *Nature*, vol. 404, no. 6774, pp. 180–183, 2000.
- [130] D. Stouffer, J. Camacho, R. Guimera, C. Ng, and L. Nunes Amaral, “Quantitative patterns in the structure of model and empirical food webs,” *Ecology*, vol. 86, no. 5, pp. 1301–1311, 2005.
- [131] R. J. Williams and N. D. Martinez, “Success and its limits among structural models of complex food webs,” *Journal of Animal Ecology*, vol. 77, no. 3, pp. 512–519, 2008.
- [132] B. C Rall, C. Guill, and U. Brose, “Food-web connectance and predator interference dampen the paradox of enrichment,” *Oikos*, vol. 117, no. 2, pp. 202–213, 2008.
- [133] J. A. Dunne, R. J. Williams, and N. D. Martinez, “Food-web structure and network theory: the role of connectance and size,” *Proceedings of the National Academy of Sciences*, vol. 99, no. 20, pp. 12917–12922, 2002.
- [134] P. Staniczenko, O. T. Lewis, N. S. Jones, and F. Reed-Tsochas, “Structural dynamics and robustness of food webs,” *Ecology Letters*, vol. 13, no. 7, pp. 891–899, 2010.
- [135] J. M. Montoya, S. L. Pimm, and R. V. Solé, “Ecological networks and their fragility,” *Nature*, vol. 442, no. 7100, pp. 259–264, 2006.
- [136] T. C. Ings, J. M. Montoya, J. Bascompte, N. Blüthgen, L. Brown, C. F. Dormann, F. Edwards, D. Figueroa, U. Jacob, J. I. Jones, *et al.*, “Review: Ecological networks—beyond food webs,” *Journal of Animal Ecology*, vol. 78, no. 1, pp. 253–269, 2009.
- [137] E. Anderson, Z. Bai, C. Bischof, S. Blackford, J. Demmel, J. Dongarra, J. Du Croz, A. Greenbaum, S. Hammarling, A. McKenney, and D. Sorensen, *LAPACK Users’ Guide*. Philadelphia, PA: Society for Industrial and Applied Mathematics, third ed., 1999.
- [138] C. McWilliams, “Ibm animations.” <http://chrismcwilliams201.wix.com/bristol#!animations/twkh3>.

Accessed: 2016-03-30.

BIBLIOGRAPHY

- [139] C. Gardiner, “Blue crystal.” <https://www.acrc.bris.ac.uk/acrc/>. Accessed: 2016-04-12.
- [140] R Core Team, *R: A Language and Environment for Statistical Computing*. R Foundation for Statistical Computing, Vienna, Austria, 2013.
- [141] G. B. West, J. H. Brown, and B. J. Enquist, “A general model for the origin of allometric scaling laws in biology,” *Science*, vol. 276, no. 5309, pp. 122–126, 1997.
- [142] R. H. Whittaker, “Dominance and diversity in land plant communities numerical relations of species express the importance of competition in community function and evolution,” *Science*, vol. 147, no. 3655, pp. 250–260, 1965.
- [143] B. J. McGill, R. S. Etienne, J. S. Gray, D. Alonso, M. J. Anderson, H. K. Benecha, M. Dornelas, B. J. Enquist, J. L. Green, F. He, *et al.*, “Species abundance distributions: moving beyond single prediction theories to integration within an ecological framework,” *Ecology letters*, vol. 10, no. 10, pp. 995–1015, 2007.
- [144] J. B. Wilson, “Methods for fitting dominance/diversity curves,” *Journal of Vegetation Science*, vol. 2, no. 1, pp. 35–46, 1991.
- [145] J. Oksanen, R. Kindt, P. Legendre, B. O’Hara, M. H. H. Stevens, M. J. Oksanen, and M. Suggs, “The vegan package,” *Community ecology package*, vol. 10, 2007.
- [146] P. J. Mumby, I. Chollett, Y.-M. Bozec, and N. H. Wolff, “Ecological resilience, robustness and vulnerability: how do these concepts benefit ecosystem management?,” *Current Opinion in Environmental Sustainability*, vol. 7, pp. 22–27, 2014.
- [147] I. Donohue, O. L. Petchey, J. M. Montoya, A. L. Jackson, L. McNally, M. Viana, K. Healy, M. Lurgi, N. E. O’Connor, and M. C. Emmerson, “On the dimensionality of ecological stability,” *Ecology letters*, vol. 16, no. 4, pp. 421–429, 2013.
- [148] V. Campbell, G. Murphy, and T. N. Romanuk, “Experimental design and the outcome and interpretation of diversity–stability relations,” *Oikos*, vol. 120, no. 3, pp. 399–408, 2011.
- [149] M. R. Dale and M.-J. Fortin, *Spatial analysis: a guide for ecologists*. Cambridge University Press, 2014.
- [150] M. Almeida-Neto, P. Guimaraes, P. R. Guimarães, R. D. Loyola, and W. Ulrich, “A consistent metric for nestedness analysis in ecological systems: reconciling concept and measurement,” *Oikos*, vol. 117, no. 8, pp. 1227–1239, 2008.
- [151] C. F. Dormann, B. Gruber, and J. Fründ, “Introducing the bipartite package: analysing ecological networks,” *interaction*, vol. 1, pp. 0–2413793, 2008.

- [152] M. J. Pocock, D. M. Evans, and J. Memmott, “The robustness and restoration of a network of ecological networks,” *Science*, vol. 335, no. 6071, pp. 973–977, 2012.
- [153] J. W. White, A. Rassweiler, J. F. Samhouri, A. C. Stier, and C. White, “Ecologists should not use statistical significance tests to interpret simulation model results,” *Oikos*, vol. 123, no. 4, pp. 385–388, 2014.
- [154] M. Lin, H. C. Lucas Jr, and G. Shmueli, “Too big to fail: large samples and the p-value problem,” *Information Systems Research*, vol. 24, no. 4, pp. 906–917, 2013.
- [155] J.-S. Lee, T. Filatova, A. Ligmann-Zielinska, B. Hassani-Mahmooei, F. Stonedahl, I. Lorscheid, A. Voinov, J. G. Polhill, Z. Sun, and D. C. Parker, “The complexities of agent-based modeling output analysis,” *Journal of Artificial Societies and Social Simulation*, vol. 18, no. 4, p. 4, 2015.
- [156] P. Runkel, “Large samples: Too much of a good thing?.” <http://http://blog.minitab.com/blog/statistics-and-quality-data-analysis>.
Published: 2012-06-04.
- [157] W. H. Greene, *Econometric analysis*. Pearson Education India, 2003.
- [158] A.-M. Neutel, J. A. Heesterbeek, and P. C. de Ruiter, “Stability in real food webs: weak links in long loops,” *Science*, vol. 296, no. 5570, pp. 1120–1123, 2002.
- [159] G. Kokkoris, A. Troumbis, and J. Lawton, “Patterns of species interaction strength in assembled theoretical competition communities,” *Ecology Letters*, vol. 2, no. 2, pp. 70–74, 1999.
- [160] K. Z. Coyte, J. Schluter, and K. R. Foster, “The ecology of the microbiome: Networks, competition, and stability,” *Science*, vol. 350, no. 6261, pp. 663–666, 2015.
- [161] R. M. May, “Patterns in multi-species communities,” *Theoretical ecology: principles and applications*, pp. 197–227, 1981.
- [162] G. F. Gause, “Experimental analysis of Vito Volterra’s mathematical theory of the struggle for existence,” *Science*, vol. 79, no. 2036, pp. 16–17, 1934.
- [163] R. A. Desharnais, *Population dynamics and laboratory ecology*, vol. 37. Elsevier, 2005.
- [164] G. E. Hutchinson, “The paradox of the plankton,” *The American Naturalist*, vol. 95, no. 882, pp. 137–145, 1961.

BIBLIOGRAPHY

- [165] M. Holyoak and S. P. Lawler, “Persistence of an extinction-prone predator-prey interaction through metapopulation dynamics,” *Ecology*, pp. 1867–1879, 1996.
- [166] H. P. Hsu, *Schaum’s outline of theory and problems of probability, random variables, and random processes*. McGraw-Hill, 1997.
- [167] D. Kwiatkowski, P. C. Phillips, P. Schmidt, and Y. Shin, “Testing the null hypothesis of stationarity against the alternative of a unit root: How sure are we that economic time series have a unit root?,” *Journal of econometrics*, vol. 54, no. 1, pp. 159–178, 1992.
- [168] S. E. Said and D. A. Dickey, “Testing for unit roots in autoregressive-moving average models of unknown order,” *Biometrika*, vol. 71, no. 3, pp. 599–607, 1984.
- [169] M. Priestley and T. S. Rao, “A test for non-stationarity of time-series,” *Journal of the Royal Statistical Society. Series B (Methodological)*, pp. 140–149, 1969.
- [170] N. Marwan, M. C. Romano, M. Thiel, and J. Kurths, “Recurrence plots for the analysis of complex systems,” *Physics reports*, vol. 438, no. 5, pp. 237–329, 2007.
- [171] T. Aparicio, E. F. Pozo, and D. Saura, “Detecting determinism using recurrence quantification analysis: Three test procedures,” *Journal of Economic Behavior & Organization*, vol. 65, no. 3, pp. 768–787, 2008.
- [172] S. Hazledine, *The Analysis and modelling of chaotic calcium oscillations*. PhD thesis, Department for Computational Systems Biology, John Innes Centre, 2009.
- [173] R. Mac Nally, “Use of the abundance spectrum and relative-abundance distributions to analyze assemblage change in massively altered landscapes,” *The American Naturalist*, vol. 170, no. 3, pp. 319–330, 2007.
- [174] J. A. Rudgers and K. Clay, “An invasive plant–fungal mutualism reduces arthropod diversity,” *Ecology Letters*, vol. 11, no. 8, pp. 831–840, 2008.
- [175] K. R. Keller, “Mutualistic rhizobia reduce plant diversity and alter community composition,” *Oecologia*, vol. 176, no. 4, pp. 1101–1109, 2014.
- [176] M. L. Rosenzweig and R. H. MacArthur, “Graphical representation and stability conditions of predator-prey interactions,” *American Naturalist*, vol. 97, no. 895, p. 209, 1963.
- [177] A. Mitra, “Are closure terms appropriate or necessary descriptors of zooplankton loss in nutrient–phytoplankton–zooplankton type models?,” *Ecological Modelling*, vol. 220, no. 5, pp. 611–620, 2009.

- [178] A. Hastings, *Population biology: concepts and models*. Springer Science & Business Media, 2013.
- [179] A. Hastings and L. J. Gross, *Encyclopedia of theoretical ecology*. No. 4, Univ of California Press, 2012.
- [180] S. Carpenter, K. Cottingham, and C. Stow, “Fitting predator-prey models to time series with observation errors,” *Ecology*, pp. 1254–1264, 1994.
- [181] G. Hutchinson, “An introduction to population ecology yale university press,” *New Haven*, 1978.
- [182] M. Solomon, “The natural control of animal populations,” *The Journal of Animal Ecology*, pp. 1–35, 1949.
- [183] K. Aho, D. Derryberry, and T. Peterson, “Model selection for ecologists: the worldviews of aic and bic,” *Ecology*, vol. 95, no. 3, pp. 631–636, 2014.
- [184] M. Sunnåker, A. G. Busetto, E. Numminen, J. Corander, M. Foll, and C. Dessimoz, “Approximate bayesian computation,” *PLoS Comput Biol*, vol. 9, no. 1, p. e1002803, 2013.
- [185] S.-B. Hsu and T.-W. Huang, “Global stability for a class of predator-prey systems,” *SIAM Journal on Applied Mathematics*, vol. 55, no. 3, pp. 763–783, 1995.
- [186] M. H. Cortez and J. S. Weitz, “Coevolution can reverse predator–prey cycles,” *Proceedings of the National Academy of Sciences*, vol. 111, no. 20, pp. 7486–7491, 2014.
- [187] N. C. Stenseth, W. Falck, O. N. Bjørnstad, and C. J. Krebs, “Population regulation in snowshoe hare and canadian lynx: asymmetric food web configurations between hare and lynx,” *Proceedings of the National Academy of Sciences*, vol. 94, no. 10, pp. 5147–5152, 1997.
- [188] D. Straile, “Meteorological forcing of plankton dynamics in a large and deep continental european lake,” *Oecologia*, vol. 122, no. 1, pp. 44–50, 2000.
- [189] K. H. Wiltshire, A. Kraberg, I. Bartsch, M. Boersma, H.-D. Franke, J. Freund, C. Gebühr, G. Gerdts, K. Stockmann, and A. Wichels, “Helgoland roads, north sea: 45 years of change,” *Estuaries and Coasts*, vol. 33, no. 2, pp. 295–310, 2010.
- [190] L. S. Luckinbill, “The effects of space and enrichment on a predator-prey system,” *Ecology*, vol. 55, no. 5, pp. 1142–1147, 1974.
- [191] L. Fahrig, J. Baudry, L. Brotons, F. G. Burel, T. O. Crist, R. J. Fuller, C. Sirami, G. M. Siriwardena, and J.-L. Martin, “Functional landscape heterogeneity and animal biodiversity in agricultural landscapes,” *Ecology letters*, vol. 14, no. 2, pp. 101–112, 2011.

BIBLIOGRAPHY

- [192] J. Elith, J. R. Leathwick, and T. Hastie, “A working guide to boosted regression trees,” *Journal of Animal Ecology*, vol. 77, no. 4, pp. 802–813, 2008.
- [193] J. C. Helton and F. J. Davis, “Latin hypercube sampling and the propagation of uncertainty in analyses of complex systems,” *Reliability Engineering & System Safety*, vol. 81, no. 1, pp. 23–69, 2003.
- [194] J. S. Lefcheck, “piecewisesem: Piecewise structural equation modelling in r for ecology, evolution, and systematics,” *Methods in Ecology and Evolution*, 2015.
- [195] G. Yvon-Durocher, A. P. Allen, M. Cellamare, M. Dossena, K. J. Gaston, M. Leitao, J. M. Montoya, D. C. Reuman, G. Woodward, and M. Trimmer, “Five years of experimental warming increases the biodiversity and productivity of phytoplankton,” *PLoS Biol*, vol. 13, no. 12, p. e1002324, 2015.

List of changes